Numerical Simulation of Carbonated Water Injection (CWI) Process in Live Oil Systems and Its Influences on Enhanced Oil Recovery

By

Ali Hassan Mohamed Al Basri Almesmari

Submitted for the degree of Doctor of Philosophy

Heriot-Watt University

School of Energy, Geoscience, Infrastructure and Society

Institute of Petroleum Engineering

September 2019

ABSTRACT

This thesis utilised the results of novel direct pore-scale experiments to develop a new and improved methodology for simulating the performance of Carbonated Water Injection (CWI) that is capable of reproducing the multiple physics observed in micromodel and core flood experiments. The method relied on the effectiveness of the transferred CO_2 from carbonated water on the compositional phase behaviour of the oil phase, and subsequent formation of an additional phase. Then, based on that, the equation of state was tuned to adopt this behaviour This methodology was applied and tested by history-matching core flood experiments in live oil systems. Through an integrated automatic-history matching algorithm, the proposed method was then employed to examine the ability of compositional reservoir simulators (CMG-GEM) to couple mass transfer and multi-phase flow during CWI.

The results revealed that the binary interaction coefficients between oil components and CO_2 would control the extent of the gaseous-phase formation. A unique and unusual negative binary interaction coefficient (BIC) was obtained between CO_2 and methane during the history match of tertiary CWI core displacement rather than the formal positive BIC in conventional CO_2 injection. Also, a relatively high value for critical gas saturation, as well as much lower k_{rg} values, were obtained to history match the coreflood experiments, which was in agreement with direct pore-scale observations of the immobility of the gas phase to reconnect the oil phase.

Next, a CW multiple-contacts equilibrium test was performed to study the compositional phase behaviour of the live oil, with the results being used to tune the equation of state (EOS). The results verified that the formation of a gas phase occurs after the oil became saturated with CO_2. Given the necessity for a negative CO_2 BIC to methane, different sets of BIC's were tested. Then, the EOS achieved during the test was used to simulate the CWI core displacement tests that successfully predicted the experimental outcomes, with the negative CO_2 BIC to C1, set producing the closest prediction. Therefore, this test verified the proposed method in tuning the EOS through history-matching the formation of gaseous phase saturation in tertiary CWI core displacement test. For the solidity of the simulation method, the applicability of the proposed method was verified in a new set of core displacement experiments. Having history matched the tertiary CWI core displacement experiment, the tuned EOS, and the collected relative permeability data

were used to predict the CWI in secondary mode (pre-WF) successfully. Thus, both conventional water and carbonated water would follow a unified flow path in a porous medium in a mixed wet system.

Finally, field-scale application scenarios of CWI for enhancing oil recovery in comparison with other recovery methods [mainly conventional water flooding and immiscible gas (CO_2 and methane) injections] was conducted. The outcomes of this study suggested that the injection of CW in secondary mode (pre-WF) is more attractive to produce additional oil. The increase of CO_2 content in the carbonated water by reducing the brine salinity or adding CO_2 solubility promoters would lead to further improvement in oil recovery as the amount of the formed gaseous phase which responsible in displacing more oil, would increase. Furthermore, the injection of CW uses the least net CO_2 about 1 MSCF/STB to recover 10% additional oil and has the highest CO_2 retention rate in the reservoir which about 50% of injected CO_2 compared to other CO_2 recovery methods.

DEDICATION

To

My father "Hassan" who once told me that only the education, not your origin or your money, will raise you in your life and in front of others. Please, forgive my negligence toward you, but you are always in my heart and my prayers.

To

My paradise in this life and after life, my mother and my spirit "Shaikha", many thanks to you. First "Allah" then your prayer that make me strong and persistent to accomplish my goal

To

My gorgeous and lovely wife "Mariam" for her continuous support and sacrifice throughout my studies. For my dearest children "Amna, Abdulla, Sultan, Hassan and Hind", thanks for sharing your moments with me.

Acknowledgment

Glory and praise be to "Allah", the Most Beneficent, the Most Merciful

I would like to express my truthful appreciation and gratitude to my supervisor, Professor Mehran Sohrabi, for his support, guidance, encouragement and patience throughout my research studies. This thesis would never have been completed without his constructive criticism and help.

I would like to thank ADNOC for their financial support during my studies, and their continuous follow up in order for me to achieve my goal through completing my thesis, thereby receiving my PhD. This work was carried out as part of the ongoing Enhanced Oil Recovery by Carbonated Water Injection (CWI) joint industry project (JIP) in the Institute of Petroleum Engineering of Heriot-Watt University. The project is equally sponsored by ADNOC, BG Group, Eni, Galp Energia, Oil India, and the UK DECC, all of whom are gratefully acknowledged.

I would like to thank Dr Pedram Mahzari and Dr Amir Farzanah for their invaluable technical support and motivation throughout my research. Also, many thanks to my colleagues Mohamed Al Hammadi, Hassan Al Zayer and Bashir Al Khazemi for their advice, encouragement, and their technical discussion, which triggered many thoughts that helped in my research.

DECLARATION STATEMENT

(Research Thesis Submission Form should be placed here)

TABLE OF CONTENTS

TABLE OF CONTENTS.....i
LISTS OF FIGURES.....iv
LISTS OF TABLES.....xi
NOMENCLATURE.....xiii
LIST OF PUBLICATIONS.....xix
Chapter 1 - Introduction.....1
1.1 Global Energy Demand.....1
1.2 Oil Recovery Techniques.....3
1.2.1 Primary Recovery Method.....3
1.2.2 Secondary Recovery Method.....4
1.2.3 Enhanced Oil Recovery (EOR) Methods.....5
1.2.4 CO_2-EOR.....6
1.3 Carbonated Water Injection (CWI).....9
1.4 Problem Statement and Research Objectives.....10
1.4.1 Problem Statement.....10
1.4.2 Research Objectives.....11
1.5 Summary of Chapter One and Overview of the Structure of the Thesis.....12
Chapter 2 – Literature Review.....14
2.1 Introduction.....14
2.2 CO_2 Phase Behaviour.....14
2.2.1 CO_2 Solubility in Brine.....15
2.2.2 CO_2-Oil Physical Properties.....18
2.3 Laboratory Experiments for CWI-EOR.....22
2.3.1 Direct Pore-Scale Tests.....23
2.3.2 CWI Coreflood and Sand-pack Experiments.....28
2.3.3 Slim-tube Experiments.....33
2.3.4 Role of CW on Wettability Alteration.....34
2.4 Theoretical and Numerical Modelling of CWI Process.....37
2.4.1 Frontal Advance Theory for CWI.....37
2.4.2 Numerical Modelling of CWI.....39
2.5 Conclusion.....41
Chapter 3 - Numerical Simulation of CWI in Water-Wet Core.....43
3.1 Introduction.....43
3.2 Methodology.....44
3.3 Direct Pore-Scale Visualisation Experiments.....44
3.4 Coreflood Experiments.....48
3.4.1 Fluid samples.....49

3.4.2 Core samples 50
3.4.3 Experimental procedure and results 51
3.5 New Gaseous Phase Saturation in Tertiary CWI 54
3.6 Multi-Phase Flow in Porous Media 57
3.7 Numerical Simulation of CWI 59
3.7.1 Model Description 59
3.7.2 Reservoir Fluids Model 61
3.7.3 Modelling the Formation of the New Phase 64
3.7.4 Simulation of Core Displacement Experiments 77
3.8 Overall Summary 101
3.9 Conclusions 103
Chapter 4 – CW Multiple-Contacts Equilibrium in Live Oil Systems 106
4.1 Introduction 106
4.2 CW Multiple-Contacts Equilibrium Test in Under-Saturated Oil 107
4.2.1 Experiment Setup 107
4.2.2 Preparation and Properties of Fluids 108
4.2.3 Experiment Procedure 109
4.3 Fluid Modelling 110
4.3.1 Modelling CW Multiple-Contacts Equilibrium Test 113
4.4 Results and Discussions 118
4.4.1 Characterisation of Carbonated Water 118
4.4.2 Phase Behaviour of CO_2-Oil mixture 119
4.4.3 Characterisation of the New Phase 122
4.4.4 CO_2-Oil Mixture Density and Viscosity 124
4.4.5 CO_2 Partition Coefficient 125
4.5 Predicting Coreflood Experiments 126
4.5.1 Methane-Saturated Oil Fluid PVT Data 128
4.5.2 Simulation Core Displacement Experiments 129
4.6 Summary and Conclusions 139
4.6.1 Multiple-Contacts Equilibrium PVT Test 139
4.6.2 Modelling CW Multiple-Contacts Equilibrium Test 140
4.6.3 Prediction of Core Displacement Experiments 141
Chapter 5 – Numerical Simulation of CWI in a Mixed-Wet Core 143
5.1 Introduction 143
5.2 Methodology 144
5.3 Direct Pore-Scale Experiments 144
5.4 Core Displacement Experiments 147
5.4.1 Fluid Samples 148
5.4.2 Core Samples 149

5.4.3 Coreflood Tests and Results 150
5.4.4 Third Phase Saturation during Tertiary CWI 151
5.5 Simulating the Performance of CWI 154
5.5.1 Model Description 154
5.5.2 Modelling Reservoir Fluids 155
5.5.3 Reproducing the Formation of the Third Phase 158
5.5.4 History Matching EXP01-SWF-TCWI 160
5.5.5 Prediction EXP02-SCWI 172
5.5.6 Effect of Carbonation Level on Oil Recovery 180
5.6 Summary and Conclusions 182
Chapter 6 – Technical Quality of Simulating CWI on the Reservoir-Scale 185
6.1 Introduction 185
6.2 Trials of CWI on the Field-Scale 185
6.3 Overall Approach 188
6.3.1 Statistical Estimates for RF, UF_{netCO2}, CO_2 Retention, and Storage 189
6.4 Homogeneous Box Model 189
6.4.1 Model Description 189
6.4.2 Simulation Results 192
6.5 SPE-5 Comparative Solution Model 201
6.5.1 Model Description 201
6.5.2 Simulation Results 207
6.6 Operational Concerns Associated with CWI 224
6.6.1 Preparing CWI 225
6.6.2 Corrosion Problems 226
6.7 Summary and Conclusion 226
Chapter 7 – Conclusions and Recommendations 230
7.1 Conclusions 230
7.1.1 Numerical Simulation of CWI in Core-Scale 231
7.1.2 CW Multiple-Contacts Equilibrium in Live Oil Systems 234
7.1.3 Technical Quality of Simulating CWI on a Reservoir Scale 237
7.2 Practical guidelines to simulate the performance of CWI 238
7.3 Future works and recommendation 240
References 243

LISTS OF FIGURES

Figure 1-1 Average annual growth in energy demand [1] 1
Figure 1-2 Various oil recovery stages and their corresponding recovery factors [7] 3
Figure 1-3 Typical MMP measurement of CO_2 Injection at fixed oil composition and temperature [16] 7
Figure 1-4 Schematic of a realistic WAG process (conceptually in horizontal reservoirs) [25] 9
Figure 2-1 Phase behaviour of Carbon Dioxide [29] 15
Figure 2-2 Solubility of different gases in pure water at 1 atmospheric pressure and various temperatures in Celsius (Created from www.engineeringtoolbox.com)[31] 16
Figure 2-3 Effect of temperature and pressure upon the solubility of CO_2 in pure water [33] 17
Figure 2-4 CO_2 Solubility in pure water, seawater and various NaCl salinities (calculated using Duan et al.'s model) [35, 36] 18
Figure 2-5 Solubility of CO_2 in an oil sample with a molecular weight (MW) of 268 g/mol and an API gravity of 21° at various temperatures and pressures (calculated using Emera and Sarma's correlation)[42] 19
Figure 2-6 oil viscosity reduction due to CO_2 solubility in oil at various CO_2 saturation pressures and two constant reservoir temperatures of 140 and 200 degrees F for two oil samples [45] 21
Figure 2-7 (left) mass transfer of CO_2 from CW into oil due to the difference in solubility between the aqueous phase and the oil phase (right) as more CO_2 is transferred into oil. The CO_2 stripped (expelled) light and intermediate components from the oil, allowing more CO_2 to be dissolved in the oil. 25
Figure 2-8 comparison of typical carbonated water injection with plain WF as proposed by de Nevers in [91] (A) the CO_2 concentration in water and its frontal advance, (B) water saturation as the water moves from injection well (C), and, (D), cumulative CO_2 and oil production as pore volume injected, respectively 39
Figure 3-1 a magnified section of the micromodel visualisation experiment of tertiary CWI in live oil system (A) after establishment of initial oil saturation at Swi (B) at the end of water flooding (C) after 24 minutes of CWI (scattered new phase bubbles are formed) (D) after 1 hour of CWI (increase in the size and numbers of new phase bubbles) (E) after 2 hours of CWI (where the reconnection of oil blobs) (F) at the end of CWI after 1 day of injection [66] 46
Figure 3-2 enlargement of the oil phase as a result of oil swelling and formation of the new phase during CWI in a live (methane-saturated) oil sample [66] 47
Figure 3-3 List of coreflood experiments [66] 48
Figure 3-4 the extended composition of stock tank oil crude B had been provided by Sohrabi et al. [66] 49
Figure 3-5 Oil recovery and differential pressure across the core during secondary WF and tertiary CWI in test no. 1 [66] 52
Figure 3-6 Oil recovery and differential pressure across the core during secondary CWI in test no. 2 [66] 53
Figure 3-7 Oil recovery and differential pressure across the core during secondary CWI followed by CO_2 injection in test no. 3 [66] 54
Figure 3-8 Calculated average gas (new phase) saturation during tertiary CWI of core displacement test no.1 55
Figure 3-9 Fractional flow of different viscosity ratios, showing the effect of a reduction in oil viscosity in a light oil system 56
Figure 3-10 linear relationship between calculated new gaseous phase saturation and reduction in residual oil saturation during tertiary CWI 58

Figure 3-11 the core physical dimensions....60
Figure 3-12 Schematic display showing the 1D model setup....60
Figure 3-13 Crude B stock tank oil and its recombined methane-saturated oil....62
Figure 3-14 Phase diagram of methane-saturated crude oil (B) based on the tuned PR-EOS....64
Figure 3-15 Flow diagram for liquid-vapour-water flash calculation as proposed by Li and Nghiem [116]....69
Figure 3-16 Bayesian framework explaining the inverse problem of history matching process [123]....73
Figure 3-17 flow diagram of CMG DECE optimisation method [126]....74
Figure 3-18 Different realisation of binary interaction coefficients in EOS to predict the average gas saturation by using assist history matching technique....76
Figure 3-19 Simulated average gas saturation using the optimum BIC realisations....77
Figure 3-20 flow diagram of assisted-history matching for tertiary CWI core displacement test no. 1....80
Figure 3-21 Comparison of experimental and simulated oil recovery during secondary WI and tertiary CWI core displacement test no. 1....83
Figure 3-22 simulated average oil saturation against the calculated one during secondary WI and tertiary CWI core displacement test no. 1....83
Figure 3-23 Comparison of simulated cumulative GOR to the cumulative GOR measured when performing test no. 1....84
Figure 3-24 Comparison of simulated cumulative WOR to the cumulative WOR measure when performing test no. 1....84
Figure 3-25 the simulated differential pressure in the core against the differential pressure measured during test no.1, showing a gradual increase as a result of the formation of the third phase....85
Figure 3-26 over-estimation of the simulated average gas (third phase) saturation compared to the saturation during CWI in test no. 1....86
Figure 3-27 the resulting relative permeability curves from matching SWI & TCWI core displacement test no. 1 (right) water-oil relative permeability and (left) oil-gas relative permeability....87
Figure 3-28 Predicted cumulative oil and differential pressure when simulating secondary CWI in test no.2 using the tuned EOR and relative permeability curves obtained from the previous test, set against the data measured experimentally in test no. 2....88
Figure 3-29 flow diagram of assisted-history matching for secondary CWI core displacement test no. 2....90
Figure 3-30 Comparison between measured and simulated oil recovery for secondary CWI test no. 2....92
Figure 3-31 Slight reduction in simulated oil saturation in comparison to the oil saturation calculated from the performance of secondary CWI in test no. 2....92
Figure 3-32 (Left) Comparison of simulated cumulative GOR to the cumulative GOR measured when performing test no. 2 (Right) Comparison of simulated cumulative WOR to the cumulative WOR measured during secondary CWI in test no. 2....93
Figure 3-33 the simulated differential pressure against measured differential pressure across the core in test no.2, showing a gradual increase as a result of the formation of the third phase....93
Figure 3-34 the estimated water-oil relative permeability curves for TCWI and SCWI 96
Figure 3-35 flow diagram of assisted-history matching for secondary CWI core displacement test no. 3....98
Figure 3-36 the history matched and predicted oil recovery during SCWI and TCO_2I in comparison with the experimental data from test no. 3....99

Figure 3-37 (Left) Simulated cumulative GOR against the experimental data for history matched SCWI and predicted TCO_2I in the core flood experiment no. 3 (Right) The match between cumulative WOR during SCWI and TCO_2I in the simulation model comparing to the measured data....99
Figure 3-38 the simulated differential pressure against the differential pressure measured across the core in test no.3, showing a gradual increase as a result of the formation of the third phase and then a sudden drop due to the mobility of the gas phase after CO_2 injection....100
Figure 3-39 the relative permeability curves resulting from matching SCWI core displacement test no. 3 (right) water-oil relative permeability and (left) oil-gas relative permeability....101
Figure 4-1 Schematic layout of CW multiple-contacts equilibrium PVT test....108
Figure 4-2 CW multiple-contacts equilibrium test in under-saturated oil at a temperature of 100 °F and pressure of 2500 psi....110
Figure 4-3 the recombined reservoir oil (B)....111
Figure 4-4 Flow diagram for liquid-vapour-water flash calculation as proposed by Li and Nghiem [116]....114
Figure 4-5 Systematic flow diagram on tuning the EOS to reproduce first equilibrium contact properties and predict the succeeding contacts....118
Figure 4-6 (A) Experimental and modelled variation in GWR of CW at each equilibrium contact, and (B) measured composition of gas content in CW in comparison with modelled composition by EOS after first equilibrium contact....119
Figure 4-7 (A) measured CO_2 solubility in oil at each saturation pressure representing equilibrium contacts with predicted values from EOS and correlations, (B) change in saturation pressure of under-saturated oil during CW equilibrium contacts....120
Figure 4-8 Modelled phase diagram of the oil phase at each equilibrium contact using the tuned EOS with negative and positive CO_2-C_1 BIC sets....121
Figure 4-9 (A) changes in measured GOR after each CW equilibrium contact with oil in comparison with predicted values using EOS (B) measured and predicted oil swelling factor at equilibrium contacts....122
Figure 4-10 Experimental and EOS predicted composition and volume of new gas phase after the sixth equilibrium contact....124
Figure 4-11 predicted change in live oil density and viscosity with an increase in CO_2 solubility in oil....125
Figure 4-12 Calculated CO_2 equilibrium coefficient in each contact....126
Figure 4-13 flow diagram showing the proposed methodology for numerically simulating the performance of CWI....127
Figure 4-14 the approach to prepare the modelled methane-saturated oil using the tuned EOS for the multiple-contact equilibrium test....128
Figure 4-15 Comparison between measured and simulated oil recovery during tertiary CWI (test no.1) where the black circles represent the experimental data, the blue plot is the simulation run using the first EOS that is tuned using assisted history matching, and the green and magenta plots are simulation runs using the second EOS that is tuned to match the MCET test....131
Figure 4-16 (A) oil viscosity reduction profiles during CWI in three simulation runs and (B) change in CO_2 and methane mole fraction in oil while CO_2 is transferred from CW to oil during CWI in test no. 1....131
Figure 4-17 Calculated cumulative GOR in three simulation scenarios in comparison to measured experimental data of EXP01....132
Figure 4-18 Predicted and history matched differential pressure across the core comparing with the measured experimental result of EXP01....133

Figure 4-19 calculated cumulative WOR in three simulation models in comparison to measured experimental data of EXP01 134
Figure 4-20 Predicted average gas (new phase) saturation in three simulation models comparing with the constructed gas saturation using EXP01 experimental data 134
Figure 4-21 Comparison between measured and simulated oil recovery during secondary CWI (EXP02) where the black circles represent the experimental data, the blue plot is the simulation run using the first EOS that is tuned using assisted history matching, and the green and magenta plots are the simulation runs using the second EOS that is tuned to match the MCET test 135
Figure 4-22 the average oil saturation in three simulation runs comparing to experimental data of EXP02 135
Figure 4-23 Calculated cumulative GOR in three simulation scenarios in comparison to measured experimental data EXP02 136
Figure 4-24 Predicted and history matched differential pressure across the core comparing with the measured experimental results of EXP02 137
Figure 4-25 Comparison between measured and simulated oil recovery during secondary CWI and tertiary CO_2I (test no.3) where the black circles represent the experimental data, the blue plot is the simulation run using the first EOS that is tuned using assisted history matching, and the green and magenta plots are simulation runs using the second EOS that is tuned to match the MCET test..... 138
Figure 4-26 sensitivity of changing CO_2-C_1 BIC on oil recovery using MCET 2^{ND} (-ve) EOS SIM 138
Figure 5-1 magnified snapshots of fully-saturated tertiary CWI micromodel to highlight the mechanism of oil swelling and reconnection of the oil phase, illustrated in the area with the blue circle, as well as the mobility of the third phase saturation alongside the oil phase (highlighted with red arrows) [121]..... 145
Figure 5-2 micromodel snapshots of (A) formation of third phase bubbles, (B) aggregation of the bubbles to form a third phase batch, (C) combined multiple patches to create a third phase chunk (D and E) third phase chunk displacing the stationary oil blobs during secondary CWI [71] 146
Figure 5-3 (A) the calculated oil saturation in visualisation experiments at the end of three injection scenarios (B) the estimated third-phase saturation during three visualisation experiments [71] 147
Figure 5-4 oil recovery and differential pressure across the core during secondary WF and tertiary CWI in crude S – EXP01 [71] 150
Figure 5-5 recorded oil recovery and differential pressure across the core during secondary fully-saturated CWI in crude S EXP02 [71] 151
Figure 5-6 calculated average (gas) new phase saturation during tertiary full-saturated CWI of coreflood EXP01..... 152
Figure 5-7 minimal oil saturation between two extreme residual oil saturations during the formation of the gas phase in tertiary CWI 153
Figure 5-8 Schematic diagram showing the 1D model setup for Crude-S coreflood experiments 155
Figure 5-9 recombined reservoir live oil – crude (S)..... 156
Figure 5-10 phase diagram of crude (S) live oil before and after EOS tuning 157
Figure 5-11 impact of adjusting the BICs in EOS with the aim of generating the third phase saturation during the tertiary CWI core displacement test..... 160
Figure 5-12 flow diagram of assisted-history matching for tertiary CWI core displacement in mixed-wet core..... 162
Figure 5-13 sensitivity of CO_2-hydrocarbon binary interaction coefficients between values obtained through assist history matching and values calculated using generalized correlation for simulating the average gas saturation 164

Figure 5-14 sensitivity of CO_2-hydrocarbon binary interaction coefficients between values obtained through assist history matching and values calculated using generalized correlation for simulating the average oil saturation....164
Figure 5-15 sensitivity of CO_2-HC BIC sets in the estimation of the phase behaviour in terms of oil (solid lines) and gas (dashed lines) viscosities and oil density in the last grid block (100, 1, 1)....165
Figure 5-16 sensitivity of CO_2-HC BIC sets for the estimation of the gas density, and the role of C_7 plus fractions in changing the gas density....165
Figure 5-17 history matched (A) oil recovery and (B) cumulative WOR compare to the experimental values during SWF and TCWI core displacement test EXP01....166
Figure 5-18 simulated (A) average oil saturation and (B) average gas saturation in comparison with calculated experimental values in EXP01 SWF-TCWI....166
Figure 5-19 illustration of the definition of wettability in porous media with oil/water/rock and their contact angles and capillary pressure behaviour [148]....168
Figure 5-20 the simulated differential pressure with recorded experimental data in EXP01 showing a gradual increase then a decline after the oil production commenced, even with formation of the third phase....169
Figure 5-21 obtained relative permeability curves from history matching the EXP01 coreflood experiment (A) water-oil relative permeability and (B) oil-gas relative permeability....170
Figure 5-22 calculated capillary pressure function during history matching the performance of secondary waterflooding in EXP01....171
Figure 5-23 comparison between produced CO_2 in simulation and the recorded experimental values....172
Figure 5-24 (A) comparison of predicted oil recovery and measured values during SCWI, and (B) the predicted cumulative WOR compared with the recorded data from EXP02-SCWI....173
Figure 5-25 predicted average oil saturation against experimentally calculated oil saturation of EXP02-SCWI....173
Figure 5-26 top cross-sections are the simulated CO_2 concentrations in oil and water close to water breakthrough, as indicated by the bottom cross-sections, which show oil and water saturation along the core close to water breakthrough....174
Figure 5-27 (A) the simulated GLR in comparison with the measured GLR during SCWI in EXP02 and (B) the recorded mole percentage of CO_2 concentration during the experiment in comparison with different simulation scenarios on the impact of mechanical dispersion on earlier CO_2 production....175
Figure 5-28 top cross-sections are the simulated CO_2 concentrations in oil and water close to water breakthrough, as indicated by the bottom cross-sections which are oil and water saturations along the core close to water breakthrough after introducing into the simulation model both CO_2 diffusion in oil and a dispersion of 0.7 ft....177
Figure 5-29 simulated oil recovery and differential pressure with and without introducing CO_2 diffusion in oil and a dispersion factor....178
Figure 5-30 CT-scan images of the core sample before and after mineral dissolution while injecting carbonated water (red circle is showing the formation of wormholes at the inlet of the core) [71]....180
Figure 5-31 sensitivity of the impact of the change in permeability due to dissolution of minerals on differential pressure across the core during SCWI EXP02....180
Figure 5-32 Effect of carbonation level on oil recovery during CWI in different modes....182
Figure 6-1 3-D homogeneous model....190
Figure 6-2 grid size (X-Y grid and layers) sensitivity of secondary WF and CWI....191
Figure 6-3 ultimate oil recovery of secondary WF and CWI with total brine/CW PVI193

Figure 6-4 oil recovery of SWF and SCWI and incremental oil recovery at 1.5 PVI of various injection rates 194
Figure 6-5 (A) ultimate oil recovery over total injected PV for the SWF, SCWI and SCWI scenarios with dispersion (B) CO_2 retention comparison between SCWI with and without the dispersion effect 195
Figure 6-6 effect of dispersion on (A) oil recovery factor of SCWI and (B) cumulative water and CO_2 mass productions 195
Figure 6-7 effect of dispersion on CO_2 concentration in oil (top) and water (bottom) at time of water breakthrough (0.12 PVI) 196
Figure 6-8 effect of dispersion on the formation of the gas phase (top gas saturation) and oil sweep efficiency (bottom oil saturation) at time of water breakthrough (0.21 PVI) 197
Figure 6-9 Impact of carbonation level on oil recovery during secondary CWI 198
Figure 6-10 impact of carbonation level on CO_2 retention during secondary CWI..... 199
Figure 6-11 comparison of oil recovery between SCWI and tertiary CWI at various SWF PVI 200
Figure 6-12 comparison of CO_2 retention between SCWI and tertiary CWI at various SWF PVI 200
Figure 6-13 a relationship between incremental oil recovery with total CO_2 PVI 201
Figure 6-14 a relationship between CO_2 retention with total CO_2 PVI 201
Figure 6-15 oil recovery at different X-Y grid sizes and number of layers 203
Figure 6-16 SPE-5 reservoir model showing the inverted five-spot pattern..... 203
Figure 6-17 a typical oil-gas relative permeability curves produced following those in [177] 207
Figure 6-18 ultimate oil recovery of secondary CWI in comparison with other injection methods 209
Figure 6-19 (A) CO_2 retention and (B) CO_2 storage during SCWI and SCO_2I with different injection rates 209
Figure 6-20 instantaneous voidage replacement ratio of SWF, SCWI and SCO_2I versus pore volume injected 210
Figure 6-21 impact of oil-gas relative permeability on oil recovery for secondary CWI and CO_2 injection (solid lines represent the results when using the oil-gas relative permeability from CW and the dashed lines representing the results when using the oil-gas relative permeability from CO_2I) 211
Figure 6-22 *impact of oil-gas relative permeability on* CO_2 retention *for secondary CWI and* CO_2 *injection* (solid lines represent the results when using the oil-gas relative permeability from CW and the dashed lines representing the results when using the oil-gas relative permeability from CO_2I) 211
Figure 6-23 oil recovery of four CO_2-related injection methods versus total pore volume injected 213
Figure 6-24 CO_2 utilisation factor of four CO_2-related injection methods versus total pore volume injected 213
Figure 6-25 CO_2 retention in various CO_2-related injection methods 214
Figure 6-26 percentage of CO_2 pore volume storage in various CO_2-related injection methods 214
Figure 6-27 oil recovery of SWF and SCWI at 0.5 PVI 215
Figure 6-28 incremental oil recovery of tertiary CWI and CO_2-related injection methods versus total pore volume injected 216
Figure 6-29 net CO_2 utilisation factor of tertiary CWI and CO_2-related injection methods versus total pore volume injected 217
Figure 6-30 CO_2 retention in the tertiary mode of various CO_2-related injection methods 218

Figure 6-31 percentage of CO_2 pore volume stored in the tertiary mode of various CO_2-related injection methods 218
Figure 6-32 cross-section of oil saturation after injecting 1.5 PV of (left top) TCWI, (right top) TCO_2I, (left bottom) TWAGI, and (right bottom) TSWAGI 219
Figure 6-33 cross section of gas saturation distribution after injecting 1.5 PV of (left top) TCWI, (right top) TCO_2I, (left bottom) TWAGI, and (right bottom) TSWAGI .. 220
Figure 6-34 comparison of incremental oil recovery during tertiary CO_2 injection methods after SCWI (dashed lines) and those after SWF (solid lines)..... 222
Figure 6-35 comparison of CO_2 storage during tertiary CO_2 injection methods after SCWI (dashed lines) and those after SWF (solid lines)..... 223
Figure 6-36 comparison of incremental oil recovery during tertiary CO_2 injection methods after SCWI using oil-gas relative permeability during CWI (dashed lines) and those using typical gas injection oil-gas relative permeability (solid lines) 224
Figure 6-37 comparison of CO_2 storage during tertiary CO_2 injection methods after SCWI using oil-gas relative permeability during CWI (dashed lines) and those using typical gas injection oil-gas relative permeability (solid lines) 224
Figure 6-38 Schematics of CO_2 mass transfer process in a Gas Infusion Unit [195] ... 225
Figure 7-1 flow diagram of the practical guilines in successfully simulating the performance of CWI core displacement experiments 240

LISTS OF TABLES

Table 2-1 Summary of direct pore-scale experiments 27
Table 2-2 Summary of CWI in core and sandpack displacement tests using dead oil systems 31
Table 2-3 Summary of CWI in coreflood tests using live oil systems 33
Table 3-1 measured basic fluid properties of fully methane-saturated reservoir oil B [66] 49
Table 3-2 Ionic content of the synthetic seawater [66] 50
Table 3-3 Physical and rock properties of the cores used in the experiments [66] 50
Table 3-4 Measured and modelled fluid properties of crude oil (B) 62
Table 3-5 Fluid description of reservoir oil (B) 63
Table 3-6 the most important cubic EOS's and their classical critical properties 67
Table 3-7 Optimum realisations of BICs for a EOS tuned to match the calculated average gas saturation 76
Table 3-8 effectiveness matrix of input parameters on objective functions of tertiary CWI core displacement test no. 1 80
Table 3-9 Binary interaction coefficients between CO_2, H_2O and hydrocarbon components 81
Table 3-10 Obtained water-oil relative permeability end points and LET correlation exponents 87
Table 3-11 Obtained oil-gas relative permeability end points and LET correlation exponents 87
Table 3-12 overall effectiveness matrix of uncertain parameters on objective function variables of secodanry CWI core displacement test no. 2 91
Table 3-13 Estimated water-oil relative permeability end points and LET correlation exponents for SCWI test no. 2 95
Table 3-14 overall effectiveness matrix of input parameters on objection function variables of secondary CWI core displacement test no. 3 98
Table 3-15 Estimated water-oil relative permeability end points and LET exponents 100
Table 3-16 Estimated oil-gas relative permeability end points and LET exponents 100
Table 3-17 Summary of the experimental and simulated oil recoveries from different core displacement tests (EXP referred to experimental data and SIM referred to simulation results) 103
Table 4-1 Composition of the synthetic gas, which was recombined with dead crude oil (B) 109
Table 4-2 Measured fluid properties of under-saturated crude oil (B) 109
Table 4-3 Fluid description of under-saturated oil (B) 113
Table 4-4 Modelled oil properties by EOS with measured experimental data 113
Table 4-5 Correlations to estimate the binary interaction parameters of CO_2 and hydrocarbons 116
Table 4-6 the calculated and manually adjusted BICs between CO_2 and hydrocarbons (MT stands for manual tuning and (-ve or +ve) is the negative or positive BIC between CO_2 and C_1 116
Table 4-7 Experimental and EOS calculated first equilibrium contact phase properties using four methods (MT stands for manual tuning and (-ve or +ve) is the negative or positive BIC between CO_2 and C_1 117
Table 4-8 Calculated methane-saturated oil compositions for two sets of EOSs where the first EOS was used in history matching the core displacement experiments in chapter 3 and the second EOS was used in matching the multiple-contacts equilibrium test 129

Table 4-9 Measured and two modelled EOS-based fluid properties of fully methane-saturated reservoir oil (B).....129
Table 5-1 Crude S stock tank oil composition and make-up gas for reservoir oil recombination [71].....148
Table 5-2 measured basic live oil properties of crude S [71].....148
Table 5-3 Composition of the seawater brine used in the coreflood experiments [71] 149
Table 5-4 the physical and rock properties of the composite core used in the coreflood experiments [71].....149
Table 5-5 detailed description of crude (S) live oil.....157
Table 5-6 comparison between the basic fluid properties that calculated by EOS and the measured values of crude (S) live oil.....158
Table 5-7 effectiveness matrix of input parameters on objection functions of tertiary CWI core displacement in mixed-wet core.....162
Table 5-8 CO_2-hydrocarbon BICs were estimated using various methods.....163
Table 5-9 obtained water-oil relative permeability end points and LET correlation exponents.....170
Table 5-10 obtained oil-gas relative permeability end points and LET correlation exponents.....170
Table 5-11 estimated capillary pressure parameters.....171
Table 6-1 Summary of the main field trials on carbonated water injection and their main results.....187
Table 6-2 X-Y grid size and layers sensitivity analysis.....190
Table 6-3 grid properties of the synthetic 3D homogeneous model.....191
Table 6-4 various injection rates over 25 years.....192
Table 6-5 CO_2 solubility in brine for different carbonation levels.....198
Table 6-6 reservoir properties in the SPE-5 grid model.....202
Table 6-7 Sensitivity of X-Y grid size and number of layers.....203
Table 6-8 Different injection and production perforation layer cases and their oil recovery at 1 PVI of SWF and CWI.....204
Table 6-9 Yuan et al. CO_2 MMP correlation coefficients.....205
Table 6-10 different reservoir injection rates over 25 years with their equivalent surface injection rates.....208

NOMENCLATURE

SF	swelling factor
$V_{CO_2-oil}(P_R, T_R)$	volume of oil and CO_2 mixture at reservoir conditions
$V_{oil}(P_b, T_R)$	oil volume at bubble point pressure and reservoir temperature
M	ratio of the mobility
λ_{ing}	the mobility of the displacing fluid
$\frac{k_{eff}}{\mu_{ing}}$	the ratio of the effective permeability of a porous medium of a displacing fluid to the viscosity of that fluid
λ_{ed}	the mobility of the displaced fluid
$\frac{k_{eff}}{\mu_{ed}}$	the ratio of the effective permeability of a porous medium of a displaced fluid to the viscosity of the fluid
S_o^{CWI}	the oil saturation in the core during CWI
S_{NP}^{CWI}	the saturation of new gaseous phase dormed during CWI
S_{orw}	residual oil saturation after conventional water injection
k_{rw}	water relative permeability
S_w	water saturation
$k_{rw}(S_w)$	water relative permeability as a function to water saturation
S_g	gas saturation
k_{rg}	gas relative permeability

$k_{rg}(S_g)$ gas relative permeability as a function to gas saturation

S_{om} the residual oil saturation in the three-phase region related to S_{orw}

α constant coefficient indicating the gas trapping

S_{gt} the trapped gas saturation or small mobile gas saturation

$k_{ro}(S_w, S_g)$ oil relative permeability as a function of water and gas saturation in three-phase region

Swc = Swcon connate water saturation

Swi initial water saturation

krow two-phase oil relative permeability for water/oil system

krog two-phase oil relative permeability for oil/gas system

So oil saturation

krocw oil relative permeability at connate water saturation

krwiro water relative permeability at residual oil saturation

Swcrit criticat water saturation

Lw, Ew, and Tw L.E.T exponents related to water in water/oil system

Low, Eow, and Tow LET exponents related to oil in water/oil system

krgc gas relative water saturation at connate water saturation in oil/gas system

krogcg oil relative permeability at connate gas saturation in oil/gas system

Sgcrit critical gas saturation

Sorg residual oil saturation to gas in oil/gas system

Sgcon connate gas saturation

Lg, Eg, and Tg L.E.T exponents related to gas in oil/gas system

Log, Eog, and Tog L.E.T exponents related to oil in oil/gas system

p experimentally measured pressure

v molar volume

R universal gas constant

α measure of the kinetic energy of the molecule (attraction parameter)

b the repulsion parameter

T the temperature

Zc critical compressibility

k_{ij} and l_{ij} binary interaction coefficients for components i and j

φ_{iv}, φ_{il} and φ_{iw} fugacity coefficients of components i in vapor, liquid and water, respectively

x_{iv}, x_{il} and x_{iw} mole fractions of component *i* in vapour, liquid and aqueous phases, respectively

z_i the feed composition (global mole fraction)

F_m the mole fraction of phase m (m = liquid, vapour or water)

Misfit the objective function

Np the number of measured data

Mi the measured data for point i

Si the simulated data for point i

Wi the weight factor of the measured point i

p(x) the posterior probability distribution function

$P_o(x)$ the prior probability function which describes the uncertainty of parameter x

L(x) the likelihood function that depends on assumptions about modelling errors and measurement errors of the observation

K_{CO2} the CO_2 partition coefficient in a mixture of water and oil

Pc	capillary pressure
a_w, a_o, c_w, and c_o	Skjaeveland correlation constants for imbibition and drainage in water/oil system

Abbreviations

CWI	Carbonated Water Injection
CO_2	Carbon Dioxide
BIC	Binary Interaction Coefficient
CW	Carbonated Water
EOS	Equation of State
WF	Water Flooding
IEA	International Energy Agency
IPCC	Intergovernmental Panel on Climate Change
GHG	Greenhouse Gas
CCS	Carbon Capture and Sequestration
CCUS	Carbon Capture Utilisation and Storage
EOR	Enhanced Oil Recovery
SPE	Society of Petroleum Engineers
OOIP	original oil in place
MMP	minimum miscibility pressure
HCPV	hydrocarbon pore volume
WAG	water-alternating gas injection
SWAG	simultaneous water and gas injection

ORCO	Oil Recovery Corporation
GWR	gas-water ratio
IFT	Interfacial Tension
ADSA	Axisymmetric drop shape analysis
WOR	water-oil ratio
PV	pore volume
BHIP	bottom-hole injection pressure
PR-EOS	Peng-Robinson's Equation of State
JST	Jossi-Stiel-Thodos viscosity model
Cn	hydrocarbon component where (n) is carbon number
GOR	gas-oil ratio
FVF	formation volume factor
STO	stock tank oil (dead oil)
FSO	fully saturated oil
Pc	critical pressure, atm
Tc	critical temperature
ω	acentric factor
VH	volume shift
vdW EOS	Van der Waals Equation of State
RK EOS	Redlich and Kwong Equation of State
SRK EOS	Soave-Redlich and Kwong Equation of State
vdW1f	Van der Waals one fluid mixing rule

WI	conventional water injection
SCWI	secondary carbonated water injection
SWF	secondary water flooding or conventional water injection
TCWI	tertiary carbonated water injection
TCO2I	tertiary CO_2 injection
SWAGI	secondary water-alternating gas injection
SSWAGI	secondary simultaneous water and gas injection
TWAGI	tertiary water-alternating gas injection
TSWAGI	tertiary simultaneous water and gas injection
SCO2I	secondary CO_2 injection
WAG-CO_2	water alternating CO_2 injection
LPG	liquified petroleum gases
STOOIP	stock tank original oil in place

LIST OF PUBLICATIONS

1. **AlMesmari, A**., Mahzari, P., and Sohrabi, M. *"**An Improved Methodology for Simulating Oil Recovery by Carbonated Water Injection: Impact of Compositional Changes**",* SPE-181630-MS, SPE Annual Technical Conference and Exhibition, Dubai, UAE, 26-28 September 2016

2. **AlMesmari, A.**, Mahzari, P., and Sohrabi, M., *"**Modelling Formation of a New Fluid Phase During Carbonated Water Injection**",* IPTC-18925-MS, International Petroleum Technology Conference, Bangkok, Thailand, 14-16 November 2016

Chapter 1 - Introduction

1.1 Global Energy Demand

The International Energy Agency (IEA) announced that global energy demand grew by 2.1% in 2017, more than the double that of 2016, with fossil fuels continuing to account for the majority (more than 70%) of this growth [1]. Figure 1-1 demonstrates the contribution of each energy sector to the growth in global energy demand over the last ten years. It is apparent from the figure that oil and gas resources are the main contributors, although renewable energy has grown strongly to subsidise around a quarter of the growth in global energy demand in 2017.

World consumption of petroleum and other petrochemicals is projected to rise from 95 million barrels per day (bbl/day) in 2015 to 113 million bbl/day in 2040 [2]. Furthermore, the net growth rate of global oil demand has shown a continuing increasing trend ever since oil prices fell in 2014. In 2017, the rate of growth of 1.6% was more than twice the average annual growth rate seen over the past decade [1]. The biggest drivers of this growth are coming from transportation and from the use of oil as a petrochemical feedstock in the production of plastics. In order to keep up with the growing global oil demand, additional investment in oil production is needed to increase volumes by an average of 18 million bbl/day from the 2015 figures by 2040.

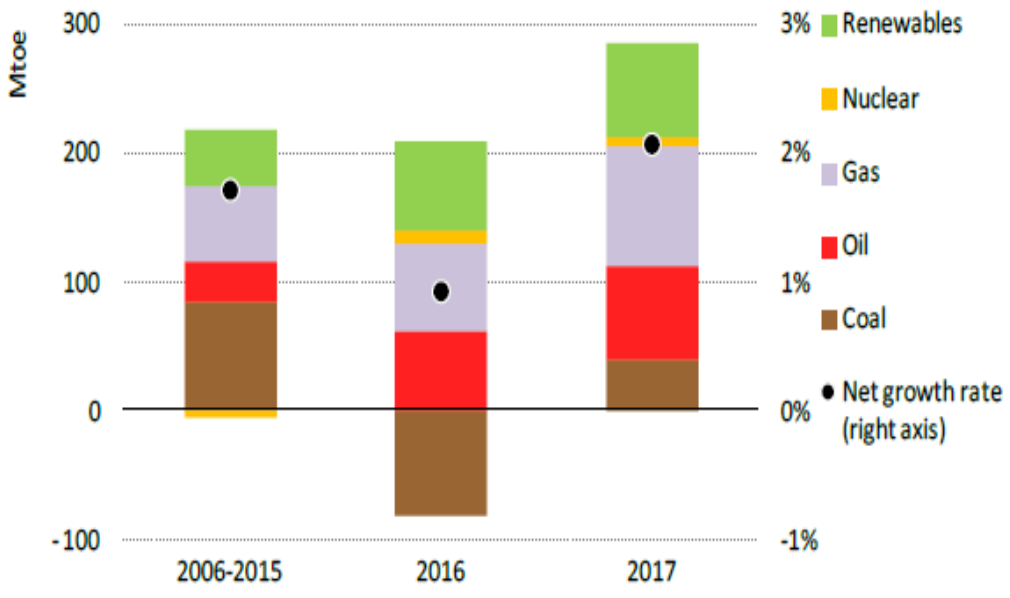

Figure 1-1 Average annual growth in energy demand [1]

These increases in the demand for oil have contributed to global energy-related carbon dioxide (CO_2) emissions increasing by 1.4% in 2017. According to the Intergovernmental Panel on Climate Change (IPCC), cumulative CO_2 emissions from fuel combustion and flaring have tripled during industrial era and contribute about 78% of all greenhouse gas (GHG) emissions [3]. Efforts to alleviate GHG emissions, particularly CO_2, in order to prevent further changes to the global climate, have focused on avoiding the production of carbon dioxide by improving dependency on renewable energy and thus reducing the need to use fossil fuels, a process that is typically referred to as "CO_2 abatement" [4]. Alternatives to CO_2 abatement given the likely continuing dependency on fossil fuels to meet global energy demand in the next decade include capturing the anthropogenic CO_2 emissions and sequestering them in geological reservoirs such as deep saline aquifers and deep ocean beds, which is referred to as Carbon Capture and Sequestration (CCS), or utilising them for enhancing the rates of oil recovery from oil reservoirs, which is referred to as Carbon Capture Utilisation and Storage (CCUS) [5].

An additional factor informing the above debates is that that the IEA estimates that most conventional oil fields experience a decline of 2% per year in available hydrocarbons, and this decline was expected to reach 4.7% per year by 2020, despite the drop in oil prices [6]. The declining conventional hydrocarbon resources due to the need for high oil production to meet the rising demand for energy has an additional effect of reducing the reservoir pressure as the leading natural forces of the reservoir. Reservoir pressure refers to the natural forces that assist in the extraction of the hydrocarbon and can be divided into three distinct phases in the lifetime of an oil reservoir: primary – where extraction can be achieved mainly through the natural forces of the reservoirs; secondary and tertiary, where external techniques are needed to assist the oil recovery. These are referred to as enhanced oil recovery (EOR) methods and these are increasingly needed to maintain the reservoir pressure for further oil production in the context of continuing demand and maturing oil fields.

Reducing the carbon footprint and enhanced oil recovery are the main drivers in injecting the CO_2 in the oil reservoirs. In this case, the CO_2 would increase the oil micro-displacement for more production, and at the same time, the trapping of CO_2 in the reservoir would store it.

1.2 Oil Recovery Techniques

The recovery lifecycle of a conventional oil reservoir would usually span from natural depletion drivers to external intervention techniques that can be used to improve oil recovery. When a reservoir begins production, oil naturally flows to the surface as a result of the interference of reservoir pressure in primary stage. As reservoir pressure depletes, immiscible fluid is typically injected in order to maintain the pressure to displace the oil (the secondary stage). Finally, additional oil can be recovered by introducing methods that can interact microscopically with oil to improve the flow efficiency. This is the tertiary or enhanced oil recovery (EOR) stage. A diagram of the various oil recovery stages, as defined by the Society of Petroleum Engineers (SPE), and their corresponding recovery factors, is shown in figure 1-2 [7].

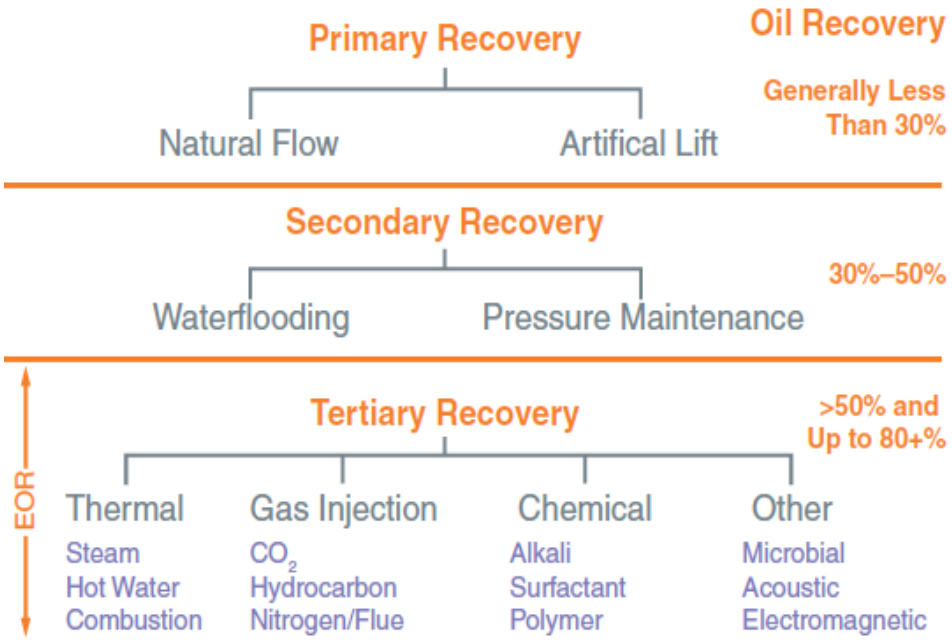

Figure 1-2 Various oil recovery stages and their corresponding recovery factors [7]

1.2.1 Primary Recovery Method

During primary recovery, the hydrocarbon can be produced from the reservoir using its natural energy source as the main driving mechanisms. This is affected significantly by factors like the viscosity of the oil, the reservoir pressure, the strength of any aquifer, and the geological and petrophysical characteristics of the reservoir. Each reservoir can be characterised by different natural energy sources which can comprise the main driving mechanism. There are five main driving mechanisms are:

- Solution gas drive
- Gas cap drive
- Water encroachment drive
- Gravity drainage
- Combination or mixed drive

In the early stage of the reservoir's life the driving mechanism is not recognised. It is determined through analysing the production data such as reservoir pressure and production ratios. The primary method is able to recover up to 50% of the original oil in place (OOIP), with an average of 20% of OOIP depending upon reservoir characteristics [8]. Primary recovery reaches its end when the pressure of the oil reservoir around the production wells becomes insufficient to maintain economic production rates, either through natural flow or mechanically assisted flow using an artificial lift.

1.2.2 Secondary Recovery Method

Once primary oil recovery is no longer sustainable, oil will no longer be produced without the contribution of additional techniques. The second stage of oil recovery involves the injection of an immiscible fluid, such as water and/or gas, into the reservoir via injection wells located in areas that have flow communication with the oil production wells.

Water flooding, or injection, is where water is injected into oil reservoirs. Because of its availability in the form of produced water or aquifer water and its competence in maintaining the reservoir pressure (known as voidage replacement), while sweeping or displacing the oil to the production wells, water flooding has been the most widely used secondary recovery method since its implementation in 1920 in the Bradford oil field of Pennsylvania, US [9]. The performance of water injection can be strongly affected by discrepancies in the mobility ratio of the injected fluid (water) to the displaced fluid (oil), however, in addition to microscopic displacement factors such as reservoir heterogeneity and wettability.

Gas flooding or injection is where the natural gas produced from the reservoir is re-injected into the reservoir gas cap in order to maintain its pressure, despite the fact that oil displacement is not the target. The gas flooding method of secondary recovery,

therefore, is a pressure maintenance technique to allow the natural reservoir dynamics to displace the oil towards the production wells. Other gas injection methods, such as the use of Carbon Dioxide or Nitrogen, are considered to be enhanced oil recovery methods which work by displacing the remaining oil by targeting the microscopic capillary and viscous forces.

In essence, therefore, primary and secondary recovery methods aim to extract mobile oil in the reservoir, whereas tertiary recovery, or EOR, aims to extract immobile oil that cannot otherwise be produced due to capillary and viscous forces [7]. In the long run, many oil fields usually produce only 15-20% of the OOIP during the primary recovery method. Another 15-20% of incremental oil recovery may be produced by secondary recovery methods [10]. As a result, there remains a great opportunity to increase oil recovery from matured oilfields by deploying other enhanced oil recovery (EOR) techniques.

1.2.3 Enhanced Oil Recovery (EOR) Methods

Enhanced oil recovery is the process whereby the physical and chemical properties of the reservoir oil/rock are modified to boost the production of hydrocarbon. In this method, the oil is recovered through the injection of fluids that are not normally present in the reservoir. These fluids are injected either to boost the natural energy in the reservoir or to interact with the reservoir oil/rock system in order to create more favourable conditions for the recovery of residual oil. These favourable conditions could be achieved in a number of ways, such as: the reduction of the interfacial tension between the displacing fluid and displaced oil so as to increase the capillary number; either increasing the injected water viscosity by polymer injection or reducing the resident oil viscosity by thermal injection to offer enhanced mobility-control; or, the promotion of oil swelling and reduction in oil viscosity through miscible injection. In addition, although the process of oil migration from source rock to reservoir rock may change the rock wettability towards mixed or oil wet, but this can be altered by the injection of surfactant through EOR methods [11].

EOR methods have the potential in increasing the production life of matured and depleted oil reservoirs, as well as having the ability to effect production from difficult, inaccessible

formations. EOR schemes fall into the broad categories of thermal, chemical, gas injection and other R&D methods such as microbial and acoustic [7]. Among all the EOR techniques, the Carbon dioxide (CO_2) solvent-based technique (CO_2-EOR) is considered to be one of the most efficient. CO_2-EOR uses the advantageous properties of supercritical CO_2 to enhance oil displacement efficiency, improving oil recovery by 5-15% beyond conventional water flooding [12].

1.2.4 CO_2-EOR

CO_2 has been increasingly used to enhance oil recovery during the past 40 years, and this expansion is likely to continue. As an example, CO_2 injection contributes over 5% of the total U.S. oil production [13]. In this context, the availability of large volumes of high-pressure CO_2 could become the limiting factor for the expansion of CO_2 injection. For example, the current CO_2 suppliers in the U.S. are operating at their full capacity [14]. Furthermore, almost two-thirds of the CO_2 utilised for EOR in the U.S. is provided from CO_2-rich natural gas formations.

Since in CO_2-EOR projects all of the injected CO_2 is either trapped in the reservoirs or is produced, recycled and then re-injected in subsequent projects, therefore the potential for using captured anthropogenic CO_2 for EOR in places which are far from natural sources of CO_2 is easy to execute. However, utilising anthropogenic CO_2 for EOR requires significantly better knowledge of reservoir characterisation. The lack of knowledge of fluid flow in reservoirs and understanding reservoir structure has been a key factor in the problems encountered in many of the EOR injection projects, including chemical and gas floods [15].

An important contribution of reservoir characterisation in the context of CO_2-EOR is to determine the reservoir conditions and the composition of the resident reservoir fluid in order to inform the decision as to whether CO_2 should be injected to encourage immiscible or miscible displacement.

Miscible Mode. If the injected fluid is completely or partially saturated with oil and oil-in-place mix in all proportions, then the process is called first contact miscibility. The injected fluids in these cases are often light or intermediate hydrocarbons, such as butane

and propane. Conversely, the injected gas and oil may initially form separate phases, meaning that they are not in first-contact miscibility; but, due to mass transfer between the gas and oil, and long contact between the fluids, miscibility may still be achieved. This is so-called multiple-contact miscibility, and it is this that occurs, for instance, with CO_2 injection [16]. Additionally, the miscibility is controlled by the pressure at which miscibility occurs. Holm and Josendal [17] defined the minimum miscibility pressure (MMP) as the pressure at which more than 80% of OIP is recovered at CO_2 breakthrough whereas, Yellig and Metcalfe [18] estimated the MMP to be the point at which no less than 90% of OIP is recovered at 1.2 HCPV (hydrocarbon pore volume) of CO_2 injected, as demonstrated in figure 1-3. It is this that is mostly used as a rule of thumb for estimating MMP.

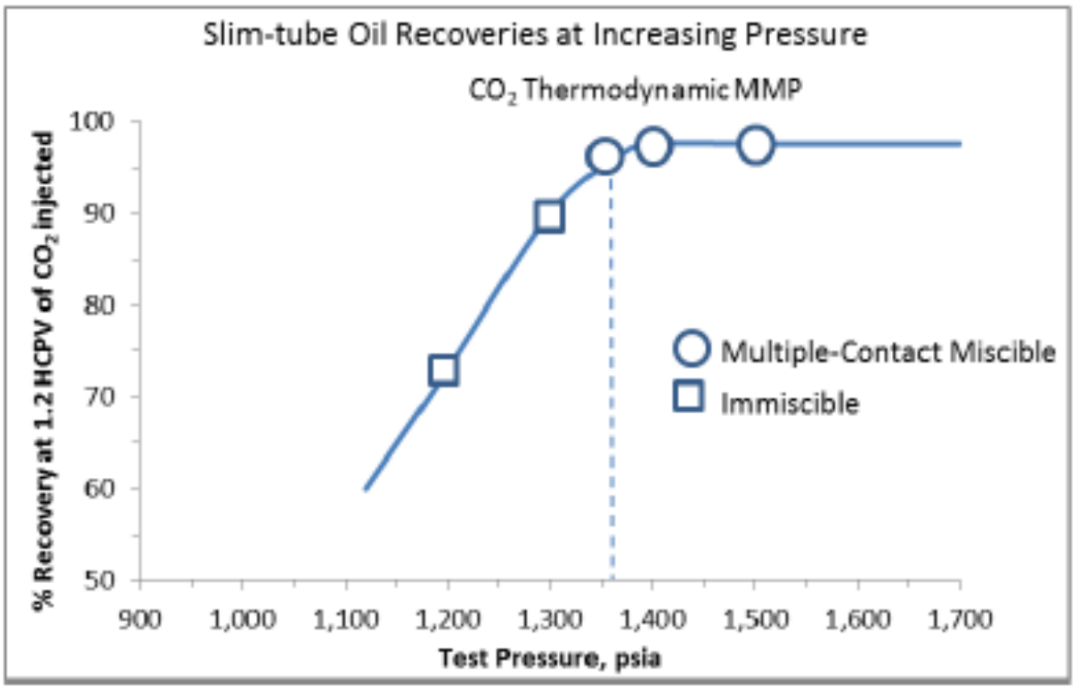

Figure 1-3 Typical MMP measurement of CO_2 Injection at fixed oil composition and temperature [18]

Usually four types of hydrocarbon miscible processes are used: (1) in a first-contact miscible injection, a slug of ethane or a light hydrocarbon mixture is used; (2) vaporising gas drive, also known as a high pressure gas drive, wherein lean hydrocarbon gas, nitrogen, or flue gas are used for injection; (3) condensing gas drive, wherein rich hydrocarbon gas is used for injection; and (4) vaporising-condensing gas drive, also known as CO_2 injection [19-21]. In fact, the CO_2 displacement process can fall into either the vaporising gas or vaporising-condensing drive processes, depending upon whether the reservoir pressure is below or above MMP. The use of CO_2 to extract lighter and

intermediate components from crude oil occurs at pressures below the MMP results in the enrichment of the driving CO_2, and is referred as vaporising drive. In addition to vaporising drive, however, when the pressures are above the MMP, CO_2 may also be transferred to the crude oil, which is referred to as condensation drive [21].

Immiscible Mode. When the reservoir pressure is not sufficient to build the miscibility, or when intermediate hydrocarbon components are not able to enrich the reservoir oil, the CO_2 and oil will not achieve miscibility. Nonetheless, CO_2 can dissolve in the oil to bring about oil swelling and a reduction in the oil viscosity, and this will still improve sweep efficiency and enable additional oil recovery [22, 23].

Although CO_2 has the capability to sweep practically all of the oil from the portion of the porous media through which it flows, in practice with miscible CO_2 injection, even when injecting 80% of hydrocarbon pore-volume (HCPV) of CO_2, typically only about 10-20% of the OOIP is recovered. Furthermore, the recovery percentage drops by half in immiscible CO_2 injection due to the contrast in the interfacial tension between the injected CO_2 and resident viscous oil [13].

The main reasons for this low oil recovery rate can be traced to the density and viscosity of CO_2. In other words, the main problems affecting gas injection techniques such as EOR are poor sweep efficiency as a result of gravity overrides or viscous fingering [10]. On the one hand, the large density contrast between the injected CO_2 and oil in the case of immiscible CO_2 injection promotes gravity override of the CO_2. In this situation, the reduced oil recovery in the lower part of the reservoir as a result of the injected gas overrides the reservoir fluid. On the other hand, the low viscosity of supercritical CO_2 in comparison to oil or brine viscosities with typical miscible CO_2 injection results in an unfavourable mobility ratio. This causes viscous fingering which in turn leads to early CO_2 breakthrough, a high CO_2 utilisation ratio, depressed oil production rates, and low rates of OOIP recovery [13].

It is possible, however, to enhance the mobility of injected gas (CO_2) by reducing its relative permeability via a water-alternating gas injection strategy (WAG). This is the most commonly applied process to maximise the extent of the reservoir contacted by the injected gas. The alternating injection of brine and CO_2 does not make the CO_2 more

viscous; rather it increases the water saturation and thereby decreases the CO_2 saturation within the pores. Bennion and Bachu [24-26] have demonstrated that this reduction of CO_2 saturation causes a reduction in the relative permeability of CO_2, which in turn lowers the mobility ratio and constrains the existence of viscous fingering. The WAG process is a combination of microscopic displacement as a result of CO_2 injection and efficient macroscopic displacement associated with water injection. Although in most of the reservoirs where WAG has been applied the process serves to damp down the gas overriding effects due to gravity in the near wellbore region, on the other hand the effect of gravity segregation increases as the injected fluids advance away from the wellbore, resulting in a huge unswept zone as a consequence of the combination of gas override and water under-ride by gravity, as demonstrated in figure 1-4 [27].

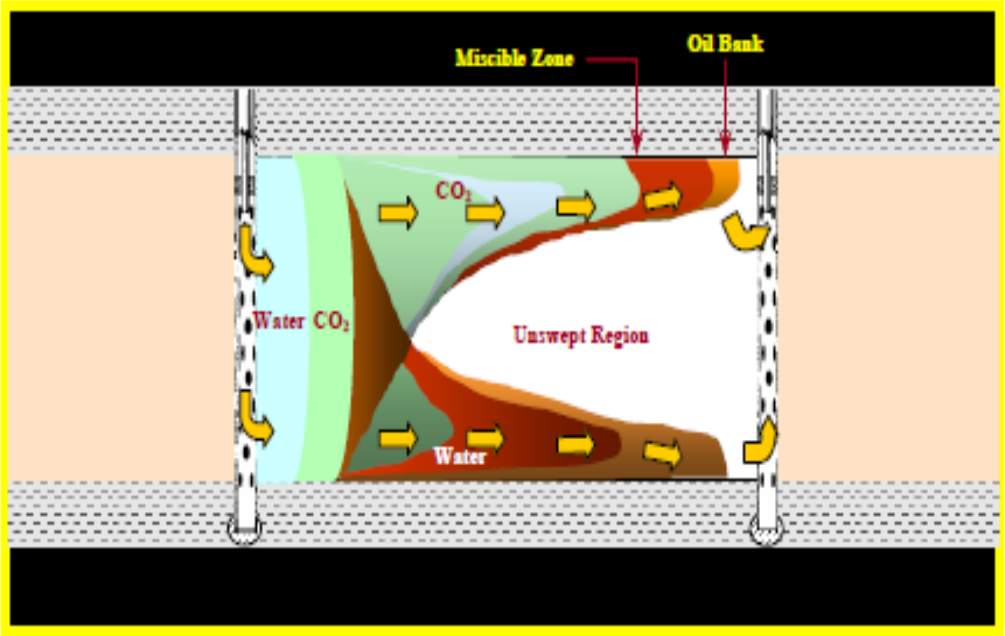

Figure 1-4 Schematic of a realistic WAG process (conceptually in horizontal reservoirs) [27]

1.2.5 Carbonated Water Injection (CWI)

In the context of the above issues, carbonated water injection (CWI) is a water-based enhanced oil recovery method, where confined and controlled amounts of CO_2 concentration are dissolved in water prior to injection and the mass transfer of CO_2 takes place from the aqueous phase into the oil phase where the water and oil come into contact. The fact that the CO_2 is dissolved in the injected water, rather than a separate phase, avoids the problems of gravity segregation and low sweep efficiency during conventional tertiary CO_2 injection methods [28]. Furthermore, the mass of CO_2 transferable to the

resident's oil results in a favourable oil swelling effect and a reduction in the oil viscosity which in turn will improve the mobility ratio and further reduce the residual oil saturation [29].

1.3 Problem Statement and Research Objectives

While the interest in CO_2 injection has grown with the need to increase oil production to meeting the global demand for energy there remain significant practical and commercial problems with the technology. Specifically, about 75% of the CO_2 used for EOR is produced by gas treating and processing facilities associated with the production of CO_2-rich natural gas reservoirs, which are mainly located in US [30]. This, in addition to the fact that anthropogenic CO_2 makes only a relatively low contribution to most of the CO_2 projects (usually less than 25%), means that capturing, treating, pressurising and transporting the CO_2 from various chemical and petroleum plants that are normally far away from the oil fields, is costly, which inhibits the use of conventional CO_2 injection in practice. Besides the lack of availability of CO_2 sources, direct injection of CO_2 may lead to poor sweep efficiency due to density and/or viscosity contrasts between the injected CO_2 and reservoir oil. This in turn leads to premature CO_2 injection, causing a deterioration in oil production and the need for CO_2 recycling facilities. Water-based CO_2-EOR methods, such as carbonated water injection, could overcome these two main complications linked to gas-based CO_2 EOR.

1.3.1 Problem Statement

Although carbonated water injection is a promising technology it involves a number of complex physical and chemical phenomena. The dynamic interphase mass transfer of CO_2 from the injected carbonated water to oil leads to fluid-fluid interactions that can bring about compositional changes in the oil and form another phase (i.e. a gas phase), thereby creating a three-phase flow regime. Furthermore, in current composition simulators, the modelling of interphase mass transfer is based on the assumption of instantaneous equilibrium which leads to rapid CO_2 transfer into oil on first contact with carbonated water. In practice, however, interphase mass transfer actually occurs slowly and in non-equilibrium manner. The main focus of this thesis, therefore, is the possibility

of modelling the non-equilibrium mass transfer of CO_2 within water and oil by using a partitioning coefficient.

Given these complex physical processes, concerns have been raised about modelling the mass transfer of CO_2 from a polar component, i.e. brine, to a non-polar substance, i.e. oil. Does the coupling of cubic equation of state (EOS) with CO_2 solubility in brine simulate the compositional change and formation of new phase resulting from the mass transfer of CO_2? How can the micromodel observations of the physics of the CWI process be fitted into numerical simulations of the process, and what are those physical processes and their impacts on the task of simulating the performance of CWI? The task, therefore, is to enhance the ability of current commercial simulators through changing the modelling approach and parameters to accommodate the reproducing of those processes by identifying feasible scientific explanations to capture the observed behaviour.

1.3.2 Research Objectives

The aim of the research is to provide scientific proofs to underpin the numerical modelling of the process of carbonated water injection (CWI) using currently available commercial reservoir simulators.

The specific objectives related to the numerical simulation of CWI process are:

- To capture the multiple physical processes and mechanisms occurring during CWI.
- To model the inter-phase mass transfer of CO_2, the formation of the new phase, and its influences on multi-phase flow, as well as the compositional changes of the resident fluids during CWI.
- To develop a method to tune the equation of state to model the fluid-fluid interaction which takes place during CWI in reservoir oil.
- To provide practical guidelines and a road map as to which parameters are responsible for improving the simulation of CWI.

1.4 Summary of Chapter One and Overview of the Structure of the Thesis

This thesis has a total of seven chapters, including this one. The subject of CWI as an enhanced oil recovery technique has received increased attention in recent years, alongside CO_2 storage and sequestration, especially in the context of the challenges faced by oil operators to produce the additional oil needed to meet global demand in the context of oil price instability. This chapter has provided a general background to global energy demand and the share of fossil fuels (oil and gas) in this demand, then different oil recovery techniques. CO_2 injection methods were shown to be the most attractive techniques for enhancing oil recovery, but it was also shown how their disadvantages, including poor sweep efficiency and limited availability of sufficient volumes of CO_2 hinder the wider adoption of CO_2 injection. In this context, carbonated water injection has been introduced as an enhanced oil recovery method that uses the water injection displacement mechanism to control the sweep efficiency and the CO_2 mechanisms to reduce the oil viscosity and increase oil swelling, with limited amounts of CO_2. Chapter 2 now moves on to present the phase behaviour of CO_2 and its solubility in brine and oil, and reviews the previous experimental and simulation trials of CWI, and how the research into CWI has developed since it was first studied. Chapter 3 introduces a new methodology that is proposed to simulate the CWI process in water-wet core displacement experiments to displace live oil. This chapter provides a comprehensive explanation using pore-scale observations and articulates how to translate the observed physics into numerical terminologies. Then, a history matching technique is used to simulate the tertiary and secondary CWI, and also to predict tertiary CO_2 injection.

Chapter 4 presents a detailed discussion of a CW multiple-contacts equilibrium PVT test, and uses its results to tune the EOS, coupling with Henry's Law for gas solubility in brine to model the PVT test results. The tuned EOS is then applied to the core flood experiments presented in the previous chapter in order to assess the method of tuning the EOS to model the average gas saturation which was calculated during tertiary CWI in chapter 3.

After establishing the method and verifying the approach to tuning the EOS, a new set of core flood experiments are performed in Chapter 5, this time in mixed-wet carbonate reservoir rock, in order to validate the method proposed in chapter 3 and refined in chapter 4. The procedure history matches the tertiary CWI, then predicts the secondary CWI

using the tuned EOS and estimated saturation function. The role of dispersion effect and mineral dissolution are discussed through the prediction procedure.

Chapter 6 investigates the performance of CWI on a reservoir-scale through technical comparison with conventional water flooding, and immiscible CO_2 and methane injection. During this technical quality screening, the effect of gridding and layering is discussed, along with the impact of dispersion and carbonation level on oil recovery and CO_2 storage. A further point of discussion in this chapter is the importance of considering an oil-gas relative permeability that is suitable for CWI, as well as one suitable for CO_2 injection, and appropriate examples are provided.

The thesis concludes in Chapter 7 with a summary of the current research study and the conclusions obtained. Recommendations for future work are also provided.

Chapter 2– Literature Review

2.1 Introduction

Carbonated water injection is a modified version of conventional water injection in so far as the water has been enriched with CO_2 to improve oil recovery. During CWI, CO_2 is transferred from the aqueous phase into reservoir oil through certain driving forces such as the contrast in CO_2 concentrations between water and oil and the fact that the solubility of CO_2 in oil is much higher than it is in water. This mass transfer causes a notable reduction in oil viscosity and an increase in swelling, improving the mobility ratio and decreasing the residual oil saturation, thereby resulting in enhanced oil recovery compared to conventional water flooding. Understanding the interaction between CO_2, brine and oil in terms of both binary systems (CO_2-brine and CO_2-oil) and a ternary system (brine-CO_2-oil), and their respective effects on oil composition is therefore fundamental to the ability accurately to model and design water-based CO_2-EOR methods for enhanced oil recovery and CO_2 storage.

2.2 CO_2 Phase Behaviour

At standard conditions, carbon dioxide behaves as a thermodynamically stable gas. It has a density higher than that of air and becomes a solid (dry ice) over a narrow temperature range at atmospheric pressure. CO_2 behaves as a supercritical fluid above its critical point (31.1°C) and pressure (72.8 atm) whereby it can adopt properties midway between those of a gas and a liquid; the entire envelope is shown in figure 2-1. For most CO_2-EOR methods, CO_2 is either in a gaseous state or is a supercritical fluid. In its supercritical state, CO_2 acts with gas-like characteristics, with its molecules moving freely similar to those of a gas, whereas its density is more like that of a liquid than a gas.

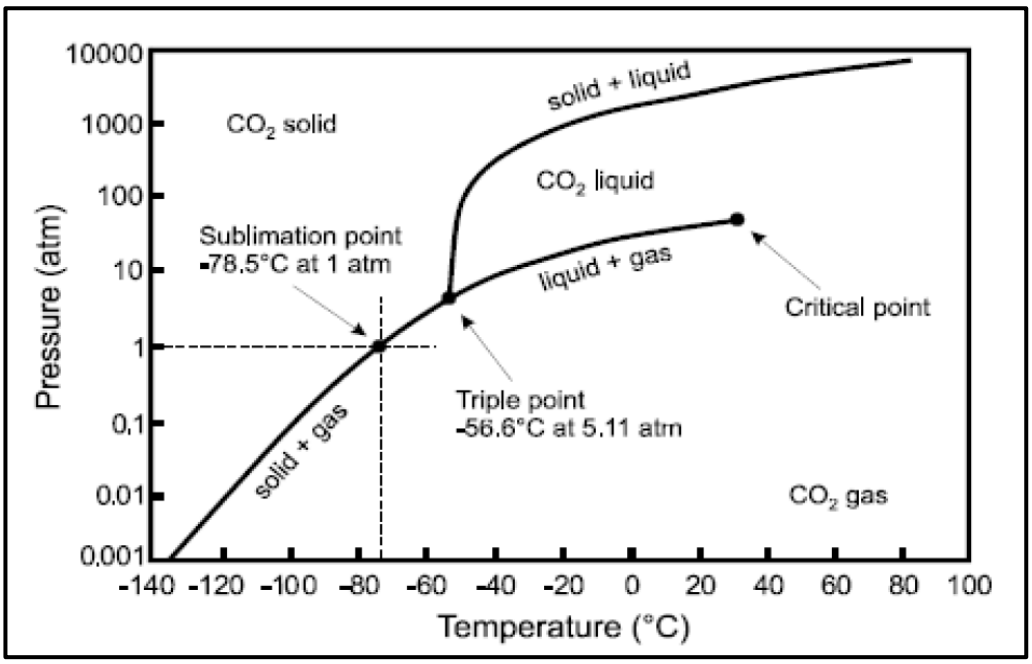

Figure 2-1 Phase behaviour of Carbon Dioxide [31]

2.2.1 CO_2 Solubility in Brine

In CWI, the amount of CO_2 used for enriching the water does not exceed what can be dissolved in the injected brine under the particular reservoir pressure and temperature, i.e., the amount of CO_2 injected is limited to CO_2's solubility in water. Generally, however, and as demonstrated in figure 2-2, CO_2's solubility in water is higher than that of other gases, due to the slight negative charge of its oxygen atoms which serve to form polar areas that attract water molecules. CO_2's solubility in water is also a somewhat complex system in that CO_2 molecules gain a shell of water molecules through polar attraction and it is through this shell that the CO_2 is transferred from its gaseous status into aqueous solution CO_2(aq), according to the following phase state reaction [32]:

$$CO_2(g) \leftrightarrow CO_2(aq) \qquad \textit{Equation 2-1}$$

In order to establish equilibrium between dissolved CO_2 and water, part of the CO_2(aq) reacts with water molecules to form carbonic acid ($H_2CO_{3(l)}$), according to:

$$CO_{2(aq)} + H_2O \leftrightarrow H_2CO_{3(l)} \qquad \textit{Equation 2-2}$$

Since the kinetic reaction is slow, however, only a small fraction (0.2 – 1%) of the dissolved CO_2 is actually converted to carbonic acid at equilibrium. Furthermore, carbonic acid is a weak acid since its ionisation in water is incomplete because it breaks

down into bicarbonate anions (HCO_3^-) when it reacts with water, which in turn forms anion carbonate (CO_3^{2-}), which is a salt of carbonic acid

$$H_2CO_3 + H_2O \leftrightarrow H_3O^+ + HCO_3^- \qquad \textit{Equation 2-3}$$

$$HCO_3^- + H_2O \leftrightarrow H_3O^+ + CO_3^{2-} \qquad \textit{Equation 2-4}$$

These carbonate anions, however, can interact with cations present in the water, especially Ca^{2+} and Mg^{2+} to form insoluble carbonate mineral deposits, as explained in equations 2-5 and 2-6. For example, if there are Ca^{2+} cations present in water, then $CaCO_3$ is formed. The formation of these precipitates, known as "*scale*", can serve to reduce the injectivity of carbonated water. On the other hand, the reverse reaction is also true, in that carbonate minerals such as calcite ($CaCO_3$) and magnesium carbonate ($MgCO_3$) themselves dissolve in the carbonated brine, leading to mineral dissolution that can alter the wettability of the rock or change the porosity and permeability in a similar way to stimulation.

$$Ca^{2+} + CO_3^{2-} \leftrightarrow CaCO_3 \downarrow \qquad \textit{Equation 2-5}$$

$$Mg^{2+} + CO_3^{2-} \leftrightarrow MgCO_3 \downarrow \qquad \textit{Equation 2-6}$$

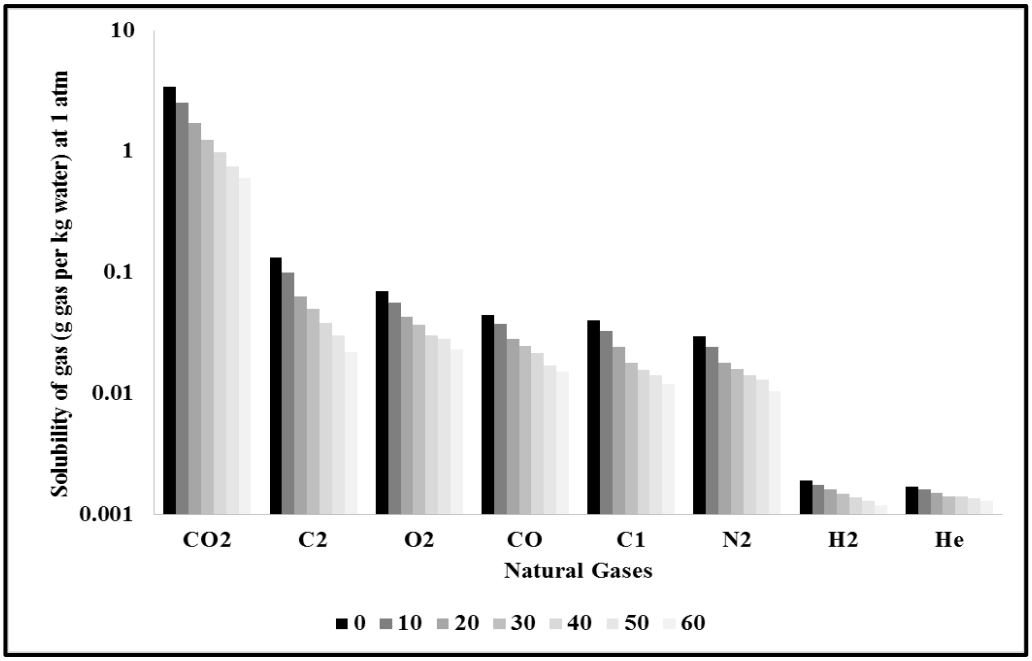

Figure 2-2 Solubility of different gases in pure water at 1 atmospheric pressure and various temperatures in Celsius (Created from www.engineeringtoolbox.com)[33]

CO_2's solubility in water/brine is affected by a number of influences, such as temperature, pressure and salinity [34]. In 1956, Dodds et al. assembled all the available experimental data on the solubility of CO_2 in pure water and to create a chart that permits more accurate determination of the changes in the solubility of CO_2 in water as a function of temperature and pressure. This is reproduced in figure 2-3 [35]. In line with Henry's Law, which states that the concentration of dissolved gas at equilibrium is directly proportional to the partial pressure of the gas, an increase in pressure has a positive effect on CO_2's solubility in water. On the other hand, an increase in temperature has the opposite effect, since the extra thermal energy gained from heating the solution is sufficient to surpass the attractive forces between the gas and solvent molecules [36]. That said, since temperature has less influence on solubility at very high pressures, the solubility of CO_2 in water increases with an increase in temperature at these pressures.

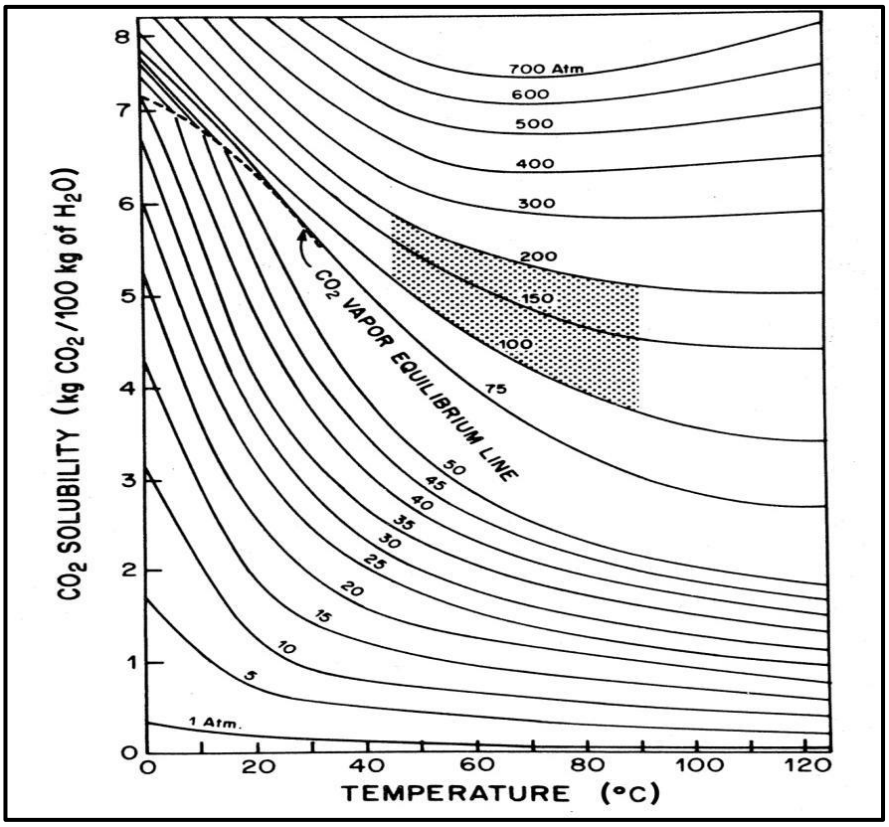

Figure 2-3 Effect of temperature and pressure upon the solubility of CO_2 in pure water [35]

CO_2's solubility in brine, meanwhile, is inversely proportional to the salinity of the brine, as exemplified in figure 2-4. This can be explained by the salting-out phenomena whereby the water molecules are attracted to the salt ions, which reduces the number of H^+ and O^{2-} ions that can surround the CO_2 molecules and transfer them into CO_2(aq).

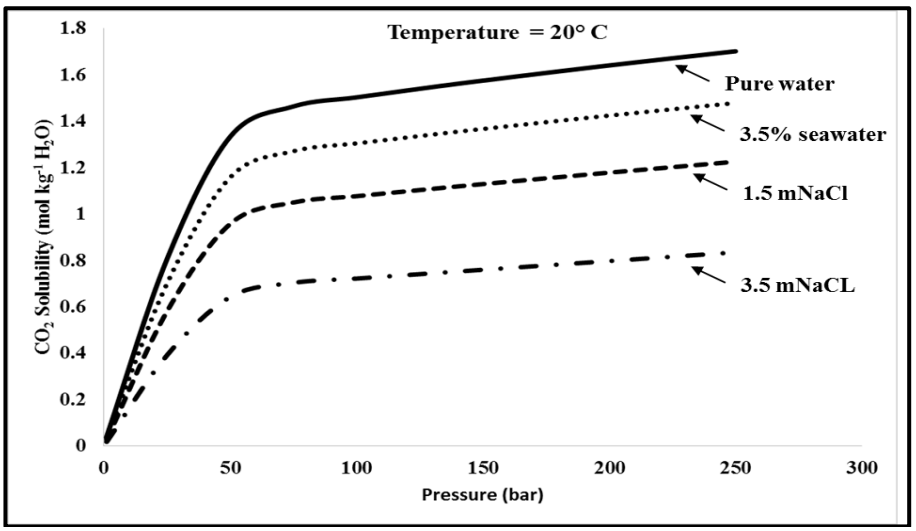

Figure 2-4 CO_2 Solubility in pure water, seawater and various NaCl salinities (calculated using Duan et al.'s model) [37, 38]

2.2.2 CO_2-Oil Physical Properties

The phase behaviour of CO_2-oil systems has been investigated by many researchers since the 1960's, especially after the implementation of many CO_2-miscible flooding projects following the increase in oil prices in the late 70's and early 80's. Interest has continued as new projects come on stream and earlier projects mature. The core mechanisms through which various CO_2 injection methods enhance oil recovery are the reduction of oil viscosity and increase in oil swelling arising from the physical and chemical interactions between CO_2 and reservoir oil. They improve the oil mobility and increase the efficiency of the oil recovery. The major parameter responsible for the reduction in oil viscosity and increase in oil swelling is CO_2's solubility in oil.

2.2.2.1 CO_2's Solubility in Crude Oil

In line with Heldebrand's [39] definition, the solubility of one substance in another substance is essentially directed by the feasibility of mixing one compound in another one as a result of the attractive forces between molecules. CO_2's solubility in oil has a significant linkage with saturation pressure, temperature and the oil's API gravity [40-43]. While CO_2 solubility increases with increasing pressure and oil API gravity, its solubility decreases with increases in temperature. There are other factors affecting CO_2's solubility in oil, namely the oil composition and CO_2's liquefaction pressure, given that gaseous CO_2 is more soluble in oil than liquid CO_2 [44]. This can be attributed to the degree of freedom available for CO_2 molecules in the gaseous state than in the liquid state due to attractive forces between molecules. In the gaseous state the CO_2 molecules can

easily move and diffuse at the CO_2-oil interface. The composition of the oil can also affect CO_2's solubility through the oil molecular weight. Emera and Sarma show that there is an inverse proportional relationship between CO_2's solubility in oil and oil's molecular weight [44].

Moreover, as more CO_2 is injected at reservoir conditions and the crude oil saturation pressure increases, Chung and Burchfield [42] observe that the solubility of CO_2 in oil would gradually increase. They explain this as resulting from CO_2 stripping the solution gas causing the methane to be liberated from the crude oil. Several researchers have developed correlations to estimate CO_2's solubility in oil based on experimental measurements [40, 41, 44-46]. Emera and Sarma [44], however, have developed a more reliable and predictable correlation for CO_2's solubility in oil and the resultant oil swelling effect and reduction on viscosity using a genetic algorithm, and the results of this model have been verified using experimental data. These correlations are appropriate for covering a wide range of oil properties such as oil specific gravities, pressures up to 34.5 MPa (~ 5000 psi), oil molecular weight greater than 490 g/mol, oil viscosities up to 12,000 cp, and temperatures as high as 140 °C. Figure 2-5 is a graphical representation of CO_2's solubility in an oil sample with a molecular weight of 268 g/mol and API gravity of 21° at different temperatures and pressures, using Emera and Sarma's correlation. It can be observed that at temperatures below the CO_2 critical temperature of $T_{c,CO2}$ = 88 °F and pressures higher than liquefaction pressure of CO_2, the solubility of CO_2 in oil reaches a maximum before the liquefaction pressure is reached.

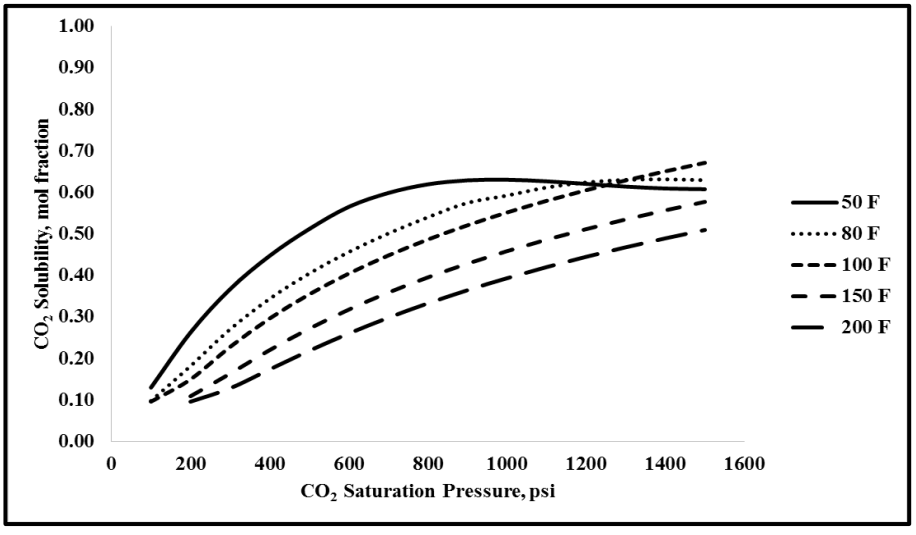

Figure 2-5 Solubility of CO_2 in an oil sample with a molecular weight (MW) of 268 g/mol and an API gravity of 21° at various temperatures and pressures (calculated using Emera and Sarma's correlation)[44]

2.2.2.2 Oil Swelling

Oil swelling is the expansion of oil volume that can occur due to the partial or complete dissolution of the CO_2 molecules into the reservoir oil. The amount of swelling is dependent on the CO_2 solubility and on the size of the oil molecules [40, 41, 44], meaning that since CO_2 is more soluble in lighter oil than in heavier oil, lighter oil swells more than heavier oil. According to Emera and Sarma, the oil swelling factor is defined as the ratio of CO_2-saturated oil volume at reservoir pressure and temperature to the oil volume at reservoir temperature and bubble point pressure [44].

$$SF = \frac{V_{CO_2-oil}(P_R,T_R)}{V_{oil}(P_b,T_R)} \qquad \textit{Equation 2-7}$$

where SF is the swelling factor, $V_{CO_2-oil}(P_R, T_R)$ is the volume of oil and CO_2 mixture at certain reservoir conditions, and $V_{oil}(P_b, T_R)$ is the oil volume at bubble point pressure and reservoir temperature. The expansion of oil volume due to oil swelling serves to reconnect otherwise isolated oil globules and this in turn mobilises trapped residual oil in inaccessible pore spaces [28, 29, 46], therefore increasing the oil recovery.

2.2.2.3 Oil Viscosity Reduction

The addition of CO_2 to the reservoir oil increases the saturation pressure, which causes the viscosity of oil to reduce significantly, resulting in increasing oil mobility and therefore increased oil recovery. The viscosity of the fluid mixtures initially reduces rapidly, followed by a shallower slope at higher CO_2 saturation pressures, as shown in figure 2-6 [47]. At higher pressures, the oil viscosity tends to increase as a result of the pressure and oil compressibility [47, 48]. Furthermore, the oil viscosity reduction due to CO_2 dissolution is more pronounced for highly viscous oil (heavy oil) than it is for (lighter) oil with a lower viscosity.

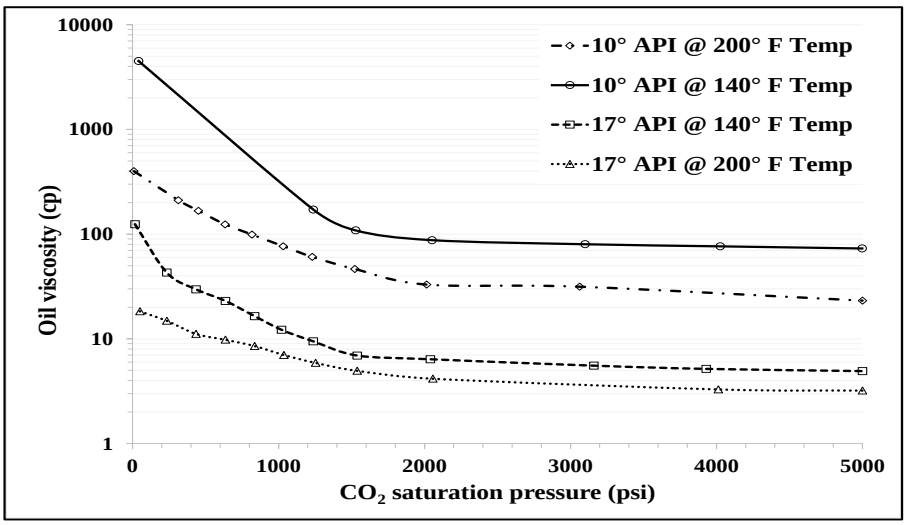

Figure 2-6 oil viscosity reduction due to CO_2 solubility in oil at various CO_2 saturation pressures and two constant reservoir temperatures of 140 and 200 degrees F for two oil samples [47]

Emera and Sarma developed a genetic algorithm-based CO_2-oil viscosity correlation based on the CO_2 solubility in oil, initial oil viscosity, saturation pressure, and temperature and oil specific gravity. Their findings summarise that the influence of these factors on the viscosity reduction is superior with live oil than with dead oil, although the effect of the initial oil viscosity is more predominant in the dead oil [44]. CO_2 solubility in either brine and oil and its effects on compositional behaviour and physical properties in both aqueous and oil phases is key driver in the performance of any CO_2-EOR methods such as carbonated water injection.

CO_2 can be introduced continuously with no added water, alternated with water in the form of water-alternating-gas (WAG), or even injected simultaneously with water (SWAG) through paired injection wells. In WAG or SWAG, water is injected with CO_2 in order to reduce the unfavourable mobility ratio between the injected CO_2 and the resident oil.

Another technique that can control that mobility ratio is through the injection of dissolved CO_2 in water in a noticeably immiscible way that enhances the mobility of oil through oil swelling and viscosity reduction, consequently recovering more oil [49]. The mobility ratio, is defined by Thomas as the ratio of the mobility of the displacing phase to the mobility of the displaced phase. It is usually expressed mathematically as follows:

$$M = \frac{\lambda_{ing}}{\lambda_{ed}}$$ Equation 2-8

where λ_{ing} is the mobility of the displacing fluid as the ratio of the effective permeability of a porous media of a displacing fluid to the viscosity of that fluid, $\frac{k_{eff}}{\mu_{ing}}$, and λ_{ed} is the mobility of the displaced fluid as the ratio of the effective permeability of a porous medium of a displaced fluid to the viscosity of that fluid, $\frac{k_{eff}}{\mu_{ed}}$

Carbonated water injection has been tested for its ability to produce significant incremental enhancement in oil recovery in comparison to water flooding since CO_2 partitioning into the reservoir oil results in a continuous reduction of oil viscosity as the solubility of CO_2 in oil increases. As explained above, this brings about higher oil mobility and thus a more favourable mobility ratio. Furthermore, the oil swelling effect due to CO_2 solubility in oil leads to a more suitable oil relative permeability, which also has a favourable effect on oil mobility [28, 29, 49-56].

2.3 Laboratory Experiments for CWI-EOR

Many laboratory studies of carbonated water injection have been conducted over the past years. These provide clear agreement as to the improvement in oil recovery that can be achieved by carbonated water injection in comparison to water flooding alone under the same conditions. Most of the comprehensive work on carbonated water injection was conducted from the late 1940's to the 1980's. At that time, the Oil Recovery Corporation (ORCO) first introduced the injection of carbonated water to improve oil recovery in sand-pack experiments conducted by Monteclaire Research in late 1940s [57]. The results showed a further reduction in oil saturation by up to 15 percent of pore volume (%PV) during carbonated water injection after secondary injection of conventional water (WF) [57].

Moreover, the period from the early 1950s until the late 1980s can be considered to be the most comprehensive in CWI laboratory research. In 1951, Martin reported an improvement of 12% in oil recovery during CWI, which positively correlated with the carbonation level [49]. On other hand, Saxon et al., in their experiments, did not achieve any significant improvement in oil recovery through CWI compared to conventional WF [58]. Later in 1952, Johnson et al. investigated the impact of different oil viscosities on

enhanced oil recovery during tertiary CWI in coreflood experiments. They found that when oil viscosities of 1.42 cp and 2.86 cp were used under test conditions there could achieve incremental recovery factors of 15% and 25%, respectively [55]. They also reported high levels of incremental oil recovery by CWI at lower temperatures, as a result of the higher CO_2 solubility in brine at lower temperatures precipitating more oil swelling. This also explained the additional oil recovery reported during the blow out process (depressurisation) at the end of CWI [55].

In 1959, Holm conducted a series of coreflood experiments using both a CO_2 slug and carbonated water. He observed that the oil recovery is a function of CO_2 solubility in oil. Furthermore, he observed the formation of a light hydrocarbon bank during CO_2-carbonated water injection which could be some kind of miscibility between CO_2 and oil that partially contributed to enhance oil recovery [59]. His results also showed an increase in the permeability of carbonate rock during CO_2-carbonated water injection. Shell also reported noticeable an increase in oil recovery during CWI in both sand-pack experiments and etched-glass models [60-64].

The incremental oil recovery and reduction of oil saturation were the primary outcomes of these experimental works in CWI. However, the lack of identifying the mechanisms responsible for enhancing oil recovery creates a limitation on further progressing in maturing the CWI as an EOR method. For that, it becomes looking at fluid-fluid interaction caused by the mass transfer of CO_2 from CW to oil through direct pore-scale observation experiments.

2.3.1 Direct Pore-Scale Tests

Focussing on pore-scale physics by using micromodel visualisation experiments to investigate the mechanisms responsible for improving oil recovery when injecting carbonated water, Sohrabi et al. [29, 65, 66] and Riazi et al. [28, 52] conducted a series of direct flow visualisation experiments at a pressure of 2000 psi and a temperature of 100 °F using n-Decane, representing a light oil and a viscous mineral oil. Their results revealed the good potential of CWI for increasing oil recovery after secondary water-flood for both light and viscous mineral oil; although more light oil was recovered than viscous oil due to the better swelling in the former. Their results identified that the two main mechanisms that contribute to improving oil recovery were:

1. Oil swelling, which causes the amalgamation of trapped oil ganglia, resulting in fluid redistribution, and a consequent improvement in displacement efficiency. The enlargement of oil volume due to oil swelling also causes local flow diversion of the CW stream to unswept areas in porous media.

2. Reduction in oil viscosity due to CO_2 partitioning between CW and resident oil.

While the oil swelling effect is the dominant mechanism for improving oil recovery in light oil systems, the reduction in oil viscosity is the main mechanism in viscous oil systems.

In 2010, Kechut et al. [67] performed direct pore-scale experiments using the same micromodel system and at similar conditions, but using a 145 cp stock tank oil (dead oil) taken from a North Sea oil reservoir. During injection of CW in tertiary mode (post-WF), oil swelling and reconnection of separated oil ganglia along with flow diversion were observed, where the maximum swelling factor was around 15%. An additional phenomenon noticed was that the resident oil's colour got brighter. This change in colour was related to the change in oil phase behaviour where the oil density and viscosity were altered due to CO_2 dissolution in oil.

For the purpose of comparison in experimental research, most of the previous experiments were carried out in either mineral oil or stock tank oil containing no dissolved gas. In realistic reservoir conditions, however, the oil always contains varying amounts of dissolved gas (solution gas) depending on the oil types. Thus, Sohrabi et al. [68] recently examined the effect of dissolved (solution) gas in reservoir oil on the performance of CWI through direct pore-scale visualisation experiments in which the transfer of CO_2 from carbonated water into live reservoir oils would generate a new gaseous-like phase inside the resident oil. They performed two micromodel experiments injecting CWI at tertiary mode in medium to low viscosity stock tank (dead) oil and live (methane-saturated) oil at a reservoir pressure of 2500 psi and a temperature of 100 °F. In the first micromodel test, the CW was injected to displace the dead oil after secondary conventional WF, in addition to the aforementioned mechanisms, like oil swelling and oil viscosity reduction, a third phase was formed at a later time after a sufficient amount of CW was injected. The formation of this new phase was mainly due to extraction of hydrocarbon components as a result of achieving the saturation limit of CO_2 in oil, which could be observed by total oil enlargement. In the second micromodel experiment,

meanwhile, where the CW was injected to displace the live oil after water flooding, the formation of the new phase occurred early and quickly since the oil was saturated with dissolved gas, and CO_2 has the ability to extract the hydrocarbon components to take their place in saturation with the oil. This new gas-like phase subsequently expands as more CO_2 is transferred from the aqueous phase to the oil phase, which contributes to further oil recovery. Compared to the normal oil swelling mechanism that takes place during CO_2 dissolution in oil, these results showed that, as the quantity of solution gas increased, the new gaseous phase formed more quickly and grew more rapidly to bring about a more substantial gaseous expansion to its surrounding oil. For live oil systems, therefore, the formation of this third phase could be considered to be the dominant mechanism driving the improved performance of CWI.

Based on micromodel observations, the new phase during CWI was formed due to the "one way" nature of the transfer of CO_2 from CW to oil when carbonated water came in contact with the oil in a reservoir. CO_2 solubility in oil is much higher than that in water, therefore, CO_2 transferred from preferentially from the aqueous phase to the oil phase. This process also caused multi-component competitions between CO_2 and the dissolved light hydrocarbon components of oil (methane), resulting in the liberation of a gaseous phase composed of methane in the very early stages which became heavier later.

During CWI, therefore, CO_2 transfer to the oil phase results in the CO_2 expelling the light and intermediate components of the oil. The expelled light and intermediate components of the oil form a new phase inside the oil phase which are nucleated as small bubbles. With more CO_2 transfer, the size and the number of these bubbles increases as more light and intermediate components are expelled from the solution, as illustrated in figure 2-7.

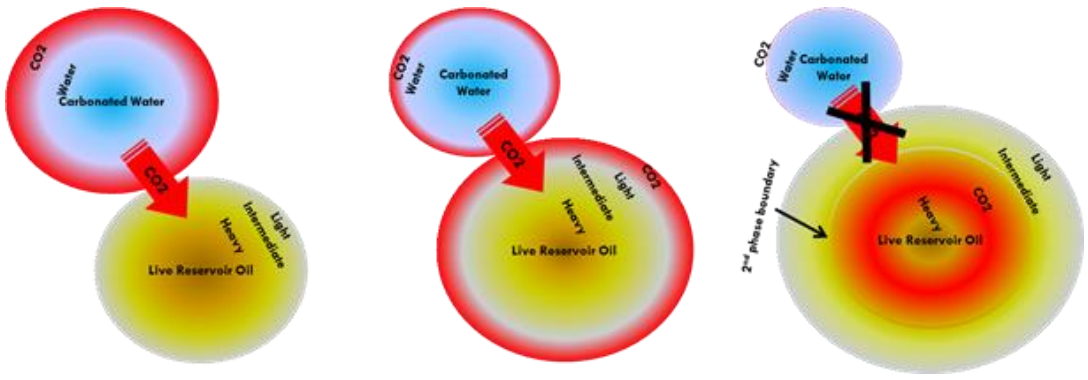

Figure 2-7 (left) mass transfer of CO_2 from CW into oil due to the difference in solubility between the aqueous phase and the oil phase (right) as more CO_2 is transferred into oil. The CO_2 stripped (expelled) light and intermediate components from the oil, allowing more CO_2 to be dissolved in the oil.

Similar work was conducted by Seyyedi et al. [69-72], injecting secondary and tertiary CW in a pore-scale micromodel apparatus to displace heavy crude (dead) and live oil. The dead and live oil viscosities were, respectively, 83 cp and 14 cp at a test temperature of 100 °F. The heavy live oil was fully saturated with methane only at a pressure of 2500 psi and temperature of 100 °F. Their results showed that the interaction at the interface between CW and resident live oil caused the formation of an additional phase inside the oil due to CO_2 partitioning between CW and oil, and they characterised this as a gas phase by analysing its composition while performing a multiple-contact equilibrium PVT test [69]. In the dead oil, meanwhile, two immiscible fluids, oil and injected CW, were observed without any formation of a new phase, even 24 hours after injecting CW. Based on pore-scale observations, the live oil grew to 34% more than its original volume, with about 60% of that enlargement being due to the formation and growth of the new gaseous phase [70]. The authors claimed that the scattered formation of gas bubbles throughout the porous medium away from the contact interface between CW and oil, would lead to efficient delivery of CO_2 by CW rather than the adverse frontal instability displacement resulting from conventional CO_2 injection [69, 71].

A summary of the micromodel experiments that observed the machnisms of CWI on enhancing oil recovery presented in table 2-1. Those observations defined three main mechanisms, e.g. the classic oil swelling and reduction of oil viscosity as a result of CO_2 dissolution in the oil phase, furthermore the formation of a new phase due to stipping of hydrocarbon components by CO_2 which observed in live oil systems. The role of those mechanisms in enhancing oil recovery depends on the original oil viscosity, the amount and type of dissolved gas in the oil, and in the least degree the oil capacity in dissolving more CO_2 such as nDecane case.

Table 2-1 Summary of direct pore-scale experiments

Previous Studies	Test Conditions	Oil type	CWI Mechanism	Limitation
Riazi et al. (2009) [28]	p = 2000 psi and T = 100 °F, (distilled water, CO_2 solubility = 29 scc/cc)	nDecane viscosity = 0.83 cp	significant oil swelling as a result of partitioning of CO_2 from CW and dissolving into oil	nDecane, synthetic and/or stock tank oil are not representing the actual reservoir fluid and does not produce all CWI mechanisms
Sohrabi et al. (2009) [29]		mineral oil viscosity = 16.5 cp	Reduction of oil viscosity due to mass transfer of CO_2 into oil	
Kechut et al. (2010) [67]		Stock tank oil viscosity = 145 cp	Oil swelling and reduction of oil viscosity	
Sohrabi et al. (2015) [68]	p = 2500 psi and T = 100 °F, sea water (salinity = 3.5%, CO_2 solubility = 28.7 scc/cc)	stock tank oil viscosity = 31 cp	Reduction of oil viscosity and oil swelling as a result of CO_2 diffusion into oil phase from CW, limited formation of a new phase	The used oil is free of dissolved gas in which limiting the formation of a new phase, subsequently, not bringing the full potential of CWI mechanisms
		(live oil) Methane-saturated oil vicosity = 1 cp, GOR = 107 cc CH4/cc	Formation of a new phase inside the oil phase makes the more oil swollen in which the water flow diverted to recover the unswept oil	the oil saturated only with methane
Seyyedi et al. (2017) [72]	p = 2500 psi and T = 100 °F, sea water (salinity = 5.4%, CO_2 solubility = 26 scc/cc)	(Live oil) Methane-saturated oil vicosity = 14 cp, GOR = 51 cc CH4/cc	Oil swelling due to the formation of a new phase within the oil and reduction of oil viscosity	Formation of a new phase inversely proportional to dissolved gas in the oil. Additionally the absence of light hydrocarbon components in live oil
Mahzari et al. (2017) [73]	p = 3100 psi and T = 212 °F, sea water (salinity = 5.9%, CO_2 solubility = 22 scc/cc)	(Live oil) Saturated oil with maltiple HC gas components, viscosity = 0.9 cp, GOR = 82 cc/cc	Oil swelling due to the formation of a new phase within the oil and the formed phase contains light hydrocarbon components which creates favourable miscibility condition with oil	High reservoir temperature reduces the CO_2 solubility in brine

2.3.2 CWI Coreflood and Sand-pack Experiments

Dead oil systems

In order to emphasise their pore-scale results, Kechut et al. [74] and Sohrabi et al. [54] examined CWI as a method to enhance oil recovery as well as its benefit in storing CO_2. A series of CW core displacement experiments were performed using different type of cores, including a relatively unconsolidated water-wet reservoir core from a North Sea sandstone reservoir, and two outcrop Clashach sandstone cores having different wettability, one with its natural water-wet whereas the other was made mixed-wet by aging in crude oil. For consistency with the micromodel experiments, the used oil samples were n-decane representing light oil (viscosity = 0.82 cp), while a refined mineral oil, representing viscous oil (viscosity = 81 cp), and a reservoir stock tank oil (viscosity = 145 cp) were used in reservoir core displacement. Decane (C_{10}) was miscible with CO_2 at test pressure and temperature of 2000 psi and 100 °F whereas the refined oil and reservoir crude oil were immiscible with CO_2 at test conditions as they contained mainly C_{20+} hydrocarbon components. Two brine samples were used with salinities of 1.0 wt% for low salinity brine and 3.538 wt% for high salinity brine.

Two sets of coreflood experiments were performed. The first set involved injecting CW in secondary mode (pre-WF) at 100 °F and 2000 psi using Clashach cores, decane, refined viscous oil, 1.0 wt% brine and CW, with a CO_2 solubility of 31 cc/cc. This set of experiments was carried out with no initial water saturation in order to monitor the flow of injected CW, and the way in which the dissolved CO_2 was transported within the porous medium, accurately. The objective of these displacement tests was to investigate the effect of oil viscosity and initial wettability on the performance of CWI. In order to study the effect of oil viscosity, therefore, the secondary CWI in the water-wet Clashach core using decane was compared with those of the refined oil, which had a viscosity of about two orders of magnitude greater than that of decane. Injecting carbonated water improved the oil recovery with decane more than with viscous oil due to the favourable viscosity ratio of 1.2, which promoted a piston-like displacement, and since the miscibility of decane with CO_2 caused unlimited oil swelling. In the refined viscous oil tests, meanwhile, the unfavourable mobility ratio initiated an unstable displacement front which led to viscous fingering and thus early water breakthrough, while the lower CO_2 dissolution in the oil reduced the oil swelling. Together this resulted in less additional oil

recovery than in the case of decane. Although the oil swelling was low, the main driver for oil recovery in the case of the viscous oil was the reduction in its viscosity due to CO_2 mass transfer from CW to the oil.

Water-wet and mixed-wet Clashach sandstone cores were then used to perform secondary CWI in a decane system in order to evaluate the effect of wettability. It was found that injecting carbonated water into the mixed-wet core produced more additional oil recovery than in the water-wet core.

In the subsequent tests, secondary and tertiary CWI coreflood experiments were performed using reservoir stock tank oil that had 145 cp viscosity at test conditions of 2500 psi and 100 °F and 3.538wt% brine with CO_2 solubility of 29 cc/cc. Incremental oil recovery was obtained in secondary CWI as well as tertiary CWI, but the secondary CWI resulted in higher and earlier enhanced oil recovery than was the case in tertiary CWI. Additionally, a relatively high percentage of injected CO_2 was trapped and stored: about 40-50% in the form of dissolved CO_2 in the remained oil and brine at the end of the experiments. The researchers therefore concluded that the carbonated water front was able to deliver CO_2 effectively since it was depleted of its CO_2 as a result of CO_2 broken through ahead of the water.

In 2012, Sohrabi et al. [54] carried out three new core displacement tests showing that the carbonation of injected brine could significantly increase oil recovery. Three Clashach sandstone cores were used to accomplish secondary CWI and tertiary CWI using reservoir crude oil with a viscosity of 8.54 cp at a test pressure of 2500 psi and a temperature of 100 °F. Seawater brine with a salinity of 35380 ppm was injected through conventional water flooding followed by injecting carbonated water in tertiary mode with CO_2 with a solubility of 28 cc/cc. The results of these experiments were in agreement with previous CWI coreflood experiments in which the incremental oil recovery in secondary CWI was higher and faster than was the case with tertiary CWI. Here, the reduction in oil viscosity caused by the dissolution of CO_2 in oil meant that a lower differential pressure was needed for the CWI, which implies a better injectivity compared to conventional water injection.

Tavakolian et al. [75], meanwhile, investigated the potential of CO_2 storage during CWI in comparison with conventional CO_2 injection. High CO_2 retention (storage) was

obtained when a large volume of CO_2 was injected during conventional CO_2 injection before breakthrough of the CO_2, at which point the storing efficiency declined sharply leading to increased CO_2 production. During CWI, however, the CO_2 retention remained high with only a gradual decline observed after CO_2 breakthrough. Generally, CO_2 retention in CWI after CO_2 breakthrough was higher than during conventional CO_2 injection.

On the other hand, using a flooding apparatus with four sand packs, Dong et al. (2011) [76, 77] carried out eight CW injection experiments in secondary and tertiary modes using dead crude oil at a test pressure of 600 psig and a temperature of 104 °F, which were conducted in the order of 15 PV/day, 1 PV/day, 4 PV/day, and 2 PV/day. The sand packs were 100% saturated with oil and CW was generated by mixing CO_2 with distilled water at test conditions in order to achieve CO_2 solubility of 100 scf/bbl. Their main results were the reduction of oil recovery at water breakthrough with an increasing injection rate due to unstable displacement. Also, high injection rates over-flooded the sand packs, resulting in low residual oil saturation which would be unrealistic for field applications.

In 2014, Mosavat and Torabi [78, 79] reported the results of incremental oil recovery and CO_2 storage due to secondary and tertiary CWI in sand pack flooding experiments at various test pressures ranging from 100 to 1500 psi and at two temperatures: 77 °F and 104 °F. They found that injecting CW at the lower temperature produced more oil than with the higher temperature due to differences in CO_2 solubility in brine. They also found that the operating pressure played a significant role in enhancing oil recovery in CWI with the oil recovery increasing with increasing pressure because the CO_2 dissolution is directly proportional to pressure and inversely proportional to temperature. While the oil recovery improved significantly for pressures up to 855 psi, only a slight increase was observed at higher pressures, however. Mosavat also reported that the CO_2 broke through at 1 PVI after the water broke through, which indicates that the carbonated brine was free of its CO_2 content. Also, the reduction in the carbonation level resulted in less improvement in oil recovery and less storage of CO_2. Additionally, the CW injection rate was found to have little effect on the ultimate oil recovery and CO_2 storage.

Summarising the above research in table 2-2, therefore, the main factors enhancing oil recovery during CWI were the mass transfer of CO_2 from the CW to the oil phase, which resulted in oil swelling, especially in light oil; while the reduction in oil viscosity was the

main mechanism for improving oil recovery in viscous oil. The level of CO_2 solubility in brine was the main driver in the performance of the CWI process as its influenced parameters such as temperature, pressure and salinity, as well as the volume of CO_2 that could be transferred into the reservoir oil by carbonated water. Initial core wettability affects the oil recovery from CWI since the carbonated water produced additional oil in a mixed-wet core more than in a water-wet core. CWI could also be one of the best methods for storing CO_2 while enhancing oil recovery.

Table 2-2 Summary of CWI in core and sandpack displacement tests using dead oil systems

Previous Studies	Displacement Experiment	Test Conditions	Oil type and core	Main results
Kechut et al. (2011) [80] & Sohrabi et al. (2012) [54]	coreflood	p = 2000 psi and T = 100 °F, (synthetic brine -salinity = 1.0%, CO_2 solubility = 29 scc/cc)	nDecane viscosity = 0.83 cp - outcrop core	DP was almost the same in WF and CWI despite 5 %PV DP was almost the same in WF and CWI despite 5% PV oil recovery during CWI than WF, due to that Decane miscible with CO_2 resulted in continuous CO_2 dissolution
			mineral oil viscosity = 16.5 cp - outcrop core	Additional oil recovery achieved as a result of oil viscosity reduction, however, due to adverse mobility ratio, the improvement of oil recovery during CWI was less in high viscous oil than low viscous oil
		p = 2500 psi and T = 100 °F, (seawater - salinity = 3.5%, CO_2 solubility = 28 scc/cc)	Stock tank oil viscosity = 145 cp - reservoir core	Good performance of CWI in secondary and tertiary modes and more than 50% of injected CO_2 stored in the core
Dong et al. (2011) [76]	Sand-packs	p = 600 psi and T = 104 °F, distilled water (CO_2 solubility = 27 scc/cc)	stock tank oil viscosity = 70 cp	CWI recovers more oil than WF in different injection rates, however high injection rates create unstable sweep leading to unrealistic low Sor
Mosavat and Torabi (2014) [79]	Sand-packs	p = 100 to 500 psi and T = 77 and 100 °F,synthetic brine (salinity = 2.0%, various CO_2 solubility)	light stock tank oil vicosity = 2.76 cp	CWI regains more oil at low temperature and high pressure due to the increase in CO_2 solubility in brine. Increasing oil recovery due to CWI is inversely proportional to carbonation level

Live oil systems

In addition to the mechanism mentioned above which answerable on enhanced oil recovery during CWI in dead oil systems, the formation of a new phase would have a significant contribution in improving the recovery of oil as observed in micromodel tests. For that, four CWI core displacement experiments were performed by Sohrabi et al. [68] to evaluate the impact of the formation of this new gas phase on oil recovery. Dead oil with a viscosity of 8.5 cp, and methane-saturated (live) oil with a viscosity of 1.4 cp, were using in these experiments at test temperature of 100 °F and pressure of 2500 psi. Clashach sandstone cores were utilised to perform secondary and tertiary (post-WF) CWI. The brine was a seawater with a salinity of 35380 ppm and CO_2 solubility of 28 cc/cc. In tertiary CWI using dead oil, the oil recovery was 41 % OOIP after conventional WF, then the incremental oil recovery due to CWI was 61 % OOIP after injecting 8 pore-volume of water and CW. The researchers recorded an increasing trend of differential pressure at the end of the CWI period that was believed to result from the formation of the new phase in the crude oil. The total oil recovery during secondary CWI using dead oil was about the same as that in tertiary CWI. In tertiary CWI using live oil, the oil recovery reached to 43 % OOIP at the end of conventional WF, then increased to 58 % OOIP after tertiary CWI. The total oil recovery after secondary CWI using live oil was almost the same as that in tertiary CWI, where most of the oil was recovered at the time of water breakthrough which was higher than the recovered oil after conventional WF. Worth to notice that I used Sohrabi et al. [68] experimental results to develop the method that helped me in simulating the performance of CWI and its influences on enhancing oil recovery in live oil systems.

Another increasing trend in differential pressure across the core observed in the CWI core displacement experiments performed by Seyyedi et al. [70], although the initial viscosity of the live (methane-saturated) oil was about 14 cp at similar test conditions. On the other hand, in CWI core displacement test performed by Mahzari et al. [73] the differential pressure across the core initially increased with the formation of a new phase. Then, it reduced with oil production during injection of CW core displacement tests in carbonate core and reservoir oil at a pressure of 3100 psi and temperature of 212 °F. The live oil viscosity was less than 1 cp and the dissolved gas formed from C1 to C4. A summary of CWI core displacements experiments in live oil systems and their main results are shown in Table 2-3.

Table 2-3 Summary of CWI in coreflood tests using live oil systems

Previous Studies	Displacement Experiment	Test Conditions	Oil type	Main results
Sohrabi et al. (2015) [68]	coreflood - Sandstone reservoir core	p = 2500 psi and T = 100 °F, (seawater - salinity = 3.5%, CO_2 solubility = 28 scc/cc)	Stock tank (dead) viscosity = 32 cp	Good oil recovery potential as a result of injecting the CW in secondary and tertiary modes, however, the performance of CW is effective in the secondary mode in sooner recover the oil.
			(live oil) Methane-saturated oil vicosity = 1 cp, GOR = 107 cc CH4/cc	More oil recovered while injecting the CW in live oil as the outcome of the evolution of solution gas from the oil due to CO_2 dissolution in it. The pressure increased due to the formation of a new phase and cannot attribute to the release of fine particles in the rock.
Seyyedi et al. (2017) [70]	coreflood - Sandstone outcrop core	p = 2500 psi and T = 100 °F, sea water (salinity = 5.4%, CO_2 solubility = 26 scc/cc)	(Live oil) Methane-saturated oil vicosity = 14 cp, GOR = 51 cc CH4/cc	CWI recovers more oil than WF in the mixed-wet core than that in CWI recovers more oil than WF in the mixed-wet core than that in the water-wet core. In secondary mode, the oil recovery at WF and CW breakthrough were almost identical in WW or MW cases, in which no wettability alteration occurred.
Mahzari et al. (2017) [73]	coreflood - Carbonate reservoir core	p = 3100 psi and T = 212 °F, sea water (salinity = 5.9%, CO_2 solubility = 22 scc/cc)	(Live oil) Saturated oil with maltiple HC gas components, viscosity = 0.9 cp, GOR = 82 cc/cc	Secondary CWI recovered more additional oil than that in tertiary mode due to less oil saturation to dissolve CO_2 in after secondary WF. Similar performance was achieved at different injection rates (5 and 60 cc/hr) which refer stable sweep efficiency. Reducing the CO_2 content in CW would negatively impact the overall performance.

2.3.3 Slim-tube Experiments

Additionally, two slim-tube experiments were performed by Seyyedi et al. [69] to investigate the performance of CW in a long homogeneous porous medium, representing the steady and uniform flow that allows continuous dynamic interactions to take place

between CW and oil. The slim-tube apparatus was 60 ft long, containing 80-140 mesh Ottawa sand, which created a porosity of 30% and a permeability of 6 darcy. Initially, the slim-tube was 100% saturated with live oil at the same test conditions as the direct pore-scale experiments. Conventional water was injected in the first experiment to establish the base comparison with the second slim-tube experiment where the CW was injected in secondary mode. 24% more was recovered during CWI than during conventional WI. The water broke through later during CWI than in plain WI, but 0.3 PVI earlier than the CO_2, indicating the depletion of its CO_2 content. Up to 1.5 PVI, the production of CO_2 was almost negligible but it then started to increase, even though the produced GWR (referred of CO_2 solubility in brine) was less than the initially injected GWR of 26 cc/cc, indicating the continuous mass transfer of CO_2 from CW to oil, subsequently more growth of formed gas phase. The viscosity of the oil reduced by about 61% from 14 cp to 5.4 cp. Since significantly more oil was recovered in CWI equivalent to less residual oil saturation and more new gas saturation making the ultimate hydrocarbon saturation equals to residual oil saturation in WI.

2.3.4 Role of CW on Wettability Alteration

In order to evaluate the impact of initial rock wettability on oil recovery during CWI, Seyyedi et al. [70] performed two sets of core displacement experiments using un-aged outcrop Berea sandstone cores, representing a water-wet state, and aged outcrop Berea sandstone cores, representing a mixed-wet state. The oil was methane-saturated oil and the brine was seawater brine. The experiments were carried out in secondary mode at the same conditions in micromodel and slim-tube experiments. In the un-aged (water-wet) system, the incremental oil recovery after secondary CWI was 6 % higher than that after secondary WF in the same system, while in the aged (mixed-wet) system, the incremental oil recovery after secondary CWI reached 11 % more than that after secondary WF in the same system. The oil recovery at the time of water breakthrough in the mixed-wet CWI was 10 % higher than the oil recovery at water breakthrough in conventional WF, which related to the alteration of the wettability towards a more water-wet state. Unlike the slim tube tests, breakthrough of CO_2 occurred earlier than the brine in CWI, indicating the effect of dispersion as a result of local velocity and heterogeneity of the core where the permeability of those cores was about 150 md and a tracer test of the core proved of its heterogeneity [81].

Several researchers have investigated what effect the interactions between CO_2, oil, brine, and rock have on the wettability, and thence on the oil recovery. Altering the wettability might affect electrical properties of porous media [82], capillary pressure [83, 84], relative permeability [84, 85], and flooding performance [86, 87]. In 1990, Grape et al. [88] carried out imbibition tests including carbonated water. The results of their laboratory experiments proved that the imbibition rate and oil recovery improved when the imbibed water contained CO_2. They explained this as being caused by a shift in the wettability towards water-wet state since the acidic nature of the CO_2-saturated water reduced the interfacial tension (IFT) thereby also reducing both the effect of capillary forces and the contact angle. They also mentioned other significant factors behind this improvement as being matrix dissolution and clay mineral clean-up, since they used sandstone and limestone rock in their experiments.

In 2008, Yang et al. [89] measured the dynamic and equilibrium contact angles between the crude oil and the reservoir rock in the presence of CO_2-enriched brine at various high pressures and constant temperatures. They developed an experimental method to measure the contact angle of the brine-CO_2 saturated brine-reservoir rock system using the axisymmetric drop shape analysis (ADSA) technique for the sessile drop case [89]. They measured an almost constant dynamic contact angle between crude oil and rock in the occurrence of carbonated brine at a given pressure and temperature, even with the gradual dissolution of CO_2 into the oil until it became saturated with CO_2. They also found an increasing equilibrium contact angle with increasing pressure, whereas it decreased with increasing temperature. They measured a low equilibrium contact angle in a crude oil-reservoir brine-reservoir rock system with CO_2 dissolution in comparison with the other system without CO_2 dissolution. A low contact angle between CO_2-saturated oil and reservoir rock could be an indication of a change in the wettability towards a more water-wet state.

Another observation of changing wettability in the presence of carbonated water was explained by Riazi et al. [90] and Sohrabi et al. [54] when comparing two magnified sections of pore-scale images after secondary conventional water and carbonated water injection in a viscous mineral oil system. By observing the shape of the fluid interface, they found the oil phase snapped off as the water films around the oil blob thickened after injecting plain water, whereas the oil-water interface showed a more rounded shape after CWI. They claimed that since the interfacial tension between oil and water decreased in

the presence of CO_2, this most likely affected the balance of capillary forces, thus shifting the wettability to a more water-wet state. In the same research group, in 2015 Seyyedi et al. [91] published the results of their series of experiments on contact angle measurements to evaluate the change of wettability during CWI using three un-aged (water-wet) and aged (mixed-wet) substrates of quartz, representing the main mineral in sandstone, mica representing the shale and clay materials, and calcite, representing the main mineral in carbonate rock. The experiments were performed at various pressure ranges from 100 psi to 3500 psi and a constant temperature of 100 °F using a high pressure-temperature drop shape analyser. Their results were consistent with other researchers who showed that the equilibrium contact angles between oil-brine and three substrates dropped in the presence of CO_2, which changed the wettability from water-wet to more water-wet in the case of un-aged substrates and from mixed-wet to water wet in case of aged substrates. In order to confirm their findings, Seyyedi et al. [92] performed a series of spontaneous imbibition experiments in carbonate and sandstone rock to evaluate the potential of carbonated water in increasing the imbibition rate and enhancing oil recovery. The experiments were carried out in un-aged (water-wet) and aged (mixed-wet) carbonate and sandstone, using crude oil at a pressure of 2500 psi and a room temperature of 68 °F. The results of their experiments showed an acceleration in imbibition rate and an improvement in oil recovery after introducing the CW in tertiary mode, where the enhancement in those parameters was more pronounced in the aged (mixed wet) core. This confirmed that changes to wettability from mixed wet to water-wet would be more effective than from water wet to more water-wet.

Overall, the results of these previous experiments summarise that CWI recovers more oil than the conventional water injection and has better performance in secondary mode (pre-WF) than in tertiary mode (post-WF). Furthermore, an additional mechanism contributing to enhanced oil recovery during CWI was observed in live oil where the transfer of CO_2 into the oil expelled the light hydrocarbon components of the oil, which then formed a new gas phase creating apparent oil swelling, and thereby improving oil recovery. Wettability alterations could also contribute to enhancing oil recovery by shifting the core towards more water-wet forms, affecting the capillary pressure and relative permeability and, again, the oil recovery rates.

2.4 Theoretical and Numerical Modelling of CWI Process

Despite the active laboratory research on CWI in recent years, only limited attempts have been made to model the performance of CWI in comparison to the large number of available modelling studies on CO_2 EOR.

2.4.1 Frontal Advance Theory for CWI

De Nevers in 1964 [93] was the first to develop a calculation method for CWI based on a frontal advance theory, Buckley-Leverett Theory, 1942 [94] and Welge's method, 1961 [95], for one dimensional linear flow. His calculation method presented the effects on oil recovery of both the size of the slug of CW and the CO_2 to water ratio. Two mechanisms were proposed to increase the oil recovery. Firstly, that the mass of CO_2 transferred from the CW into the oil reduced oil viscosity and increased oil mobility. Secondly, the oil swelling followed by a shrinking effect as the residual oil, stripped of CO_2, led to lower residual oil saturation.

In his calculation, the partial pressure of CO_2 in water is the same as it is in oil at any given point in the formation, which leads to instantaneous equilibrium. In addition, the viscosity and density of carbonated water and CO_2-oil mixture are a function of the concentration of CO_2 in each phase at reservoir temperature, while the solubility of CO_2 in each phase is a function of the CO_2 pressure at reservoir temperature.

He described the method by comparing the results of CW with that of plain water injection. Figure 2-8 demonstrates the cumulative oil and CO_2 production, water saturation and CO_2 concentration in the reservoir for CW in comparison with plain WI. From this graph, it can be seen that, in a plain water injection (A to F in figure 2-8B), the water saturation jumps from its initial level (S_{wi}) to the breakthrough value (point A), then gradually increases so that the cumulative oil production is high and the water oil ratio (WOR) is zero until breakthrough. The oil rate then declines as the WOR progressively increases, as illustrated in figure 2-8C (A to F).

Figure 2-8A, meanwhile, shows that the carbonated water is advanced (G to E), with a leading edge (E to C). In figure 2-8B, at region (G to E), where the CO_2 concentration is high, the water saturation is higher than it would have been in the plain water flood due

to the increase in the density and viscosity of carbonated water, and the additional oil recovered from this region would advance and accumulate in the region (C to B) to form a constant water saturation (or oil bank). The recovered oil in this region, therefore, has no CO_2 as it is driven ahead of the carbonated water. Looking at figure 2-8D, from O to B, the carbonated water injection produces the same oil production as the plain water flood. Then, at time B, the oil bank reaches the producer and the WOR remains constant until time C. The leading edge of carbonated water arrives at the production well and the extra oil produces at the same time as WOR starts to increase again, although CO_2 would be produced first in the producing well, as illustrated in figure 2-8C. As the leading part of the carbonated zone is produced (C to E), the rate of CO_2 production and the WOR increase. Then, the region of high CO_2 concentration reaches the producing well at point E, at which point the oil production rate drops to zero (E to G) and the CO_2 production rate remains high [93].

With this calculation method, the CO_2 content of the injected carbonated water would be depleted so that it moves forward as plain water. De Nevers concluded that the oil viscosity reduction was the predominant mechanism to improve oil recovery, although oil swelling also plays some role.

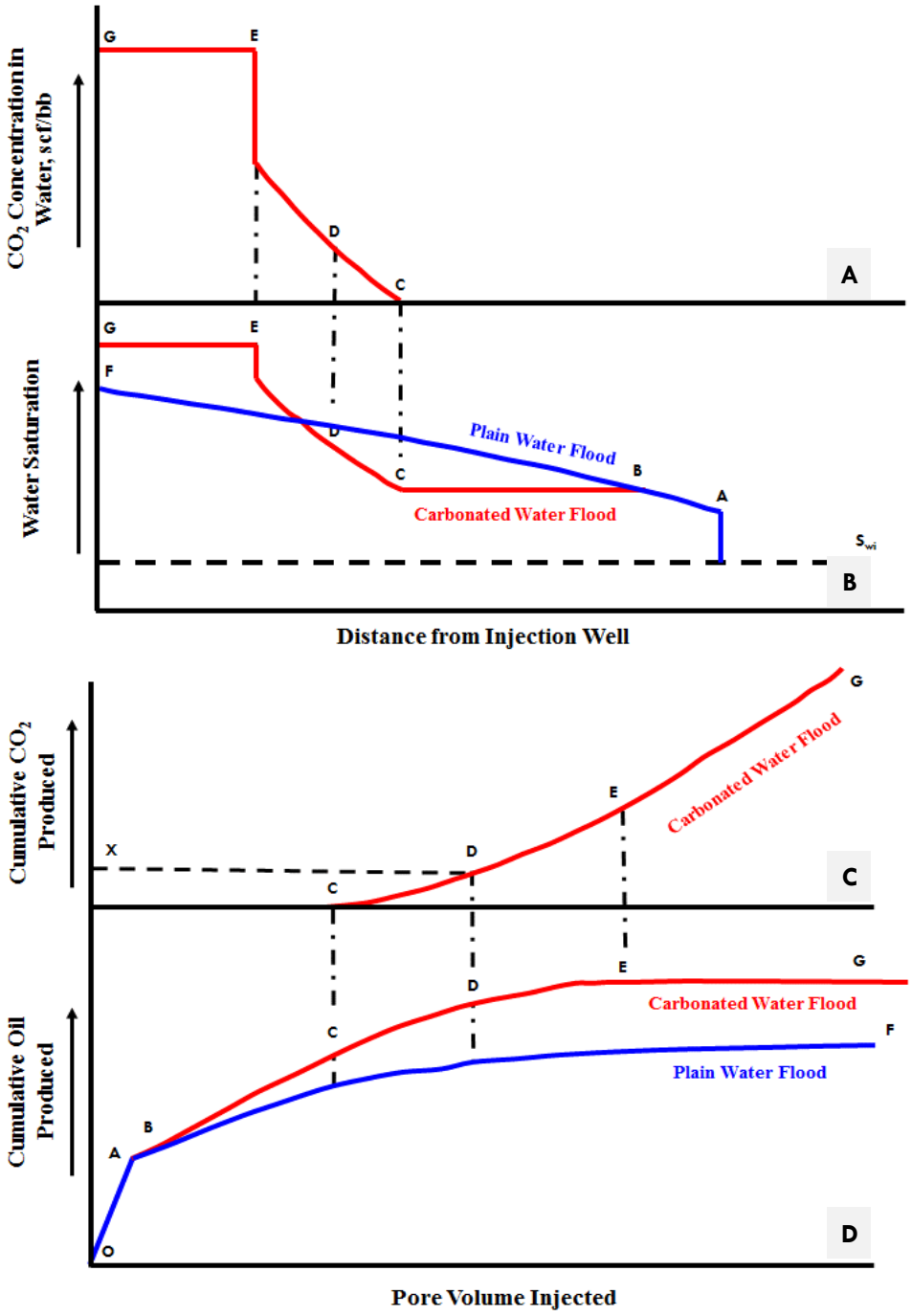

Figure 2-8 comparison of typical carbonated water injection with plain WF as proposed by de Nevers in [93] (A) the CO_2 concentration in water and its frontal advance, (B) water saturation as the water moves from injection well (C), and, (D), cumulative CO_2 and oil production as pore volume injected, respectively

2.4.2 Numerical Modelling of CWI

About ten years later, Ramesh and Dixon [96] developed a two-dimensional time-dependent three-phase flow mathematical model to predict the performance of CO_2 injection and CWI in heterogeneous reservoirs. They extended the black oil model formulation to include the solubility of CO_2 in water. In their study, they assumed that

the distribution of CO_2 between oil and water is proportional to the relative abilities of these phases to dissolve CO_2 at saturation point based on simultaneous saturation of CO_2 in the oil and water phases. CO_2 solubility in each saturated phase is only a function of pressure, and instantaneous equilibrium occurs between the oil and water phases containing CO_2. They assumed that the existence of the oil phase would not have an impact on the CO_2 solubility in water and vice versa. Consequently, they used different solubility data for CO_2-oil and CO_2-water systems for a three phase (oil-CO_2-water) system. The development of free hydrocarbon gas in the reservoir was not allowed.

Shenawi and Wu [97] developed a three-dimensional, three-phase and dual porosity compositional numerical simulator to describe the performance of CWI in enhancing oil recovery during an imbibition experiment conducted on chalk cores at high pressures and temperatures. They neglected the diffusional mass transfer between the matrix and fracture, and also the gravity effect on the matrix/fracture fluid exchange transfer function. The equilibrium of CO_2 between CW and oil was again achieved instantaneously within each gridblock and no free gas was allowed in the system. Partitioning of CO_2 from carbonated water into oil was mainly based upon the solubility of CO_2 in the oil phase. Also, the wettability was altered upon the interaction between CW and the matrix, causing a reduction in the oil saturation and a variation in the relative permeability and capillary pressure, taking into consideration a constant interfacial tension between CW and oil. The results of this simulation indicated the enhancement of the water imbibition rate and oil recovery during CWI due to wettability alterations, consequently changing the water-oil relative permeability and capillary pressure. On the other hand, the effects of the reduction in oil viscosity and changes in oil density were minimal.

In 2011, Riazi et al. [51] constructed a mathematical model to simulate the dynamic process of oil swelling at a pore-scale level as a result of CO_2 partitioning between the contacted CW to oil ganglion. Their model took into account the oil drop swelling in two cases: where the CO_2 indirectly transferred into oil through a water shield, and where there was direct contact between the oil and the CO_2 source (CW). They assumed that the diffusion of CO_2 in oil and water were constant, and that oil, water, CO_2 and CW were at equilibrium conditions at the interface. They concluded that the molar density of CO_2, and its solubility in oil, were the main factors influencing the percentage of oil ganglion swelling during CWI.

More recently, Kechut et al. [67, 74, 80] used the results of core flooding experiments of CWI in dead oil to assess the capabilities and limitations of a commercial reservoir simulator for modelling the CWI process. Secondary conventional water injection followed by tertiary CWI and secondary CWI were simulated using the ECLIPSE (E300) commercial reservoir simulator. The EOS used was tuned based on advanced PVT experiments where the CO_2 swelling test was conducted in reservoir oil. Then, the reservoir oil was flashed to obtain stock tank oil at standard conditions, and this was used to generate the dead oil at coreflood conditions. Noticeably, the tuned EOS was suitable for CO_2 injection where the maximum swelling was achieved with injected CO_2 rather than that soluble in CW. The simulation results showed an over-estimation of oil recovery in comparison with the experimental data on CWI.

It is evident, therefore, that the currently available compositional simulators have been developed based on assumptions of instantaneous equilibrium and complete mixing which would be unlikely in CWI in practice, given that the continuous mass transfer of CO_2 from carbonated water to oil plays a major role in creating non-equilibrium conditions. That is, in practice, the resistance of CO_2 transfer at the interface between water and oil phases prevents immediate partitioning of CO_2 between the phases. In the author's preliminary analyses, however, it was observed that, in live oil systems, the predominant mechanism (new phase formation) would start immediately, which implies minimal impact of time on the formation of the new phase [68]. This therefore showed that in order to form a new (gas) phase, the CO_2 mass transfer from CW to oil should be fast to allow the oil to reach its saturation limit, and that, subsequently, CO_2 strips the light hydrocarbon components to form a gas phase.

2.5 Conclusion

In the previous CWI modelling experiences, the developing of the method relied on considering one of CWI mechanisms to be the predominant mechanism and neglecting the other as in chosen the oil viscosity reduction only [93] or in selecting the oil swelling effect only [51] or wettability alteration only [97]. Although the micromodel observations showed the importance of all CWI mechanisms on enhancing oil recovery, however, they differentiate in effectiveness based upon the oil viscosity, dissolved gas content, and rock wettability. On the other hand, The other researchers who developed numerical models of CWI performance assumed no mutual interaction between CO_2 solubility in brine and

CO_2 dissolution in the oil. Therefore, those mathematical and numerical models lacked in proper capturing the mechanisms, and subsequently, the multiple physics associated with injecting CW. The observed physics in the direct pore-scale tests were used to quantify the saturation of the formed gas phase and then connecting the behaviour of the three-phase flow regime to increase oil swelling through trapping of the new phase. In addition to that, the existence of CO_2-oil mixture interacted with CO_2 solubility in brine in which the equation of state was tuned based on brine-CO_2-oil interaction not as CO_2-oil interaction only as in conventional CO_2 injection. Also, through this procedure, the mechanisms of CWI were numerically incorporated as following:

- The oil viscosity would be reduced by viscosity model connected with EOS that reproduces the CO_2 dissolution into the oil.

- The formation of a new phase that creates apparent oil swelling would be modelled through the tuned EOS and critical gas saturation in oil-gas relative permeability

- The three-phase flow regime is also reduplicated through selecting the right 3-phase oil relative permeability function and adjusting the oil-gas relative permeability curves.

In this work, a new methodology has been developed to numerically simulate coreflood experiments in which carbonated water was injected in tertiary and secondary modes to displace live oil. Firstly, an approach was put forward to estimate the profile of the average gas saturation in the core and this profile was used to tune EOS for reproducing the phase behaviour. After that, the oil-water and gas-oil relative permeabilities were adjusted to history-match the coreflood experimental data. The results would demonstrate that the proposed methodology is capable of capturing the complex processes taking place during CWI.

Chapter 3- Numerical Simulation of CWI in Water-Wet Core

3.1 Introduction

For any recovery method, the main purpose of a reservoir simulation model is its ability to simulate the different mechanisms involved in oil production and subsequent fluid flow in porous media. This ability is crucial to evaluating the effects on recovery of different operational conditions and to compare the economics of different recovery methods. Appropriate modelling of the CWI process is therefore vital for assessing its feasibility and design, and for forecasting its performance under various operational conditions and scales.

The injection of carbonated water into an oil reservoir involves a number of complex physical and chemical phenomena. Continuous interphase transfer of CO_2 from injected carbonated water to oil due to the contact between the oil and the carbonated water stream will lead to fluid-fluid interactions that can bring about compositional changes in the oil so as to form another phase (i.e. a gas phase), which then creates a three-phase flow regime. This means that it is necessary to understand the fluid/fluid interactions and phase equilibria that take place in complex processes such as carbonated water injection in order to evaluate how the distribution of CO_2 amongst the three phases may affect fluid flow in porous media. Although the complex phase behaviour involved in the dissolution of CO_2 and crude oil has been investigated extensively, there is a fundamental difference between plain CO_2 injection and carbonated water injection which necessitates special modelling approach for CWI: whereas a two-way condensing-vaporising mass transfer occurs in plain CO_2 injection, only a one-way CO_2 dissolution takes place in the oil phase in CWI. Given this complexity, involving multiple physical processes, concerns have been raised about the ability of current commercial simulators to model those processes in such a way as to both capture and explain scientifically the observed behaviour.

The accurate modelling of CWI requires a proper methodology to capture the complicated physics in this process. This chapter takes a comprehensive and systematic simulation approach to provide historical models to verify actual core-flood experiments that have studied the performance of carbonated water injection in a live oil system. A new methodology has been developed to simulate numerically core-flood experiments in

which carbonated water has been injected in tertiary and secondary modes. Firstly, an approach is put forward to estimate the profile of the average gas saturation in the core, and this profile has been used to tune a cubic equation of state (EOS) so as to reproduce the phase behaviour. After that, the oil-water and gas-oil relative permeabilities were adjusted to history-match the core-flood experimental data. The results demonstrate that the complex processes taking place during CWI can be captured through the proposed methodology.

3.2 Methodology

The building block of this method of simulating the performance of CWI is the calculation of the saturation of the new gas-like phase from a tertiary CWI core displacement test. This has been observed from the direct pore-scale (micromodel) visualisation experiments to be one of the mechanisms through which enhanced oil recovery is achieved during CWI, along with the oil swelling effect and oil viscosity reduction. Then, the Peng-Robinson cubic equation of state (PR-EOS78) is tuned in order to produce the constructed gas phase saturation through an assisted history matching algorithm by modifying the interaction coefficient of CO_2 to other hydrocarbon components. This enables the modelling of the fluid-fluid interaction and compositional changes that take place as a result of CO_2 transfer from aqueous phase to oil. After that, based on the physics observed in direct pore-scale visualisation experiments, a proper three phase relative permeability function is selected to capture the overall behaviour of oil/gas/water flow in the areas where the three phases co-exist. Finally, using an integrated automatic-history matching algorithm, the proposed method is implemented to couple the thermodynamic processes with the associated physical phenomena during CWI in numerical terms.

3.3 Direct Pore-Scale Visualisation Experiments

In a series of micromodel visualisation experiments at a pressure of 2500 psi and temperature of 100 °F, Sohrabi et al. [68] discovered the formation of bubbles and then the accumulation of a new gaseous phase during continuous CWI using 28.5° API reservoir oil . The formation of this gas-like phase has been discovered in both dead and live (oil with dissolved gas) systems through different durations of carbonated water

injection but has not been observed when using mineral (nDecane) oil. The results of the micromodel observations show that, while the formation of the gas-like phase during CWI was not a deterministic pore-scale phenomena in dead oil systems due to its late occurrence, it plays a crucial role during injection of carbonated water in live (oil with dissolved gas) systems, which represent a more realistic system in practice.

Figure 3-1 shows magnified sections of a micromodel visualisation experiment at different stages of a tertiary CWI test in a live (methane-saturated) oil system. Details of the experimental information and procedure can be found in [68]. In summary, however, the experiment was used to explain the method of estimating the formation of the third phase while injecting tertiary CWI in core displacement tests so as to observe physical mechanisms that could be correlated later on to suitable numerical simulation modelling. In this visualisation test, after water flooding, the trapped oil phase can be seen in the form of patches of scattered oil ganglia in the porous medium (figure 3-1B). After the breakthrough of water and after the point at which no more oil displacement or production was observed, carbonated water was injected into the micromodel for a period of 24 hours. Significant oil swelling was observed during CWI due to dissolution of CO_2 into the oil phase and, at the same time, the oil's colour changed to a brightener brown [68]. Figure 3-1C shows a magnified section of the micromodel after 24 minutes of CWI, when a number of scattered bubbles of the new phase (indicated by red arrows) appeared and increased inside the crude oil. An analogy might be drawn between the formation of gas bubbles during CWI and in-situ gas liberation during a depressurisation process (i.e. pressure blow down) where the pressure is reduced below the saturation pressure. The nucleation and growth of the new phase is fast and takes place simultaneously with oil swelling mechanisms, which explains the rapid increase in total oil enlargement during CWI in live oil systems, as observed in figure 3-2.

Furthermore, figure 3-1D shows another magnified section of the same snapshot of the micromodel visualisation where the scattered bubbles of the new phase have grown in size as more CO_2 is transferred from the aqueous phase to the crude oil. This growth of the bubbles in the new phase enables the oil blobs to reconnect with each other, as in the area highlighted by a red circle in figure 3.1E, while also serving to restrict the water path and increase the resistance of water to flow, all of which influences the relative permeability of the three-phase water. Oil remobilisation and recovery as a result of the preceding nucleation and growth of the new phase and process of reconnection described

above, occurred at later point in the CWI and can be clearly observed in the area highlighted by blue rectangles in figure 3-1F. The new phase bubbles that are located nearby each other combine together to form a larger growth of the new phase that can be mobile at a certain saturation, as observed in figure 3-1F.

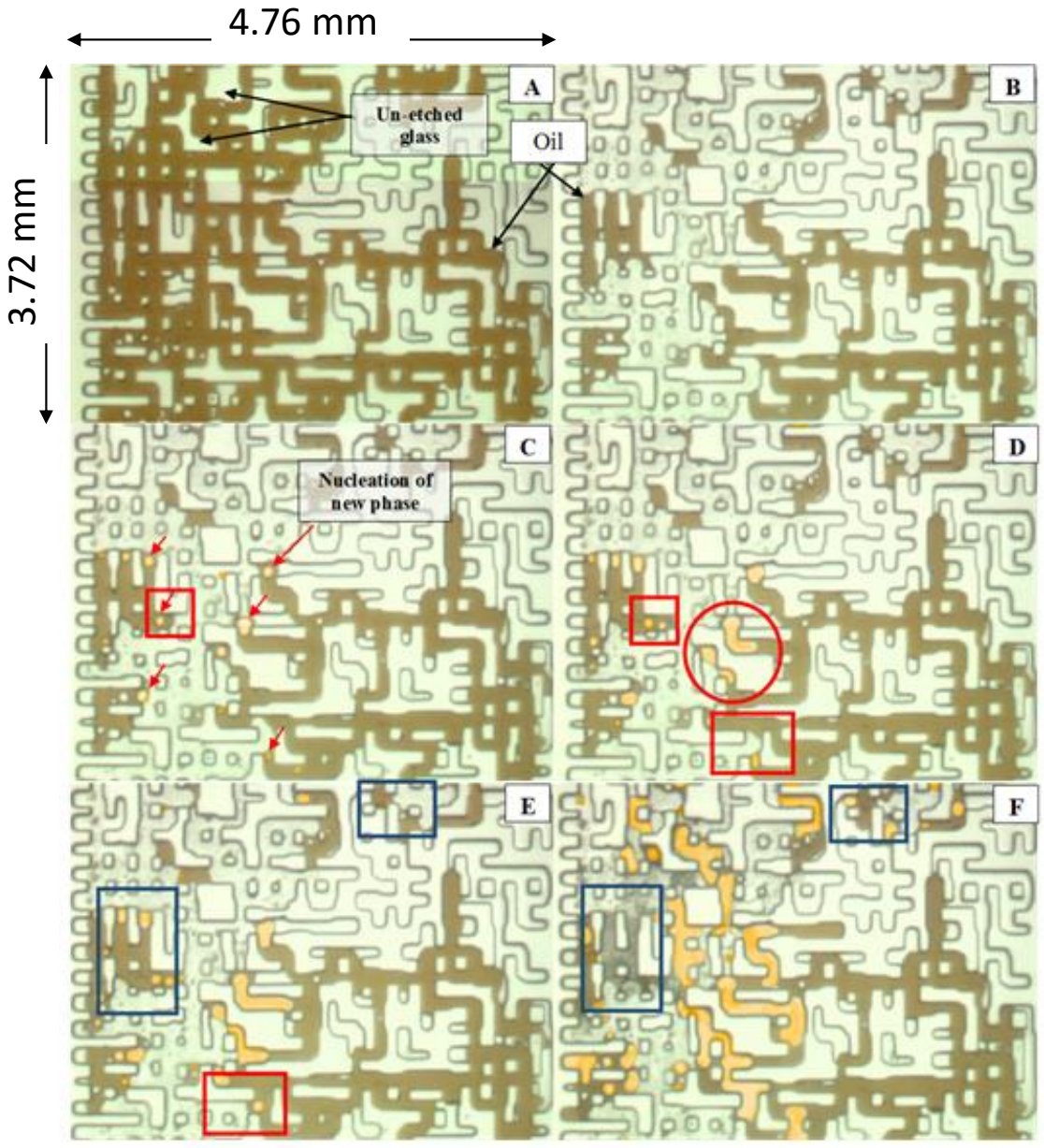

Figure 3-1 a magnified section of the micromodel visualisation experiment of tertiary CWI in live oil system (A) after establishment of initial oil saturation at Swi (B) at the end of water flooding (C) after 24 minutes of CWI (scattered new phase bubbles are formed) (D) after 1 hour of CWI (increase in the size and numbers of new phase bubbles) (E) after 2 hours of CWI (where the reconnection of oil blobs) (F) at the end of CWI after 1 day of injection [68]

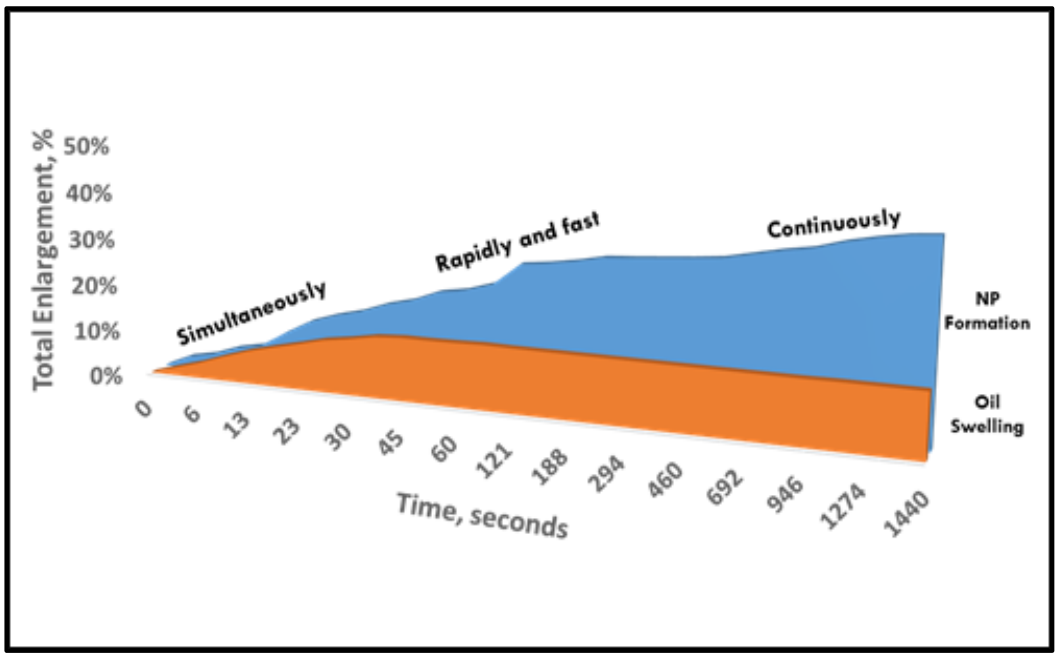

Figure 3-2 enlargement of the oil phase as a result of oil swelling and formation of the new phase during CWI in a live (methane-saturated) oil sample [68]

Based on these micromodel observations, the mechanism through which this new phase is formed during carbonated water injection is related to the "one way" nature of the transfer of CO_2 from CW to oil when the CW comes into contact with the oil in a reservoir. Multi-component competitions between CO_2 and the dissolved light hydrocarbon components of oil (methane) result initially in the liberation of a gaseous phase composed of methane, which becomes heavier later due to the ability of CO_2 to strip out more of the intermediate hydrocarbon components. This new phase subsequently expands and contributes significantly to oil recovery. Nucleation and growth of a new phase within the oil was first observed in micromodel tests when CW was injected for an extended period of time in a dead oil system [74]. After performing the experiments in live-oil (methane-saturated oil) systems, the new gaseous phase was found to form predominantly within the oil and to grow more rapidly, serving to increase the oil volume beyond the normal oil swelling mechanism that takes place during CO_2 dissolution into oil. Consequently, the formation of the third phase could be considered to be the dominant mechanism involved in improving the performance of CWI.

To all intents and purposes, the mechanisms through which the new phase is formed during CWI will influence many processes that need to be considered when simulating CWI. The appearance of the gaseous phase, and its accumulation in volume within the resident oil would cause apparent oil swelling that will be more pronounced than the well-

known oil swelling effect. Also, the rapid growth in the saturation of the new phase would keep the total hydrocarbon (liquid and vapour) saturation constant until the new phase becomes mobile and can be displaced. Utilising these findings, I can calculate the saturation of the new phase during CWI in tertiary recovery mode. This is the foundation of my method for calculating the saturation of the new phase in the absence of other in-situ saturation measurements during the experiment. By those mechanisms, the mobility of the new gaseous phase towards other phases can be considered when simulating the process of CWI through critical saturation of that phase and its influences in relative permeability and three-phase flow regime.

3.4 Coreflood Experiments

This section provides a brief description of the three coreflood experiments that were performed by Sohrabi et al. [68] to corroborate the observations made in the direct pore-scale experiments and to evaluate the performance of CWI. In order to allow a valid comparison between the pore-scale and coreflood experiments, the same experimental conditions and fluids were used. Experiment No. 1 is a sequential fluid displacement test starting with secondary conventional water flooding followed by tertiary carbonated water injection, whereas experiment No. 2 involves secondary carbonated water. Experiment No. 3 is a sequential fluid displacement test, but this time starting with secondary carbonated water followed by tertiary continuous CO_2 injection, as illustrated in figure 3-3.

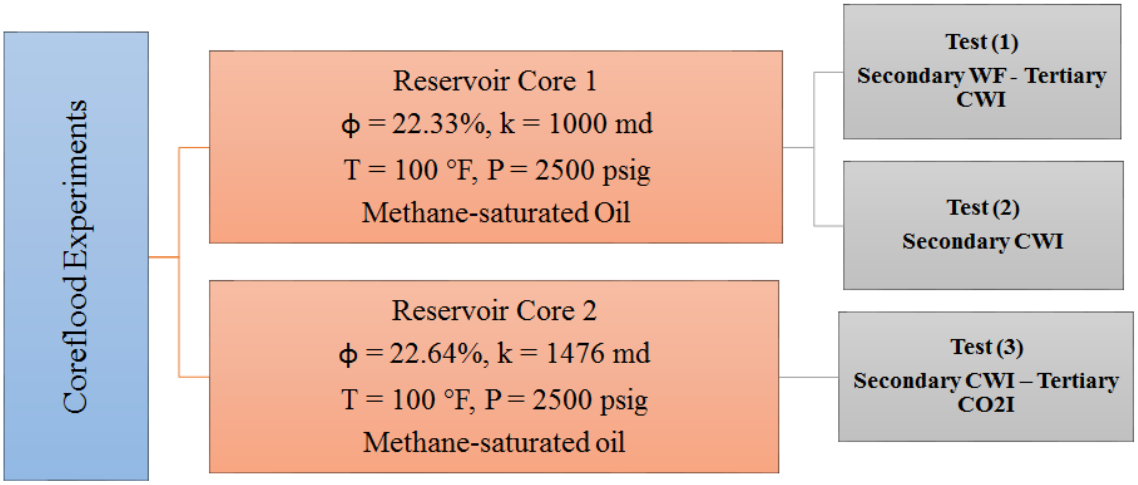

Figure 3-3 List of coreflood experiments [68]

3.4.1 Fluid samples

A stock tank crude oil B with composition as presented in figure 3-4 was recombined with methane with a gas-oil ratio of 107 ccGas/ccOil (~ 599 scf/stb) at test conditions of 2500 psi and 100 °F in order to generate a fully saturated live oil sample. The stock tank oil sample is a medium crude oil with API gravity 28.5° and its viscosity at the test temperature of 100 °F is 31.50 cp. Other measured oil properties are shown in table 3-1.

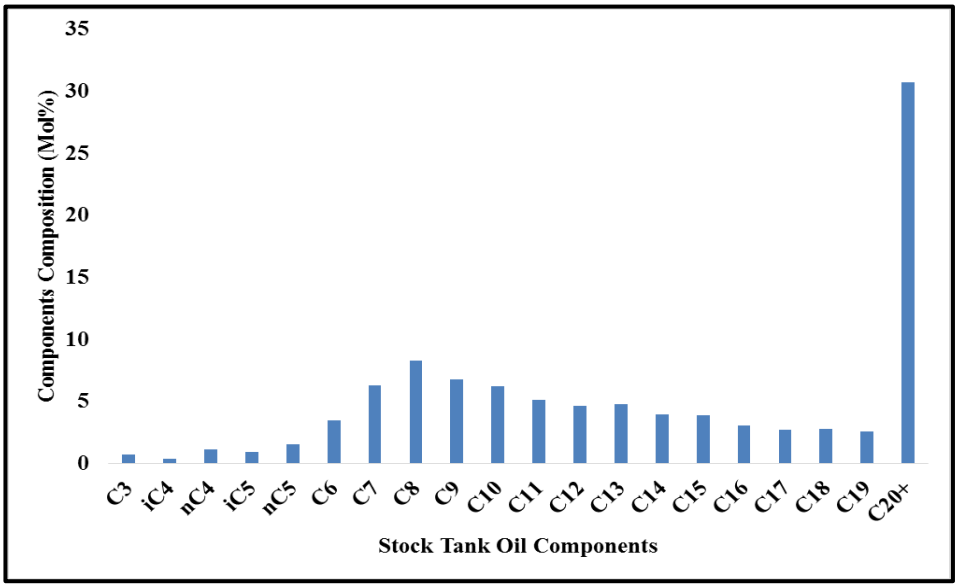

Figure 3-4 the extended composition of stock tank oil crude B had been provided by Sohrabi et al. [68]

Table 3-1 measured basic fluid properties of fully methane-saturated reservoir oil B [68]

Methane-saturated oil saturation pressure at 100 °F	2500 psi
Gas-oil ratio (Rs)	599 SCF/STB
Stock tank API gravity	28.5°
Stock tank oil viscosity at 100 °F	31.50 cp
Live oil viscosity	1.417
Formation Volume Factor	1.240

The water used in the experiments is a high salinity brine (seawater) where its salinity of 35380 ppm represents typical injection brine in familiar waterflood experiments. The ionic contents of the brine are given in table 3.2. To make up the carbonated brine, the seawater brine was mixed with CO_2 in a rocking cell at the required carbonation pressure of 2500 psi and temperature of 100 °F. The mixture was shacked to expedite the CO_2 dissolution in brine until the pressure stabilised, which was taken as an indication that the mixture had reached its equilibrium. The CO_2 content of carbonated water at the test conditions is 28.7 ccCO_2/ccBrine (161 scf/bb).

Table 3-2 Ionic content of the synthetic seawater [68]

Ion	Concentration, ppm
Na^{+}	11700
Ca^{++}	1170
Mg^{++}	326
K^{+}	123
Sr^{++}	31
Cl^{-}	18200
$SO4^{-}$	3180

3.4.2 Core samples

Two Clashach sandstone cores were used in the coreflood tests, which were made to be mixed-wet by ageing them in a crude oil. The ageing procedure followed has been widely applied and shown to be reputable through numerous coreflood tests over years of laboratory experience in our lab. The procedure initially brings about favourably water-wet wettability before becoming mixed wet. Since the same ageing procedure was implemented for the cores used in these experiments, it is hereafter supposed that the aged cores became mixed wet following the ageing process.

The dimensions and other rock properties of these cores are given in table 3-3. The porosities of the cores were determined using a helium porosity test, then confirmed through the calculation of the ratio of the pore volume and the bulk volume, where the pore volume of the core was taken to be the total volume of brine saturating the core. The permeability of the core was measured at test pressure of 2500 psi and temperature of 100 °F using the brine.

Table 3-3 Physical and rock properties of the cores used in the experiments [68]

Experiments	Length (cm)	Diameter (cm)	Porosity (%)	Permeability (md)	PV (cc)
Tests 1 and 2	32	5.012	22.33	1000	141
Test No. 3	32	5.064	22.64	1476	146

3.4.3 Experimental procedure and results

3.4.3.1 Tertiary CWI (Test No. 1)

The experiment started with an imbibition process where the live oil (oil saturated with methane) was displaced with methane-saturated brine, in which the initial water saturation (Swi) was achieved at 21% pore volume (PV). In order to minimise any methane mass transfer from the resident oil to the injected brine during the conventional waterflooding period, since all the displacement experiments are performed with live oil (methane-saturated oil), the brine was pre-equilibrated with methane before conducting the waterflooding. The injection was stopped after 1.73 PV of total injections, when no more oil was being produced. The water breakthrough happened after 0.319 PV of water injection, which brought about an oil recovery of 39.6 % of OOIP. About 45.1% of OOIP was recovered during secondary conventional water flooding.

Then, carbonated water that contained 28.7 scc of CO_2 per cc of brine was injected in order to quantify the performance of carbonated water injection in improving oil recovery in tertiary (post-WF) mode. Almost an additional 15 % of OOIP was recovered after injecting 8 PV of carbonated water. Figure 3-5 presents the recovery of the oil and the differential pressure measured across the core during the secondary waterflood and tertiary CWI in test no. 1. The differential pressure dropped after water breakthrough, then it remained flat at the end of the waterflooding period where there was no further oil production and only water was flowing in the core. Shortly after the start of CWI, the differential pressure across the core increased from around 0.7 psi to nearly 2.0 psi, while the oil production started at a low rate after 0.3 PV of injected CW. After that, the rate of oil production increased significantly, recovering additional oil. The increase in the differential pressure across the core during CWI could be attributed to the formation of the new gaseous phase, as observed in the pore-scale visualisation experiment.

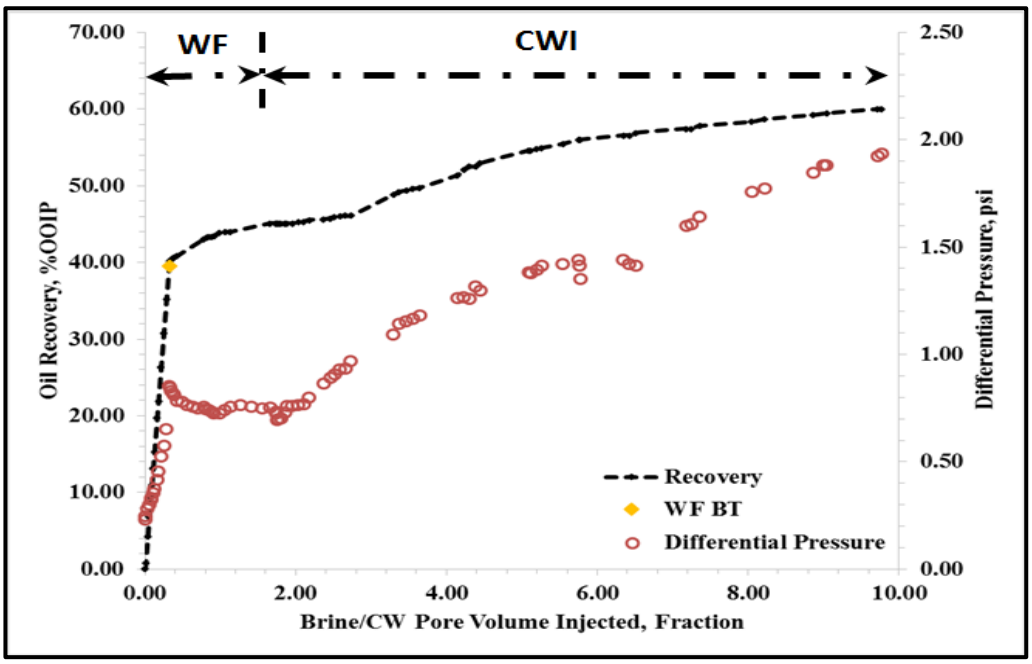

Figure 3-5 Oil recovery and differential pressure across the core during secondary WF and tertiary CWI in test no. 1 [68]

3.4.3.2 Secondary CWI (Test No. 2)

For the sake of comparison, all test parameters, such as injection rate, test pressure and temperature, and fluid samples were kept the same as in the previous tertiary CWI experiment. After achieving the initial water saturation of 21% PV, the carbonated water containing 27.8 cc of CO_2 per cc of brine, was injected. Figure 3-6 shows the experimental results of oil recovery and differential pressure across the core during secondary CWI in test no. 2. The injection of CW continued until a total of approximately eight pore volumes have been injected. Initially, differential pressure across the core steadily increased due to displacement of oil by injected brine, as is typically seen in conventional water flooding. Afterwards, water breakthrough occurred after 0.39 PV of carbonated water injection, which resulted in oil recovery of 48 % of OOIP. After water breakthrough, a gradual increase of both oil recovery and differential pressure was observed, which is not in line with what is generally seen in typical conventional waterflooding, where the differential pressure trends downwards as the rate of oil production decreases. The oil recovery reached approximately 64 % of OOIP which was higher by almost 19 % of OOIP compared to the recovery arising from the conventional waterflooding in the previous test.

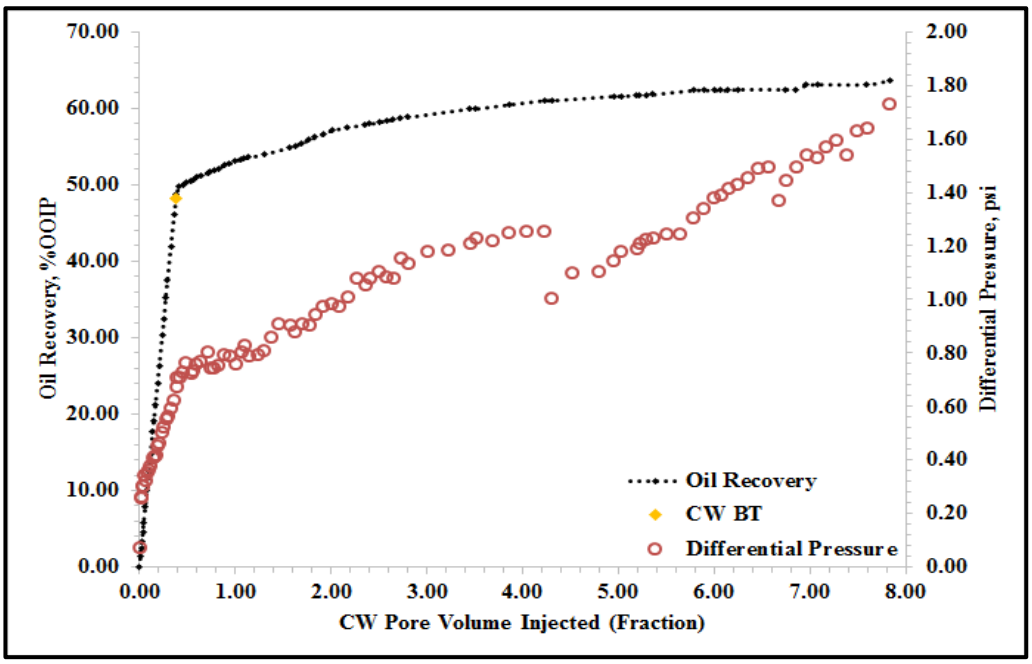

Figure 3-6 Oil recovery and differential pressure across the core during secondary CWI in test no. 2 [68]

3.4.3.3 Secondary CWI Followed by CO_2 Injection (Test No. 3)

As with the previous core displacement tests, all the operational parameters were maintained except that the core used had about 48% higher absolute brine permeability. The objective of test no. 3 was to investigate performance of tertiary CO_2 injection in a live oil system after secondary carbonated water injection. Diffusion of CO_2 into the mobile water after secondary waterflooding would increase the contact time needed for the CO_2 to dissolve in the resident oil, therefore delaying additional oil recovery [98, 99]. On the other hand, the residual oil and mobile water after secondary CWI would be saturated with CO_2, which facilitates the mass transfer of the CO_2 in tertiary CO_2 injection mode.

In this experiment, the core was flooded with carbonated water after establishing the initial oil and water saturation. The initial water saturation (Swi) was established at 20% PV. The injection of CW continued until a total of approximately 5.8 pore volume had been injected, by which point oil recovery of 60.5 % of OOIP was achieved. During the injection of CW, the new gaseous phase was formed, which resulted in an increase in the differential pressure across the core up to 1.2 psi after the CW breakthrough. The CW breakthrough took place at about 0.36 PV, bringing about oil recovery of 46.9 % of OOIP.

After that, nearly four pore volumes of CO_2 were injected. An immediate response in oil recovery occurred, even in the presence of 68% PV of water saturation after secondary CWI. The differential pressure across the core increased to overcome the capillary forces, then dropped sharply, indicating the mobility of the three phases inside the core, in tandem with a stepped increase in oil recovery. The ultimate oil recovery reached was 69.5 % of OOIP, in other words about 9 % additional OOIP due to the tertiary immiscible CO_2 injection. Figure 3-7 presents the recovery of the oil and the differential pressure measured across the core during all stages of test No. 3.

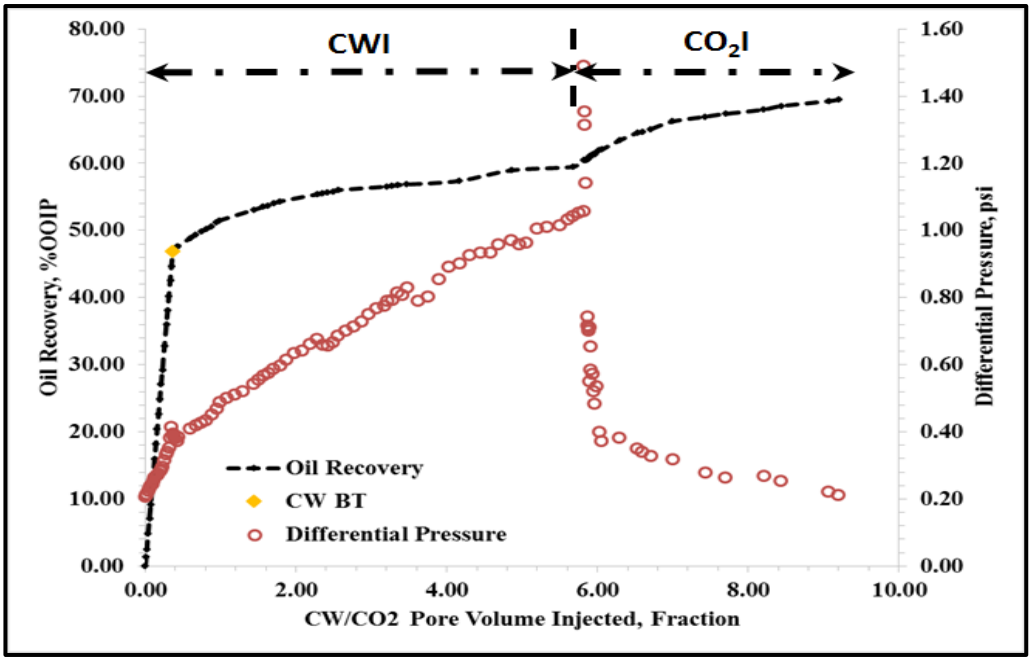

Figure 3-7 Oil recovery and differential pressure across the core during secondary CWI followed by CO_2 injection in test no. 3 [68]

3.5 New Gaseous Phase Saturation in Tertiary CWI

Considering the tertiary CWI coreflood experiments, only residual oil saturation (S_{orw}) remained in the porous medium, as indicated by the fact that there was no further oil production at the end of conventional secondary waterflooding. The observation from the pore-scale experiment, during CWI that was performed in the same conditions, was that the oil ganglia had started to develop a gaseous phase which resulted in apparent swelling of those oil ganglia. Subsequently, the swollen oil drops reconnected with neighbouring oil drop, and were then displaced by CW. Furthermore, the oil ganglia shrank back to the original saturation despite the high immobile gas saturation held inside the oil ganglia. In other words, the total hydrocarbon saturation encompassing both the

oil and new phase saturations remained constant during tertiary CWI since the new phase is formed as part of the total hydrocarbon saturation so the saturation in the oil would decrease as the saturation in the new gaseous phase increases. The following equation (3-1) expresses the methodology mathematically.

$$S_o^{CWI} + S_{NP}^{CWI} = S_{hydrocarbon} \qquad \text{Equation 3-1}$$

Where S_o^{CWI} is the oil saturation in the core during CWI, and S_{NP}^{CWI} is the saturation of new gaseous phase formed during CWI. At the start of tertiary CWI, the gas saturation is zero and hence the above equation 3-1 would become S_{orw}, but as the gas forms in the core some of the oil would be produced, leading to a reduction in oil saturation. In other words, during tertiary CWI, it will be as in equation 3-2:

$$S_o^{CWI} + S_{NP}^{CWI} = S_{orw} \qquad \text{Equation 3-2}$$

Where S_{orw} is residual oil saturation after conventional water injection. The results of the oil recovery profile from the tertiary coreflood experiment were used to obtain the oil saturation in the core and, from those data and equation 3-2, the average gas formed in the core was estimated. The result of adopting this approach is illustrated in figure 3-8. The average gas (new phase saturation) calculated during CWI in tertiary mode of experiment no. 1 reached approximately 12%. This method is clearly adoptable in the absence of conventional WF mechanisms where the performance of CWI is the only active oil recovery process.

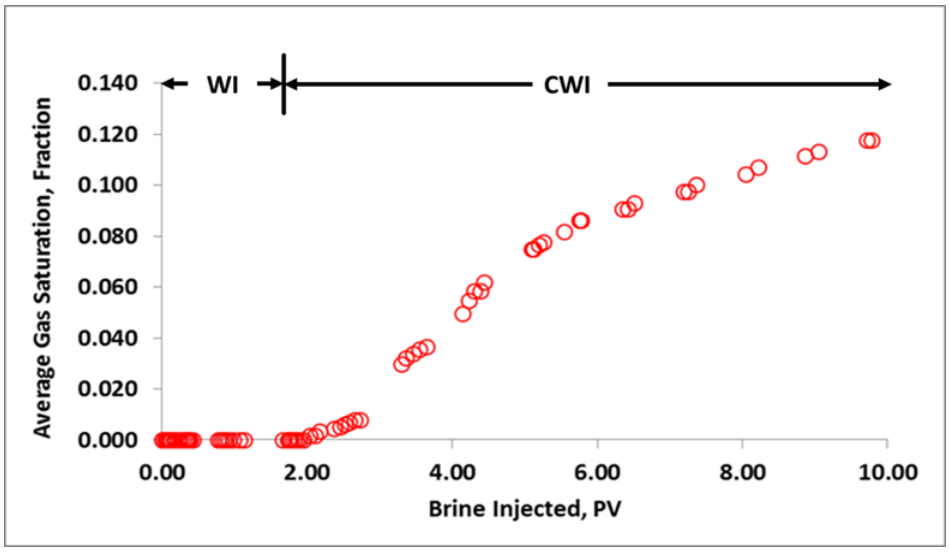

Figure 3-8 Calculated average gas (new phase) saturation during tertiary CWI of core displacement test no.1

The contribution of other mechanisms, such as normal oil swelling and reduction of oil viscosity, are limited. Most of the oil enlargement is due to the formation of the new phase, whereas the normal oil swelling is limited and only occurred at very early stages, as observed in figure 3-2. In respect to the effect of viscosity, the live oil viscosity was 1.4 cp and the injected plain brine viscosity was 0.8, whereas the calculated carbonated brine viscosity increased to approximately 0.88 cp. The dissolution of CO_2 in oil would change the oil's colour to a brighter colour, as was observed in the micromodel experiments [68], and this change of colour also reflects the change in the physical properties of the crude oil, e.g. reduction in oil viscosity and density, but that reduction would take place at the same time as the increasing in the carbonated water viscosity compared to normal water. The oil/water viscosity ratio is 1.77 in conventional waterflooding, whereas, if we assume that the oil viscosity is reduced to 1 cp due to CO_2 dissolution, then the viscosity ratio will drop to 1.14 in the carbonated water scenario. If there is no evidence of an alteration in wettability during CWI, then the relative permeability will remain constant in both injection scenarios. Figure 3-9 shows the fractional flows at different oil-water viscosity ratios. As can be seen, therefore, these improvements in mobility ratio cannot be the main contributors to the improvement in oil recovery during CWI where a slight delay in water breakthrough occurred when the oil viscosity reduced.

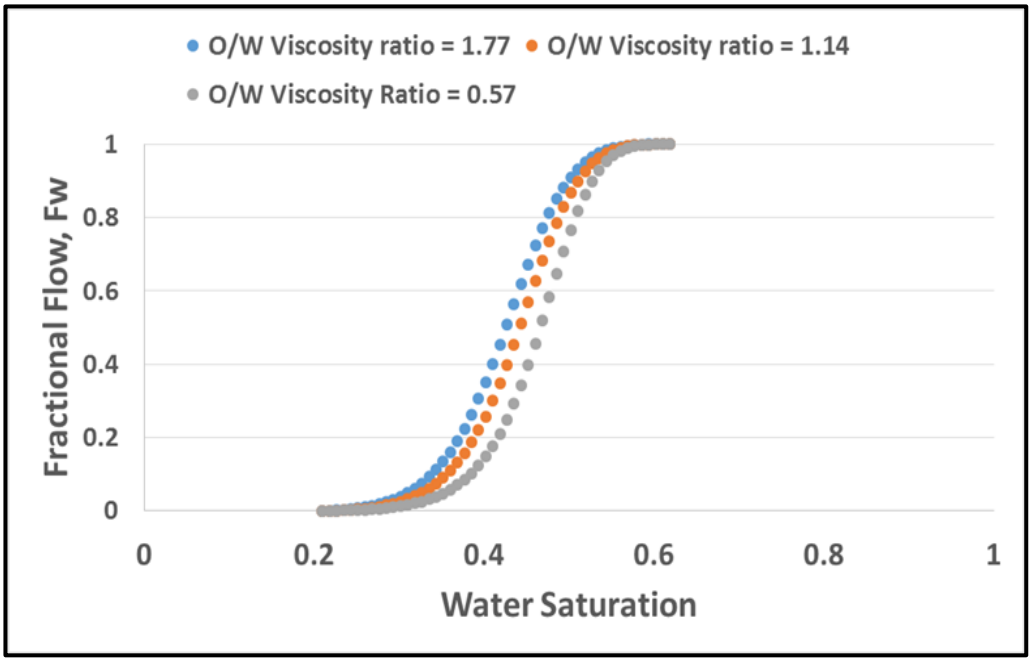

Figure 3-9 Fractional flow of different viscosity ratios, showing the effect of a reduction in oil viscosity in a light oil system

3.6 Multi-Phase Flow in Porous Media

The formation of the new phase as a result of CO_2 dissolution into live oil during CWI brings about a three-phase flow regime in the porous medium. This means that additional aspects of multiphase flow need to be considered when simulating the process of injecting carbonated water, such as:

- Modelling the relative permeability of the oil and the new phase
- Changes in the saturation of the oil and new phase

In the micromodel visualisation experiment, as demonstrated in Figures 3.1D to 3.1F, a thin film of oil was always present between the new (gaseous) phase/oil region and the water/oil region, which served to separate the gas from the flowing water. This film creates an additional (apparent) oil swelling effect. Due to the extreme increase in size and volume of the new phase within the oil, the oil volume increases, resulting in the oil being remobilised. This may also connect the oil ganglia to form a continuous low mobility flow of oil. The way we represented this phenomenon in our numerical simulation model was by designing a model for oil-gas relative permeability and three phase oil relative permeability.

Generally, in the presence of three-phase flow in a porous medium, three-phase relative permeabilities are considered to account for the interaction in flow between the different phases. Due to the complexities and time involved in the laboratory measurement of three-phase relative permeabilities, correlations or models of three-phase relative permeabilities are often estimated from two-phase relative permeability data . Standard three-phase relative permeability models have been developed for water-wet systems, where the water is the most wetting phase and the gas the least wetting phase. The water and gas relative permeabilities are therefore functions only of their own saturations ($k_{rw} = k_{rw}(S_w)$ and $k_{rg} = k_{rg}(S_g)$), whereas the oil relative permeability depends on both the water and gas saturations (i.e. $k_{ro} = k_{ro}(S_w,S_g)$). Various three-phase relative permeability models have been proposed to predict the oil's relative permeability in a three phase region, while the most common and widely used methods for interpolating the oil's relative permeability are those in Stone I & II [100, 101]. Another classic method is the saturation-weighted interpolation originally proposed by Baker (1988) [102].

The micromodel experiments demonstrated a relationship between the increase in the new phase saturation and the decrease in the oil saturation during CWI, as illustrated in Figure 3-10. Although it should be noted that the residual oil saturation is not a constant, but continuously changes depending on the amount of the formed gas; therefore, the residual oil saturation is in fact a function of gas saturation.

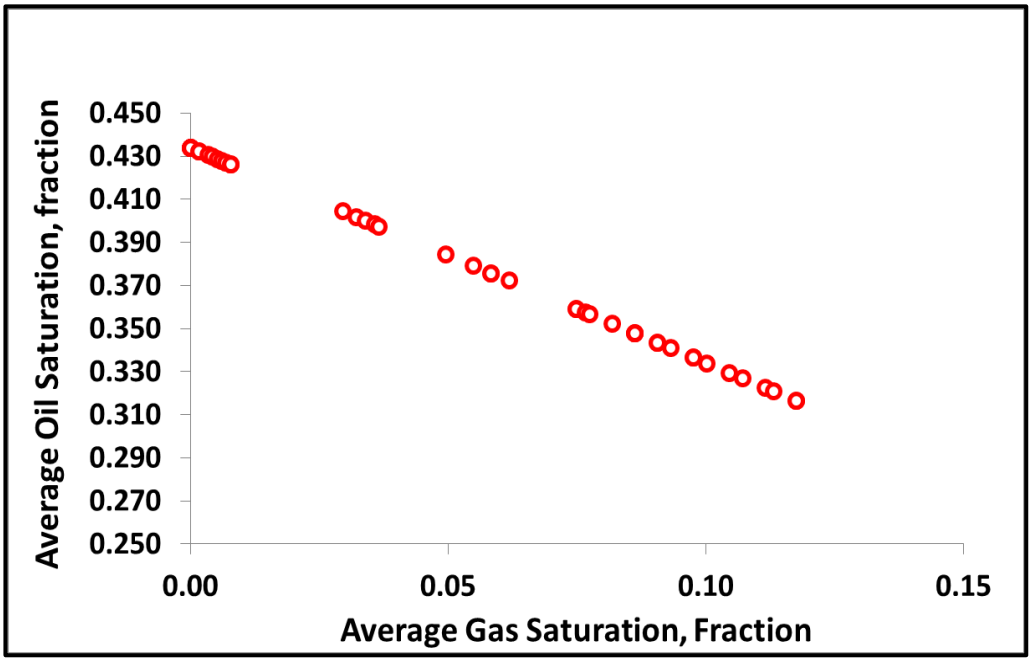

Figure 3-10 linear relationship between calculated new gaseous phase saturation and reduction in residual oil saturation during tertiary CWI

Correlation of this concept could be linked when S_g is slightly larger than S_{gc} = critical gas saturation, k_{rg} remains small, so the overall behaviour is still close to a trapped gas saturation. Thus for small values of S_g, it is argued by Fayers in 1989 [103] that:

$$S_{om} = S_{orw} - \alpha(S_{gt}) \qquad \text{Equation 3-3}$$

Where S_{om} is the residual oil saturation in the three-phase region related to S_{orw}, which is residual oil saturation due to water injection, and S_{gt} is the trapped gas saturation or small mobile gas saturation. The α coefficient would be a constant between 0 and 1, where a value of α = 1 means the gas saturation is totally trapped.

The pore-scale observations demonstrated that the new gaseous phase formed within the oil, and then the oil augmented promptly as the gas phase grew in size and volume. Subsequently, the swollen oil reconnected together and mobilised, at which point it shrank back to its original saturation, even though with a high immobile gas saturation

trapped inside the oil. In other words, the new gaseous saturation would enlarge the residual oil saturation, while the water saturation would displace the swollen oil in the three-phase region. The minimal oil saturation is therefore a function of the new gaseous phase saturation, where the oil relative permeability is a function of both gas and water saturation in which the relative permeability to oil in the three-phase region could be expressed using the Stone I model [100] as modified in [104]:

$$k_{ro}(S_w, S_g) = \frac{S_o^* k_{row} k_{rog}}{k_{rocw}(1-S_w^*)(1-S_g^*)} \qquad \text{Equation 3-4}$$

where, $S_w^* = \frac{S_w - S_{wc}}{1-S_{wc}-S_{om}}$, $S_w > S_{wc}$, $S_g^* = \frac{S_g}{1-S_{wc}-S_{om}}$, $S_o^* = \frac{S_o - S_{om}}{1-S_{wc}-S_{om}}$, $S_o > S_{om}$

S_{wc} = connate water saturation, k_{rocw} = two-phase oil relative permeability at $S_o = 1 - S_{wc}$, and k_{row}, k_{rog} = two-phase oil relative permeability for the water/oil and oil/gas systems, respectively. Thus, $k_{row} = k_{row}(S_w)$ and $k_{rog} = k_{rog}(S_g)$.

3.7 Numerical Simulation of CWI

To have a representative and reliable simulation model of the CWI process, it is important to understand the phenomena taking place during CWI, specifically the impact of the formation of new gaseous phase on the reservoir fluid properties, the characterisation of the different phases, and the multi-flow regime in a porous medium. Having defined the mechanisms that were observed to occur during the pore-scale visualisation of CWI, and having reflected these processes in numerical terms, the methodology is ready to be implemented using a commercial numerical simulation package.

3.7.1 Model Description

The initial step in the development of a numerical simulation mode was constructing the reservoir grid system, which was in this case a linear one-dimensional rectangular model. The one-dimension core model has a length of 32 cm and a diameter of 5 cm as shown in figure 3-11. The direction of flow is assumed to be in the I-direction. Based on the laboratory core, the cross-sectional flow area through the core would be:

$A = \pi r^2 = 3.1415 * (0.164436/2)^2 = 0.02123654$ ft^2 (19.729 cm^2)

Then, the cross-sectional area of the simulation model = DJ * DK, with the assumption that DJ and DK are the same. Therefore, the simulation model cross-sectional area = DJ^2 = DK^2 = 0.02123654 ft^2, and DJ = DK = the square root of the cross-sectional area = 0.145727611 ft (4.44 cm). The simulation model length (DI) = 1.05 ft.

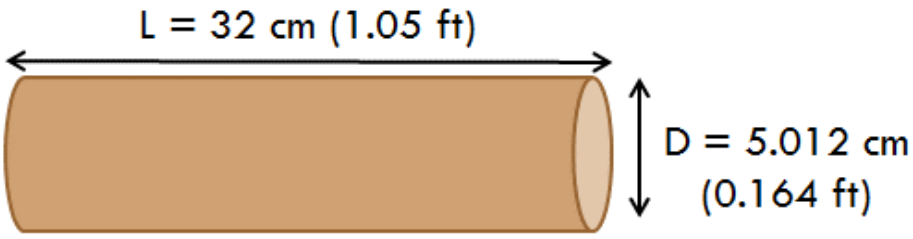

Figure 3-11 the core physical dimensions

The model was simulated using a compositional simulator (CMG-GEM) [105]. This model is to illustrate the author's methodology and workflow in studying the effect of the tuned EOS based on the formation of the new phase, and its impact on the three-phase flow model when simulating the process of CWI for improving oil recovery. The model is constructed with 200 blocks in the x-direction, and a single grid in the Y and Z directions in a Cartesian horizontal orientation. Since the rock properties (porosity and absolute permeability) have been measured for the whole core, it is assumed that the simulation model is a homogeneous porous medium in all spatial directions. Hereafter, a constant absolute permeability is assigned for the I, J, and K-directions. Figure 3-12 schematically displays a 1-D cross section with homogenous porosity and permeability in all directions. For the high permeability core used in these tests the capillary pressure is estimated to be very small. Thus, capillary pressure is ignored in this case.

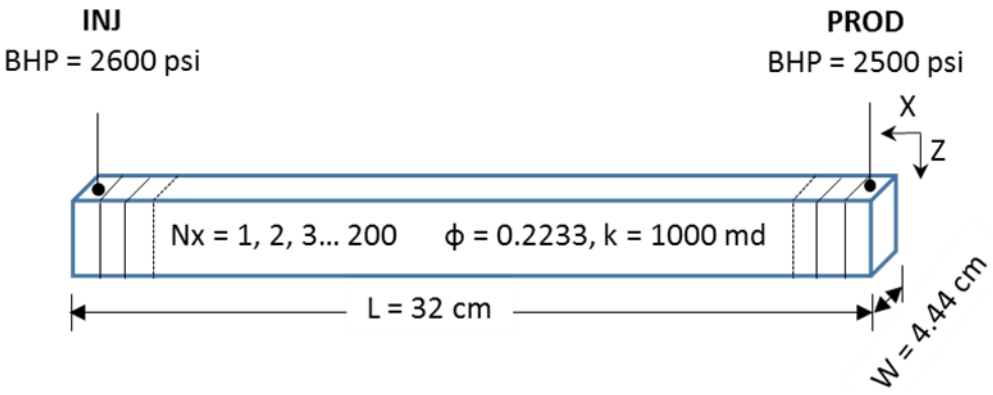

Figure 3-12 Schematic display showing the 1D model setup

Coupling the greenhouse gas module (GHG) with the compositional (GEM) models [105] can give us the opportunity to simulate the injection of carbonated water in a single well by invoking the solubility feature in injection water. Henry's Law was used to match the CO_2 solubility in water, which was measured at 28.7 cc of CO_2 per cc of brine (162 SCF/STB) at test conditions of 2500 psi and 100 °F with brine salinity of 35380 ppm. Thus, carbonated water (CW) was defined by the molality of CO_2 soluble in brine and was injected using a single well, called the 'injector'. The second well defined in the model was the 'producer'. The well at the outlet was constrained by constant bottom-hole pressures (BHP) of 2500 psi, which is the experiment pressure, whereas the injector was constrained with the constant injection rate of 0.00075477 bbl/day.

3.7.2 Reservoir Fluids Model

A CO_2-based oil recovery process involves the interface of multiple phases (e.g. oil, gas and brine), as well as the mutual interactions of the various components existing within those phases. The porous medium has reservoir oil, which typically contains light (e.g. C_1-C_4), intermediate (e.g. C_{5-12}) and heavier (e.g. C_{12+}) hydrocarbon components, in addition to formation brine, and a free gas phase; if it exists. In a conventional reservoir, the choice of recovery process depends on the extent of the various hydrocarbon fractions, which affect the compositional behaviour of the reservoir oil. In simulation modelling, however, a large number of these components (real and/or pseudo-components) require significant computational time and data storage capacity if they are to be represented fully. The procedure of lumping these components, which represent the composition of reservoir oil, and its fluid properties, and their interaction with the injected solvent, therefore forms an integral part of any reservoir fluids study.

The crude oil used in this study was a medium black oil with API gravity of 28.5° and stock tank oil viscosity of 31.25 at a test temperature of 100 °F. The crude oil was recombined with methane (C_1), representing the make-up gas with respect to a gas-oil ratio of 599 scf/stb at the test temperature and pressure of 100 °F and 2500 psi.

Peng-Robinson's (1978) cubic equation of state (PR-EOS) was selected for the fluid modelling since this yields more accurate vapour pressure predictions for the heavy hydrocarbon components, and the Jossi-Stiel-Thodos (JST) viscosity model was used for

viscosity estimation for both vapour and liquid phases. Accordingly, the JST model highly depends on the density of the mixture predicted by the cubic equation of state through the mixing rule. The recombined oil sample (hereafter methane-saturated oil) is first lumped into seven components, as shown in figure 3-13, and the parameters of the EOS and viscosity model are tuned with the available fluid properties that were measured before commencing the coreflood experiments, which are listed in table 3-4. WinProp™ [106], a CMG equation of state multiphase equilibrium property software, was used for this.

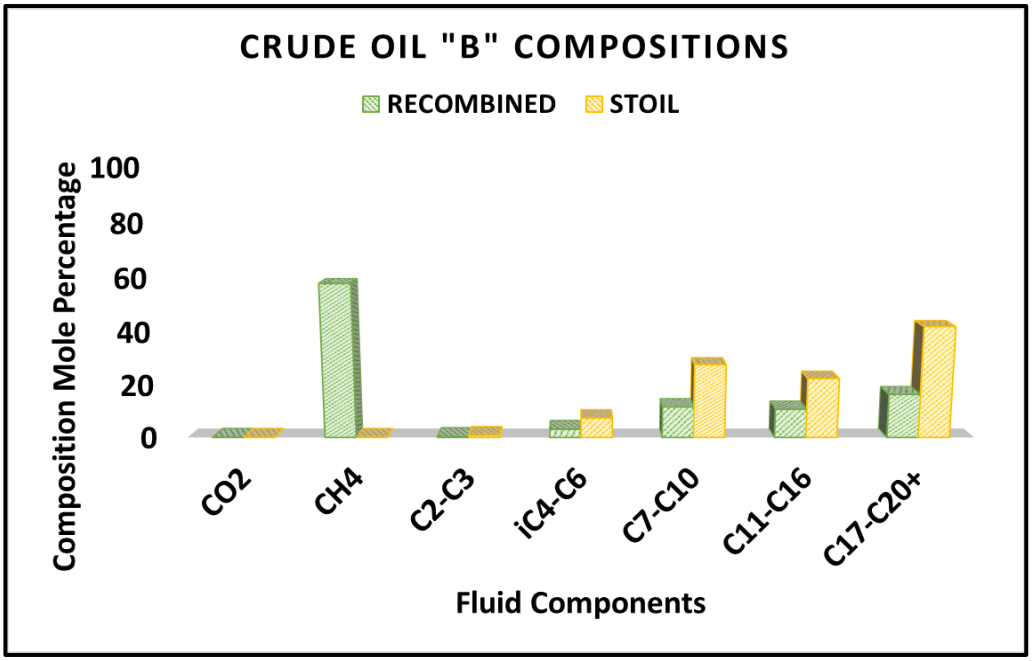

Figure 3-13 Crude B stock tank oil and its recombined methane-saturated oil

Table 3-4 Measured and modelled fluid properties of crude oil (B)

Parameter	Saturation Pressure (psi)	GOR (SCF/STB)	FVF (bbl/STB)	API Gravity	Oil Viscosity (cp)	
					Live Oil	STO
Measured [68]	2500	599	1.240	28.5	1.417	31.25
Modelled	2500	599	1.239	28.5	1.417	31.24

The lumping scheme for the reservoir fluid components took into account the recombination process of reservoir oil in such a way that the components of the model gas (methane) would be considered to be a separate component along with carbon dioxide (CO_2), which is the target component of the mass transfer from carbonated water to reservoir oil. The intermediate hydrocarbon components, C_2 to C_6, were lumped into two

pseudo-components (C_2-C_3 and iC_4-C_6) due to the fact that they comprise only a small component of the reservoir oil, and since their critical properties and molecular weight are within the same range. The C_{7+} fractions, meanwhile, are lumped into three pseudo-components (C_7-C_{10}, C_{11}-C_{16}, and C_{17}-C_{20+}), again based on their approximately equal molecular weight, in order to facilitate the optimisation of the binary interaction coefficients BIC of CO_2 and the transfer of those components to the new phase during CWI. The fluid properties of C_{7+} pseudo-components are calculated using the mixing rules as shown in table 3-5. The critical temperature and pressure of the pseudo-component (C_{17}-C_{20+}), as well as its molecular weight, were used in the tuning process, along with alteration of the volume shift of all components. Due to the limitation in respect to oil viscosity data, the tuning of viscosity model mainly depended upon the stock tank oil viscosity at test temperature and the viscosity of methane-saturated oil at test conditions. The mixing rule exponent parameter, polynomial coefficients of the JST viscosity model, were used in the viscosity regression. Table 3-4 presents the modelled fluid properties against the measured properties of crude oil B, while figure 3-14 shows the final phase diagram of the methane-saturated oil based on the tuned PR-EOS.

The available fluid properties did not provide further characterisation of CO_2-oil mixture phase behaviour during CWI, hence the equation of state has its limitations in respect to modelling the compositional changes during CWI. The average gas (new phase) saturation will therefore be used in tuning EOS to model fluid-fluid interactions during CWI.

Table 3-5 Fluid description of reservoir oil (B)

Components	FSO, Mol%	Molecular Weight	Pc (atm)	Tc (°K)	ω	VH
CO_2	0.00	44.010	72.80	304.20	0.225	0.0000
C_1	57.71	16.043	45.40	190.60	0.008	0.1427
C_2-C_3	0.31	44.097	41.90	369.80	0.152	0.0166
IC_4-C_6	3.13	75.853	33.68	477.80	0.247	0.2000
C_7-C_{10}	11.68	114.035	27.97	584.09	0.372	0.2000
C_{11}-C_{16}	10.75	179.498	20.17	628.01	0.572	-0.1540
C_{17}-C_{20+}	16.42	502.143	10.18	687.38	1.047	-0.2543

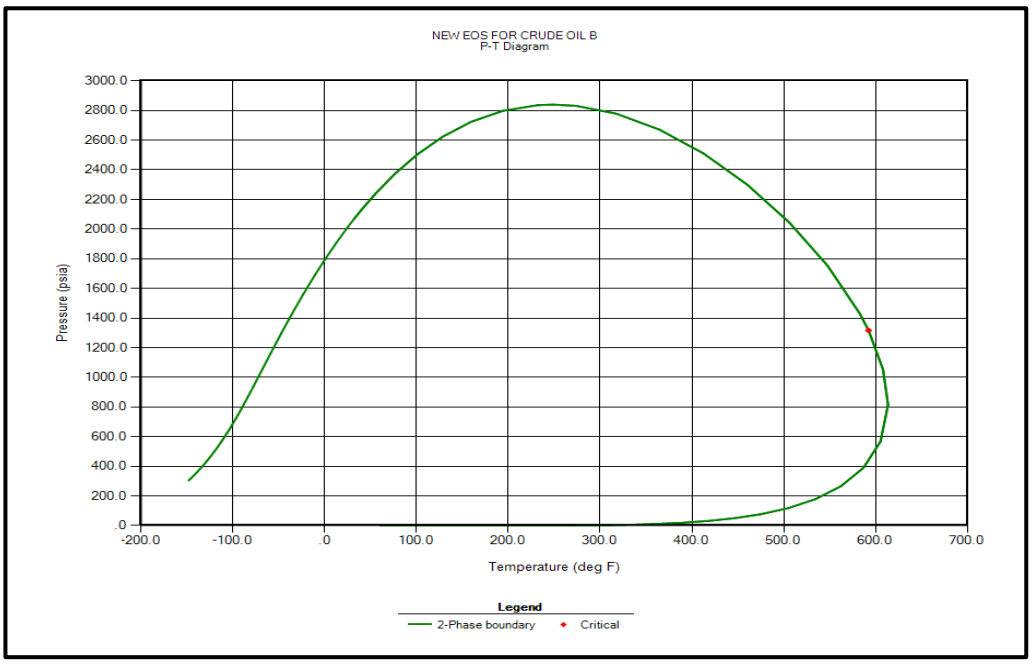

Figure 3-14 Phase diagram of methane-saturated crude oil (B) based on the tuned PR-EOS

3.7.3 Modelling the Formation of the New Phase

Cubic equations of state (CEOS) are currently the equations of state considered most applicable to performing complex phase equilibrium calculations of high-pressure multiple components containing hydrocarbon and non-hydrocarbon systems for most oil and gas operations. A large number of equations have been suggested to predict the thermodynamic properties of pure or mixed components since the first proposed CEOS by van der Waals [107]. Since the starter of the van der Waals EOS, which was the first analytical expression connecting the pressure (p) to the temperature of a fluid (T) and the volume (V), incorporating both the gas-liquid and fluid criticality [108]. Most of the equations of state that are being used widely, however, have been derived from that of van der Waals (vdW-EOS). Among these, the Redlich and Kwong (RK) [109], Soave, Redlich and Kwong (SRK) [110] and the Peng-Robinson (PR) [111, 112] are the most widely used in modelling thermodynamic phase equilibria calculations.

Van der Waals proposed for the first time physical-coherent explanation of fluid behaviour from low to high pressure. He considered the ideal-gas law (i.e., p v =RT) as the base of his equation derivation taking into account that the molecules would occupy space through replacing v by (v -b), and also they exert an attraction on each other by changing p with p+ a / v^2 (cohesion effect) [113]. The mathematical equation proposed by van der Waals [108] as follow:

$$p = \frac{RT}{v-b} - \frac{a}{v^2}$$ Equation 3-5

where p and ν are the experimentally measured pressure and molar volume, R is the universal gas constant = 8.314472 J.mol^{-1}.K^{-1}, a is a measure of the kinetic energy of the molecule (attraction parameter), b is the repulsion parameter. Then, the van der Waals (vdW) EOS improves the description of non-ideal gas behaviour, where the repulsive term ($\frac{RT}{v-b}$) approximates ideal gas behaviour, and the attractive term ($\frac{a}{v^2}$) accounts for non-ideal behaviour [107].

In 1949, Redlich and Kwong derived a new expression from vdW EOS in which the attractive term was modified and became $\frac{a_c}{\sqrt{T}v(v+b)}$, to attain better fluid phase behaviour at low and high densities with the introduction of temperature dependency term [109]. The accuracy of Redlich and Kwong (RK) EOS is moderately useful in predicting the fluid response for pure fluids with acentric factors close to zero [113]. Whereas, its accuracy much reduced in predicting the fluid behaviour for complex fluids that have nonzero acentric coefficients. In RK EOS, all components have a critical compressibility factor of Z_c = 1/3, which could be reasonable for lighter hydrocarbon components and unacceptable for the heavier one in which their Z_c values are less than 0.2 [107].

Another alteration was carried by Soave through substituting a two-parameter EOS which are Tc and Pc into a three-parameter EOS by introducing the acentric factor (ω) as a third parameter in the definition of α(T) as follow [110]:

$$\alpha(T) = \left[1 + m\left(1 - \sqrt{T/T_c}\right)\right]^2$$ Equation 3-6

Where $m = 0.480 + 1.574\omega - 0.176\omega^2$, whereas the acentric factor (ω) is used to consider the molecular size and shape effects since it varies with chain length and the spatial arrangement of the molecules [113]. The resulting model is known as the Soave-Redlich-Kwong (SRK) EOS being the most widely used RK EOS proposed up to date. The SRK EOS provides an excellent predictive model for systems require accurate predictions of vapour-liquid equilibrium (VLE) and vapour properties which most properly due to the compressibility factor of 0.333 that similar to light hydrocarbons Zc values [107]. However, it is unacceptably overestimated liquid volume and

underestimate liquid densities of petroleum mixture if no volume translation used. Therefore, in 1976, Peng and Robinson proposed recalculation of the coefficients of the (m) function that used in the Soave's alpha function (α) where $m = 0.37464 + 1.54226\omega - 0.26992\omega^2$ and also, amending the volume dependency of the attractive term [111]. It intended to create great improve on EOS prediction and particularly enhancing liquid-density calculation. A slight modification suggested by Robinson and Pang [112] to account for heavier molecules in which their acentric factors more 0.491, through recalculation the coefficients of the (m) function for those molecules as follows: $m = 0.379642 + 1.487503\omega - 0.164423\omega^2 + 0.016666\omega^3$.

The accuracy of the PR EOS is comparable to the SRK EOS, where both equations of state use widely and most popular in the oil and gas industry. Both of these models generally offer a good representation of the fluid phase behaviour that contains few associated hydrocarbon mixtures such as paraffin, naphthene, aromatics and gases. However, the difference between PR and SRK EOS liquid volumetric predictions can be substantial due to most significant improvement in critical compressibility factor (Z_c) of 0.307 offered by PR EOS which is somewhat closer to experimental values for heavier hydrocarbon and lower than that in SRK EOS [107]. Table A-1 summaries the significant differences between the most famous equations of state and their critical parameters. In summary, the Peng & Robinson (PR) and Soave-Redlich & Kwong (SRK) equations of state provide almost similar acceptance of vapour-liquid equilibrium (VLE) predictions and reasonable calculation for vapour and liquid volumes and densities when used with volume translation [107]. For that, the selection of PR-EOS (1978) for the fluid modelling carried in this research was mainly based on the acentric factor where the existence of more heavier hydrocarbon components in the reservoir oil that their acentric elements more than (0.5).

Table 3-6 the most important cubic EOS's and their classical critical properties

EOS	Equation	a	b	Z_c
Van der Waals (vdW) [108]	$p = \frac{RT}{v-b} - \frac{a}{v^2}$	$\frac{27}{64}\frac{(RT_c)^2}{P_c}$	$\frac{RT_c}{8P_c}$	0.375
Redlich & Kwong (RK) [109]	$p = \frac{RT}{v-b} - \frac{a}{\sqrt{T}v(v+b)}$	$\frac{0.42748R^2T_c^{2.5}}{P_c}$	$\frac{0.08664RT_c}{P_c}$	0.333
Soave-Redlich & Kwong (SRK) [110]	$p = \frac{RT}{v-b} - \frac{a\alpha(T)}{v(v+b)}$	$\frac{0.42748R^2T_c^2}{P_c}$	$\frac{0.08664RT_c}{P_c}$	0.333
Peng & Robinson (PR) [111]	$p = \frac{RT}{v-b} - \frac{a\alpha(T)}{v(v+b)+b(v-b)}$	$\frac{0.45724R^2T_c^2}{P_c}$	$\frac{0.0778RT_c}{P_c}$	0.307

In addition to using an appropriate cubic equation of state for an accurate prediction of vapour pressure and liquid density, the ability of a CEOS to correlate and predict the phase equilibria of mixtures requires mixing rules for the energy parameter and the covolume. The most commonly used method to extend equations of state to a non-polar mixture is by using the van der Waals one fluid (vdW1f) mixing rules and the classic combining rules (i.e. the geometric mean rule for the cross-energy and the arithmetic rule for the cross covolume parameter):

$$a = \sum_i \sum_j x_i x_j a_{ij} \qquad a_{ij} = \sqrt{a_i a_j}\left(1 - k_{ij}\right) \qquad \text{Equation 3-7}$$

$$b = \sum_i \sum_j x_i x_j b_{ij} \qquad b_{ij} = \left[\frac{1}{2}\left(b_i + b_j\right)\right]\left(1 - l_{ij}\right) \qquad \text{Equation 3-8}$$

Where k_{ij} and l_{ij} are the binary interaction parameters that are generally estimated directly from experimental equilibrium data for binary systems [114]. The van der Waals mixing rule is capable of accurately representing vapour-liquid equilibria using one binary interaction coefficient for non-polar or slightly polar systems, where $l_{ij} = 0$. Theoretically, the interaction parameter is introduced to account for the molecular interaction between dissimilar molecules. Coutinho et al. [115] describes the binary interaction coefficient as a correction for the deviations between EOS predictions and the experimental data. In fact, the interaction coefficients arise from various simplifications and assumptions used in the derivation of the mixing and combining rules, and they also take into account the various deficiencies and limitations of the EOS approach.

Coupling the model of various gas solubilities in water with a cubic equation of state would provide a lot of value in respect to simulating the mass transfer of a soluble gas in both immiscible phases (e.g. oil and water). Several researchers [116-121] have developed compositional models linking the solubility of CO_2 in the aqueous phase with a cubic equation of state. Mehra et al. [116] proposed a numerical scheme for the calculation of multiphase equilibria. In their work, the hydrocarbon phases were being predicted by the Peng-Robinson EOS and solutes in the aqueous phase were estimated by Henry's constants using the Cysewski and Prausnitz correlations [122]. Their results showed that the water phase had a significant influence on both vapour and CO_2-rich phase saturation, and that its addition to the system does not introduce new complications in the number of unstable solutions more than that already inherent in the three liquid-liquid-vapour problem. In the same year, Mansoori [119] constructed a compositional model to investigate the effect of CO_2 solubility in water on oil recovery by CO_2 flooding. His model utilised the SRK-EOS to predict the phase equilibrium and density of CO_2-hydrocarbon mixture, while Henry's law was used to obtain the solubility of CO_2 in water. The thermodynamic equilibrium between phases was enforced by the equity of component fugacities applied at each time and each grid block through the simulation. On the other hand, Chang et al. [120] built a three-dimensional three-phase compositional model for simulating CO_2 injection including CO_2 solubility in water. In his model, oil and gas densities and fugacities were predicted by a cubic equation of state, while CO_2 solubility in water was computed using correlations as a function of pressure at the reservoir temperature.

In turn, the multiphase calculation to be performed by the CMG simulation package uses the techniques described in Nghiem and Li [123] to simulate the fluid-fluid interaction behaviour during CWI. This procedure provides a gradual increase in the number of phases as shown in flow diagram figure 3-15. Where a three-phase flash calculation for vapour-liquid-water system incorporated in such a way that the vapour and liquid are modelled with a cubic equation of state, while the solubility of the gases in the aqueous phase is modelled with Henry's law, as introduced in [118].

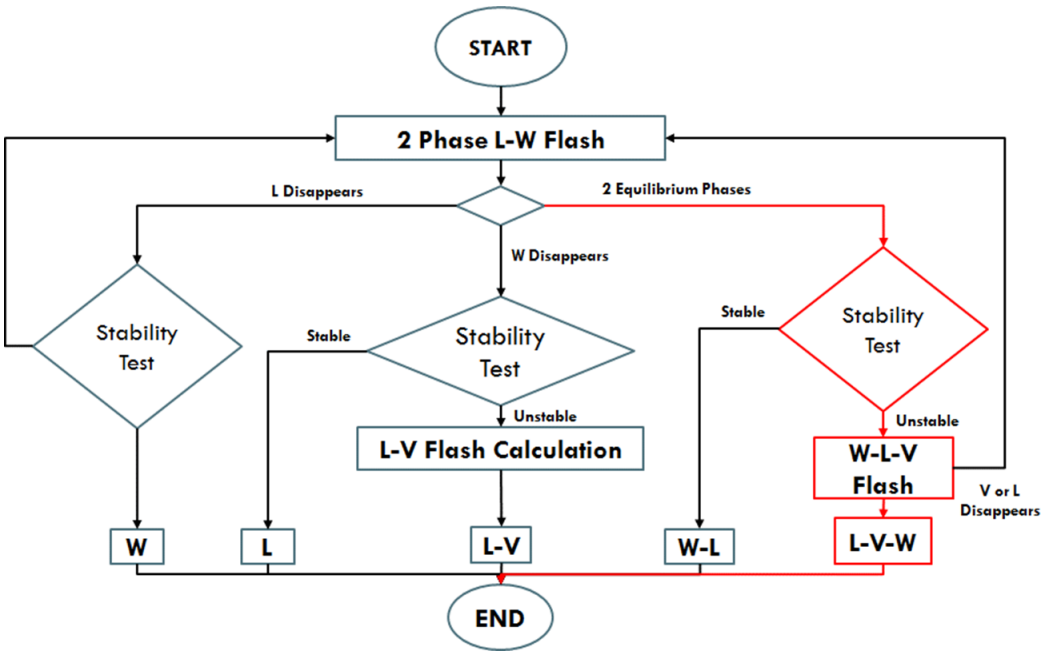

Figure 3-15 Flow diagram for liquid-vapour-water flash calculation as proposed by Li and Nghiem [118]

The three-phase (O-G-W) equilibrium would be predominantly controlled by the CO_2 mass transfer from CW to oil, and the formation of the new gaseous phase through the following thermodynamic equilibrium equations:

$$\ln k_{iv} + \ln \varphi_{iv} - \ln \varphi_{il} = 0 \qquad \text{Equation 3-9}$$

$$\ln k_{iw} + \ln \varphi_{iw} - \ln \varphi_{il} = 0 \qquad \text{Equation 3-10}$$

Where φ_{iv} and φ_{il} is the fugacity coefficient of component *i* in vapour and liquid phases, respectively, estimated from an EOS using equation 3-11, and is a function of pressure, temperature and phase compositions

$$\ln \varphi_i = \frac{b_i}{b}(Z-1) - ln(Z-B) - \frac{1}{\delta_2-\delta_1}\frac{A}{B}\left(\frac{2S_i}{a} - \frac{b_i}{b}\right) ln\left(\frac{Z+\delta_2 B}{Z+\delta_1 B}\right) \qquad \text{Equation 3-11}$$

Where Z is the compressibility factor, A = ap/(RT)^2, B = bp/RT, δ_1 and δ_2 are equation of state parameters and a & b are the van der Waals one fluid mixing rule parameters presented in equations 3-7 and 3-8.

φ_{iw}, meanwhile, is the fugacity coefficient of component *i* in the aqueous phase handled by Henrys' law through the following equation 3-12:

$$\ln \varphi_{iw} = ln(H_i/p)$$ Equation 3-12

Where, H_i is the Henry's law constant of component i in the aqueous phase. It is a measurement of gas solubility in a liquid, and expressed as the ratio of the partial pressure of gaseous solute to its equilibrium concentration in the liquid phase. Therefore, the use of Henry's law constant would relate the fugacity/molar fraction ratio of a solute in a solution to the partitioning coefficient of component i among aqueous and liquid phases as explained in equation 3-14. Therefore, equations 3-13 and 3-14 represent the equilibrium coefficient of component *i* in the vapour to liquid phase and also in the water to liquid phase.

$$k_{iv} = x_{iv}/x_{il}$$ Equation 3-13

$$k_{iw} = x_{iw}/x_{il}$$ Equation 3-14

where x_{iv}, x_{il} and x_{iw} are mole fractions of component *i* in vapour, liquid and aqueous phases, respectively. Then, the material balance on component *i* requires that:

$$z_i = F_l x_{il} + F_v x_{iv} + F_w x_{iw}$$ Equation 3-15

In this case, z_i is the feed composition (global mole fraction), and F_m is the mole fraction of phase m (m = liquid, vapour or water). Details of this procedure were introduced in [118]. The mole fractions are treated as dependent variables, however:

$$x_{im} = {k_{im} z_i}\Big/{(k_{iv} F_v + F_l + k_{iw} F_w)}$$ Equation 3-16

In CWI, although the mass transfer of CO_2 is a dynamic process due to the difference in solubility of CO_2 in two immiscible fluids, the dissolution of CO_2 into oil is controlled by the CO_2 partition coefficient between aqueous and oil. This partition coefficient could be modified by changing the binary interaction coefficient values of CO_2 and other hydrocarbon components. Providing a representative estimation of binary interaction parameters (BIC), the third phase will be formed during the injection of carbonated water. More importantly, the BIC between CO_2 and the hydrocarbon components could be modified to adjust the dissolution of CO_2 into oil, and also the consequent liberation of light HC components into the vapour phase. It should be pointed out that the default BIC (obtained from conventional CO_2 and oil interactions) cannot capture how a third phase would form as a result of CO_2 mass transfer from carbonated water to reservoir oil.

Therefore, history matches the calculated new (gas) phase saturation through adjusting the BIC between CO_2 and the hydrocarbon compounds would provide a technique to calibrate the equation of state in reproducing the new gas phase that formed as a result of transferred CO_2 from CW to oil phase, consequently simulating the mechanisms of CWI in enhancing oil recovery.

3.7.3.1 History Matching

History matching is the process of fine-tuning uncertain parameters of a simulation model to available historical data. This process is a non-linear problem where there is no clear trend between themeasured data and the model parameters. It is an inverse process that the historical data are used to optimise the simulation model parameters. Furthermore, the process ends with non-unique solutions where many possibilities of simulation model parameters can have similar simulation output responses that match the real measured data.

The process of history matching comprises adjustment of the uncertain input parameters until the simulation model prediction corresponds closely enough with the historical data. So, this task is either performed manually through the interference of an experienced and qualified engineer who has enough knowledge into edit and modifies the input parameters, or automatically in which optimisation techniques are employed. In the other hand, the manual history matching process is very time-consuming, especially in the existence of multiple input parameters that should be tuned to predict numerous historical data numerically. Also, it uses the trial-and-error method to calibrate the reservoir model with measured data and by this method, it is inefficient for generating multiple reservoir model realisations to quantify uncertainties [124].

Over the years, as a result of the development of computer hardware and software, history matching of reservoir performance developed to be performed automatically, although it is not fully automated yet, as there is some resistance by the engineers who view the role of responsibility on the history matching process. The concept laid in handling the history matching as an optimisation process, i.e., determining an objective function pointing out the difference between the measured (real) and simulated data and minimising this objective function. The minimisation of the objective function could be achieved by

applying an appropriate optimisation algorithm. Thus, optimisation and nonlinear algorithms were not new techniques in other fields like mathematics and statistics, and that knowledge is used in the petroleum industry [124]. The idea of assisted history matching suggests that reservoir engineers are still in charge of a reservoir model calibration, however, they can depend on an optimisation tool to enhance their exploration on the input parameters space and speed up the convergence into one or more solutions.

The objective function (known as misfit) generally expressed as a single-objective function or multiple-objective function, where the single-objective function is the most used ones [125]. But It demands that the user assigns the weights linked each set of data to be tuned. Coats et al. [126] were the first to employ the parameterisation when they studied the use of porosity and permeability as uncertainty parameters in their reservoir history matching study. In their work, the objective function takes a linear form which minimises the absolute difference between the measured and the simulation values as express in the following

$$\text{Misfit} = \sum_{i=1}^{N_p} |M_i - S_i| \qquad \text{Equation 3-17}$$

Where Misfit is the objective function, Np is the number of measured data, Mi is the measured and Si is the simulation data for point i. Later, Thomas et al. [127] amended the results of assisted history matching accomplished by Coats et al. by suggesting a non-linear objective function. They used weight factors to reflect the importance of each measurement in the history matching process as following

$$\text{Misfit} = \sum_{i=1}^{N_p} [W_i(M_i - S_i)]^2 \qquad \text{Equation 3-18}$$

Where Wi is the weight factor of the measured point i. As mentioned earlier, the history matching is an inverse problem which could be handled within a Bayesian framework. The Bayesian framework is used in history matching to find models with a maximum degree of similarity to historical data. The set of these models acquired during the historical matching lets us quantify the uncertainty in the input parameters of the model and, consequently, the predictions of the model. Figure 3-16 illustrated the general scheme in dealing with history matching in a Bayesian framework.

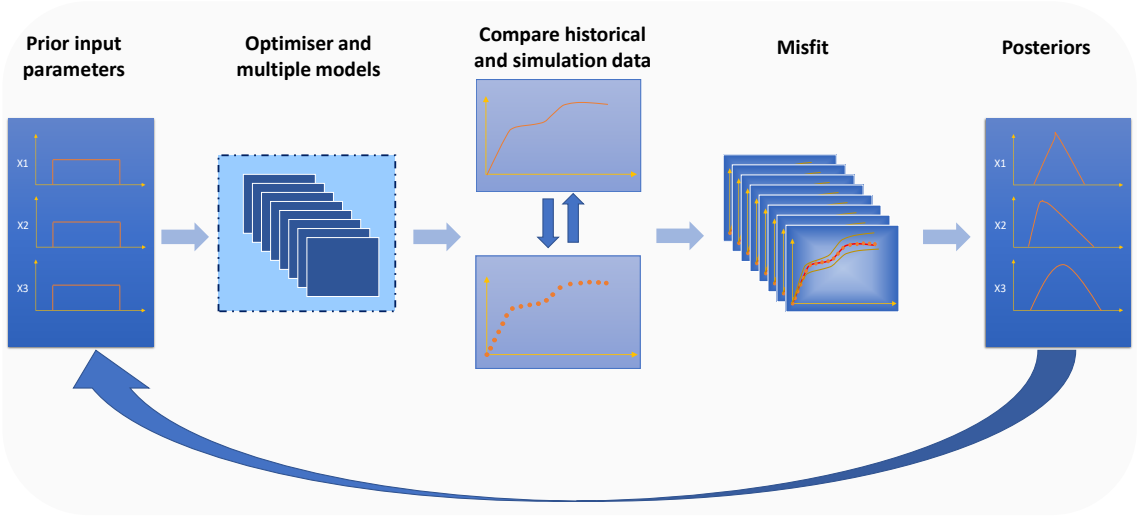

Figure 3-16 Bayesian framework explaining the inverse problem of history matching process [125]

For setting up the assisted-history matching in this study, CMOST that is a CMG assisted history-matching, optimisation, sensitivity analysis, and uncertainty assessment engine, used for minimisation of the global objective function in the history-matching process [128]. CMOST uses an optimizer such as CMG DECE, Latin hypercube plus proxy optimisation, and particle swarm optimizer, to create multiple simulation jobs from the uncertain input parameters with the intention of either converging on a better solution to some problem or seeing the impact of input parameters on simulation results.

CMG Designed Exploration and Controlled Evolution (CMG-DECE) optimizer is used to perform the assisted-history matching process for all the simulation studies in this thesis [128]. The CMG DECE Optimizer [128] is an improved genetic algorithm that implements the CMG's proprietary optimisation method which seeks to mimic the process where reservoir engineers usually use to solve history-matching or optimisation problems. It is an iterative process that implements a designed exploration stage to explore the maximum information about the solution space in a designed random pattern. By this way, representative simulation datasets are generated through experimental design and Tabu search techniques in picking up parameters values. It is followed by the evolution stage, where the simulation results obtained in the designed exploration stage statistically analysed. Based on the analyses, the DECE optimizer examines every selected value of each input parameter to decide whether there is a better chance to improve solution quality or if specific values are discarded or rejected of being chosen again. These banned values are recognised by the algorithm and do not be used in the next exploration stage, unless if there is the possibility of being trapped in local minima,

then the DECE optimiser reviews the banned values to scrutinize the previous dismissal resolutions are still valid. If the algorithm finds that certain rejection decisions are not valid, the banned decision is suspended, and the associated nominee values will be used again. The DECE optimisation method is successfully applied in a number of real reservoir simulation studies and the results prove that the method is reliable and efficient. DECE characterises to handle continuous, discrete parameters, and hard constraints and it provides complete utilization of distributed computing power in fast and stable convergence (ref). The following figure 3-17 illustrates the workflow of CMG DECE:

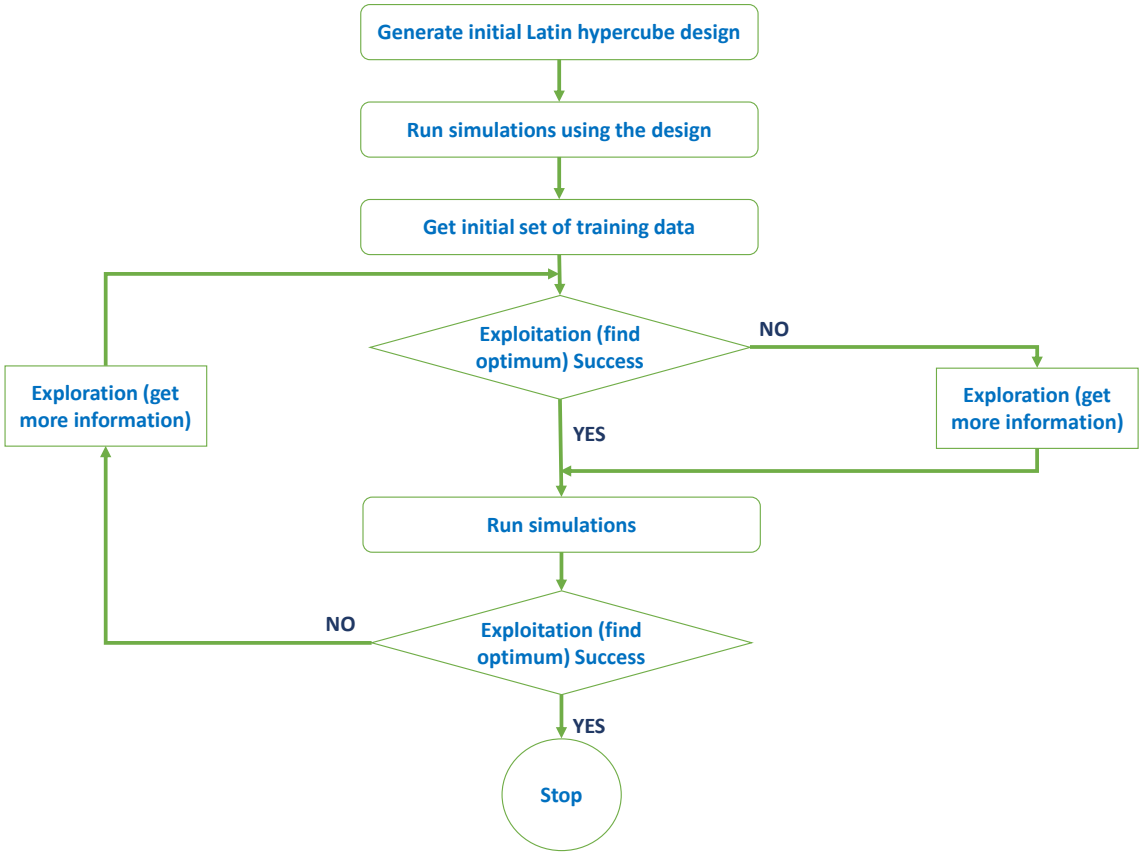

Figure 3-17 flow diagram of CMG DECE optimisation method [128]

The optimisation algorithm is based on the estimation of the posterior probability distribution of a parameter (x) that can be expressed by Bayes theorem [129] equation 3-19:

$$p(x) = \frac{P_o(x)L(x)}{\sum P_o(x)L(x)}$$ Equation 3-19

And $L(x) = e^{-Q(x)}$ Equation 3-20

Where p(x) is the posterior probability distribution function, $P_o(x)$ is the prior probability function which describes the uncertainty of parameter x, and L(x) is the likelihood function that depends on assumptions about modelling errors and measurement errors of the observation. Normal distribution for the errors as shown in equation 3-20 is the likely used expression for the likelihood function where Q(x) as the objective function (misfit).

Using the calculated average gas saturation profile (figure 3-8), the binary interaction coefficients between CO_2 and other hydrocarbon components were tuned to history match the constructed profile, and were set to be in the range between -1 and 1. In this history matching process, an optimisation was run to adjust the CO_2 interactions in order to reproduce the average gas saturation profile which has been expressed in the following equation:

$$Objective\ Function = \sum_{S_g=1}^{\mathrm{N_p}} \left[\mathrm{W_{S_g}} \left(S_g^{EXP} - S_g^{SIM} \right) \right]^2 \quad \text{Equation 3-21}$$

Then, by parameterising the binary interaction coefficients of CO_2 to the hydrocarbon components (i.e. methane and pseudo-components), the average gas (new phase) saturation formed throughout the core can be significantly affected as shown in figure 3-18. Other multi-flow parameters, such as relative permeability data, were preserved. As can be seen, the blue lines illustrate the different realisations of the binary interaction parameters, and thus indicate the high sensitivity of the gas saturation to the binary interaction coefficients, where the red line indicates the optimum solutions against the historical data presented in blue circles. Through this trial, fine-tuning the CO_2 binary interaction coefficient to hydrocarbon components has a great impact on whether the reservoir oil will dissolve the CO_2 from CW with or without the formation of a new gaseous phase.

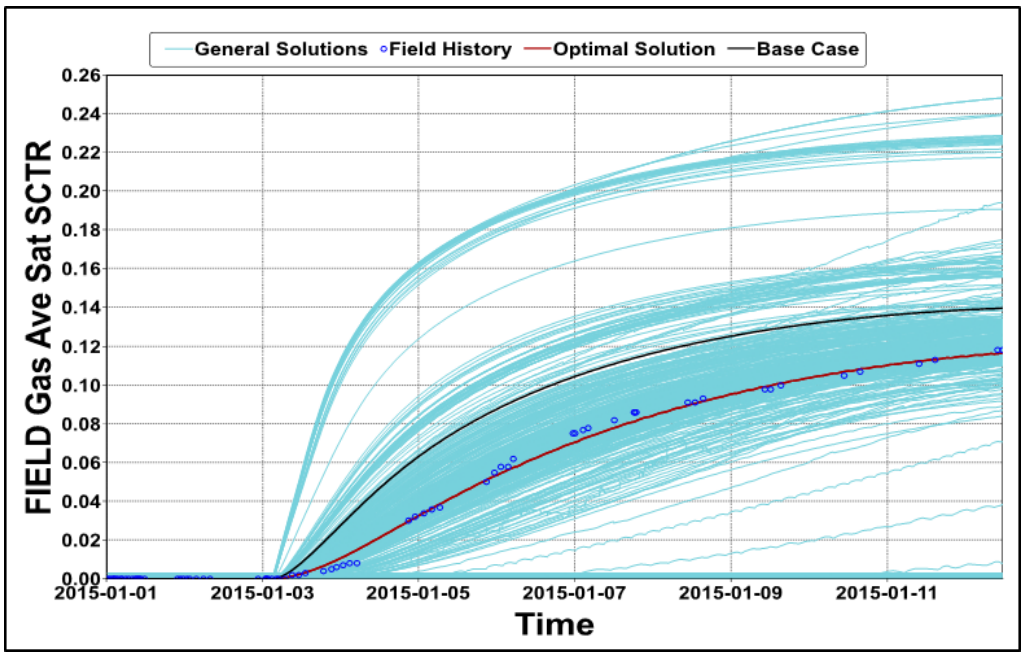

Figure 3-18 Different realisation of binary interaction coefficients in EOS to predict the average gas saturation by using assist history matching technique

3.7.3.2 Non-unique Solution

To a great extent, the proposed approach provides us an adjustment method to optimise the binary interaction coefficient (BIC) of CO_2 to hydrocarbon components in order to tune the EOS for modelling the formation of the new phase during CWI. On the other hand, this approach would deliver multiple sets of BICs that would be able to match the average new gaseous phase saturation, thus it leads to a non-unique solution. Table 3-6 shows four realisations of binary interaction coefficients, all suitable to modelling the average gas (new phase) saturation during CWI, and, as shown in Figure 3-16, the simulated average gas saturations for all realisations are matched with the calculated one. The compositional phase behaviour in the system, such as the solubility of CO_2 in oil, the concentration of CO_2 and hydrocarbon gases (e.g. methane), are affected by this lack of a unique solution, as well as the hydrocarbon densities and viscosities.

Table 3-7 Optimum realisations of BICs for a EOS tuned to match the calculated average gas saturation

Components	BIC CO_2			
	Case 1	Case 2	Case 3	Case 4
C_1 (HC)	0.105	0.105	0.105	0.105
C_7-C_{10} (HC)	0.21	0.31	0.30	0.35
C_{11}-C_{16} (HC)	0.16	0.18	0.15	0.13
C_{17}-C_{20+}(HC)	0.15	0.11	0.13	0.12
H_2O	1.46	1.44	1.63	1.42

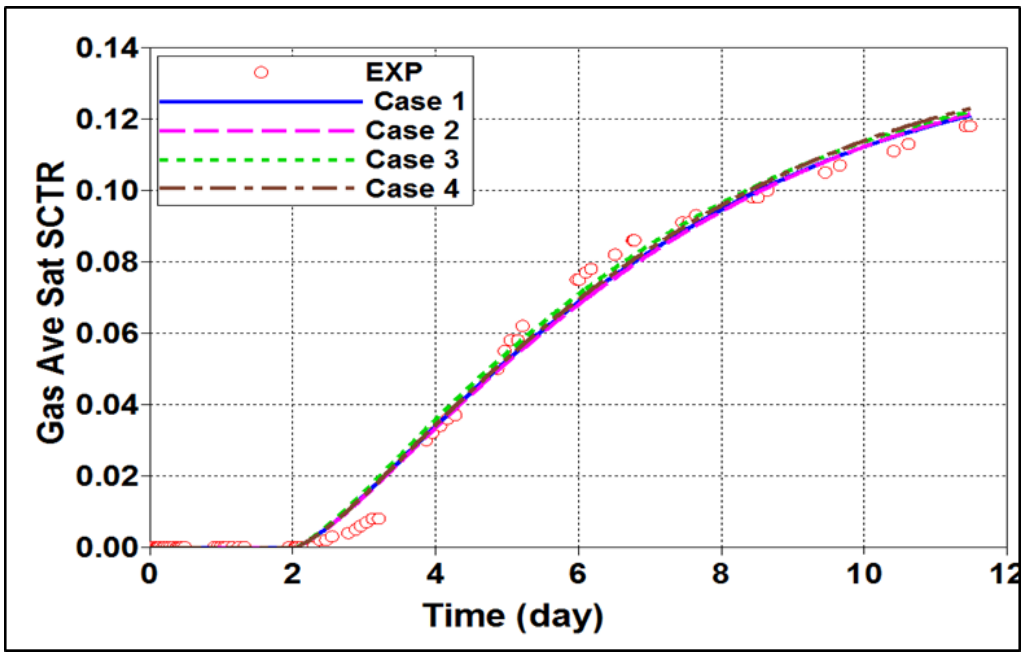

Figure 3-19 Simulated average gas saturation using the optimum BIC realisations

3.7.4 Simulation of Core Displacement Experiments

3.7.4.1 Tertiary CWI (Test No. 1)

To overcome this issue, oil-gas relative permeability has to be used in the optimisation procedure in addition to BICs to model the performance of CWI in tertiary mode. Initially, the secondary water injection period was history matched to obtain the water-oil relative permeability as a starting point, bearing in mind the fact that only two phases (oil and water) flow in the porous medium. It should be recognised, however, that the water-oil relative permeability curves that history match the experiment data provide non-unique solutions, due to the fact that most coreflood experiments are unsteady state tests. Unsteady state tests are popular because they require less time, effort and money than steady state tests to operate. Since in an unsteady state process, however, the permeability to oil reduces to zero while the permeability to water increases, these curves of relative permeability are not a unique function of saturation.

The Objective Function

Next, the objective function defined to cover more historical data during tertiary CWI to steer the optimizer in selecting proper input parameters values to minimise the objective function (misfit) as in the following expression:

$$M = \sum_{i=1}^{N_p}\left[W_{oi}\left(V_{oi}^{EXP} - V_{oi}^{SIM}\right)^2\right] + \sum_{i=1}^{N_p}\left[W_{BHIPi}\left(BHIP_i^{EXP} - BHIP_i^{SIM}\right)^2\right] + \sum_{i=1}^{N_p}\left[W_{Sgi}\left(S_{gi}^{EXP} - S_{gi}^{SIM}\right)^2\right] + \sum_{i=1}^{N_p}\left[W_{Soi}\left(S_{oi}^{EXP} + S_{oi}^{SIM}\right)^2\right]$$ Equation 3-22

The observation data include cumulative oil volume, bottom-hole injection pressure (BHIP), average oil and gas saturation, resulting in Np = 57 measurements points of each observation data during experiment time. Subscript *i* indicates the time of the measurement while the other variables are as follow:

- M is the objective function (misfit)
- W_{oi}, W_{BHIPi}, W_{sgi} and W_{soi} are the weight factors applied to oil volume, BHIP, gas and oil saturation meaurements at the time *i*.
- V_{oi}^{EXP}, $BHIP_i^{EXP}$, S_{gi}^{EXP} and S_{oi}^{EXP} are the observed value of cumulative oil volume, BHIP, gas and oil saturation at time *i*.
- V_{oi}^{SIM}, $BHIP_i^{SIM}$, S_{gi}^{SIM} and S_{oi}^{SIM} are the simulated value of cumulative oil volume, BHIP, gas and oil saturation at time *i*.

Uncertainty Parameters

The 15 uncertain parameters in the tertiary CW injection model are binary interaction coefficients of CO_2 and hydrocarbon components which are BIC CO_2-C_1, BIC CO_2-C_7-C_{10}, BIC CO_2-C_{11}-C_{16}, and BIC CO_2-C_{17}-C_{20+} in addition to L.E.T oil-gas relative permeability correlation which are Soirg, Sgcrit, Krgcl and gas and oil LET exponents (Lg, Eg, Tg, Log, Eog, and Tog). Accordingly, the CO_2 BIC's are the numerical factors forming a set that tunes the cubic EOS to allocate a specific transfer of CO_2 from CW to reservoir oil to form a gaseous phase. After that, the oil and gas two-phase flow and W-O-G three-phase flow would be reproduced through the adjustment of oil-gas relative permeability parameters.

The relative permeability curves of water-oil and oil-gas were tuned by history matching the experimental recovery and pressure drop data. The L, E and T parameters in LET correlations (Equations 3-23 through to 3-26) [130] are empirical parameters that offer more flexibility in accommodating different shapes of relative permeability curve in core

displacement experiments, unlike the shortcomings of Corey correlations to provide flexibility to construct appropriate relative permeability shapes.

$$k_{rw} = k_{rwiro}\left[\frac{\left(\frac{S_w - S_{wcrit}}{1 - S_{wcrit} - S_{oirw}}\right)^{Lw}}{\left(\frac{S_w - S_{wcrit}}{1 - S_{wcrit} - S_{oirw}}\right)^{Lw} + E_w\left(\frac{1 - S_w - S_{oirw}}{1 - S_{wcrit} - S_{oirw}}\right)^{Tw}}\right] \quad \text{Equation 3-23}$$

$$k_{row} = k_{rocw}\left[\frac{\left(\frac{1 - S_w - S_{orw}}{1 - S_{wcon} - S_{orw}}\right)^{Low}}{\left(\frac{1 - S_w - S_{orw}}{1 - S_{wcon} - S_{orw}}\right)^{Low} + E_{ow}\left(\frac{S_w - S_{wcon}}{1 - S_{wcon} - S_{orw}}\right)^{Tow}}\right] \quad \text{Equation 3-24}$$

$$k_{rg} = k_{rgc}\left[\frac{\left(\frac{S_g - S_{gcrit}}{1 - S_{gcrit} - S_{wcon} - S_{oirg}}\right)^{Lg}}{\left(\frac{S_g - S_{gcrit}}{1 - S_{gcrit} - S_{wcon} - S_{oirg}}\right)^{Lg} + E_g\left(\frac{1 - S_g - S_{oirg} - S_{wcon}}{1 - S_{gcrit} - S_{oirg} - S_{wcon}}\right)^{Tg}}\right] \quad \text{Equation 3-25}$$

$$k_{rog} = k_{rogcg}\left[\frac{\left(\frac{1 - S_g - S_{wcon} - S_{org}}{1 - S_{gcon} - S_{wcon} - S_{org}}\right)^{Log}}{\left(\frac{1 - S_g - S_{wcon} - S_{org}}{1 - S_{gcon} - S_{wcon} - S_{org}}\right)^{Log} + E_{og}\left(\frac{S_g - S_{gcon}}{1 - S_{gcon} - S_{org} - S_{wcon}}\right)^{Tog}}\right] \quad \text{Equation 3-26}$$

In CMOST, the CMG DECE optimiser applied to perform 1000 simulation runs. Figure 3-20 shows the flow diagram of the assisted-history matching of tertiary CWI experiment. The minimisation of the objective function continued until a cumulative error of less than 5% achieved. The analysis of the method results in the main and interaction effects of each input parameters with other parameters to achieve the simulation requirement. The analysis shows that BIC_CO_2_C_{17}_C_{20+} had the most effect in tuning the EOS to facilitate the transfer of CO_2 into the oil phase and form the third phase. The binary interaction coefficients had main effects and less interaction with other parameters, whereas the oil-gas relative permeability factors show more interaction effect to reproduce the flow phase of resident fluids. For example, the BIC_CO_2_C_1, BIC_CO_2_C_{11}_C_{16} and BIC_CO_2_C_{17}_C_{20+} input parameters are more effective in history-matching the average gas and oil saturation and bottom-hole injection pressure, whereas Soirg and Sgcrit are influential in simulating the cumulative oil production as shown in effectiveness matrix in table 3-8.

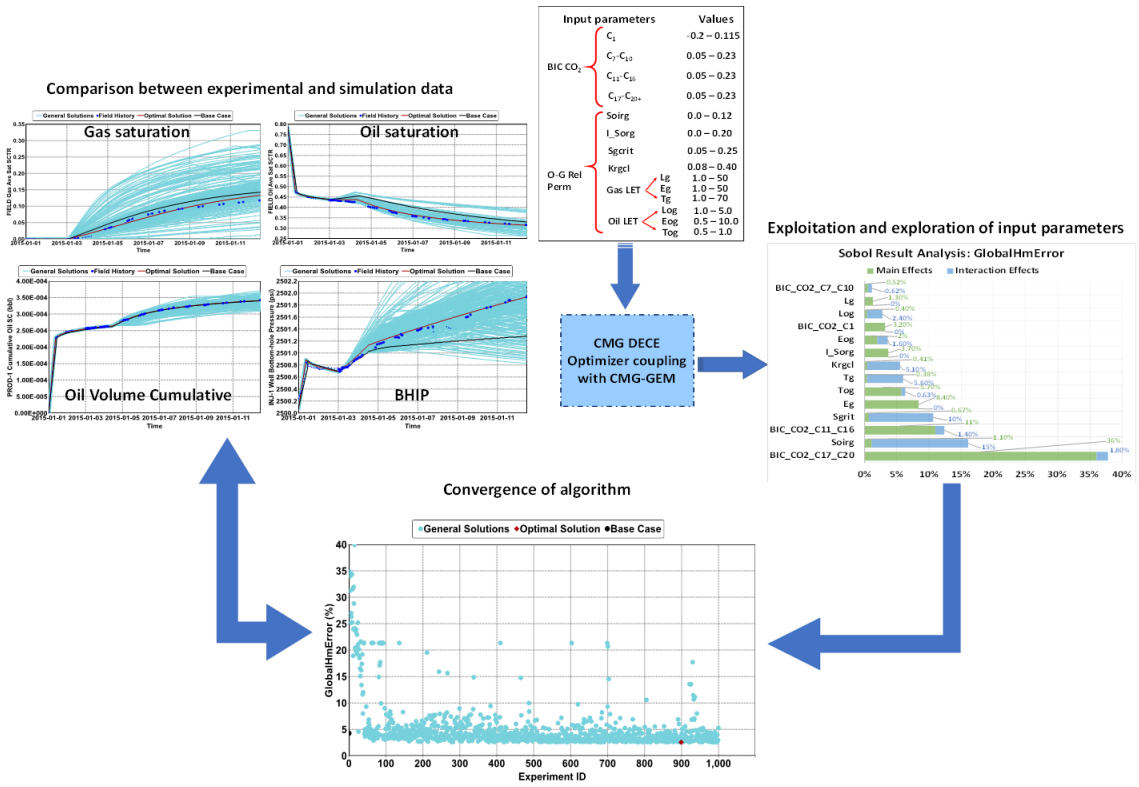

Figure 3-20 flow diagram of assisted-history matching for tertiary CWI core displacement test no. 1

Table 3-8 effectiveness matrix of input parameters on objective functions of tertiary CWI core displacement test no. 1

Input Parameters	Objective Function				
	GlobalHmError	Gas Saturation	Oil Saturation	Cumulative Oil Production	BHIP
$BIC\_CO_2\_C_1$	**15.7%**	**34.9%**	3.1%	6.3%	**18.5%**
$BIC\_CO_2\_C_7\_C_{10}$	1.1%	5.7%	6.1%	2.3%	1.5%
$BIC\_CO_2\_C_{11}\_C_{16}$	**12.4%**	1.9%	**15.0%**	8.5%	8.9%
$BIC\_CO_2\_C_{17}\_C_{20}$	**37.8%**	**38.3%**	**55.9%**	**32.0%**	**61.1%**
Soirg	**16.1%**	0.1%	0.0%	**21.1%**	1.5%
I_Sorg	3.7%	1.9%	3.3%	7.7%	**11.8%**
Sgcrit	**10.7%**	2.3%	7.4%	**13.3%**	3.6%
Krgcl	5.5%	0.1%	0.1%	7.6%	1.8%
Lg	1.3%	0.1%	0.9%	1.1%	2.1%
Eg	8.4%	0.1%	0.0%	9.6%	3.1%
Tg	6.0%	3.0%	2.2%	7.0%	1.8%
Log	2.8%	0.1%	1.2%	3.7%	1.4%
Eog	3.6%	1.4%	1.4%	5.3%	2.5%
Tog	6.3%	4.9%	2.7%	4.3%	1.7%

It has been noticed that the binary interaction coefficient between CO_2 and methane shifts toward negative values in order to fulfil the requirement to match the experimental data. Table 3-9 represents the final binary interaction coefficients between CO_2, H_2O and

hydrocarbon compounds. Although the binary interaction coefficients (k_{ij}) for any cubic EOS could be in the range between 1 to -1 as a result of using van der Waals one fluid parameter (vdW1f) mixing rules equations 3-5 and 3-6, the mixing rules themselves depend on the composition of the mixture and randomly mixing the molecules of that mixture. Two interaction parameters (k_{ij} and l_{ij}) are often needed for complex polar systems, with k_{ij} being by far the most important one and typically fitted to the phase equilibrium of non-polar mixtures. The great success of cubic EOS composed with the vdW1f mixing rules lies in their ability for fast computation and precise representation of low and high pressure vapour-liquid equilibria for mixtures of hydrocarbon compounds and mixtures of hydrocarbons with gases (e.g. methane, N_2, CO_2, and H_2S) which are important in the oil and gas industry. For mixtures that contain strongly polar compounds such as water, however, they do not yield reasonable vapour-liquid equilibrium results [131]. Usually, a positive or negative k_{ij} means deviation to ideally i.e. that it is overestimating or underestimating the attractive energy between the two molecules (CO_2 and C_1). The mass transfer of CO_2 from CW to the oil phase, and the formation of the gas phase that contains mainly methane, results in a negative BIC between CO_2 and methane in the EOS used to model the expulsion of methane to form a new phase. This means that the resulting gas phase would be immiscible and trapped in the oil-rich phase, causing an increased in the differential pressure across the core. In other words, the sign of BIC between CO_2 and C_1 might have a role in the degree of miscibility between the vapour and liquid phases.

Table 3-9 Binary interaction coefficients between CO_2, H_2O and hydrocarbon components

Components	CO_2	C_1	C_2-C_3	iC_4-C_6	C_7-C_{10}	C_{11}-C_{16}	C_{17}-C_{20+}	H_2O
CO_2	**zero**	-0.167	0.125	0.115	0.1316	0.1943	0.1696	1.29
C_1	-0.167	**zero**	0.00472	0.01204	0.02041	0.03332	0.04777	0.49
C_2-C_3	0.125	0.00472	**zero**	0.00172	0.00566	0.01345	0.02349	0.2
iC_4-C_6	0.115	0.01204	0.00172	**zero**	0.00115	0.00563	0.01273	0.2
C_7-C_{10}	0.1316	0.02041	0.00566	0.00115	**zero**	0.00171	0.00630	0.2
C_{11}-C_{16}	0.1943	0.03332	0.01345	0.00563	0.00171	**zero**	0.00147	0.2
C_{17}-C_{20+}	0.1696	0.04777	0.02349	0.01273	0.00630	0.00147	**zero**	0.2
H_2O	1.296	0.4907	0.2	0.2	0.2	0.2	0.2	**zero**

Using the tuned EOS, after modelling the saturation of the new phase and the core model described earlier, the secondary water injection period was history matched to obtain the water-oil relative permeability as a starting point, bearing in mind the fact that only two phases (oil and water) flow in the porous medium. It should be recognised, however, that

the water-oil relative permeability curves that history match the experiment data provide non-unique solutions, due to the fact that most coreflood experiments are unsteady state tests. Unsteady state tests are popular because they require less time, effort and money than steady state tests to operate. Since in an unsteady state process, however, the permeability to oil reduces to zero while the permeability to water increases, these curves of relative permeability are not a unique function of saturation.

Having performed a series of history matching attempts, the experimental data could be reasonably reproduced by simulation to obtain oil-gas relative permeability curves having in mind the relationship to the formation of the new phase during CWI and the three-phase flow regime in a porous medium as shown in final mismatch of figures 3-21 through to 3-26. Worth to mention that the cumulative oil volume converted to percentage of oil recovery through the division of original oil in place and the bottom-hole injection pressure subtracted by flowing pressure of 2500 psi to calculate the differential pressure across the core. Utilising the relationship between the reduction in oil saturation and the increase in new gas phase saturation, the simulated oil recovery and average oil saturation in the model are in good agreement with the experimental data, as shown in figures 3-21 and 3-22, respectively. The period at the beginning of the injection of CW during which oil is not produced is when the CO_2 is diffusing into the brine which was injected in secondary waterflood. One of the main assumptions in using this approach is that most of the oil recovery during CWI is a result of the formation of a new gas phase.

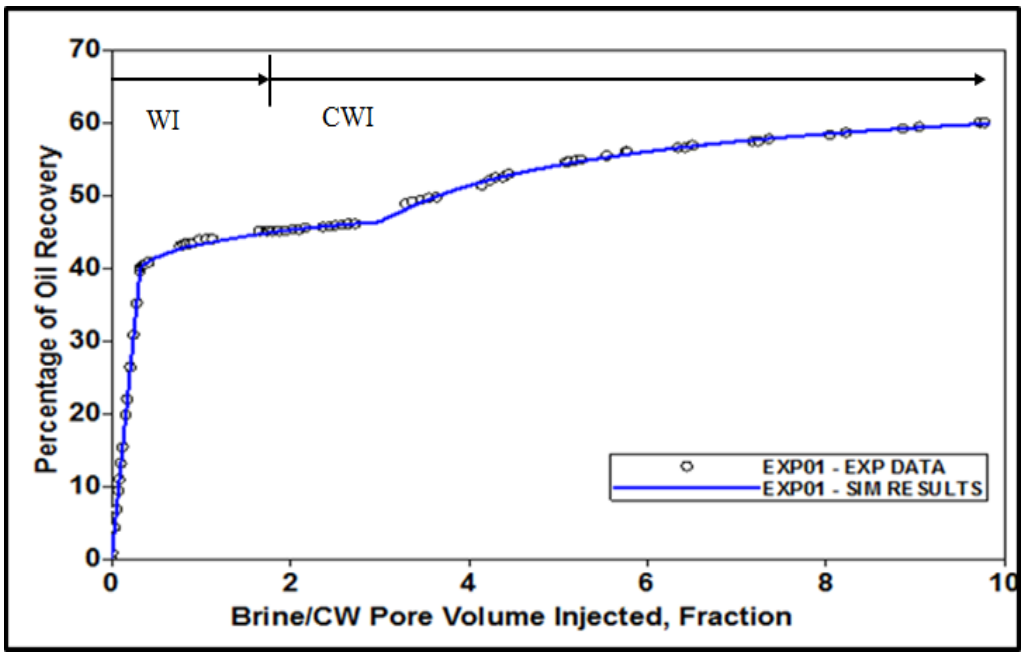

Figure 3-21 Comparison of experimental and simulated oil recovery during secondary WI and tertiary CWI core displacement test no. 1

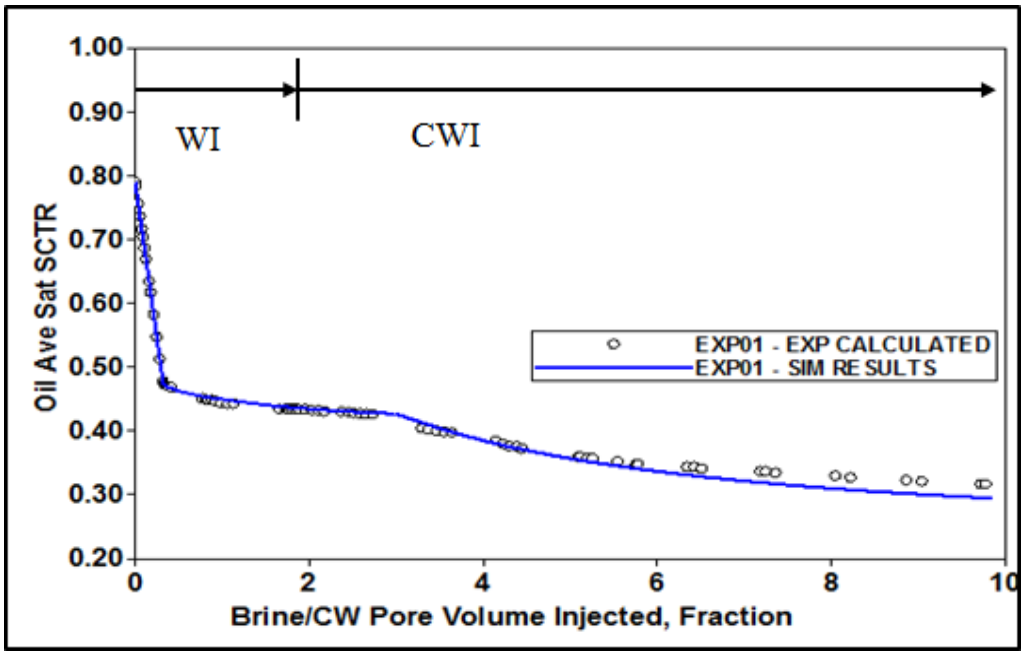

Figure 3-22 simulated average oil saturation against the calculated one during secondary WI and tertiary CWI core displacement test no. 1

Figures 3-23 and 3-24 show the ratio of cumulative production of other fluids (gas and water) to cumulative oil production in the simulation model and coreflood experiment. The formation of the gas phase during CWI and the increase in its volume is slightly reduced by the flow of water in the porous medium, whereas the simulated cumulative gas production starts to kick off approximately 1 PV earlier than the cumulative gas production measured in the coreflood experiments. Although the equation of state was

tuned to produce the average gas saturation that was calculated during tertiary CWI, the produced gas in the simulation model was faster than that in the experiment, indicating the mass transfer of hydrocarbon components into the gas phase was sufficient to lead to a larger gas saturation than what was estimated.

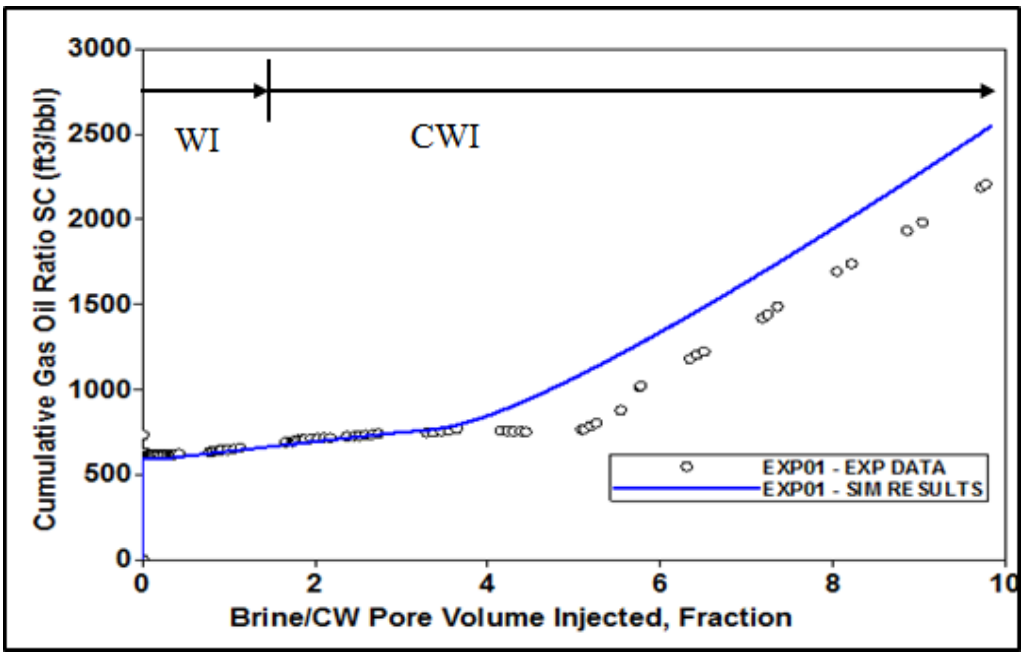

Figure 3-23 Comparison of simulated cumulative GOR to the cumulative GOR measured when performing test no. 1

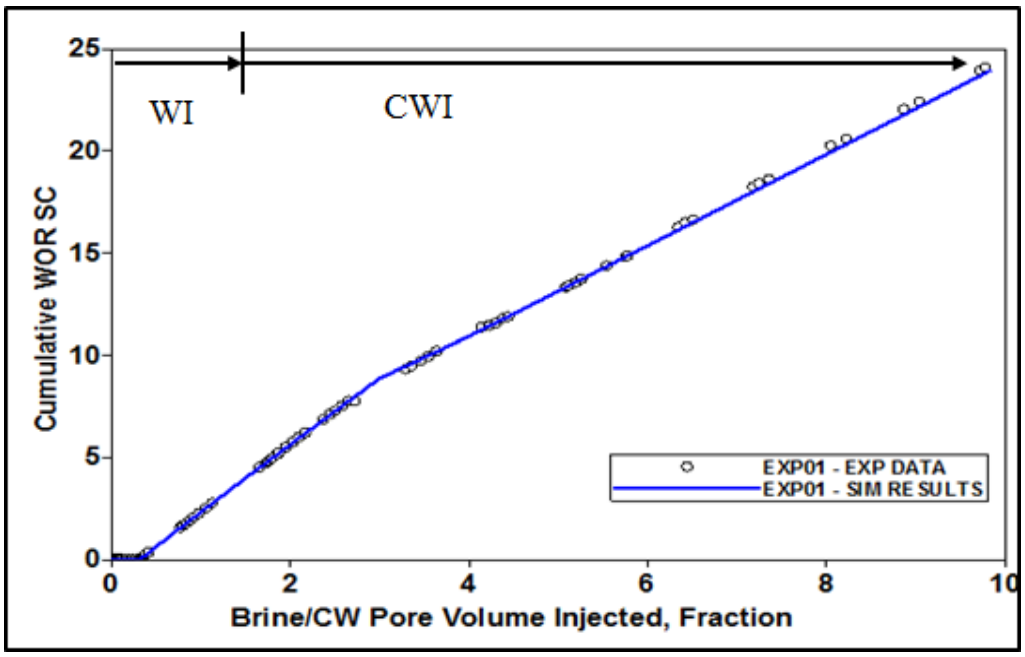

Figure 3-24 Comparison of simulated cumulative WOR to the cumulative WOR measure when performing test no. 1

The simulated differential pressure follows the gradually increasing slope of the experimental data in tertiary mode, which is due to the formation of the third phase and the consequent increase in the resistance of water to flow, as shown in figure 3-25. The simulated average gas saturation representing the formation of the third phase in figure 3-26 is overestimated, most probably due to the gas phase volume predicted by the cubic equation of state, which also led to the under-estimation the average oil saturation. Generally, however, the proposed method captures the main physics observed in micromodel experiments, namely that the formation of the new (gas) phase is the predominant mechanism involved in recovering additional oil during CWI. Also, the reduction in oil saturation is a function of gas saturation where the k_{rg} would remain small and close to trapped gas saturation. The injection of carbonated water in a live oil system could be considered to be a typical in-situ WAG injection process with high trapped gas saturation.

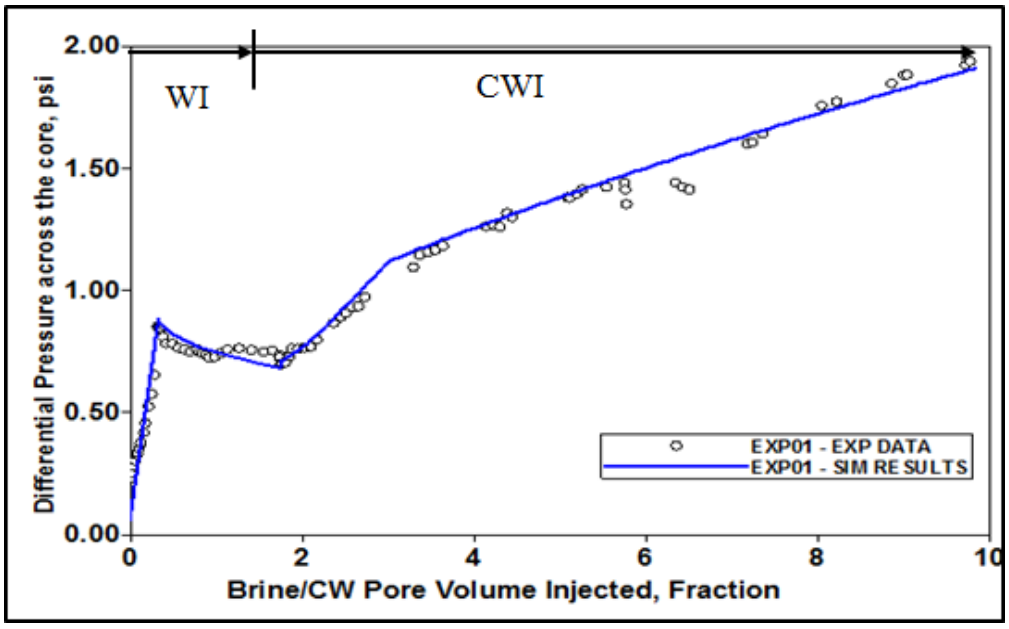

Figure 3-25 the simulated differential pressure in the core against the differential pressure measured during test no.1, showing a gradual increase as a result of the formation of the third phase

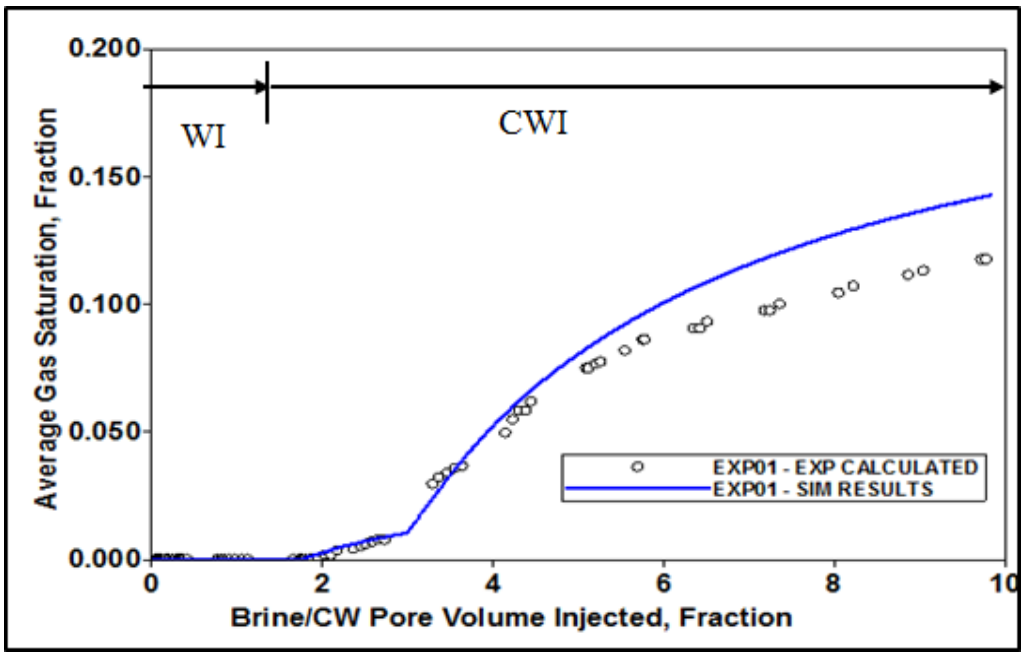

Figure 3-26 over-estimation of the simulated average gas (third phase) saturation compared to the saturation during CWI in test no. 1

The obtained water-oil and oil-gas relative permeability curves from history matching the experimental data considering the reduction of minimal oil saturation as a function of the increase in the new gaseous phase saturation, are illustrated in Figure 3-27. Tables 3-10 and 3-11 represent water-oil and oil-gas relative permeability end points, along with the LET correlation parameters that were obtained during the history matching process. According to Craig's rule of thumb on qualitatively classifying the water-wet wettability of the core based on water-oil relative permeability curves [132], end point oil relative permeability at connate water saturation ($k_{ro}|_{Swi}$) should be greater than 0.8, the connate water saturation greater than 0.2, the saturation at which the relative permeabilities of oil and water are equal should be greater than 0.5, and the end point of water's relative permeability at residual oil saturation ($k_{rw}|_{Sorw}$) should be less than 0.3. Then, based on Craig's criteria, figure 3-27A might be representing the water-oil relative permeability of a weakly water-wet core. A high value of critical gas saturation (16.2 %PV) was obtained in the simulation, which is in agreement with the direct pore-scale observations that the existence of the new phase would create apparent oil swelling which reconnects the neighbouring oil blobs and causing them to be mobilised. The estimated oil-gas relative permeability curves show clear differences compared to values obtained in reported conventional gas injection experiments. During CWI, the formed gas which is the non-wetting phase, has more effect where its k_{rg} is much lower than values obtained from gas injection experiments. This indicates the sharp reduction in gas mobility when the formed gas starts to mobilise. Also, the k_{rog} is affected by the population of gas bubbles in the

porous medium. Both Grattoni et al. [133] and Egermann et al. [134] explained similar behaviour in their study of critical gas saturation and relative permeability during depressurisation. They concluded that relatively high critical gas saturation (S_{gc}) and very low values of k_{rg} are obtained when solution gas is released from a waterflooded reservoir.

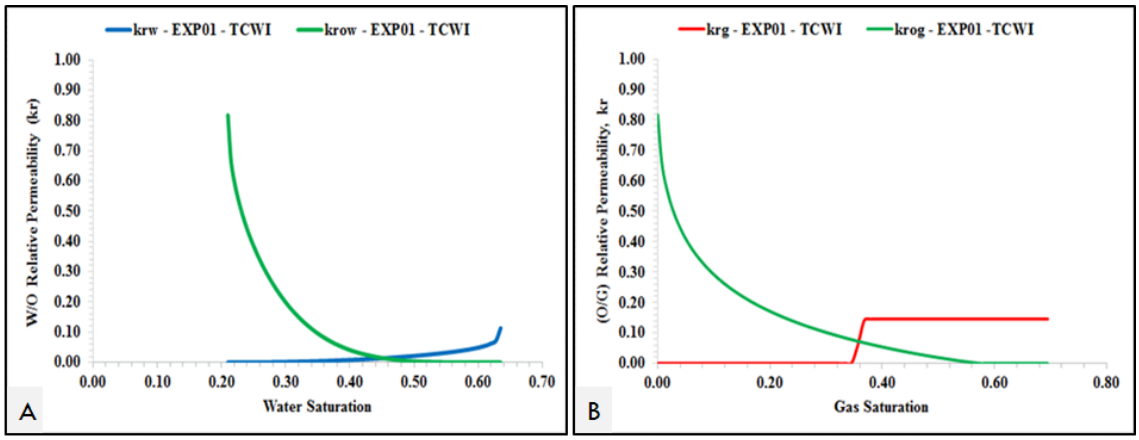

Figure 3-27 the resulting relative permeability curves from matching SWI & TCWI core displacement test no. 1 (right) water-oil relative permeability and (left) oil-gas relative permeability

Table 3-10 Obtained water-oil relative permeability end points and LET correlation exponents

S_{wi}	S_{wcrit}	S_{oirw}	S_{orw}	k_{rwiro}	k_{rocw}
0.210	0.210	0.3645	0.3645	0.113	0.817
L_w	**Ew**	**Tw**	**Low**	**Eow**	**Tow**
2.05	3.45	0.42	3.695	3.72	0.655

Table 3-11 Obtained oil-gas relative permeability end points and LET correlation exponents

S_{oirg}	S_{org}	S_{gcon}	S_{gcrit}	k_{rogcg}	k_{rgc}
0.095	0.2135	0	0.162	0.817	0.146
L_g	**Eg**	**Tg**	**Log**	**Eog**	**Tog**
30.539	36.38	58.42	1.098	4.8735	0.694

3.7.4.2 Secondary CWI (Test No. 2)

The objective of this simulation practice is to utilising the tuned PR-EOS and relative permeability data estimated from the tertiary CWI test no.1 to predict the carbonated water injection performance in secondary mode numerically, and then to compare the results with the experimental data. Although, the prediction shows an increase in oil recovery and differential pressure across the core, as shown in figure 3-28, it under-estimates the oil recovery at the CW breakthrough and, subsequently, the total oil recovery, and over-estimates the differential pressure across the core. These

discrepancies in the predicted results could be due to the influence of the formation of the new phase in the saturated oil, since oil swelling apparently occurs causing an adjustment in the relative permeability of the oil.

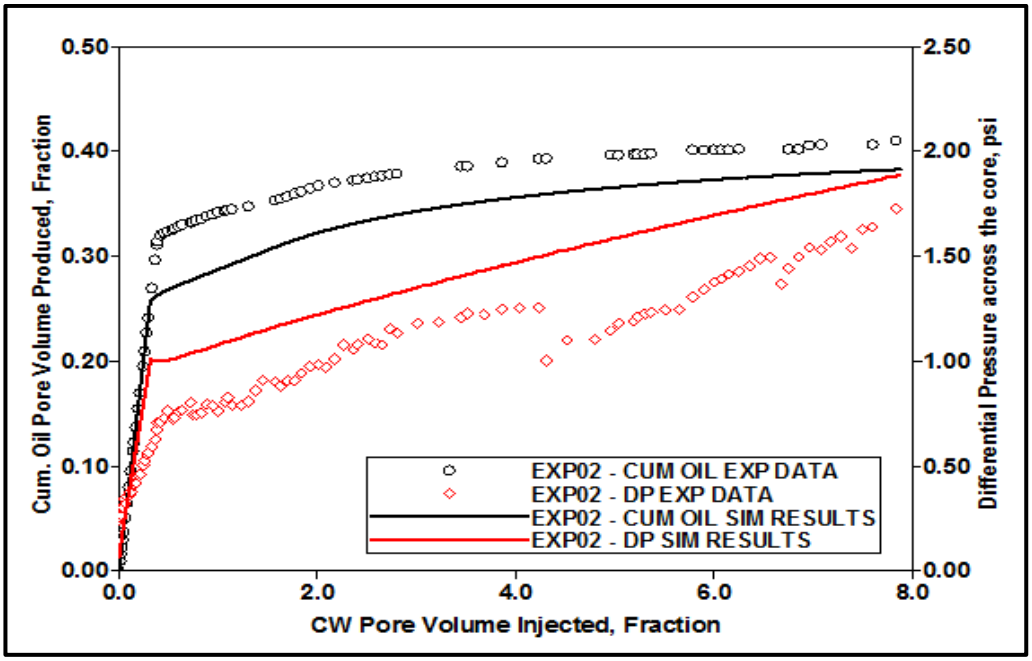

Figure 3-28 Predicted cumulative oil and differential pressure when simulating secondary CWI in test no.2 using the tuned EOR and relative permeability curves obtained from the previous test, set against the data measured experimentally in test no. 2

The Objective Function

Another history matching trial is considered to evaluate the effect of the formed gas phase on oil mobility by adjusting only the water-oil relative permeability parameters while keeping the tuned EOS and oil-gas relative permeability data the same. During the assisted-history matching process, the cumulative oil and water volumes in addition to bottom-hole injection pressure formed the objective function where its global error to be minimised as expressed in the following equation:

$$M = \sum_{i=1}^{N_p}\left[W_{oi}\left(V_{oi}^{EXP} - V_{oi}^{SIM}\right)^2\right] + \sum_{i=1}^{N_p}\left[W_{wi}\left(V_{wi}^{EXP} - V_{wi}^{SIM}\right)^2\right] + \sum_{i=1}^{N_p}\left[W_{BHIPi}\left(BHIP_i^{EXP} - BHIP_i^{SIM}\right)^2\right] \quad \text{Equation 3-27}$$

Where M is the global objective function that should be minimised and the other variables are as follow:

- W_{oi}, W_{sgi}, and W_{BHIPi} are the weight factors applied to cumulative oil and water volume and BHIP meaurements at the time *i*.

- V_{oi}^{EXP}, V_{wi}^{EXP} and $BHIP_i^{EXP}$ are the observed value of cumulative oil and water volumes and BHIP at time *i*.

- V_{oi}^{SIM}, V_{wi}^{SIM} and $BHIP_i^{SIM}$ are the simulated value of cumulative oil and water volumes and BHIP at time *i*.

A total of Np = 35 points selected from cumulative oil volumes and bottom-hole injection pressure during the experiment time to be included in the observation data. Whereas only 7 observation points formed the cumulative water volumes in order to capture the exact water breakthrough time and volume.

Uncertainty Parameters

LET water-oil relative permeability correlation (as shown equations 3-23 and 3-24) which are Soirw, krwiro, and water and oil LET exponents (Lw, Ew, Tw, Low, Eow, and Tow) are the only uncertain parameters in the secondary CWI core displacement model. The CMG DECE optimiser utilized to execute 1500 simulation runs as illustrated in the convergence of the algorithm in figure 3-29. The global error was initially small only 2.0% due to pre-tuned EOS and the calibrated oil-gas relative permeability from the previous test no. 1 and the global error of objective function reduced to less than 0.2%.

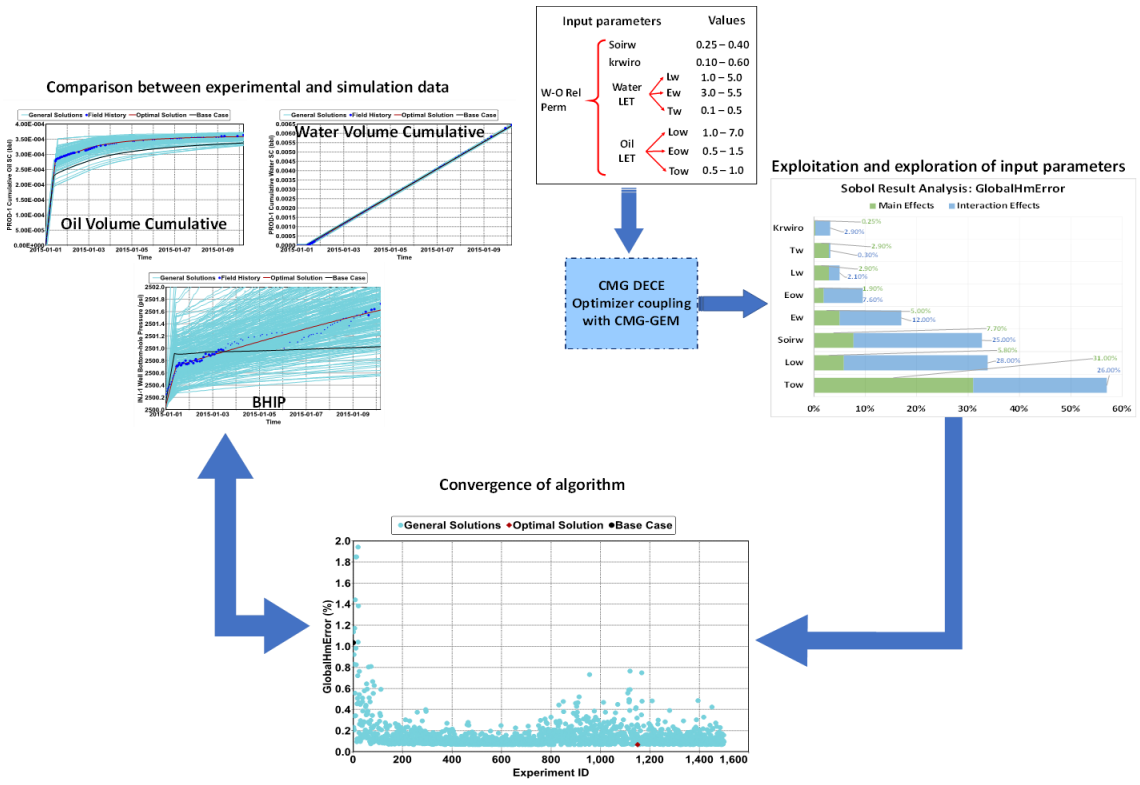

Figure 3-29 flow diagram of assisted-history matching for secondary CWI core displacement test no. 2

The input parameters are interactive with each other as shown in blue bars of exploitation and exploration of input parameters in figure 3-29, more than its main effect in the objective function as clarified in the green bars of the same plot. For example, Soirw is 8% effect in global history match error, and 25% interact with other input parameters to reduce the difference between simulation and observed data. Table 3-12 exhibits that the cumulative oil volume is the primary driver of minimising the global error of the objective function, while the simulated bottom-hole injection pressure matched with historical data through a slight adjustment in water relative permeability parameters. The most significant optimisation occurs in the input parameters that related to oil relative permeability which are Soirw, Low, and Tow as a result of the formation of the gas phase in oil that allows effectively the flow of oil by enlarging the oil volume and reducing the flow of water.

Table 3-12 overall effectiveness matrix of uncertain parameters on objective function variables of secondary CWI core displacement test no. 2

Input Parameters	Objective Function			
	GlobalHmError	Cumulative Oil Volume	Cumulative Water Volume	BHIP
Soirw	**32.7%**	**32.0%**	**23.7%**	1.9%
krwiro	3.2%	4.4%	7.5%	**19.6%**
Lw	5.0%	2.8%	2.8%	**42.3%**
Ew	**17.0%**	**10.8%**	9.2%	**27.4%**
Tw	3.2%	0.0%	1.4%	8.9%
Low	**33.8%**	**34.6%**	**39.0%**	0.5%
Eow	9.5%	8.7%	6.3%	0.3%
Tow	**57.0%**	**65.0%**	**47.0%**	**10.8%**

Figures 3-30 through to 3-33 demonstrate the simulation results in respect to oil recovery, average oil saturation, cumulative GOR, cumulative WOR and differential pressure across the core as compared with the data measured experimentally during secondary CWI, exhibiting a good match. The steady and gradual increase of oil recovery after CW breakthrough at 0.383 PV is flawlessly simulated, which indicates that the selection of the three-phase oil relative permeability function is good and that the estimation of the oil-gas relative permeability curve obtained in previous tertiary CWI experiment is appropriate. The experimental average oil saturation is calculated by subtracting the cumulative oil produced at test conditions (p_{test} = 2500 psi and T_{test} = 100 °F) from the original reservoir oil in place, divided by the core pore volume at the same conditions. The assumption that is implied in this calculation is that the effect of normal oil swelling is minimal. Then, the simulated oil saturation compared with the one which was calculated from the experimental data to act as another calibration of how efficient the tuned EOS and estimated oil-gas relative permeability. Remarkably, the average simulated oil saturation is in good agreement with the oil saturation calculated from experimental data, which indicates that the existence of the third phase does indeed act as the main driver and diverter of water flow for further oil production that could not be produced by conventional water flooding.

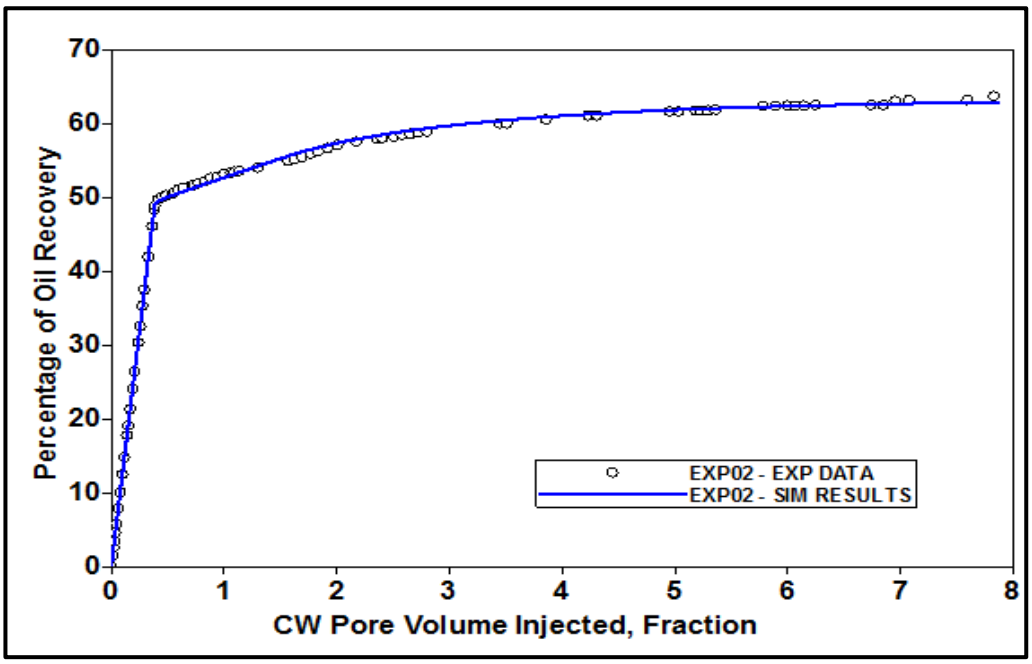

Figure 3-30 Comparison between measured and simulated oil recovery for secondary CWI test no. 2

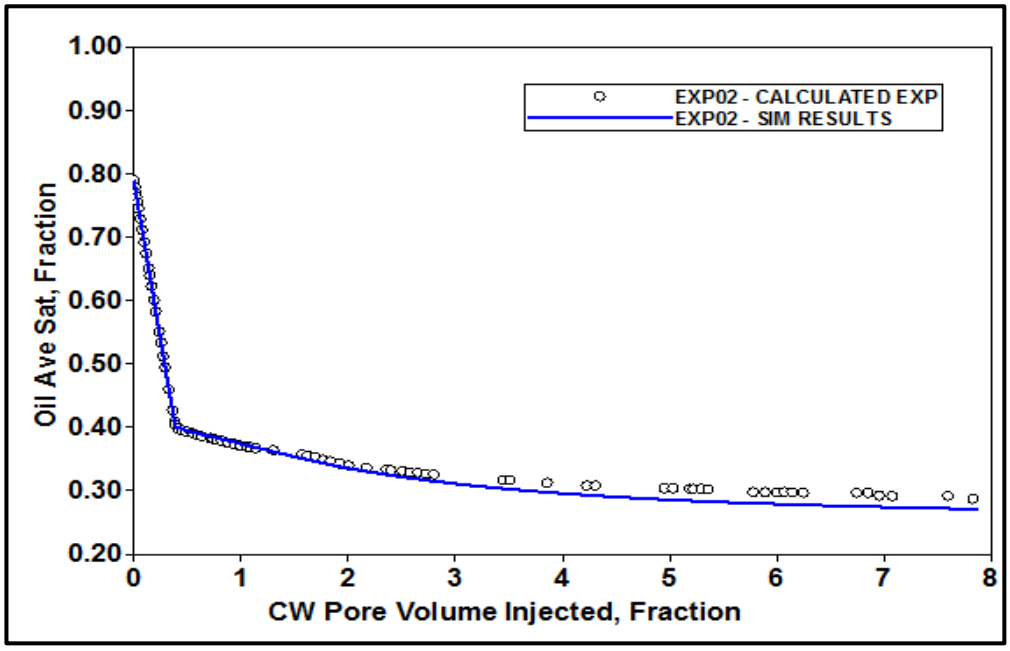

Figure 3-31 Slight reduction in simulated oil saturation in comparison to the oil saturation calculated from the performance of secondary CWI in test no. 2

Furthermore, initially, the conventional waterflooding mechanisms are the predominant process in oil recovery, with some contribution from CO_2 mass transfer and its subsequent mechanisms in improving oil production before the CW breakthrough. Then, the CW mechanisms, such as oil swelling and the existence of the third phase, leads to more oil recovery, as can be observed through the steady increase in cumulative GOR (the ratio between cumulative gas to cumulative oil volumes) after CW breakthrough, as shown in figure 3-32. Moreover, the continuing increase in differential pressure after CW

breakthrough, as illustrated in figure 3-33, due to the three-phase flow regime and the trapping mechanism of the gas phase, was reproduced in the simulation model and compared against the differential pressure measured when performing the secondary CWI test.

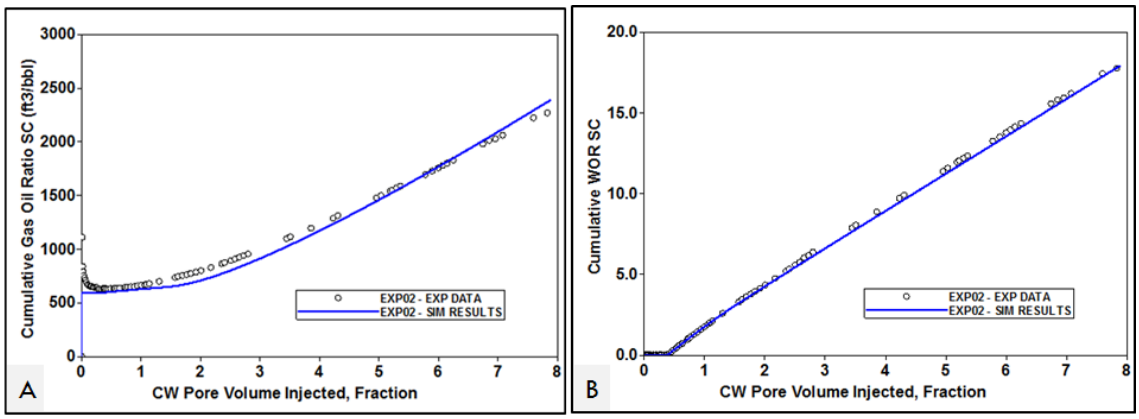

Figure 3-32 (Left) Comparison of simulated cumulative GOR to the cumulative GOR measured when performing test no. 2 (Right) Comparison of simulated cumulative WOR to the cumulative WOR measured during secondary CWI in test no. 2

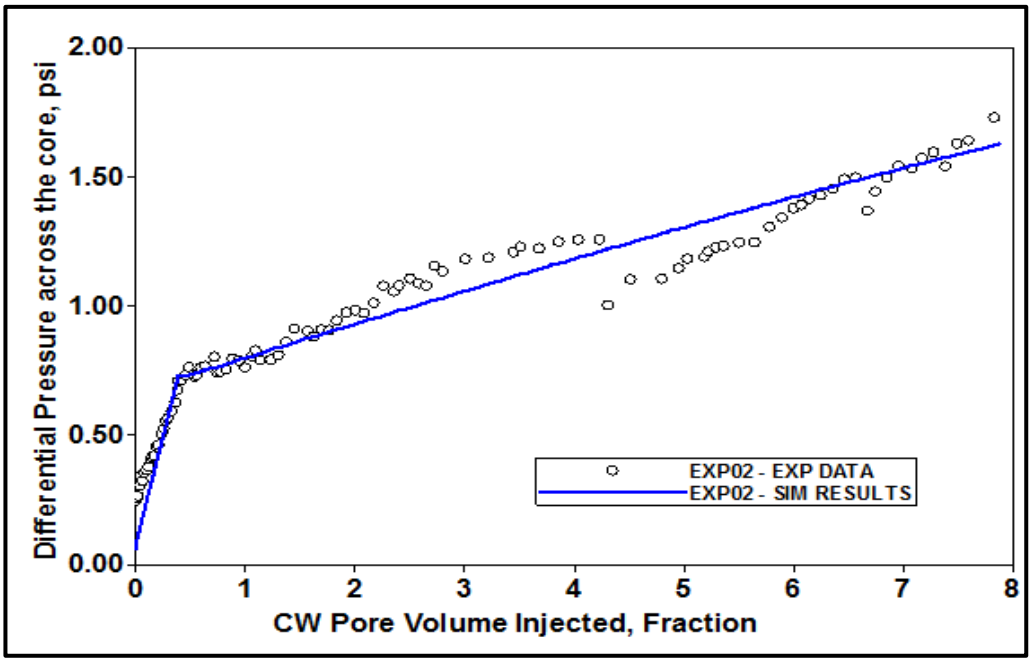

Figure 3-33 the simulated differential pressure against measured differential pressure across the core in test no.2, showing a gradual increase as a result of the formation of the third phase

In the history matching of the previous experiment, i.e. tertiary carbonated water injection, a single set of relative permeability curves could reproduce the experimental data from the secondary and tertiary sequences, which implies that behaviour of the water-oil relative permeability does not change when it was switched to tertiary CWI. In

the case of secondary CWI (test no. 2), however, a different water-oil relative permeability curve was obtained from history matching the secondary core displacement test, as shown in figure 3-34. The water relative permeability for SCWI ($k_{rw|CWI}$) is slightly lower than $k_{rw|WI}$ due to the creation of the third phase at an early stage in the secondary CWI. Additionally, the formation of the gas phase within the oil, and its subsequent three-phase flow, increases the oil's relative permeability and reduces the residual oil saturation (S_{or}), which causes the saturation function to switch to a more water-wet scenario. Table 3-13 represents the water-oil relative permeability end points and LET exponents as estimated from history matching with the SCWI experiment. Three possible causes could contribute in this discrepancy in the water-oil relative permeability, namely:

1. In the unsteady state displacements, the reliable range of the relative permeability curve can be estimated from the after breakthrough information. During tertiary CWI, the gaseous phase would form after S_{orw} to waterflood was established, while in the secondary CWI, where carbonated water meets resident oil at a high oil saturation, the three-phase flow occurs at early stages of the carbonated water injection. This means that the creation of three-phase flow conditions would be different in these scenarios, and this may be the main reason for the difference between the secondary and tertiary CWI experiments. It has been observed, however, that the formation of the third phase during secondary CWI would not change the breakthrough time, nor lead to the recovery of more oil than conventional waterflooding as clarified by Seyyedi et al. [81] and Mahzari et al. [73].

2. The water-oil relative permeability in secondary CWI was shifted towards a more water wet environment than that in tertiary CWI. This may be an indication of the change in the initial core wettability during the core preparation stage of the experiments. As mentioned earlier, the sandstone core used in the experiments was carefully cleaned after the tertiary CWI test and the same procedure was followed in both experiments, therefore the outcome of core preparation in both experiments is expected to be mainly similar. Wettability affects the shape of relative permeability curves, however, in that when the core wettability is more water-wet, the intersection of the water-oil relative permeability curves shifts

towards the right and the S_{orw} is lower, as explained by Owens and Archer [135] and Morrow et al. [136].

3. The third possibility lies in the mechanism of carbonated water injection. In the secondary CWI, the formation of the new phase takes place immediately after the carbonated water contacts the crude oil, whereas in tertiary CWI, there will be a time lapse due to the existence of a bank of preceding plain water left from the secondary water flooding. As was observed in the direct pore-scale visualisation experiments, the formation and growth of the new phase will create an apparent oil swelling. Then, practically, this process would reduce the water relative permeability and at the same time increase the oil relative permeability. As a result, the water will slowly start to flow, allowing the swollen oil to flow at oil relative permeabilities close to k_{row} at S_{wi}.

The third possibility is the most likely taken place where the oil relative permeability in secondary CWI is a function of both gas and water saturation in the three-phase region due to the formation of the gas phase. In this case, the oil volume would enlarge as observed in the pore-scale experiment and that reflects on the estimation of the oil relative permeability. Therefore, it can't fit the flow function in two-phase (water-oil) region. However, this could be the true in this case only where the oil recovery at water breakthrough in secondary CWI core displacement is higher than that in secondary WF of the same core.

Table 3-13 Estimated water-oil relative permeability end points and LET correlation exponents for SCWI test no. 2

S_{wi}	S_{wcrit}	S_{oirw}	S_{orw}	k_{rwiro}	k_{rocw}
0.210	0.210	0.315	0.315	0.340	0.817
L_w	$\mathbf{E_w}$	$\mathbf{T_w}$	$\mathbf{L_{ow}}$	$\mathbf{E_{ow}}$	$\mathbf{T_{ow}}$
2.40	7.0	0.2075	3.91	0.63	0.04

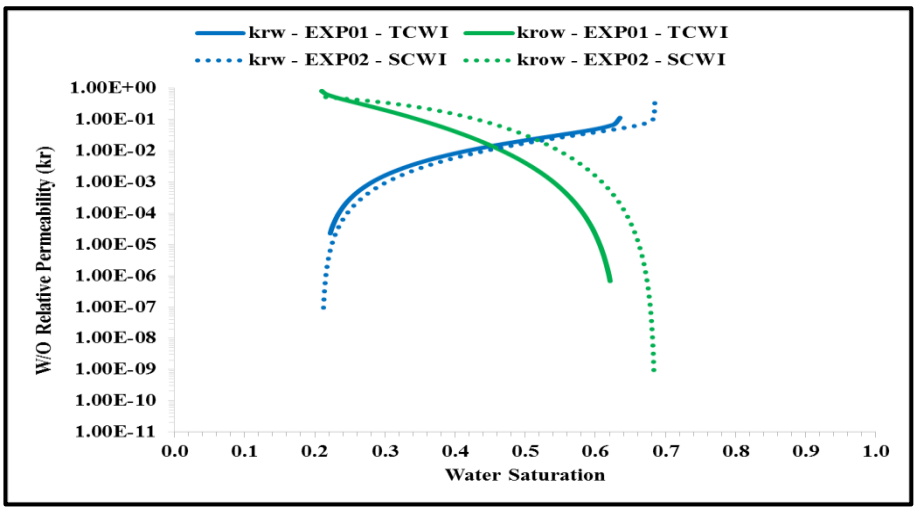

Figure 3-34 the estimated water-oil relative permeability curves for TCWI and SCWI

3.7.4.3 Secondary CWI followed by CO_2 Injection (Test no. 3)

Above we have obtained the proposed method to history match the performance of CWI in both secondary and tertiary modes through tuning the cubic EOS to reproduce the third phase observed in direct pore-scale visualisation experiments and thus defining suitable three-phase flow model. In this sub-section the focus shifts to the ability of the tuned-EOS to predict the performance of CO_2 injection after secondary carbonated water injection. The third test was performed under the same conditions as the previous experiments where the oil is methane-saturated oil under a test pressure and temperature of 2500 psi and 100 °F, respectively, but using a different core. Initially, the simulation model starts by constructing the one-dimensional grid block with the physical dimensions of the tested core. The model discretises a linear Cartesian and homogeneous gridblock that has porosity and absolute permeability values similar to the core displacement experiment.

The Objective Function

As the properties of the core were different than the previous experiments where the absolute permeability increased by about 50%. The relative permeability curves of water-oil and oil-gas were tuned by history matching the experimental recovery of secondary CWI along with differential pressure across the core. Similar to the previous experiment (test no. 2), the global objective function defined to include the cumulative volumes of

oil and water in addition to bottom-hole injection pressure and expressed in the equation 3-27.

A total of Np = 30 observation points in cumulative oil volume, ten observation points in cumulative water volume and Np = 65 pressure points in BHIP covered the historical data of secondary CWI to guide the optimizer in picking up optimum input parameters to minimise the global objective function which is the difference between the simulated values and observation data.

Uncertainty Parameters

About 19 uncertain parameters are in this assisted-history matching job in which mostly contain the relative permeability function parameters for both water-oil and oil-gas. Thus water-oil relative permeability correlation parameters are Soirw, krocw, krwiro, and LET exponents related to water and oil, while oil-gas relative permeability correlation parameters are Soirg, I_Sorg, Sgcrit, krgcl, and LET exponents related to oil and gas, as explained in equations 3-23 to 3-26 of LET relative permeability correlations.

As the initial saturation function was the estimated relative permeability in test no. 2, the global error was at first around 2.6% which is relatively small compared to the number of input parameters included. That would call the potential of not including most of the oil-gas relative permeability parameters as input values. However, the CMG DECE optimiser reduced the global percentage error to be around 0.1% as shown in figure 3-35 after about 1200 simulation runs.

Table 3-14 is showing the effectiveness of each input parameters on global history matching error and each objective function variable. Obviously, the water-oil relative permeability parameters have the significant impact on matching the cumulative oil and water volumes. Although, residual oil saturation to gas (Soirg) and E exponent related to the gas effect on reproducing the experimental cumulative oil volume, however, that would be later in experiment time after the water breakthrough where the mechanisms of CW more active. The oil relative permeability parameters effects the history-matching of the cumulative volumes whereas the water relative permeability parameters impact on reproducing the experimental BHIP.

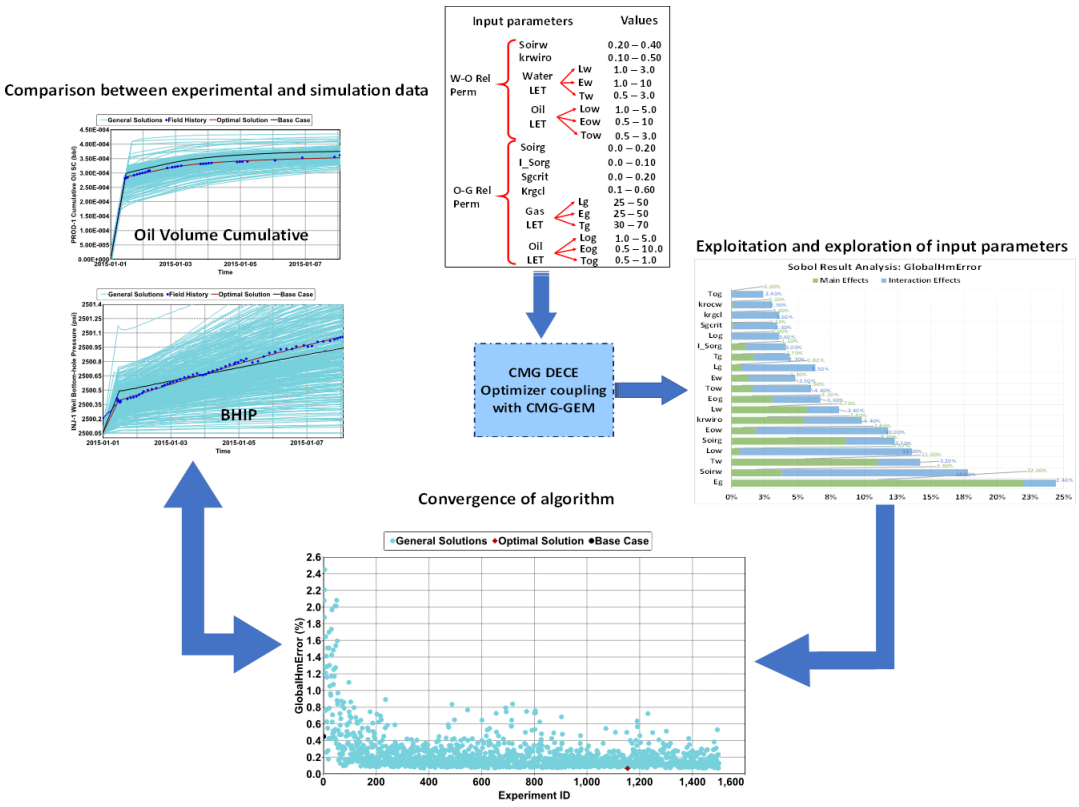

Figure 3-35 flow diagram of assisted-history matching for secondary CWI core displacement test no. 3

Table 3-14 overall effectiveness matrix of input parameters on objection function variables of secondary CWI core displacement test no. 3

Input Parameters	Objective Function			
	GlobalHmError	Cumulative Oil Volume	Cumulative Water Volume	BHIP
Soirw	**17.80%**	**18.40%**	**69.20%**	0.69%
krwiro	9.80%	9.10%	2.18%	**24.50%**
krocw	3.05%	3.16%	1.20%	1.20%
Lw	8.10%	7.90%	1.97%	6.20%
Ew	4.80%	4.70%	2.06%	**23.00%**
Tw	**14.20%**	**14.20%**	2.34%	**15.11%**
Low	**13.57%**	**14.62%**	**11.80%**	9.30%
Eow	**11.80%**	**13.00%**	3.58%	2.50%
Tow	6.00%	6.10%	2.40%	0.00%
Soirg	**12.30%**	**13.10%**	1.40%	3.50%
I_Sorg	4.10%	4.00%	3.30%	2.20%
krgcl	3.60%	3.99%	2.49%	0.91%
Sgcrit	3.43%	4.51%	1.50%	0.00%
Lg	6.32%	6.22%	2.60%	0.00%
Eg	**24.40%**	**24.50%**	7.89%	0.56%
Tg	4.40%	4.60%	3.10%	0.97%
Log	3.60%	3.66%	2.10%	1.30%
Eog	6.70%	6.90%	1.81%	0.00%
Tog	2.40%	2.49%	1.96%	3.00%

The experimental information from the secondary CWI period could be reasonably simulated, as shown in figures 3-36 through 3-38. The simulated oil recovery and both cumulative GOR and WOR with differential pressure are in good agreement with the experimental data. The performance of tertiary CO_2 injection is then predicted in order to evaluate the capability of the tuned-EOS with the saturation function, particularly in respect to oil-gas relative permeability. The simulation results are promising and could reasonably predict the behaviour of CO_2 injection in recovering additional oil.

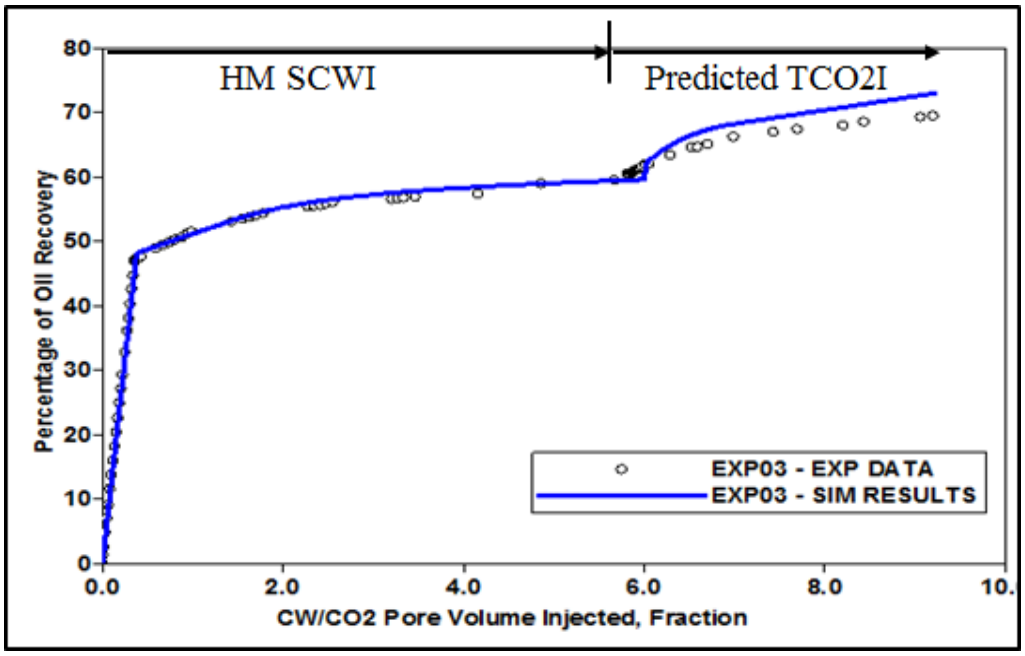

Figure 3-36 the history matched and predicted oil recovery during SCWI and TCO_2I in comparison with the experimental data from test no. 3

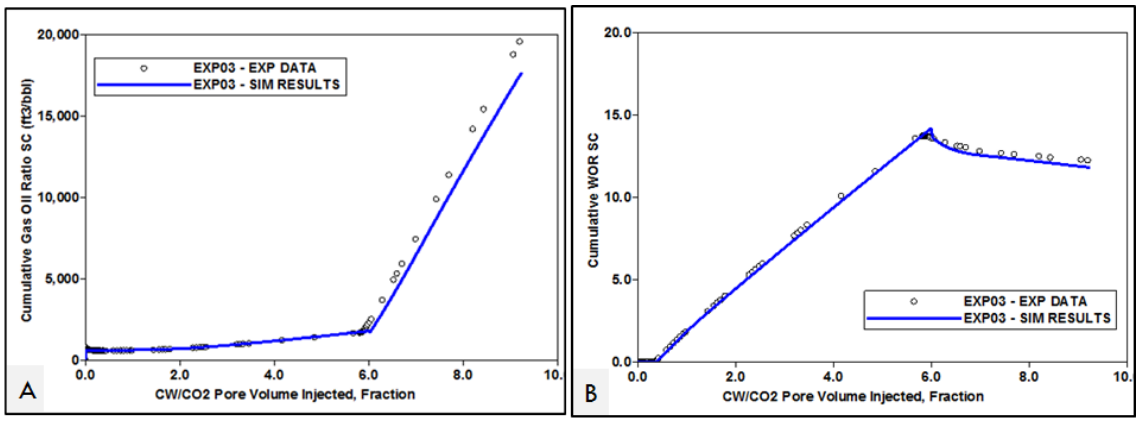

Figure 3-37 (Left) Simulated cumulative GOR against the experimental data for history matched SCWI and predicted TCO_2I in the core flood experiment no. 3 (Right) The match between cumulative WOR during SCWI and TCO_2I in the simulation model comparing to the measured data

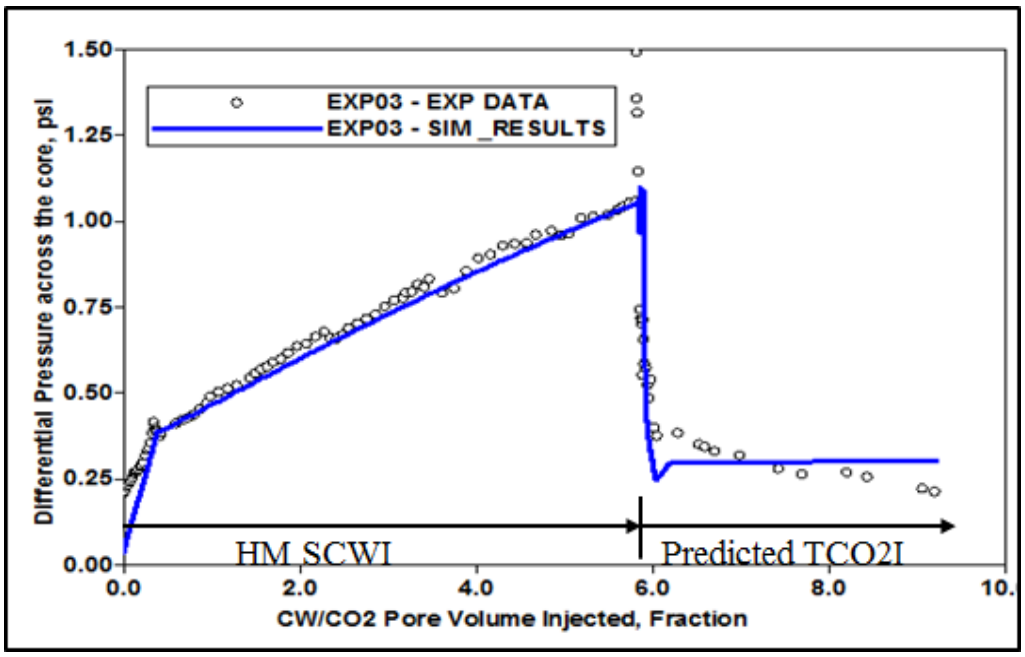

Figure 3-38 the simulated differential pressure against the differential pressure measured across the core in test no.3, showing a gradual increase as a result of the formation of the third phase and then a sudden drop due to the mobility of the gas phase after CO_2 injection

The estimated water-oil and gas-oil relative permeability curves from history matching the secondary CWI and then the predicted tertiary CO_2 injection are illustrated in figure 3-39, while their end points with LET exponents are shown in tables 3-15 and 3-16.

Table 3-15 Estimated water-oil relative permeability end points and LET exponents

S_{wi}	S_{wcrit}	S_{oirw}	S_{orw}	k_{rwiro}	k_{rocw}
0.20	0.20	0.368	0.368	0.116	0.976
L_w	**E_w**	**T_w**	**L_{ow}**	**E_{ow}**	**T_{ow}**
2.38	1.6875	0.625	2.8	1.6875	2.875

Table 3-16 Estimated oil-gas relative permeability end points and LET exponents

S_{oirg}	S_{org}	S_{gcon}	S_{gcrit}	k_{rogcg}	k_{rgc}
0.108	0.2045	0	0.048	0.976	0.274
L_g	**E_g**	**T_g**	**L_{og}**	**E_{og}**	**T_{og}**
46	28.5	61	1.86	6.04	0.9

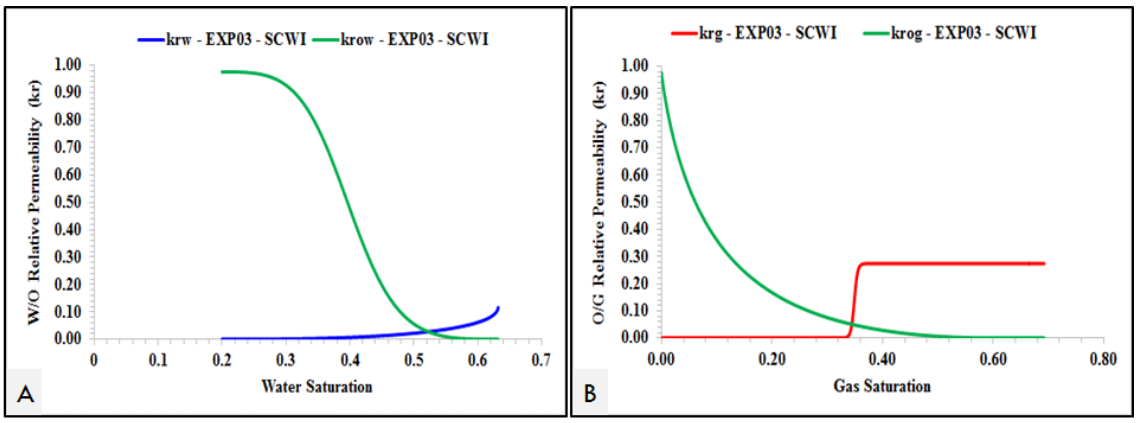

Figure 3-39 the relative permeability curves resulting from matching SCWI core displacement test no. 3 (right) water-oil relative permeability and (left) oil-gas relative permeability

3.8 Overall Summary

Simulation studies were performed on three core displacement experiments, where carbonated water was injected in different modes, such as post-waterflood or pre-CO_2 injection, in order to develop a methodology for modelling the performance of CWI in live oil systems in view of observed mechanisms of CWI in direct pore-scale experiments. Based on the micromodel observations, it was determined that the formation of the new phase during carbonated water injection occurs due to the directional mass transfer of CO_2 from CW to oil at the interface between the contacted oil and CW. Since the tendency of CO_2 to dissolve in oil is higher than that in water, CO_2 will transfer from the aqueous phase to the oil phase. In the saturated oil, multi-component competition between CO_2 and the dissolved light hydrocarbon compounds of oil will lead to unstable phase equilibrium that results in liberation of hydrocarbon gases composed of methane at an early stage in the process to form a third phase which becomes heavier. Moreover, the expelled light and intermediate components of the oil form a new phase inside the oil phase where it nucleates as a small bubble. The size and number of these third-phase bubbles increase rapidly, as more CO_2 is transferred and thus more hydrocarbon components of the oil are expelled out of the solution.

The rapid growth of the new phase brings about a gaseous expansion to its surrounding oil beyond the normal oil swelling effect that takes place during CO_2 dissolution in oil. This trapping mechanism arising from the new phase formed within the oil during CWI is different from the separated CO_2-rich phase formed during CO_2 injection. The occurrence of the third phase causes a three-phase flow phenomenon in porous medium

where the mobility of the remaining oil phase is in a linear relationship with increasing new phase saturation, which could be a representation of a localised in-situ WAG process.

Additionally, the unstable phase equilibrium established due to CO_2 dissolving in saturated oil as the latter contacts CW, and the subsequent creation of the third phase, results in complex phase behaviour in the resident oil and the subsequently formed phase. It was noted that a compositional simulator could probably model the CWI process through development of a methodology coupling a cubic equation of state responsible for modelling the hydrocarbon vapour and liquid phases with the solubility of CO_2 in the aqueous phase. It was found that GEM ver. 2014.1 and beyond has an algorithm containing the prediction and calculation of the phase equilibria of oil, gas and water/brine mixtures, which was previously developed by Li and Nghiem [118], where the oil and gas are modelled by a cubic equation of state and the gas solubility in the aqueous phase is estimated from Henry's law. Also, the selected simulator has an explicit keyword to assign carbonated water compositions as a single phase in the injection stream, which could be implemented in any scale of simulation model, whether in one, two or three dimensions.

A tertiary CWI core displacement experiment was used to calculate the third phase saturation that forms during CWI, based on observed mechanisms through direct pore-scale visualisations. Then, tuning the EOS by employing the parameterisation of binary interaction coefficients between CO_2 and hydrocarbon components to model the estimated experimental gas saturation could predict the phase behaviour during CW, while preserving the other parameters which were obtained during conventional water flooding, like water-oil relative permeability curves and estimated CO_2 solubility in brine using Henry's law. The process of tuning the EOS reveals that the solutions are not unique, since different realisations of the set of BICs could reproduce the calculated gas saturation during CWI, while none of them could repeat the performance of CWI even with history matching the production data from experiment data to obtain the oil-gas relative permeability curve.

Both the binary interaction coefficients of CO_2 to hydrocarbon components (mainly methane and pseudo-components), and the oil-gas relative permeability, were utilised to assist the history matching in modelling the performance of CWI by reproducing the experimental production data, estimated gas saturation and differential pressure across

the core. The history matching revealed that a negative binary interaction coefficient between CO_2 and methane was necessary in order to model the measured increasing trend in differential pressure during tertiary CWI. The hypothesis of a negative CO_2-C_1 BIC could be due to the limitation of the cubic EOS using the quadratic (vdW1f) mixing rules and classical combining rules to predict highly polar and hydrogen bonding mixtures, especially water. For that reason, a negative CO_2-C_1 BIC is necessary to account for the highly repulsive forces between them, and their highly interactive forces in respect to the water.

Table 3-17 summarises the simulated oil recoveries versus the experimental measurements for all the tests under investigation. The overall percentage differences at different oil recovery stages were satisfactory, even for predicted oil recovery from tertiary CO_2 injection, which was about 5%. The predicted oil recovery profile from the simulation does not exhibit an extreme shift but rather a gradual increment in oil recovery.

Table 3-17 Summary of the experimental and simulated oil recoveries from different core displacement tests (EXP referred to experimental data and SIM referred to simulation results)

Test	Process		Recovery, %OOIP			Inc. Recovery, %OOIP		
			EXP	SIM	DIFF, %	EXP	SIM	DIFF %
1	SWF	At BT	39.57	39.58	0.03	-	-	-
		At End of WF	45.08	44.83	0.56	5.51	5.25	4.83
	TCWI	At End of CWI	59.95	59.88	0.12	14.87	15.05	1.20
2	SCWI	At BT	48.27	48.56	0.60	-	-	-
		At End of CWI	62.70	62.90	0.32	14.43	14.34	0.63
3	SCWI	At BT	46.90	47.71	1.71	-	-	-
		At End of CWI	60.46	59.58	1.47	13.56	11.87	13.29
	TCO_2I	At End of CO_2I	69.50	73.10	5.05	9.04	13.52	39.72

3.9 Conclusions

Based on the physics directly observed in the pore-scale visualisations, a new methodology was developed to estimate the complex processes leading to gas saturation in the core, and an EOS was tuned to reproduce the dynamics of fluid phase behaviour and the formation of a new phase. The following conclusions can be drawn from the simulation and history matching attempts:

- The formation of the new gas phase within the oil phase could be simulated using commercial simulators. This simulation reveals that this third-phase brings about

an apparent second phase oil swelling. The increase in oil recovery and further reduction in oil saturation are linked with the amount of immobile (critical) gas saturation in the system.

- Based on the physics observed in the visualisation experiments, a new approach was developed to overcome the difficulties in measuring gas saturation. Tuning the EOS using the binary interaction coefficient between CO_2 and hydrocarbon components in order to model the estimated experimental gas saturation could help to predict the phase behaviour during CWI. The relationship between CO_2 and hydrocarbon components as represented in the binary interaction parameter values in the EOS would have either a positive or negative impact when simulating the partition coefficient of CO_2 in water and oil, and would also affect the formation of the gas phase. This means that the optimum estimation of the binary interaction parameters is the key to the successful prediction of the performance of carbonated water injection.

- A unique and unusual negative binary interaction coefficient between CO_2 and methane was obtained when history matching tertiary CWI core displacement, in contrast to the formal positive BIC in conventional CO_2 injection scenarios. The author would relate this behaviour to the existence of a highly polar compound (i.e. water). Given the solubility of CO_2 and methane in water, this could produce high interaction forces set against the opposing repulsive forces between them. Also, the cubic equation of state using quadratic (vdW1f) mixing rules and classical combining rules failed to predict the mixture of highly polar and hydrogen bonding mixtures.

- The formation of the new gaseous phase would necessitate the use of a three-phase oil relative permeability model. Furthermore, the new gaseous saturation would enlarge the residual oil saturation, while the water saturation would displace the swollen oil in the three-phase region. This means that the minimal oil saturation is a function of the new gaseous phase saturation as defined by Fayers [103], in which $\alpha=1$ represents a gas that is completely trapped in a porous medium, where the oil relative permeability is a function of both the gas and water saturation in

which the relative permeability to oil in the three-phase region could be expressed using Stone I model.

- Highly critical gas saturation was simulated to account for the observations (micromodel visualisations) of the immobility of the gas phase in the micromodel experiments. Furthermore, very low gas relative permeability, and relatively good oil relative permeability, were obtained to model the flow of oil during the formation of the new phase. The successful history matching of the coreflood experiments implies a good potential to simulate large-scale cases of carbonated water injection if the simulator is trained to capture the pertinent physics.

- The full sequence of secondary waterflood and subsequent tertiary CWI could be history matched successfully to obtain one set of oil-water and gas-oil relative permeabilities, thus indicating that commercial simulators have an acceptable potential to capture the underlying mechanisms once the dominant physics are understood and implemented in the simulation. The work in this chapter has shown that secondary CWI can be matched and that relative permeabilities can be estimated. The steady increase in the differential pressure could be reproduced, which confirmed the selection of the three-phase oil relative permeability model that fits the underlying mechanism. Furthermore, the prediction of tertiary CO_2 injection using the proposed method in history matching the secondary CWI was generally acceptable.

Chapter 4 – CW Multiple-Contacts Equilibrium in Live Oil Systems

4.1 Introduction

Recently, Sohrabi et al. [68] examined the effect on the performance of CWI of dissolved (solution) gas in reservoir oil through direct visualisation experiments in which the transfer of CO_2 from carbonated water into live reservoir oils would generate a new gaseous-like phase within the resident oil. This new gas-like phase would subsequently expand as more CO_2 was transferred from the aqueous phase to the oil phase, contributing to further oil recovery. The results showed that as the quantity of solution gas increased, the new gaseous phase formed sooner, and to a larger extent, within the oil and grew more rapidly to bring about a gaseous expansion to its surrounding oil beyond the normal oil swelling mechanism that takes place during CO_2 dissolution in an oil. For live oil systems, therefore, the formation of the third phase could be considered to be the dominant mechanism in improving the performance of CWI.

Seyyedi et al. [69, 71], meanwhile, conducted an integrated study of the dominant mechanism leading to improved oil recovery from carbonated water injection. In this study, a methane-saturated oil was used as a host fluid medium to effect a novel multiple-equilibrium contact with carbonated water at experiment conditions of 2500 psi and 100 °F. They concluded that a gas-like phase formed immediately at the first equilibrium contact, and that this phase initially consisted mainly of methane and, to lesser extent, CO_2 before becoming richer in other hydrocarbons and CO_2 in subsequent contacts. Also, a continuous mass transfer of CO_2 occurred from the carbonated water to oil, even in the latest contacts, which indicated a further oil swelling capability. Furthermore, they found that the phase behaviour of the CO_2-oil mixtures during carbonated water injection results in an improvement in oil properties and that this has different effects compared to typical CO_2 injection.

Knowledge of the fluid/fluid interactions and phase equilibria that take place in complex processes such as carbonated water injection is required to evaluate how the distribution of CO_2 amongst the three phases may affect fluid flow in porous media. In this study, a series of multiple equilibrium contacts test between under-saturated oil and carbonated water were performed in order to characterise the phase behaviour of CO_2-oil mixtures

during CW contacts and to reproduce the new gaseous-like phase in a relatively under-saturated system and understand its compositional characterisation. We studied the CO_2 partitioning interaction between CW and under-saturated oil by conducting a series of high pressure and high temperature equilibrium tests. The carbonated water was serially brought into contact with reservoir oil, and then the resultant phases were measured to track the transferred CO_2 between the different phases so as to characterise the phase behaviour in the oil and in the subsequent new phase.

Another objective in performing the PVT experiment was to evaluate the capability of the cubic equation of state, coupling with Henry's law, to model and predict the phase behaviour of the CO_2-oil mixture during the CW multiple-contact equilibrium test, and thus to reproduce the new phase and its properties. A comprehensive interpretation of the physical fluid properties, including the solubility of CO_2 in oil, the solubility of gases in water, the swelling factor, changes in saturation pressure. In addition, the third phase physical properties were measured in order to tune the cubic-EOS. The tuned EOS was then used to validate the history matched method proposed in chapter 3.

4.2 CW Multiple-Contacts Equilibrium Test in Under-Saturated Oil

4.2.1 Experiment Setup

Figure 4-1 shows the schematic layout of a PVT experiment that could be operated at high pressure and temperature. The main equipment for this test were a hassler-type cylinder for equilibrium contacts, surrounded by a heating jacket that allowed the experiment to be performed at a controlled temperature of 100 °F, and a PVT cell connected to a pump that controlled the experiment pressure at 2500 psi. While running an experiment, the fluids would flow through a backpressure regulator, where the pressure would drop to atmospheric pressure, allowing any dissolved CO_2 to be liberated and measured using a CO_2 analyser. The liberated gas would be collected in a gasometer to measure its volume, before being collected for further gas chromatography analyses. The separated liquid (water or oil) was collected in a graduated cylinder in order to measure its volume and compare it with the injected pump volume, in order to estimate the change in the formation volume factor.

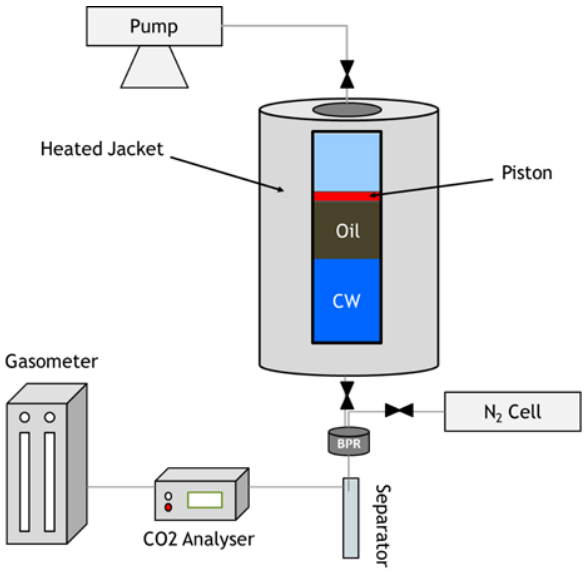

Figure 4-1 Schematic layout of CW multiple-contacts equilibrium PVT test

4.2.2 Preparation and Properties of Fluids

To achieve consistency, the stock tank oil and carbonated water used in the core displacement experiments discussed in chapter 3 were also used in these experiments under the exact same conditions. Accordingly, under-saturated live oil was pre-equilibrated by recombining a synthetic gas containing three components (Methane C_1, Ethane C_2, and Propane C_3), with stock tank crude (B) under a gas-oil ratio of 599 SCF/STB (106.7 scc/cc) at a test temperature of 100 °F and pressure of 2500 psi. The composition of this synthetic gas can be found in table 4-1, whereas figure 3.4 shows the composition of the stock tank oil. The three-components model gas is designed which could provide a solution gas content similar to actual gas at reservoir conditions. Then, the synthetic gas is prepared by 60% of real reservoir gas composition at experiment pressure and temperature, where the other light hydrocarbon compositions which available in actual gas, would be part of the methane. Crude (B) is characterised as a medium crude oil with an API gravity of 28.5° and stock tank oil viscosity of 31.25 cp at 100 °F. The basic fluid properties of the recombined live oil are shown in table 4-2. Moreover, the crude oil was intentionally recombined with three gases and made to be under-saturated in order to assess the solubility of other hydrocarbon components in water and also to point out the specific oil behaviour entailed in forming the third phase.

Table 4-1 Composition of the synthetic gas, which was recombined with dead crude oil (B)

Components	Experimental Composition (%mole)
Methane (C_1)	77.44
Ethane (C_2)	10.43
Propane (C_3)	12.13
Total	100

Table 4-2 Measured fluid properties of under-saturated crude oil (B)

Saturation Pressure (psi)	GOR (SCF/STB)	FVF (bbl/STB)	API Gravity	STO Viscosity (cp)
1743.48	599	1.265	28.5	31.25

CO_2 was dissolved in seawater with a salinity of 35,380 ppm at test conditions in order to make a carbonated water at 29.6 sccCO_2/cc. The brine composition is shown in table 3-2 in chapter 3. The viscosity of brine was 0.771 cp at test conditions.

4.2.3 Experiment Procedure

In order to replicate the dynamic CO_2 mass transfer that takes place while contacting reservoir oil with carbonated water, a multiple-contact equilibrium PVT test between carbonated water and under-saturated oil was performed at a pressure of 2500 psi and a temperature of 100 °F. The experiment started by placing almost 400 cc of under-saturated oil into a PVT cell at test conditions. After that, an exact volume of 400 cc of carbonated water was carefully transferred to the cell in order to have a 1:1 ratio, as shown in the schematic experimental procedure in figure 4-2. Then, the cell was gently shaken until equilibrium was reached, which could be observed when the pump that was connected to the cell to control the test pressure at 2500 psi began to retract. A balance between pump retraction and delivery was an indication that equilibrium had been achieved between the CW and oil. Having finished the first contact, the CW was drained out of the cell, as well as a small amount (± 20 cc) of oil, and their respective CO_2 concentration and fluid properties, such as GWR, GOR and saturation pressure, were measured.

Subsequently, a new batch of CW was transferred to the PVT cell to contact the oil remaining from the previous contact. Furthermore, the same procedure was followed for the second and subsequent contacts, until the oil became fully saturated with CO_2, and its

saturation pressure was nearly equal to the test condition pressure of 2500 psi. For subsequent contacts, and after the equilibrium between CW and oil was achieved, CW and approximately ±20 cc of oil were drained and their CO_2 concentration, GWR, GOR were measured. At that time, the PVT cell was held steady until the separation of oil and the new phase had completed. Then, the volume and CO_2 concentration of the new phase were measured and its composition was analysed. A total of six contacts of a ratio of 1:1 were performed in order to duplicate the fluid-fluid interaction that takes place from continuously bringing reservoir oil into contact with a stream of carbonated water.

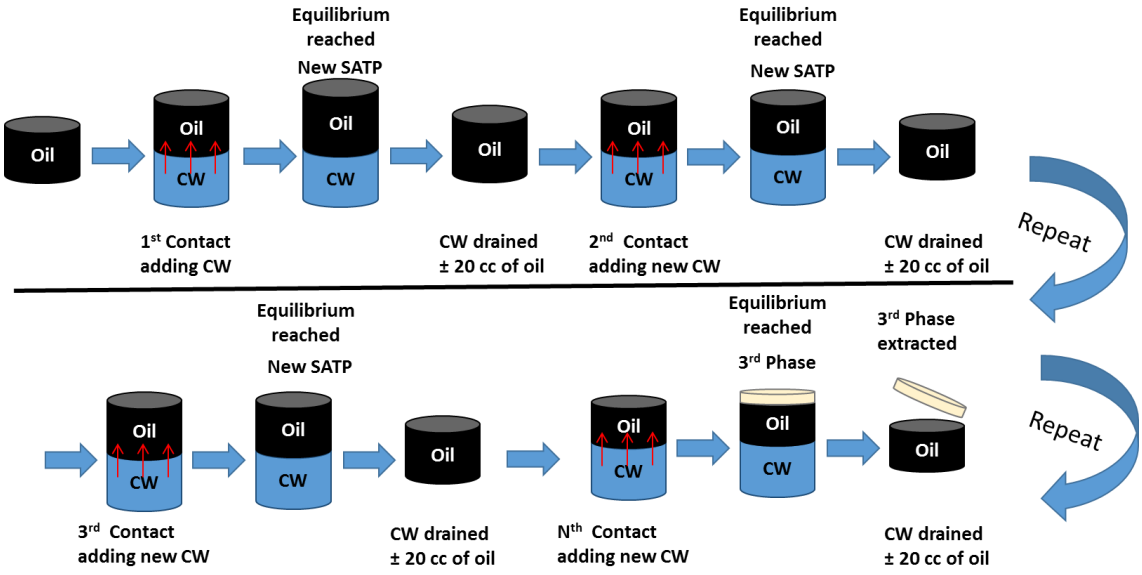

Figure 4-2 CW multiple-contacts equilibrium test in under-saturated oil at a temperature of 100 °F and pressure of 2500 psi

4.3 Fluid Modelling

The recombined composition was calculated through a global material balance:

$$z_i = \beta y_i + (1 - \beta)x_i \qquad \text{Equation 4-1}$$

Where β is the vapour-to-oil molar ratio, x_i and y_i are the mole fraction of component i in the liquid and vapour phase, respectively. The value of β was calculated through the following steps:

$$V_m = \frac{\sum x_i MW_i}{\rho_{mixture}}$$ Equation 4-2

V_m is the molar volume calculated for vapour and liquid phases, MW_i is the molecular weight for component i and ρ is the phase density. Then,

$$\frac{GOR_{ST}}{V_m}[=]\frac{599.13(scf/STB)}{379.348(scf/lb-mole)}[=]\ 1.57937\ lm-mole_{gas}/STB$$ Equation 4-3

And,

$$\frac{\rho_{oil}}{M_{wo}}[=]\frac{55.21(lb/cu\ ft)}{268(lb/lb-mole)}\times 5.615\frac{cu\ ft}{bbl}[=]\ 1.15673\ lb-mole_{oil}/STB$$ Equation 4-4

Finally,

$$\beta = \frac{1.57937\ lb-mole_{gas}/STB}{(1.57937\ lb-mole_{gas}/STB+1.15673 lb-mole_{oil}/STB)} = 0.5772345$$ Equation 4-5

Figure 4-3 shows the reservoir oil after recombining the three-component make-up gas with the stock tank oil, while respecting the gas-oil ratio. Peng-Robinson's (PR78) cubic equation of state, with Jossi-Stiel-Thodos's (JST) viscosity model were selected for modelling the recombined oil, so as to be consistent with the fluid modelling conducted previously in chapter 3.

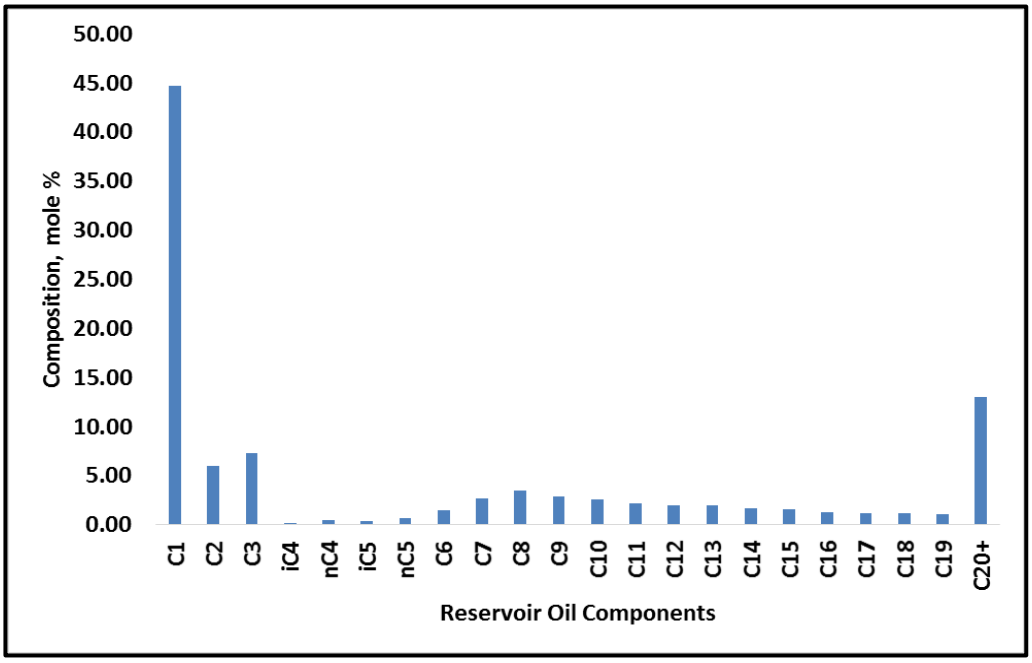

Figure 4-3 the recombined reservoir oil (B)

The hydrocarbon interaction coefficient exponent was regressed using the CMG-WinProp fluid modelling package [106] in order to match the measured saturation pressure. Then, the recombined oil was grouped into eight hydrocarbon components taking into account that the components of the make-up gas (C_1, C_2 and C_3) would be considered as a single carbon number component in addition to carbon dioxide (CO_2). The intermediate hydrocarbon components iC_4 to C_6 were lumped into a single pseudo-component (iC_4-C_6) since their concentration in the reservoir oil is minimal and their critical properties and molecular weights fall within an equivalent range. The C_{7+} fractions were lumped into four components using Whitson's lumping scheme [137] through equation 3-6:

$$N_g = \mathrm{Int}[1 + 3.3\log(N - n)][=]4.00 \qquad \text{Equation 4-6}$$

Where N_g is the number of pseudo-components, and N and n are the heavy components, numbers N = 20 and n = 7. Then, the molecular weight of each pseudo-component was obtained using equation 4-7.

$$M_I = M_{C7}\left(\frac{M_{N+}}{M_{C7}}\right)^{I/N_g} \qquad \text{Equation 4-7}$$

This resulted in the following pseudo-components: C_7-C_{11}, C_{12}-C_{16}, C_{17}-C_{19}, and C_{20+}. The thermodynamic properties of four components (C_1, C_2, C_3, iC_4-C_6, C_7-C_{11}, C_{12}-C_{16}, and C_{17}-C_{19}) have been directly used from the library in the PVT simulation package, respecting the mixing properties for the intermediate hydrocarbon pseudo-components, whereas the critical pressure and temperature of C_{20+}, in addition to the molecular weights of C_{12}-C_{16} and C_{20+}, were used in the tuning process, along with the modification of the C_{20+} volume shift in order to match with the measured saturation pressure and separator test. The detailed fluid description of the reservoir oil after tuning the EOS to match the measured fluid properties is listed in Table 4-3.

The mixing rule exponent parameter and five polynomial coefficients for the JST viscosity correlation were regressed to reproduce the viscosity of stock tank oil at 100 °F and under-saturated oil of 1.413 cp at test conditions. These data are not enough to evaluate the change in oil viscosity during CO_2 mass transfer from CW, however.

Table 4-3 Fluid description of under-saturated oil (B)

Components	Comp (mol%)	MW	Pc (atm)	Tc (°K)	ω	VH
CO_2	0.00	44.01	72.80	304.20	0.225	0.01484
C_1	44.70	16.04	45.40	190.60	0.008	0.00000
C_2	6.02	30.07	48.20	305.40	0.098	0.00000
C3	7.31	44.09	41.90	369.80	0.152	0.00000
iC_4-C_6	3.13	75.85	33.68	477.76	0.247	0.00000
C_7-C_{11}	13.84	119.18	27.14	594.21	0.389	0.00000
C_{12}-C_{16}	8.59	183.56	19.50	697.44	0.596	0.00000
C_{17}-C_{19}	3.42	250.02	15.69	760.11	0.758	0.00000
C_{20+}	12.99	556.11	7.15	801.51	1.326	0.26712

The fluid properties resulting from tuning the EOS in comparison to the measured PVT data are shown in table 4-4.

Table 4-4 Modelled oil properties by EOS with measured experimental data

Oil Properties	Measured	EOS Modelled
P_{sat} (psia)	1743.48	1743.62
GOR (SCF/STB)	599.13	598.61
FVF (res bbl/STB)	1.265	1.279
Live oil viscosity (cp)	1.413	1.414
STO viscosity (cp) at 100F	31.50	31.24
API gravity	28.5	28.5

Henry's Law constant for CO_2 can readily be estimated to match the experimental CO_2 solubility in brine of 166 SCF/bbl. The obtained Henry's Law constant for CO_2 is 2545.7281 atm, whereas about 2.2 mol% of CO_2 is dissolved in brine. Besides, reference Henry's Law constants and molar volumes at infinite dilution for other hydrocarbon gases (C_1, C_2, and C_3) are estimated using the predefined correlations specified by Li and Nghiem [118].

4.3.1 Modelling CW Multiple-Contacts Equilibrium Test

In order to predict and calculate the phase equilibria of oil, gas and water/brine mixtures, the author follows the method that has been proposed by Li and Nghiem [118], coupling the Peng-Robinson's (PR78) cubic equation of state with Henry's Law. As discussed in chapter 3, Li and Nghiem developed a robust algorithm for three-phase flash calculation

involving an aqueous phase by which the partitioning and fugacity coefficients of any components, such as CO_2, would control its mass transfer within three phases. The oil and gas are modelled by a cubic equation of state, and the gas solubility in the aqueous phase is estimated from Henry's Law. Figure 4-4 shows a flow diagram of their procedure for LVW flash calculations. In their procedure, the oil phase contains CO_2 at the start, and then the flash between oil and water is performed in order to compute the amount of CO_2 in water and the composition of the hydrocarbon phase. In contrast, in the procedure followed here, the water phase contains CO_2 at the beginning so the flash calculation between the oil and water phases is performed to compute the partitioning of CO_2 among both phases, and then to provide the remaining CO_2 in water and the CO_2-oil mixture composition. The computed hydrocarbon composition is then tested against the stability if the hydrocarbon phase is not in equilibrium, and a three-phase flash calculation is performed to determine the compositions of the oil, gas and aqueous phases.

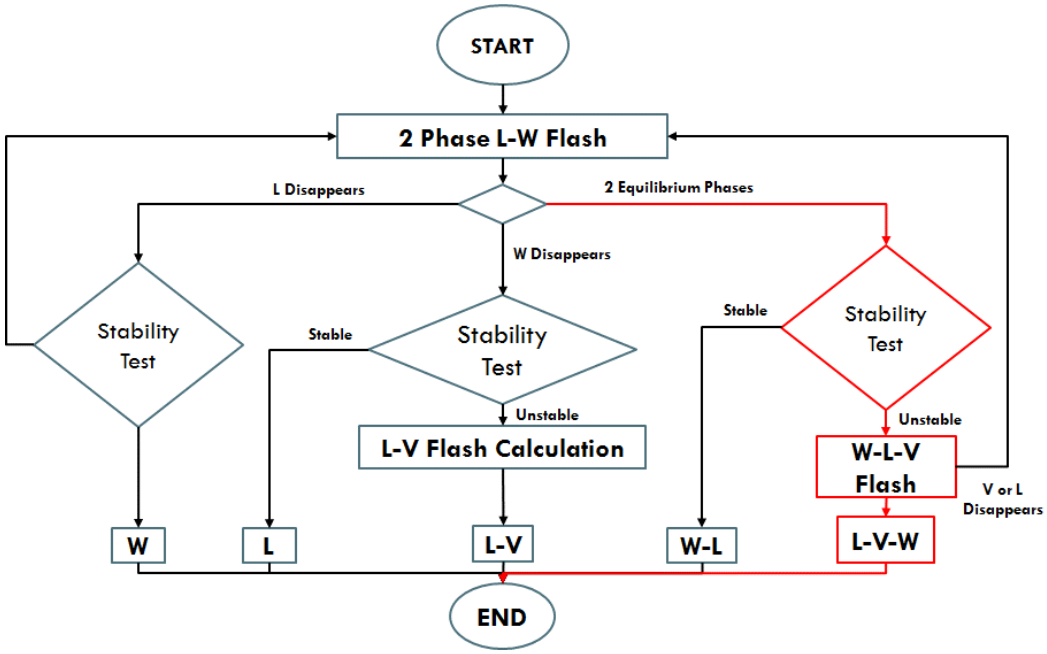

Figure 4-4 Flow diagram for liquid-vapour-water flash calculation as proposed by Li and Nghiem [118]

Using the results of the CW multiple-contacts equilibrium test, the binary interaction coefficients (BIC = k_{ij}) between CO_2 and hydrocarbon components were optimised to reproduce the measured phase behaviour in the equilibrium test at the first contact. Initially, the BIC's were estimated using generalised correlations developed for systems containing CO_2 and other hydrocarbons. Several researchers have suggested correlations to estimate the BIC for systems containing CO_2 and hydrocarbons where the k_{ij} is far from zero [138-143]. For example, Graboski and Daubert developed a correlation for SRK

EOS that is suitable for mixtures including CO_2 and paraffins [139], but it is necessary to know the solubility parameters to use this correlation. Kato et al., meanwhile, developed a correlation which has the advantage of being temperature dependent [138]. Their correlation can be applied to Peng-Robinson's EOS and is useful for mixtures containing CO_2 and n-alkanes whose acentric factor is less than 0.8, also the three parameters for this correlation depend only on the acentric factor of the n-alkanes, as shown in table 4-5. Nikos et al. constructed a generalised correlation to calculate the interaction coefficients for CO_2/hydrocarbon, as shown in table 4-5, N_2/hydrocarbon and CH_4/hydrocarbon [142]. Through this, they found the dependency of BICs on temperature, pressure and the acentric factor. In their approach, the k_{ij} depends on the hydrocarbon reduced temperature ($T_{rj} = T/T_{cj}$) and the logarithmic of the hydrocarbon acentric factor (ω_j). The authors explain that their correlation can tune EOS accurately to simulate multiple contacts of injection gases and reservoir fluids. On the other hand, alternative approaches have tuned the EOS by manually adjusting the BICs of CO_2 and hydrocarbons until a satisfactory match is achieved between the model and the measured experimental data at first contact.

In this thesis, the BIC between CO_2 and methane was adjusted to a negative value as a result of previous practice in chapter 3, which is referred to as MCET 2^{ND} (-ve), in table 4-6. The second manual adjustment of BICs, meanwhile, which is referred to as MCET 2^{ND} (+ve) in table 4-6, was a modified version of the correlation outputs in [125] and [129]. Specifically, the BICs between CO_2 and methane are calculated using Nikos et al. the correlation from [129], while the BICs of other hydrocarbons, whose acentric factors are less than 0.8, are computed using the Kato et al. correlation from [125]. The BICs between CO_2 and C_{20+} were tuned to achieve results that are consistent with the data at the first contact. The list of binary interaction parameters between CO_2 and hydrocarbons in each method are presented in Table 4-6.

Table 4-5 Correlations to estimate the binary interaction parameters of CO_2 and hydrocarbons

Author	Generalised BIC correlation	Correlation parameters
Kato et al. [138]	$k_{ij} = a'(T - b')^2 + c'$	$a' = -0.70421 \times 10^{-5} log(\omega_j) - 0.132 \times 10^{-5}$ $b' = 301.58\omega_j + 226.57$ $c' = -0.0470356\left[log(\omega_j) + 1.08884\right]^2 + 0.13040$
Nikos et al. [142]	$k_{ij} = \delta_2 T_{rj}^2 + \delta_1 T_{rj} + \delta_o$ Pressure correction $k'_{ij} = k_{ij}(1.044269 - 4.375 \times 10^{-5} p)$	$\delta_o = 0.4025635 + 0.1748927 \times log(\omega_j)$ $\delta_1 = -0.94812 - 0.6009864 \times log(\omega_j)$ $\delta_2 = 0.741843368 + 0.441775 \times log(\omega_j)$ $T_{rj} = \frac{T}{T_{cj}}$

Coutinho et al. [115] stated the difficulty in describing the binary interaction parameter of a CO_2-methane system with any of the proposed correlations, because methane has a critical temperature lower than the critical temperature of CO_2. They found the mean value of k_{ij} for CO_2-methane mixture as equalling 0.097 by using the data in the temperature ranges between 200° and 250° K. Kato et al. [138], meanwhile, estimated k_{ij} to equal 0.15 for the PR-EOS at a temperature of 293.2° K, while for temperatures below 200° K; k_{ij} is about 0.095. On the other hand, Kordas et al. [143] recommended that k_{ij} equals a constant value of 0.1 for temperatures greater than 300° K, although they excluded the CO_2-methane system from their generalised correlation for k_{ij}.

Table 4-6 the calculated and manually adjusted BICs between CO_2 and hydrocarbons (MT stands for manual tuning and (-ve or +ve) is the negative or positive BIC between CO_2 and C_1

BIC CO_2	Kato et al.	Nikos et al.	MCET 2ND (-ve)	MCET 2ND (+ve)
C_1	0.181672	0.050404	-0.013068	0.050404
C_2	0.151395	0.173049	0.068024	0.151395
C_3	0.135482	0.135223	0.094253	0.135482
iC_4-C_6	0.119911	0.109769	0.109769	0.119911
C_7-C_{11}	0.111860	0.109581	0.129581	0.111860
C_{12}-C_{16}	0.109562	0.120131	0.132531	0.109562
C_{17}-C_{19}	0.103642	0.129485	0.142484	0.103642
C_{20+}	0.148564	0.137813	0.159913	0.198564

Table 4-7 shows a comparison between the phase behaviour of first equilibrium contact and EOS-modelled properties using the four methods above. Although the results from using the generalised correlations of BICs are very close to the measured data, Kato et al. and Nikos et al. correlations under-estimate the saturation pressure and over-estimate the CO_2 concentration in oil, which represents the solubility of CO_2 in oil. The manual

adjustment of BICs in methods 3 and 4 could predict the saturation pressure with a percentage error of 0.7% and 0.04%, respectively, but they still over-estimate the solubility of CO_2 in oil. Although the GWR, CO_2 and methane concentrations in brine can be estimated using Henry's Law for gas solubility, due to the thermodynamic partitioning coefficient in the flash calculation method, all the methods show greater values in these parameters.

Table 4-7 Experimental and EOS calculated first equilibrium contact phase properties using four methods (MT stands for manual tuning and (-ve or +ve) is the negative or positive BIC between CO_2 and C_1

1st Contact Flash	Exp	Kato et al.	Nikos et al.	MCET 2ND (-ve)	MCET 2ND (+ve)
CO_2 in oil, mol%	17.77	19.91	20.07	19.97	19.72
Sat. pressure, psi	1865.63	1790.98	1804.80	1852.59	1864.84
GOR, SCF/STB	737.53	737.84	739.61	738.80	736.28
GWR, SCF/bbl	46.19	47.96	46.43	47.25	49.48
CO_2 water, mol%	69.8	74.69	74.21	74.80	75.72
C_1 water, mol%	28.7	22.85	23.31	22.76	21.87
Oil swelling factor	1.332	1.338	1.339	1.337	1.336

After screening the selected methods used in the estimation of the BICs for CO_2 to hydrocarbons, the two manual optimised methods were selected to predict the succeeding equilibrium contacts. Due to the dependency of the subsequent equilibrium contacts on previous contacts, the tuned EOS was evaluated when predicting the following contacts, as illustrated in the systematic flow diagram in figure 4-5, reproducing the gas phase in the last contact. At each contact, a new batch of CW that was fully saturated with CO_2 was placed in contact with the pre-equilibrated oil from the previous contact. The properties of the pre-equilibrated oil and drained CW were measured, for example the CO_2 concentration in oil and water, gas-water ratio, gas-oil ratio, swelling factor and oil saturation pressure. A similar procedure was applied in the fluid modelling, namely a multiple three-phase flash calculation was performed using the composition of the pre-equilibrated oil from post contact with the original CW composition. Then, the cubic EOS reproduced the saturation pressure and separation tests.

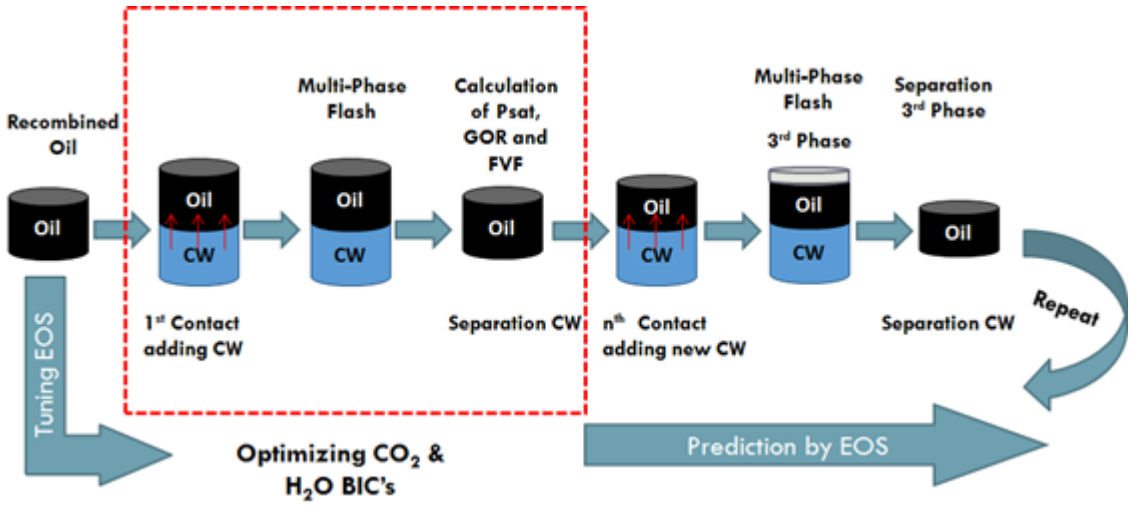

Figure 4-5 Systematic flow diagram on tuning the EOS to reproduce first equilibrium contact properties and predict the succeeding contacts

4.4 Results and Discussions

4.4.1 Characterisation of Carbonated Water

Carbonated water was serially brought into contact with under-saturated oil through multiple-equilibrium contacts. The compositional changes in the contacted CW can be explained through the variation of the gas-water ratio of CW in each contact compared with the initial gas-water ratio (GWR) of 29.6 scc/cc. A sharp reduction in the CO_2 content in the CW was measured after each contact, as shown in figure 4-6A, which indicates a continuous mass transfer of CO_2 into the oil, even after the oil became saturated with CO_2 and formed a gas phase. There is a large contrast between the solubility of CO_2 in water and its solubility in oil, in that CO_2 favours dissolving in oil, but, due to thermodynamic partitioning, the CW was not deprived of CO_2, i.e., the concentration of the CO_2 in the water phase did not reduce to zero. Nonetheless, the concentration of CO_2 in the water phase did drop very rapidly as the carbonated water came into contact with oil. Also, during the equilibrium contacts, there was a dual mass transfer between carbonated water and oil, where light hydrocarbon components, mainly C_1, C_2, and C_3, transferred from the oil to the brine. The concentrations of these hydrocarbon components in brine are well connected to their solubility in brine at test conditions, as shown in figure 4-6B.

Coupling the tuned equation of state with Henry's Law to estimate the gas solubility in brine showed its ability to model the immediate and sharp reduction in CO_2 concentration

in brine after first contact. Also, the Henry's Law coefficient estimated using the proposed correlations could predict the concentrations of hydrocarbon gases in brine, and are in good agreement with the measured concentrations.

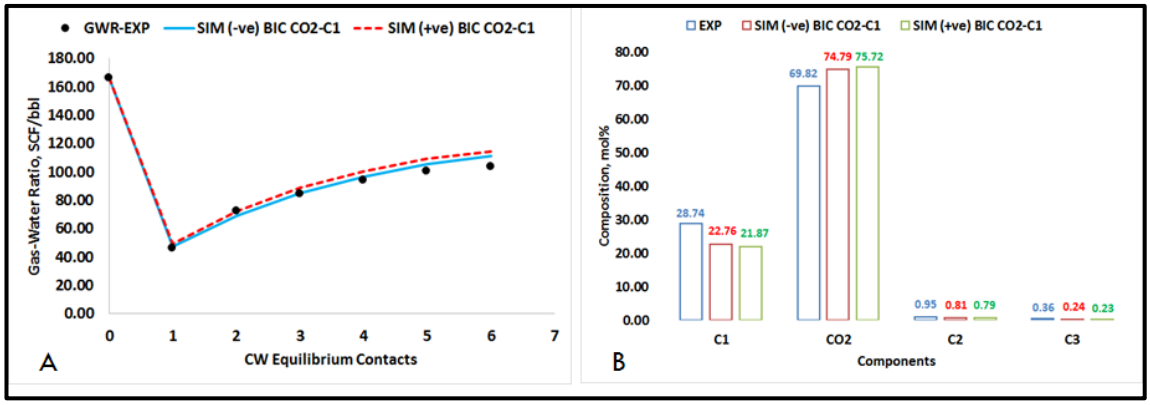

Figure 4-6 (A) Experimental and modelled variation in GWR of CW at each equilibrium contact, and (B) measured composition of gas content in CW in comparison with modelled composition by EOS after first equilibrium contact

4.4.2 Phase Behaviour of CO_2-Oil mixture

4.4.2.1 Saturation pressure and solubility of CO_2 in oil

The continuous dissolution of CO_2 in oil as it was transferred from the CW would lead to a steady compositional change in the oil to form a gas phase, even though the oil was under-saturated with hydrocarbon gases, therefore contributing to further oil recovery. The results indicate that the pressure builds up as the CO_2 dissolved in the carbonated water transfers to the oil phase, as shown in figure 4-7B. At first, there is an immediate increase in CO_2 solubility, represented by the CO_2 concentration in oil at each saturation pressure, then a slight stabilisation in solubility of CO_2 as the oil becomes saturated with CO_2, as illustrated in figure 4-7A. After that, the trend of CO_2 solubility resumes its increase as the gas phase continues to be formed as the CO_2 expels the light hydrocarbons. The extraction process may not take place immediately in a live oil system, therefore, with its timing depending on the degree of dissolved gas saturated in the oil. In the micromodel visualisation experiments presented by Sohrabi et al. [68], the timing to form the new phase during CWI reached 6 minutes in fully-saturated oil but this increased to 4 hours in a stock tank (dead) oil system. In another pore-scale visualisation test performed in a partially saturated oil system, the time required to form the new phase was 20 minutes. There is therefore an acceptable agreement between the PVT test and the direct pore-scale visualisation experiments.

In order to make a fair comparison between measured solubility of CO_2 in oil and that predicted using the cubic equation of state, the solubility of CO_2 at each saturation pressure was computed using correlations from the literature that were developed based on various experimental data, as illustrated in figure 4-7A. Simon and Graue suggested a graphical correlation, where the solubility of CO_2 in dead oil is a function of the saturation pressure and temperature [40]. Additionally, Emera and Sarma developed a genetic algorithm package of polynomial correlations for computing the solubility of CO_2 in live oil [44, 144]. Their correlation is a function of specific gravity, molecular weight, temperature, initial saturation pressure and CO_2 saturation pressure. On the other hand, Rostami et al. estimated the solubility of CO_2 in live oil by introducing a gene expression programming method (GEP) [46]. As a result of their programming, the determination of CO_2 solubility would depend on molecular weight, specific gravity, reservoir temperature, CO_2 saturation pressure, and initial oil saturation pressure.

Applying these correlations to our work, the solubility of CO_2 in oil calculated by tuned Peng-Robinson's (PR78) EOS using two sets of BICs over-predicted the measured data and under-predicted the ultimate solubility before forming the gas phase. They do, however, show a satisfactory increase in CO_2 solubility after the gas phase is formed and after stabilising the solubility of CO_2 in the CO_2-saturated oil. The correlations of Emera & Sarma and Rostami et al. showed a reasonable calculation of the solubility of CO_2 in oil compared to the measured data, whereas Simon and Graue graphical correlation of CO_2 solubility did not get any closer to the measured data. These correlations, however, all failed to compute CO_2 solubility at fully saturated oil pressure, where its pressure was equal to the reservoir pressure.

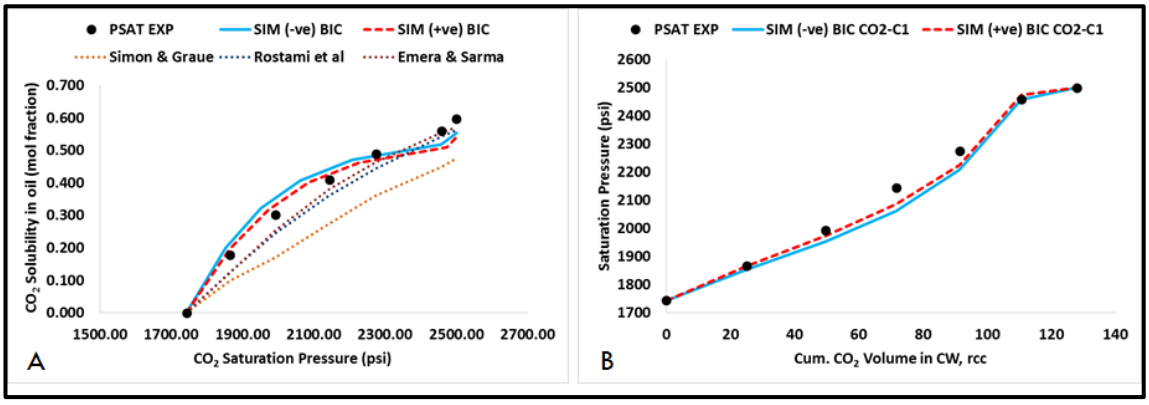

Figure 4-7 (A) measured CO_2 solubility in oil at each saturation pressure representing equilibrium contacts with predicted values from EOS and correlations, (B) change in saturation pressure of under-saturated oil during CW equilibrium contacts

Figure 4-8 is a variation in oil phase behaviour while it was saturated with CO_2 at each equilibrium contact, modelled using two sets of BIC's for tuning EOS. The solid black phase diagram represents the original under-saturated oil, while the solid coloured phase diagrams characterise the equilibrium contacts before the formation of the gas phase using the tuned EOS with negative CO_2-C_1 BIC. The dashed phase diagrams, meanwhile, characterise the equilibrium contacts using the tuned EOS with positive CO_2-C_1 BIC. The figure exhibits the enlargement of oil saturation with more CO_2 dissolution. This can also indicate which tuned EOS predicted un-physical fluid properties. The changes in compositional phase behaviour in both methods are almost identical.

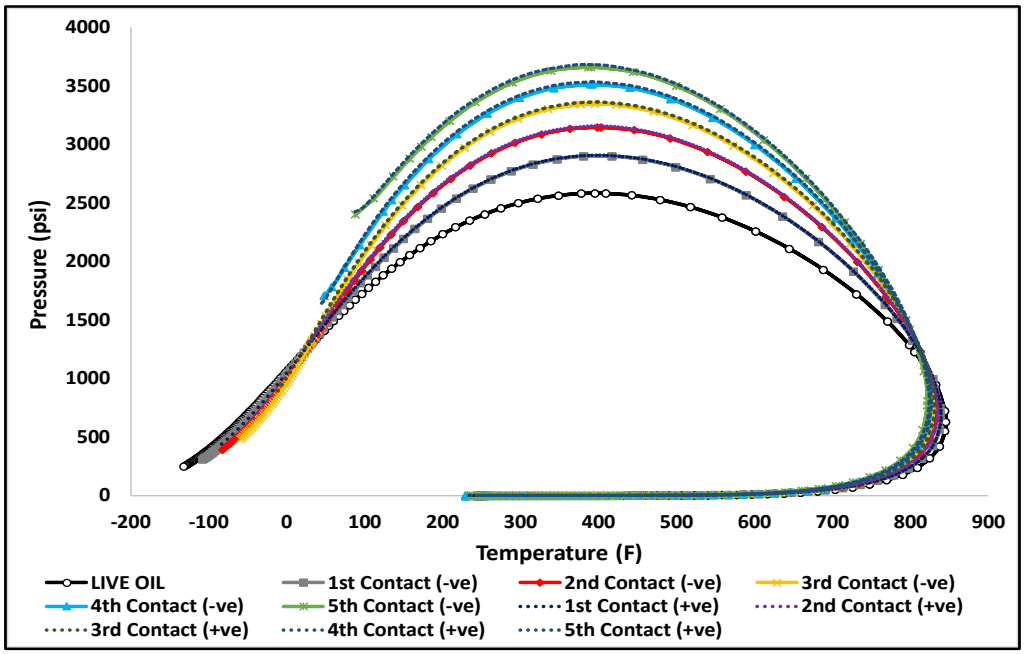

Figure 4-8 Modelled phase diagram of the oil phase at each equilibrium contact using the tuned EOS with negative and positive CO_2-C_1 BIC sets

4.4.2.2 GOR and Oil Swelling Effect

The initial measurement of the gas-oil ratio in under-saturated oil was about 599 scf/stb, at which no CO_2 was initially dissolved in the oil. The CO_2 concentration continually increased in each equilibrium contact, however, as shown in figure 4.7B, confirming the dynamic inter-phase mass transfer of CO_2 from carbonated water to oil. Accordingly, the gas-oil ratio is progressively amplified to almost twice its initial value, even though the new phase would form when the oil reached its saturation limit, as shown in figure 4-9A.

One of the observed mechanisms in direct pore-scale visualisation experiments during CWI with different oil saturation levels was the oil swelling effect. Oil swelling is a result of CO_2 dissolution in oil that will enlarge the oil volume to more than the original. In conventional CO_2 injection, the oil would be swollen to almost 2.5 times its initial volume. During the PVT, the oil swelling factor was measured and revealed an increasing trend from its initial value of about 1.27 up to 1.5, as shown in figure 4-9B. Based on this figure, as the CO_2 content of oil increases, the swelling factor increases. While the gas-oil ratio increases even after the formation of gas phase, the oil swelling is almost stabilised at its maximum value after the formation of the gas phase. The continuous increasing in GOR after formation of gas phase is probably due to that the measured gas-oil ratio after the formation of gas phase could contain bubbles of gas phase even after carefully separating the two hydrocarbon phases. The tuned EOS therefore has the ability to reproduce the measured GOR and swelling factor before the formation of the gas phase, whereas the difficulty occurred in estimating the GOR after the gas phase formed, which most likely lies in the accuracy of the measured value.

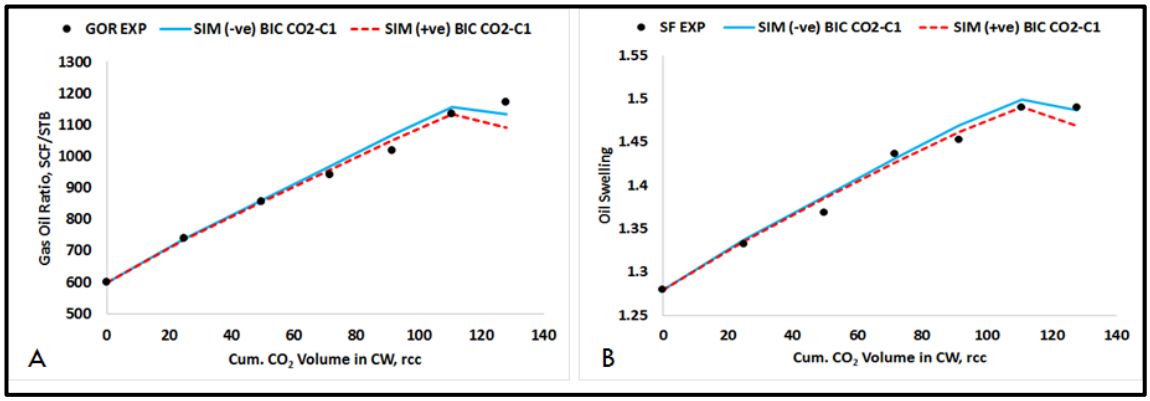

Figure 4-9 (A) changes in measured GOR after each CW equilibrium contact with oil in comparison with predicted values using EOS (B) measured and predicted oil swelling factor at equilibrium contacts

4.4.3 Characterisation of the New Phase

To achieve a comprehensive study of the fluid-fluid interaction that takes place throughout the process of carbonated water contacting oil, the full characterisation of the gas phase that formed in this process is crucial. To that end, the accumulated gas phase was separated at the sixth equilibrium contact in the PVT test. The assumption was that the new phase would not be formed unless the reservoir oil became fully saturated with CO_2. The increase in the saturation pressure is therefore the clue to address the formation of the gas phase, which in this experiment occurred at contact number six, when the

saturation pressure in the previous contact reached 2457 psi, i.e. close to the experimental pressure.

The sample that was taken after the sixth contact was analysed using gas chromatography. This sample contained 62.7 Mol% of CO_2, which was slightly higher than the CO_2 concentration measured in the oil phase; Figure 4.10. In contrast to the findings by Seyyadi et al., [69], where the composition of the new phase at the early stage consisted mainly of methane (C_1) before becoming richer in CO_2 and other hydrocarbon components in subsequent contacts, in this experiment, the main component in the third phase composition was CO_2, and this continued to increase in subsequent contacts. Another observation was the concentration of hydrocarbon components, suggesting the ability of CO_2 to expel a variety of light hydrocarbon components starting with the lightest (methane) and then, to a lesser degree, the other components. The amount of produced gaseous phase after the sixth contact was 3.2 cc. The formation gas volume factor (Bg) of the new gaseous phase was also measured to be 0.00397 rcc gas/scc gas, confirming the availability of other richer components than methane in the composition of the formed gas.

The formation of the gas phase at the sixth equilibrium contact was predicted by the tuned EOS and its composition was reproduced and compared with the measured new gas phase composition, as shown in figure 4-10. The compositions of CO_2 and C_1 were close to the measured values, with percentage differences between 4.5 to 11.7%, however both BIC sets that were used to tune the EOS under-estimated the composition of C_2 and C_3 by between 25 and 60%, and over-estimated the concentration of heavier hydrocarbon components by about 181%. For that reason, the gas phase volume calculated using the tuned EOS was higher than the measured volume from the PVT test due to the increase in the composition of C_{4+} which enlarges the volume of the new phase in modelled experiment.

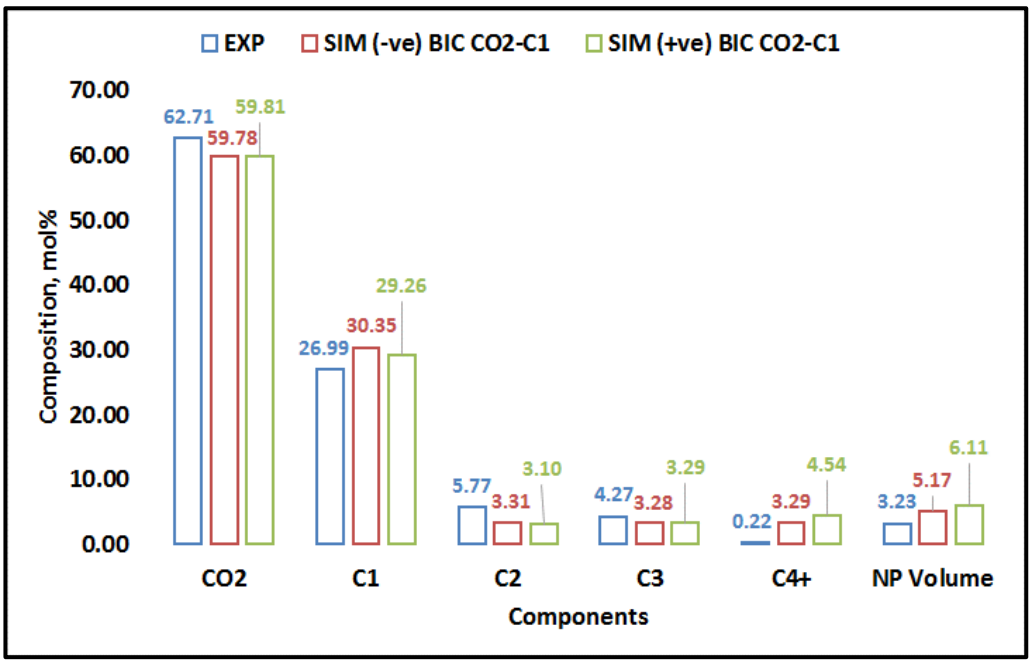

Figure 4-10 Experimental and EOS predicted composition and volume of new gas phase after the sixth equilibrium contact

4.4.4 CO_2-Oil Mixture Density and Viscosity

As a result of the tuned EOS, the JST viscosity model calculated a decrease in the modelled CO_2-oil mixture viscosity under test conditions (pressure = 2500 psi and temperature = 100 °F), which is in line with the proven mechanism of oil viscosity reduction during CO_2 dissolution in oil (see figure 4-11). The viscosity reduction was steady, with about a 44.8% drop in viscosity when the oil came to be saturated with CO_2. The cubic EOS, however, calculated a continuing increase in reservoir oil density before the phase split to form the gas phase. After the phase split, both the oil density and viscosity demonstrate an increasing trend. These fluid modelling results do not conclusively evaluate the CO_2-oil mixture characterisation in terms of viscosity and density, although the equation of state could predict the general behaviour of the CO_2-oil mixture reported in the literature. DeRuiter et al. studied the solubility and displacement of viscous crudes with CO_2 and found that the oils exhibit an increase in density due to the solubility of CO_2 [48]. The two samples in their study, with API gravities of 18.5° and 14°, exhibited an increase in density upon CO_2 dissolution. In a study of a West Texas crude oil, Grigg observed a 2% increase in oil density (after the addition of CO_2 and before the phase split), while the viscosity decreased [145]. After the phase split, the traditional viscosity-density relationship was observed; i.e. viscosity increased when density increased, and vice versa.

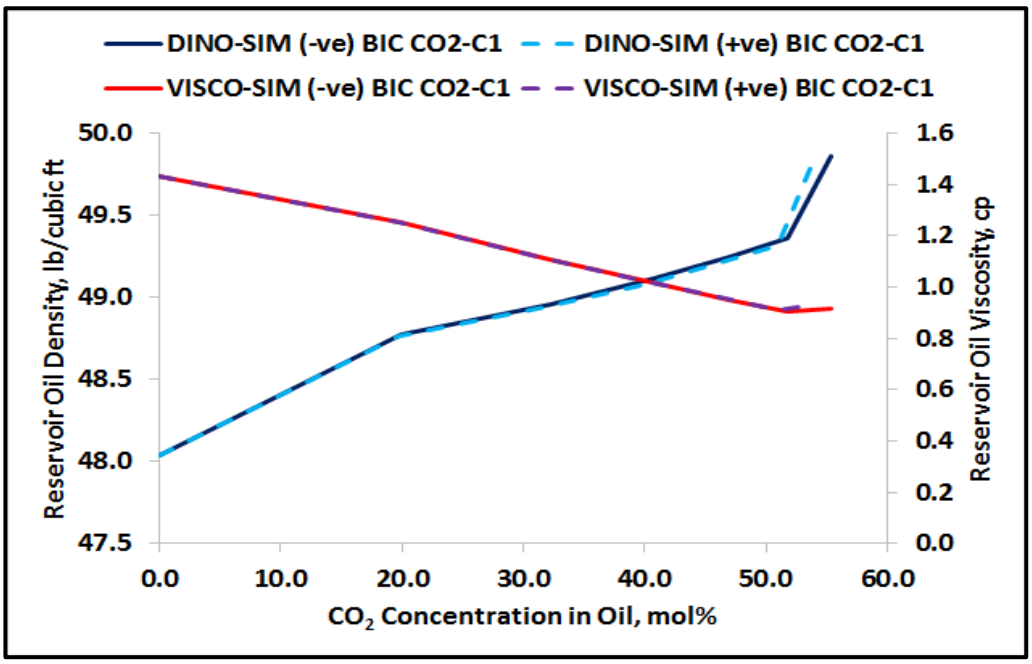

Figure 4-11 predicted change in live oil density and viscosity with an increase in CO_2 solubility in oil

4.4.5 CO_2 Partition Coefficient

A partition, or equilibrium, coefficient (K) is the ratio of the concentration of a compound (CO_2) in a mixture of two immiscible phases (CW and oil) at equilibrium and is expressed mathematically as follows:

$$K_{CO_2} = {C_{CO_2(HC)}}/{C_{CO_2(W)}} \qquad \text{Equation 4-8}$$

Where, K_{CO_2} is the CO_2 partition coefficient in a mixture of carbonated water and oil. A partition coefficient is therefore a measurement of the different solubility of CO_2 compound in the aqueous and oil phases. In this PVT test, as the carbonated water comes into contact with the oil, CO_2 is distributed between the two phases. Consequently, the dissolution of CO_2 in the oil phase leads to oil swelling and compositional changes that in return will form a new third phase, as noticed before. Figure 4-12 is the calculation of CO_2 partition coefficient in each equilibrated contact during the PVT experiment. The trend of the CO_2 partitioning coefficient exhibited a slight steadiness during the first two contacts, then the ratio of distributed CO_2 in oil to carbonated water increased. The presence of the third phase would enhance the mass transfer of CO_2 from carbonated water to the oil phase, which would be reflected in a continuing increase in the equilibrium ratio as the concentration of CO_2 in the hydrocarbon phases increases.

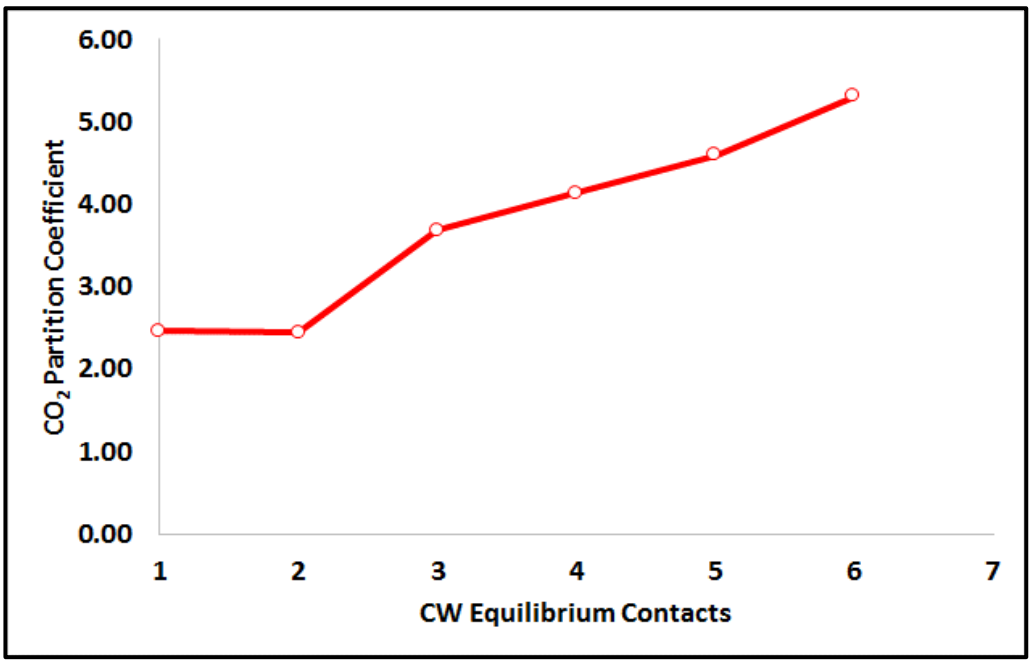

Figure 4-12 Calculated CO_2 equilibrium coefficient in each contact

4.5 Predicting Coreflood Experiments

We started by establishing a methodology to simulate the performance of carbonated water injection core displacements by analysing the physics that takes place during CWI in pore-scale micromodel observations. In chapter 3, this methodology was applied and tested with history matching core displacement experiments in methane-saturated oil systems in which the optimisation of CO_2 BICs to hydrocarbons assisted the history matching process. Then, the other key process involved as a result of the presence of the third phase is the creation of a three-phase flow region, meaning that a two-phase flow regime would no longer govern the saturation distributions. Additional aspects of multi-phase flow should therefore be considered while simulating the process of injecting carbonated water and can be drawn in pore-scale observations. For that reason, the author called it backward method which has been illustrated in figure 4-13.The backward method involves enhancing the binary interaction coefficient (BIC) of CO_2 and hydrocarbon components in Peng-Robinson's (PR78) EOS to predict the change in phase behaviour of oil composition as it forms an additional gas phase in which its saturation can be matched with the calculated gas saturation during tertiary CWI core displacement, as explained in chapter 3.

Non-unique solutions are reached, wherein multiple sets of BIC's are applied to obtain a match with the calculated average gas saturation, in addition to the unexpected negative

value of CO_2-C_1 BIC. Changing the CO_2 BIC to hydrocarbon components impacts the characteristics of both oil and gas in terms of compositional changes. Also, selecting a set of BIC realisations would affect the interaction of three-phase flow behaviour in a porous medium.

In order to validate the backward method, the CW multiple-contacts equilibrium test (MCET) is introduced to measure the changes in the compositional characteristics of oil during its contact with carbonated water. The multiple-contact equilibrium test is a thermodynamic PVT test in which carbonated water was brought into contact with live (gas dissolved) oil through a series of equilibrium contacts. Consequently, the results of the equation of state reveal its capability to model the fluid-fluid interaction taking place when CW contacts oil. In view of the necessity of having a negative CO_2-C_1 BIC, two sets of BICs were used to tune the EOS and reproduce the measured CW and CO_2-oil mixture properties. Furthermore, it was decided to utilise the tuned EOS to mimic MCET when simulating the performance of CWI in core displacement tests after recombining stock tank oil with methane to generate methane-saturated oil. This was done in order to predict the experimental outcomes and validate the backward method.

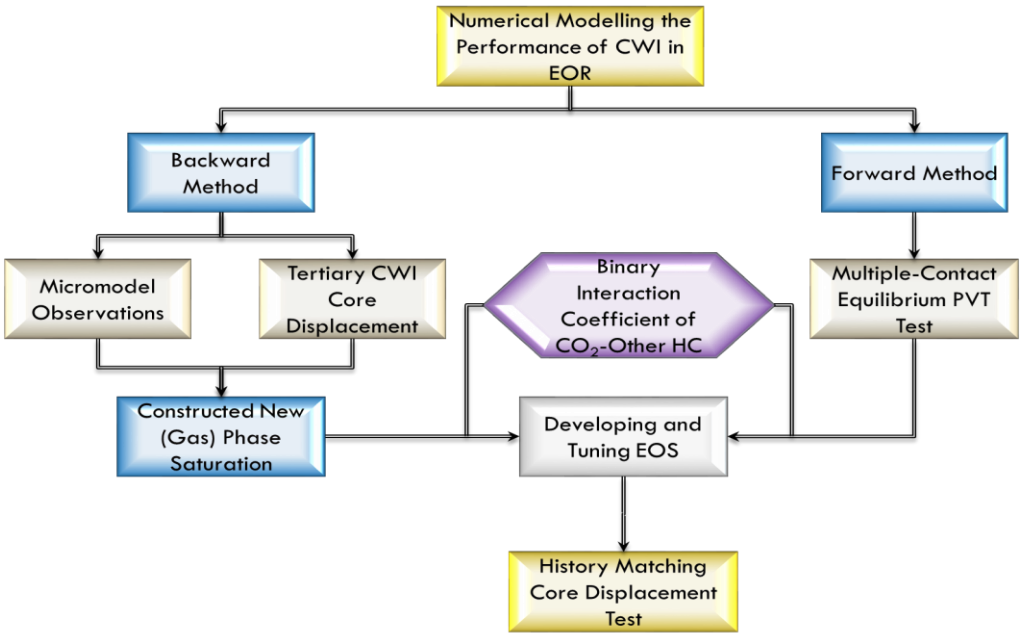

Figure 4-13 flow diagram showing the proposed methodology for numerically simulating the performance of CWI

4.5.1 Methane-Saturated Oil Fluid PVT Data

After a satisfactory match was achieved in the multiple-contacts equilibrium test, the reservoir oil was numerically flashed at standard conditions of 60 °F and 14.7 psi using the CMG-WinProp fluid modelling package [106] to produce the stock tank oil following the approach shown in figure 4-14. The flashed stock tank oil (dead oil) was recombined with methane at the experimental GOR of approximately 599 scf/stb to generate methane-saturated oil similar to what was used in the core displacement experiments. As shown in table 4-8, the calculated methane-saturated oil compositions in the two set of EOSs are reasonably alike. In 1st EOS reservoir oil composition, the ethane (C_2) and propane (C_3) were lumped in single pseudo-component (C_2-C_3) as their compositions are traces. Then, their CO_2 BIC would not affect the modelling of formation of new phase in methane saturated oil system, whereas in 2nd EOS reservoir oil composition they have quantified mole fractions. For that, two single components (C_2 and C_3) are considered in modelling the reservoir oil compositions.

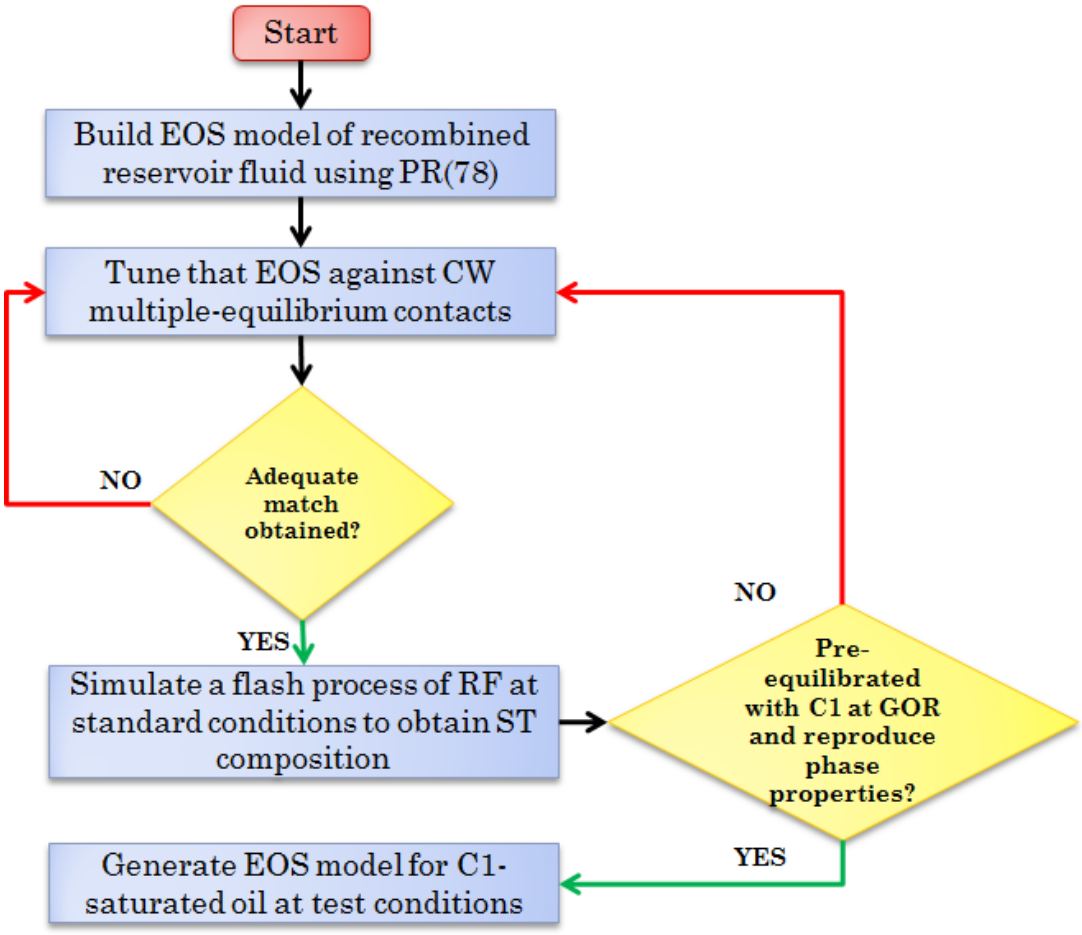

Figure 4-14 the approach to prepare the modelled methane-saturated oil using the tuned EOS for the multiple-contact equilibrium test

Table 4-8 Calculated methane-saturated oil compositions for two sets of EOSs where the first EOS was used in history matching the core displacement experiments in chapter 3 and the second EOS was used in matching the multiple-contacts equilibrium test

Reservoir Oil (B) Components	1st EOS Compositions, mol%	2nd EOS Compositions, mol%	
C_1	57.71	58.59	
C_2-C_3	0.31	**C_2**	0.16
		C_3	0.67
iC_4-C_6	3.13	1.91	
C_7-C_{10}	11.68	**C_7-C_{11}**	13.67
C_{11}-C_{16}	10.75	**C_{12}-C_{16}**	8.59
C_{17}-C_{20+}	16.42	**C_{17}-C_{19}**	3.41
		C_{20+}	12.99

The physical fluid properties of the fully methane-saturated oil that was calculated using the second EOS are given in table 4-9 in comparison with the experimental measured and calculated properties using the first EOS model. The second EOS predicts that the reservoir oil is nearly saturated with methane as the saturation pressure is 8.5 psi below the experimental pressure of 2500 psi, although the gas phase would still form immediately after the CW contacts the reservoir oil. Although the numerically flashed stock tank oil is recombined with methane at 599 SCF/STB, however the EOS is over estimated the predicted GOR. The oil viscosity at experiment conditions of 100 °F and 2500 psi is calculated to be 1.293 cp which is almost 10% lower than the measured and first EOS values. Nevertheless, the impact in terms of reducing the oil viscosity during mass transfer of CO_2 from CW to oil is minimal in the case of low viscosity oil.

Table 4-9 Measured and two modelled EOS-based fluid properties of fully methane-saturated reservoir oil (B)

Parameters	Saturation Pressure (psi)	GOR (SCF/STB)	FVF (bbl/STB)	API Gravity	Oil Viscosity (cp)	
					Live Oil	STO
Measured	2500.0	599.0	1.240	28.5	1.417	31.25
1st EOS	2500.0	599.0	1.239	28.5	1.417	31.24
2nd EOS	2491.5	624.5	1.259	27.9	1.293	31.24
Diff. % (EOS 1 & 2)	0.341	4.2	1.6	2.13	9.15	0

4.5.2 Simulation Core Displacement Experiments

In order to evaluate the impact of using another EOS which was tuned to match the multiple-contacts equilibrium test when simulating the performance of CWI, the rock properties, saturation function and three-phase flow oil relative permeability function

were kept similar to the previous simulation model in chapter 3. The only difference was fluid modelling through changing the equation of state and the binary interaction parameters of CO_2 to other hydrocarbon components. As described earlier, the second EOS has two version to match the MCET. The first version, which is called the MCET 2^{ND} (-ve) EOS, has a negative binary interaction coefficient between CO_2 and C_1, while the other version, which is called the MCET 2^{ND} (+ve) EOS, combines the calculation of the binary interaction coefficient between CO_2 and other hydrocarbons using the correlations in [125] and [129]. C3 1^{ST} (-ve) EOS is the first equation of state whose binary interaction coefficients of CO_2 and other hydrocarbon components were optimised using assisted history match to match the calculated average gas (new phase) saturation in the tertiary CWI coreflood experiment following the backward method.

4.5.2.1 Tertiary CWI (Test No. 1)

In the following figures 4-15 to 4-20 there are three simulation runs modelling the secondary conventional waterflooding and tertiary carbonated water injection core displacement experiment. The blue profiles represent the simulation run using the first EOS from chapter 3, whereas the green and magenta profiles characterise the simulation runs using the second EOS that is tuned to match the MCET PVT test by adjusting the CO_2-C_1 BIC to either negative or positive, respectively. The difference in oil recovery among the three simulation runs in conventional waterflooding before 1.73 PVI is a result of the modelled oil viscosities as shown in figure 4-16A that impacts the mobility ratio between the water and oil. Where the oil viscosity in the second EOS (MCET 2^{nd} EOS) scenarios is lower than the oil viscosity obtained in the first EOS by about 9%. Overall, the MCET 2^{ND} (-ve) EOS simulation run shows reasonable prediction of oil recovery during tertiary CWI, as shown in figure 4-15, although at the early stage the oil recovery is over-predicted due to large oil viscosity reduction rate and high CO_2 solubility in oil, as demonstrated in figure 4-16A. On the other hand, the MCET 2^{ND} (+ve) EOS simulation attempt under-predicts the oil recovery during CWI as a result of low CO_2 solubility in oil in comparison to the MCET 2^{ND} (-ve) EOS run, as illustrated in figure 4-16B, where the figure is showing the concentration of CO_2 and C_1 in the oil phase of three runs at the last grid block of 200, 1, 1.

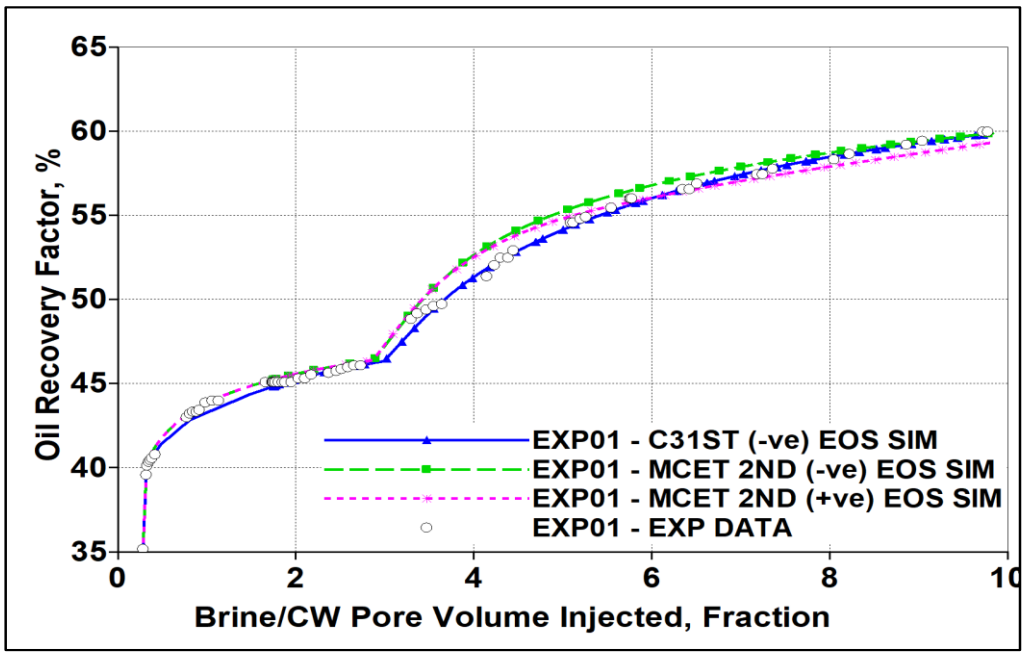

Figure 4-15 Comparison between measured and simulated oil recovery during tertiary CWI (test no.1) where the black circles represent the experimental data, the blue plot is the simulation run using the first EOS that is tuned using assisted history matching, and the green and magenta plots are simulation runs using the second EOS that is tuned to match the MCET test

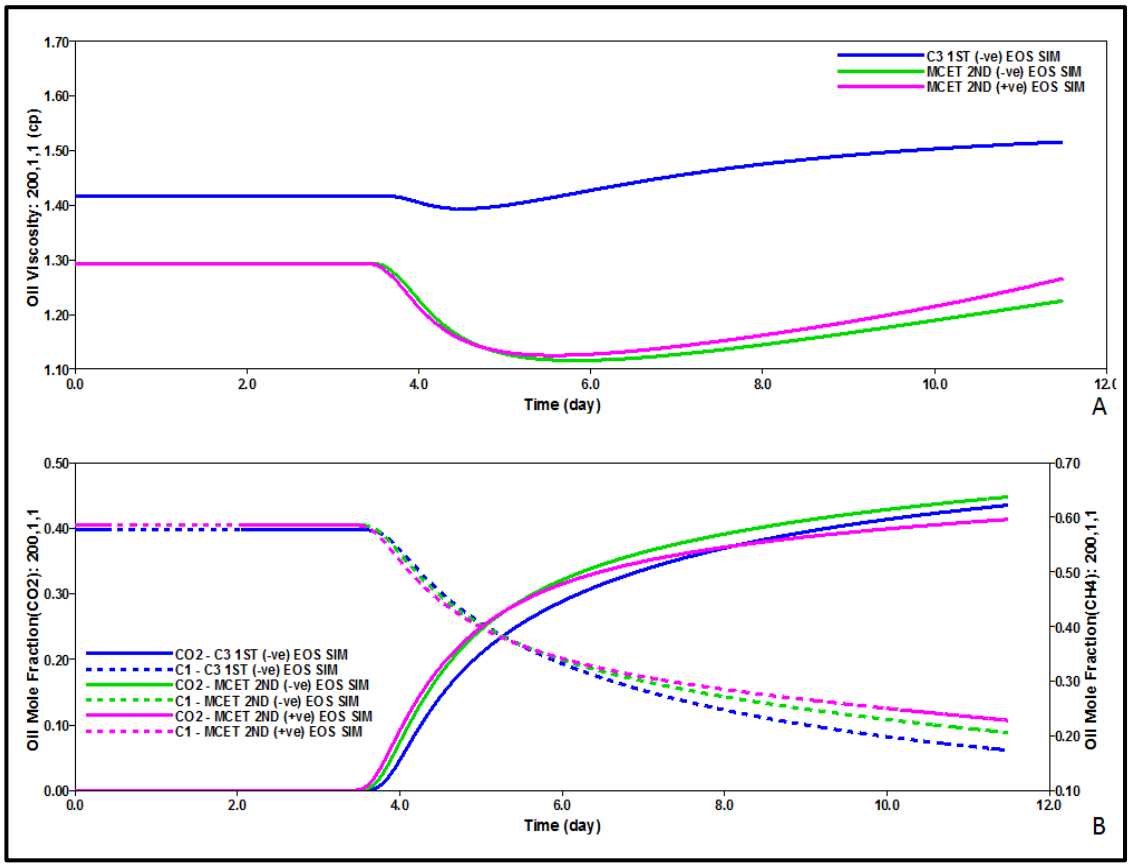

Figure 4-16 (A) oil viscosity reduction profiles during CWI in three simulation runs and (B) change in CO_2 and methane mole fraction in oil while CO_2 is transferred from CW to oil during CWI in test no. 1

One of the differences between conventional water injection and carbonated water injection is the effect of the GOR on the differential pressure across the core. In conventional waterflooding, the displacement between two immiscible fluids result in a fixed ratio of gas to oil, meaning that the drop in differential pressure after water breakthrough, and its stability, is due to the flow rate of each fluid (water and oil) in porous medium. In CWI, meanwhile, the gas to oil ratio has an effect on the differential pressure as a result of the formation of the new gaseous phase and its trapping mechanism in porous medium. As demonstrated in figure 4-17, the increase in GOR occurs earlier before a drop in differential pressure across the core as the trapped gas phase becomes mobile. This figure compares the cumulative GOR between the three simulation scenarios with the experimental data, and figure 4-18 shows the resulting differential pressure generated across the core in these simulation scenarios.

Generally, the second EOS simulation scenarios could realistically predict the increase in differential pressure across the core which gives a good indication of the appropriateness of the obtained oil-gas relative permeability curves and also the effect of the binary interaction coefficients on fluid phase behaviour.

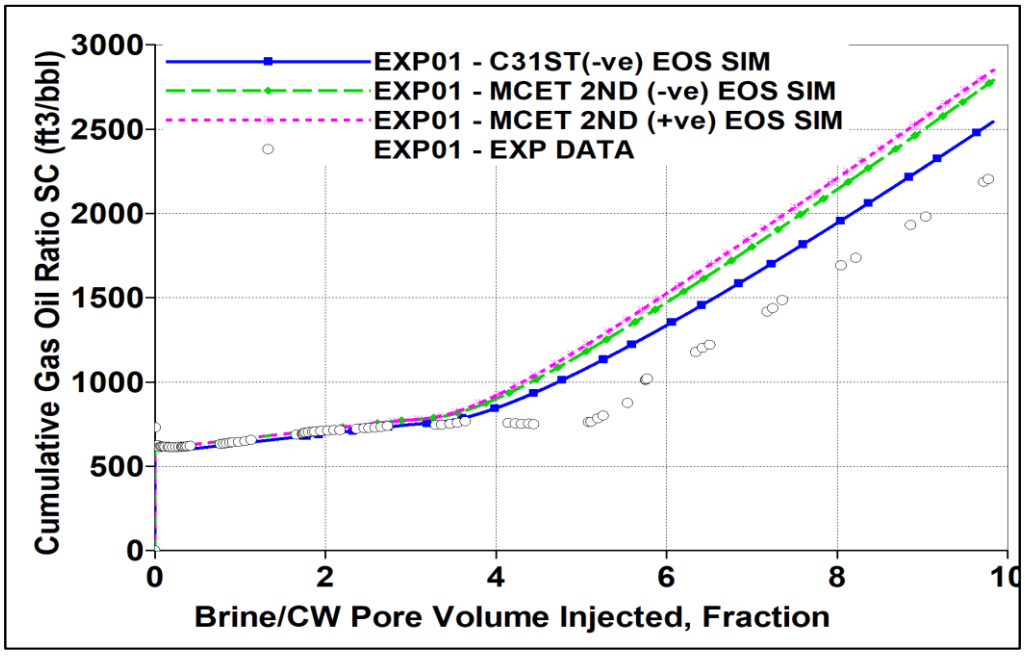

Figure 4-17 Calculated cumulative GOR in three simulation scenarios in comparison to measured experimental data of EXP01

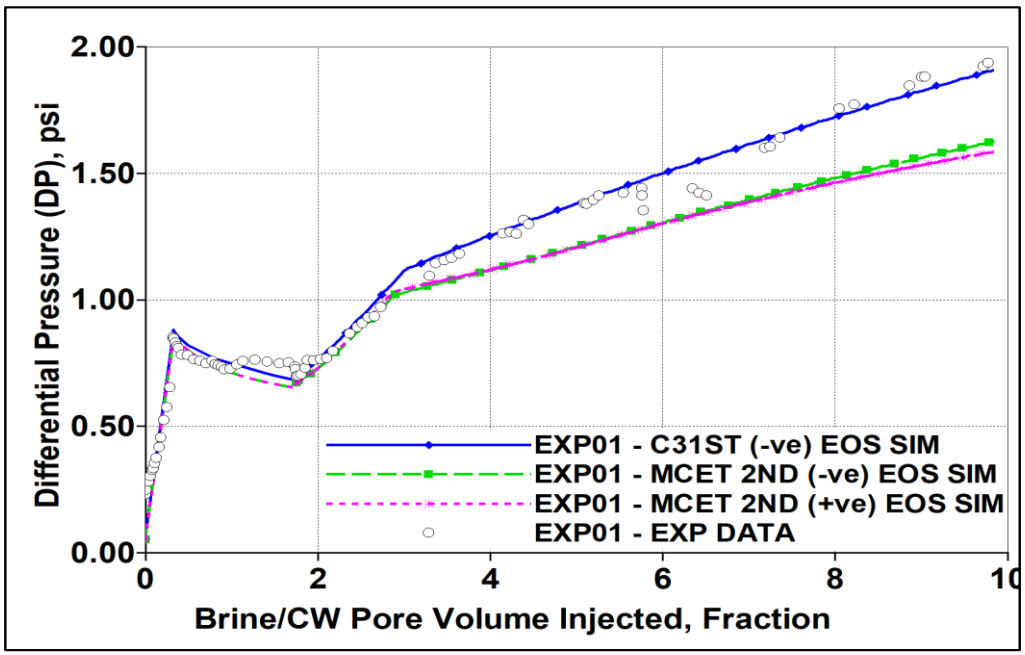

Figure 4-18 Predicted and history matched differential pressure across the core comparing with the measured experimental result of EXP01

In figure 4-19, the two MCET 2ND EOS simulation runs successfully predict the cumulative WOR. Due to the fact that the solubility of CO_2 solubility in oil is less than was calculated using the positive CO_2-C_1 BIC in the MCET 2ND (+ve) EOS simulation run, the new gaseous phase saturation is propagated as exemplified in figure 4-20. Thus, the positive CO_2-C_1 BIC would limit the CO_2 dissolution in the oil phase after the oil becomes saturated with CO_2, whereas the negative CO_2-C_1 BIC allows the oil continually to dissolve more CO_2.

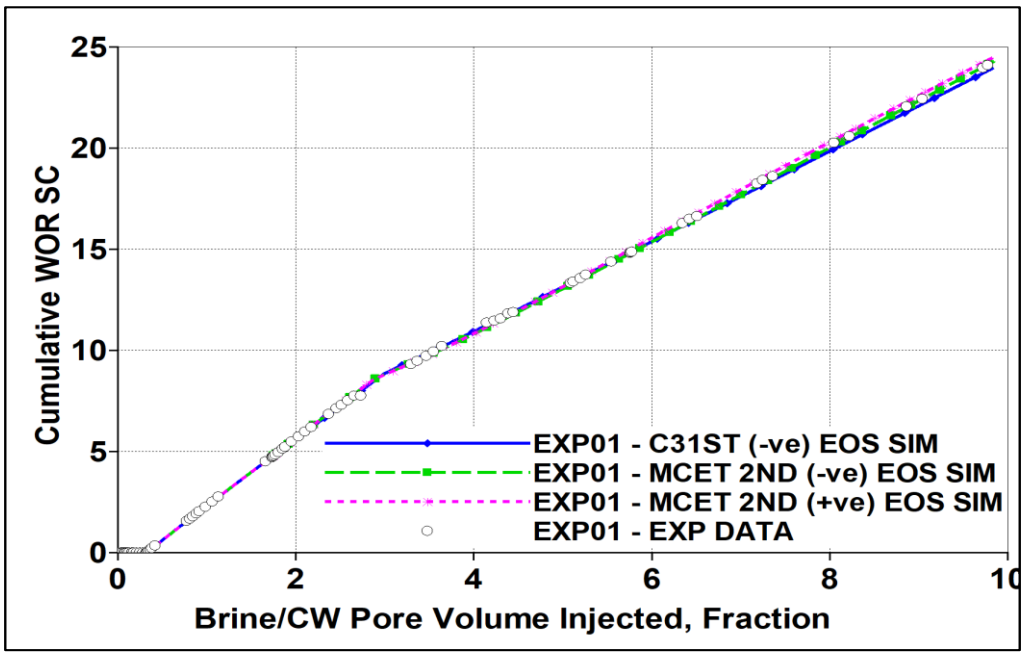

Figure 4-19 calculated cumulative WOR in three simulation models in comparison to measured experimental data of EXP01

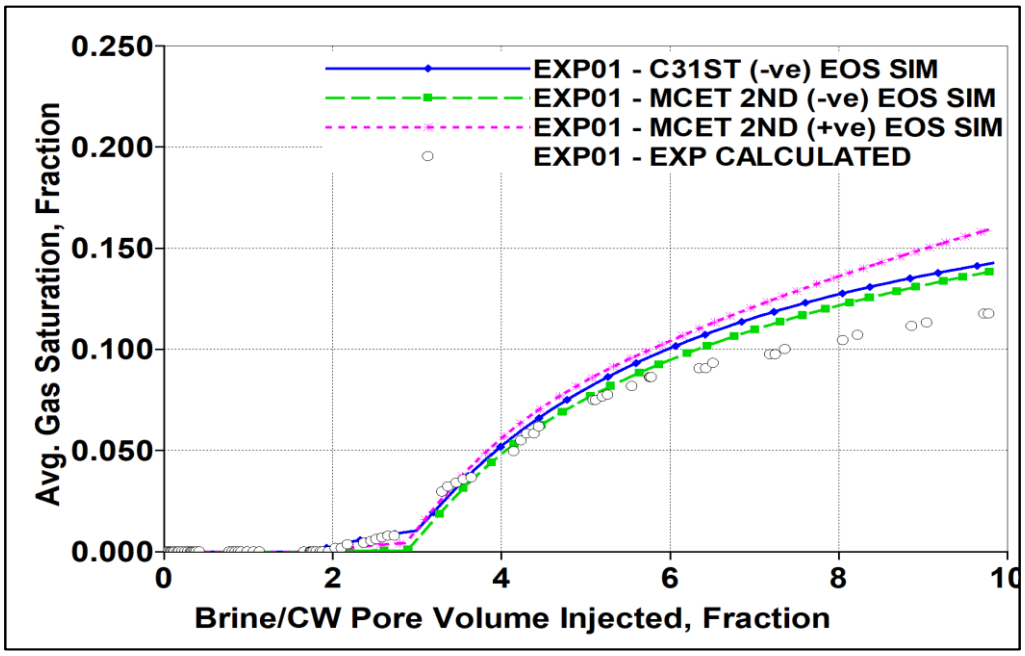

Figure 4-20 Predicted average gas (new phase) saturation in three simulation models comparing with the constructed gas saturation using EXP01 experimental data

4.5.2.2 Secondary CWI (Test No. 2)

In secondary CWI, the EOS tuned through matching with multiple-contacts equilibrium test could rationally predict the performance of CWI similar to both the experimental results and the first EOS tuned by the assisted history matching technique. It is evident that the over estimation of the solubility of CO_2 solubility in oil calculated by the second

MCET equation of state results in higher oil recovery after water breakthrough, as demonstrated in figure 4-21. The only difference between MCET 2ND (-ve) EOS SIM and MCET 2ND (+ve) EOS SIM is the binary interaction coefficients of CO_2 to other hydrocarbon components, however the MCET 2ND (+ve) EOS SIM has predicted smaller values of average oil saturation than calculated experimentally, and even lower than the other simulation runs, as illustrated in figure 4-22.

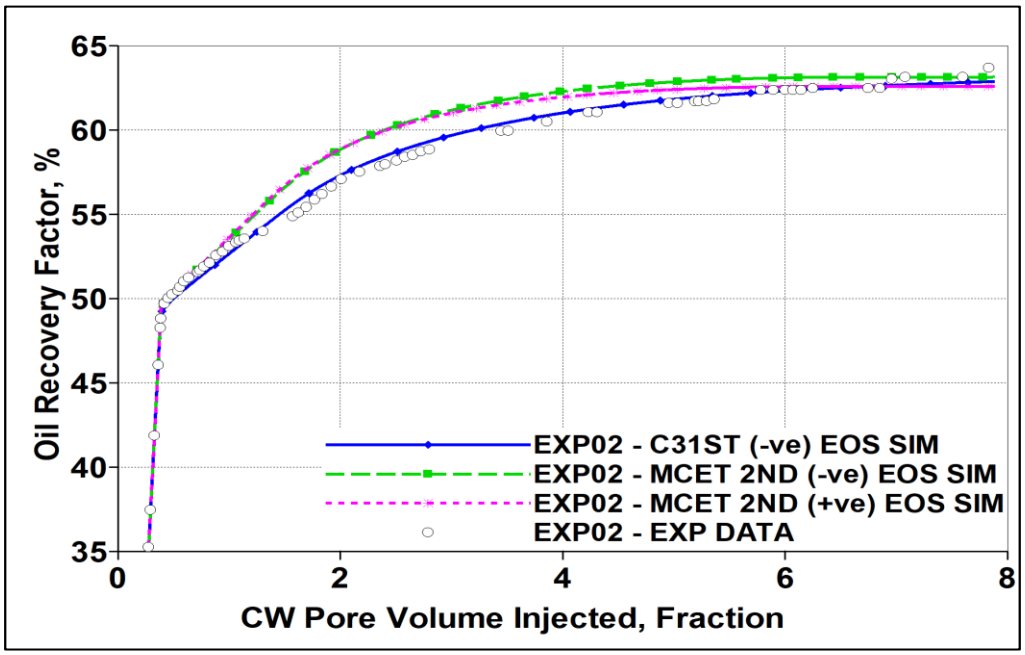

Figure 4-21 Comparison between measured and simulated oil recovery during secondary CWI (EXP02) where the black circles represent the experimental data, the blue plot is the simulation run using the first EOS that is tuned using assisted history matching, and the green and magenta plots are the simulation runs using the second EOS that is tuned to match the MCET test

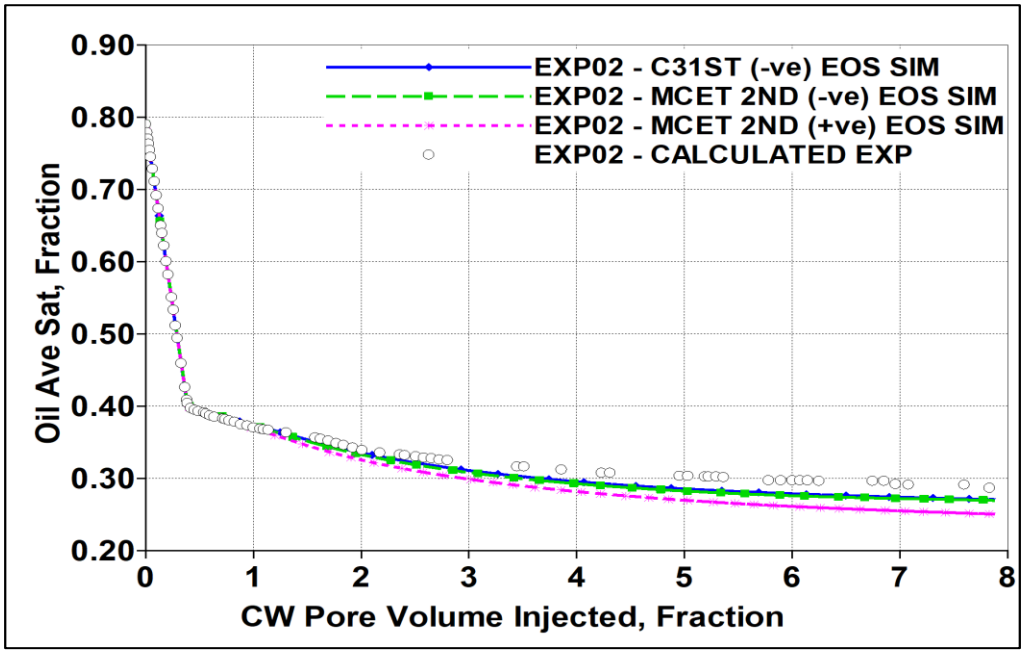

Figure 4-22 the average oil saturation in three simulation runs comparing to experimental data of EXP02

In the second EOS simulation scenarios, the system started to lose its energy (pressure) as shown in figure 4-24 when the gas production increased after 3 PV of injected CW, which means the trapped gas became mobile, as shown in figure 4-23. By reviewing the prediction results in secondary and tertiary CWI, using the negative CO_2-C_1 BIC for tuning the EOS is essential to mimicking the phase behaviour taking place during CWI.

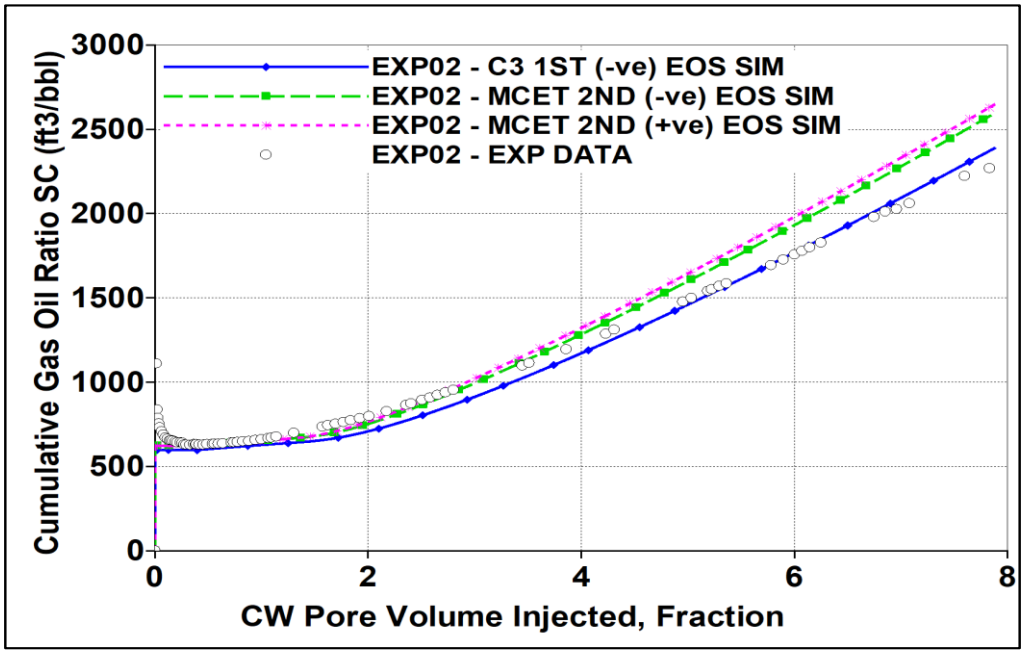

Figure 4-23 Calculated cumulative GOR in three simulation scenarios in comparison to measured experimental data EXP02

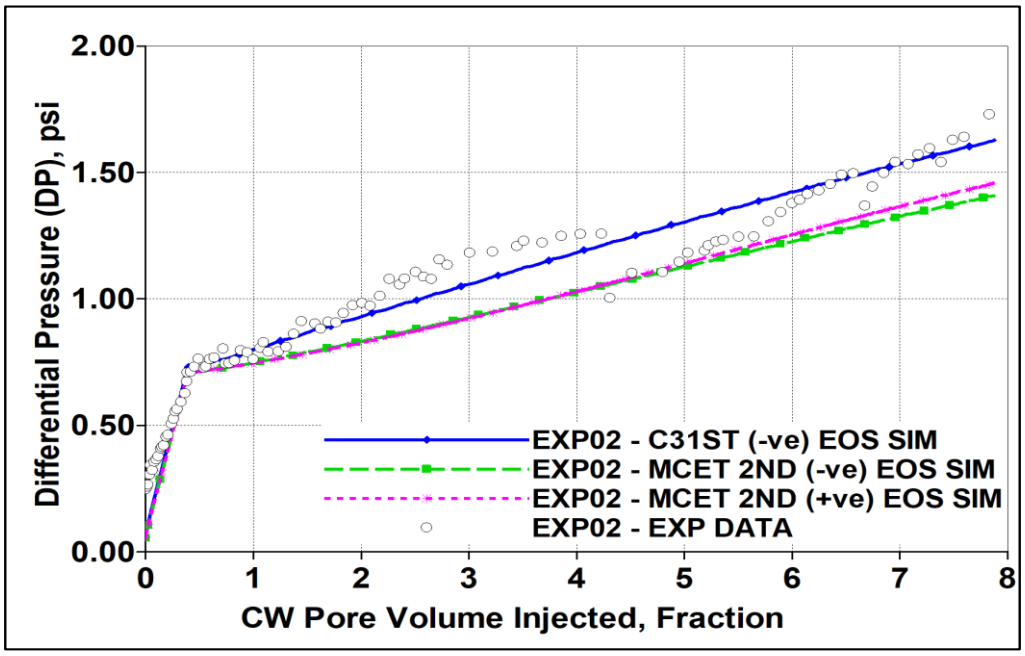

Figure 4-24 Predicted and history matched differential pressure across the core comparing with the measured experimental results of EXP02

4.5.2.3 Secondary CWI followed by CO_2 Injection (Test No. 3)

The prediction of tertiary CO_2 injection in test no. 3 revealed acceptable estimation of tertiary CO_2 injection performance, using the EOS that was tuned utilising the assist history matching technique for optimising the binary interaction coefficients of CO_2 to hydrocarbon components. After secondary CWI, the remaining oil is gradually recovered by the injected CO_2 in tertiary mode due to dynamic and non-equilibrium CO_2 diffusion via water phase to oil phase. The flash calculation carried out by the EOS computes the mixing between the three phases (CO_2, oil and water) instantaneously, however.

Looking at figure 4-26, the simulation runs that were performed utilising the EOS that was tuned by adjusting the BIC to match the multiple-contacts equilibrium PVT test, predict higher oil recovery than both the experimental data and the C3 1^{ST} (-ve) EOS SIM simulation run. The reason for this is that the EOS was tuned to model the behaviour change in oil due to CO_2 mass transfer from carbonated water to oil without taking into consideration the compositional change that takes place during conventional CO_2 injection.

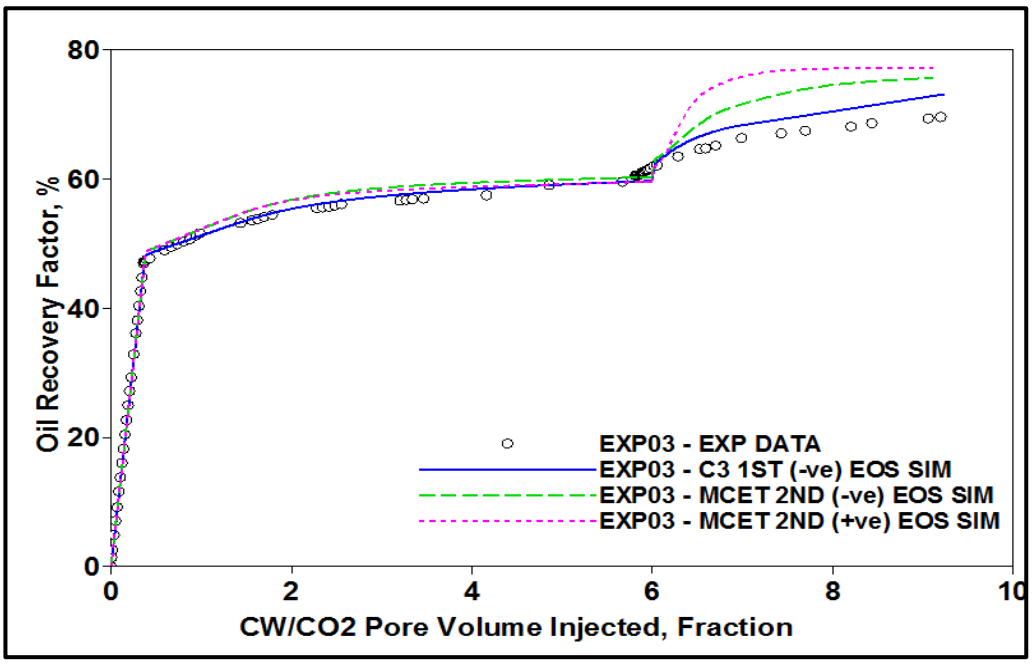

Figure 4-25 Comparison between measured and simulated oil recovery during secondary CWI and tertiary CO_2I (test no.3) where the black circles represent the experimental data, the blue plot is the simulation run using the first EOS that is tuned using assisted history matching, and the green and magenta plots are simulation runs using the second EOS that is tuned to match the MCET test

Considering now the MCET 2ND (-ve) EOS SIM that was tuned by manually adjusting the binary interaction coefficients of CO_2 and other hydrocarbon components and setting up CO_2-C_1 BIC with a negative value to match the multiple-contacts equilibrium PVT test. Changing the CO_2-C_1 BIC towards more negative values would decrease the CO_2 solubility in oil, consequently reducing the oil swelling and the rate of oil viscosity reduction. Subsequently, the oil recovery would reduce, as demonstrated in figure 4-27.

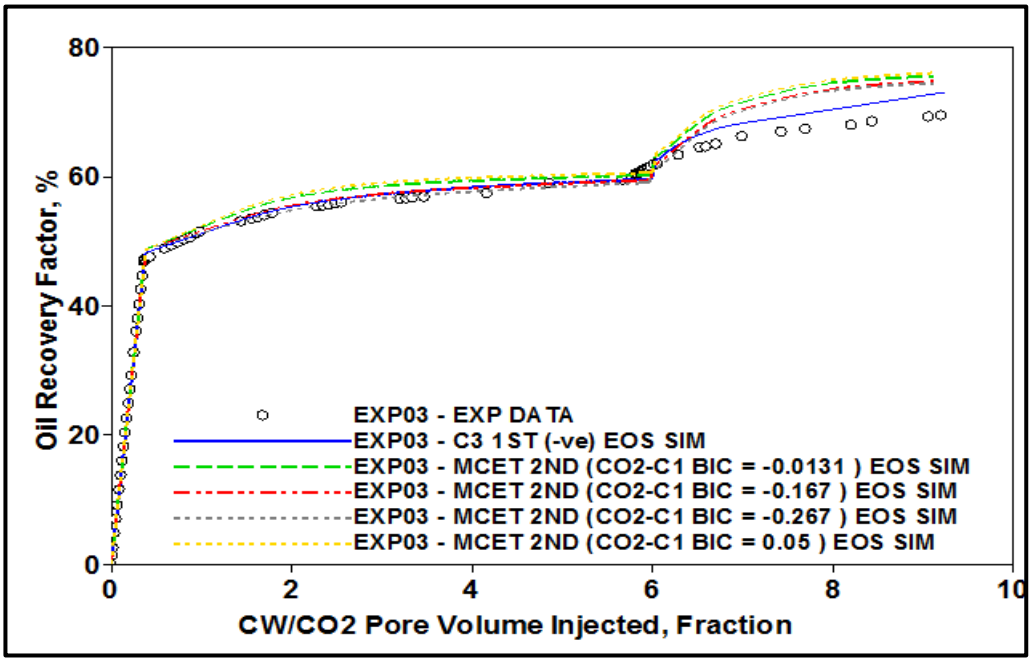

Figure 4-26 sensitivity of changing CO_2-C_1 BIC on oil recovery using MCET 2ND (-ve) EOS SIM

4.6 Summary and Conclusions

4.6.1 Multiple-Contacts Equilibrium PVT Test

In the multiple-contacts equilibrium PVT test, the carbonated water was brought into contact with under-saturated oil in a series of equilibrium contacts. Increasing trends in saturation pressure and GOR were measured while the solubility of CO_2 in the oil phase increased as a result of the CO_2 mass transfer from CW to oil. The outcome of this equilibrium PVT test verified the fluid-fluid interaction taking place while CW contacts oil. The following conclusions were summarised from this test:

- There was a dual mass transfer between carbonated water and oil where light hydrocarbon components, mainly C_1 to C_3, transferred from oil to the brine while CO_2 transferred from CW to oil.

- There was an incessant mass transfer of CO_2 into oil, which can be observed by the low GWR after each contact, even after the oil became saturated with CO_2 and formed a gas phase.

- A continuous CO_2 dissolution in oil, which was transferred from the CW, would lead to steady compositional changes in the oil to form a gas phase, even though the oil was under-saturated with hydrocarbon gases.

- The formation of the new gas phase during CWI depends on the amount of gas dissolved in the oil. The continuous and dynamic dissolution of CO_2 into the oil phase that takes place during the interphase mass transfer happening during CWI would expel the lighter hydrocarbon components of the oil to form a new gaseous phase with a tendency to enlarge the oil phase to a much greater extent than the effect of normal oil swelling.

- The formation of the new gas phase occurred after the oil became saturated with CO_2, which was reflected through an increase in the saturation pressure. The new phase is characterised as a gaseous phase. Furthermore, its early formation composition consists mainly of methane (C_1) in fully saturated oil, while in under-

saturated oil, its composition contains a higher concentration of CO_2 than of other light hydrocarbon components. The reason for this is the initial saturation level of each type of oil.

- The formation of the new phase would enhance the mass transfer of CO_2 from the aqueous phase to the oil phase that was clearly observed in the calculation of the CO_2 partition coefficient among the two immiscible phases.

4.6.2 Modelling CW Multiple-Contacts Equilibrium Test

In this fluid modelling, an attempt was made to predict the results of different equilibrium contacts in the MCET experiment using the cubic equation of state coupling with Henry's Law for the solubility of gases in brine. The results of the equation of state reveal the ability of the EOS to simulate the fluid-fluid interactions taking place when CW contacts oil. The following conclusions were drawn from this work:

- This a confirmation with the conclusion of the previous chapter that by adjusting the binary interaction coefficients between CO_2 and hydrocarbon components, the CO_2 mass transfer from CW to oil will change, and, as a result of that, the new (gas) phase will form containing the light hydrocarbon components. While Henry's Law controls the solubility of various gases in brine and through the flash calculation, the partitioning coefficients of soluble gases in brine to oil will mimic the mass transfer of those gases from CW to oil, and vice versa.

- The two manually adjusted BIC sets are mainly distinguished by the negative CO_2-C_1 BIC in one, referred to as MCET 2^{ND} (-ve) EOS, which was able to predict the CO_2 dissolution in oil through a noticeable increase in oil saturation pressure. The tuned EOS has the ability to reproduce the measured GOR and swelling factor before the formation of the gas phase, whereas the difficulty occurred in estimating the GOR after the gas phase formed, most likely due to an inaccuracy in the measured value.

- Successful prediction of the new (gas) phase composition and volume compared to measured composition after the sixth CW equilibrated contact. The tuned EOS calculated more extraction of C_{4+} than the measured experimental composition, however.

- The tuned cubic EOS calculated a continuing increase in reservoir oil density and a reduction in oil viscosity before the phase split to form the gas phase. After the phase split, both the oil density and viscosity demonstrate an increasing trend. These results of fluid modelling did not conclusively evaluate the CO_2-oil mixture characterisation in terms of viscosity and density, although the equation of state could predict the general behaviour of the CO_2-oil mixture as reported in the literature.

4.6.3 Prediction of Core Displacement Experiments

To evaluate of the necessity of having a negative CO_2-C_1 BIC, two sets of BIC's were used to tune the EOS and reproduce the measured CW and CO_2-oil mixture properties. Then, the tuned cubic EOS to mimic the MCET was used to simulate the performance of CWI in core displacement experiments. This very closely predicted the experimental outcomes and enabled a full comparison between the two sets of BICs. The resulting conclusions were obtained from the simulation practice:

- Changing the CO_2-C_1 BIC towards more negative values would decrease the solubility of CO_2 in oil, consequently reducing the oil swelling and the rate of oil viscosity reduction. A positive CO_2-C_1 BIC would limit the dissolution of CO_2 in the oil phase after the oil became saturated with CO_2, whereas the negative CO_2-C_1 BIC allows the oil continually to dissolve more CO_2.

- Generally, the second EOS simulation scenarios could realistically predict the increase in differential pressure across the core, which gives a good indication of the appropriateness of the obtained oil-gas relative permeability curves and also the effect of the binary interaction coefficients on fluid phase behaviour.

- The prediction of tertiary CO_2 injection in test no. 3 using the second EOS showed an overestimate of tertiary CO_2 injection performance. This was because the EOS was tuned to model the phase behaviour change in oil due to CO_2 mass transfer from carbonated water to oil without taking into consideration the compositional change that takes place during conventional CO_2 injection.

- In conventional waterflooding, the displacement between two immiscible fluids results in a fixed ratio of gas to oil, where the drop in differential pressure after water breakthrough and its subsequent stability is due to the flow rate of each fluid (water and oil) in a porous medium. In CWI, meanwhile, the effect of the gas to oil ratio on the differential pressure is a result of the formation of the new gaseous phase and its trapped mechanism in a porous medium.

Chapter 5 – Numerical Simulation of CWI in a Mixed-Wet Core

5.1 Introduction

In previous chapters, a methodology to numerically simulate the performance of CWI in core displacement experiments was successfully designed and implemented on Clashach sandstone cores using methane-saturated oil to history match the improvement in oil recovery. The method of tuning the EOS by optimising the binary interaction coefficients between the oil's CO_2 and hydrocarbon components and using assisted history matching to mimic the calculated new (gas) phase saturation from tertiary CWI coreflood experiments could be an effective and reliable way to simulate the performance of carbonated water injection in live oil core displacement experiments. Furthermore, positively or negatively adjusting the CO_2-C_1 BIC when tuning the EOS would increase or decrease the CO_2 dissolution in oil, with a consequent impact on oil swelling and the rate of oil viscosity reduction.

After that, continuous CO_2 mass transfer from the injected carbonated water to the oil phase would bring about compositional changes in the oil and extract the light hydrocarbon components forming a new gas phase. The physics observed in micromodel experiments proved the formation of that new gas phase within the resident oil which acts like oil swelling, and the reduction in oil saturation, with the subsequent increase in oil recovery relying on the enlargement of the volume of the gas phase. Additionally, the formed gas phase would create a three-phase flow regime such that a proper three-phase relative permeability function should be considered.

The proposed method was tested in a new set of experimental results where the carbonated water was injected into the reservoir core, which was aged with reservoir oil in order to evaluate and confirm its applicability in a real reservoir environment. Overall, the investigation of CWI performance in carbonate reservoirs using a live oil that was created by recombining the crude oil with a multi-components gas so as to represent a realistic oil system can be of great interest in terms of tuning the cubic equation of state for modelling phase behaviour in reservoir oil during CWI. In 2017, a series of integrating direct pore-scale micromodel visualisations and core-flood experiments performed to carry on a comprehensive analysis of the processes leading to additional oil

recovery in carbonate reservoir rocks by Mahzari et al. [73, 146]. Their observations endorse that the performance of CWI would be more representative under reservoir conditions using multi-component live oil and reservoir cores. On the other hand, using a single component (methane) make-up gas or reduced reservoir pressure and temperature, and any other form of simplification, would speciously change the pore-scale physics, and subsequently the performance of the CWI. The author uses their test results as a basis to apply his method for numerically simulating the performance of CWI in a tertiary coreflood experiment through a history matching technique. Then, the obtained saturation function, including the set of relative permeability and capillary pressure curves, were used in tandem with the tuned EOS to predict the performance of CWI for enhancing oil recovery in secondary mode.

5.2 Methodology

The method is mainly reliant on the formation of an additional phase when the interphase transfer of CO_2 occurred as a result of the interaction between the oil phase and the injected carbonated water. The formation of the new gas phase, and when exactly this occurs, could be observed through analysing the direct pore-scale observations, and serve to improve the tuning of the equation of state and thus the modelling of the fluid-fluid interaction and compositional changes that take place as a result of the transfer of CO_2 from the carbonated water to the oil phase. Furthermore, the formation and in-situ growth of the new phase within the oil during CWI, as observed in pore-scale experiments, controlled the need for modelling the immobility of this phase. According to the relationship between the saturation of gas and oil, and consequently the enhancement in oil recovery, Stone I three-phase relative permeability function was the suitable formulation to model the oil flow in the areas where three phases exist. Also, the strategy entailed history matching the tertiary fully-saturated CWI coreflood experiment and predicting the secondary fully and half-saturated CWI coreflood experiments.

5.3 Direct Pore-Scale Experiments

The formation of the new gas phase when the injected carbonated water comes into contact with the oil happens as a result of mass transfer of CO_2 to the oil phase, given that the CO_2 has a higher tendency to dissolve in oil than in water. This dissolution of CO_2

within it causes the oil to start to swell. Although the oil is initially saturated by hydrocarbon gases, the transferred CO_2 extracts the light hydrocarbon components, replacing them in the oil, subsequently forming an additional gas phase. Furthermore, the contrast between the solubility of CO_2 in oil and in water allows continuous, dynamic and non-equilibrium mass transfer of CO_2 to oil, which results in the rapid growth of gas bubbles within the oil that eventually reconnect the oil blobs and drive further production. The occurrence of the new phase, and its growth in volume, within the resident oil would result in apparent oil swelling. Also, although the saturation of the new phase rapidly increases, the oil saturation decreases, because the total hydrocarbon saturation remains constant due to the immobility of new (gas) phase saturation.

Mahzari et al. carried out three micromodel experiments on the recombined live oil at a reservoir pressure of 3100 psi and temperature of 212 °F to detect the mechanisms arising during CWI [73, 146]. In the first pore-scale experiment, fully-saturated carbonated water was injected in tertiary mode after secondary conventional water injection. In this experiment, a third (gaseous) phase started to form within the oil after injecting one pore volume of carbonated water, as a result of mixing between the carbonated water and the preceding conventional water, which may weaken the CO_2 mass transfer process. Despite the slightly late appearance of the gas phase, its formation introduced two mechanisms; (i) oil swelling and reconnection of trapped oil ganglia after waterflooding and (ii) movement of the third phase alongside the mobilised oil, as can be seen in the magnified snapshots in figure 5-1.

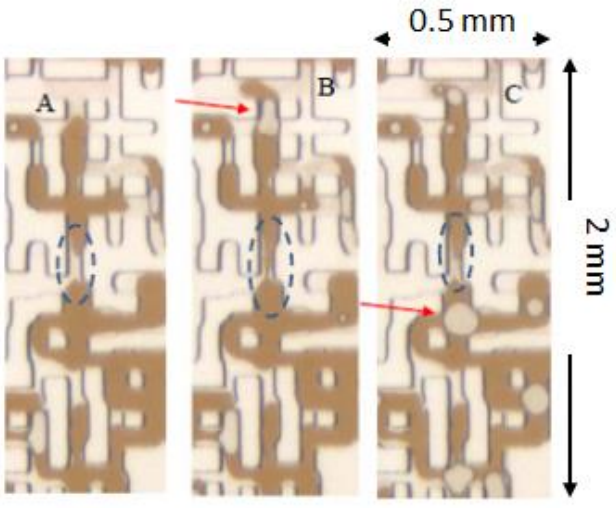

Figure 5-1 magnified snapshots of fully-saturated tertiary CWI micromodel to highlight the mechanism of oil swelling and reconnection of the oil phase, illustrated in the area with the blue circle, as well as the mobility of the third phase saturation alongside the oil phase (highlighted with red arrows) [121]

The second micromodel observation was performed to explore the mechanisms occurring in a secondary fully-saturated carbonated water injection scenario [73, 146]. Whilst the formation of the gas phase depends primarily on oil volume and its gas saturation level, the third phase forms ahead of the CW front, which indicates stronger CO_2 mass transfer in secondary CWI due to direct contact between the injected CW and in-situ oil. The bubbles of third phase combine to form larger patches, as indicated by the red arrows in figures 5-2A to 5-2C, then these patches relocate, displacing the oil blobs and allowing them to be produced, as shown in figures 5-2D and 5-2E.

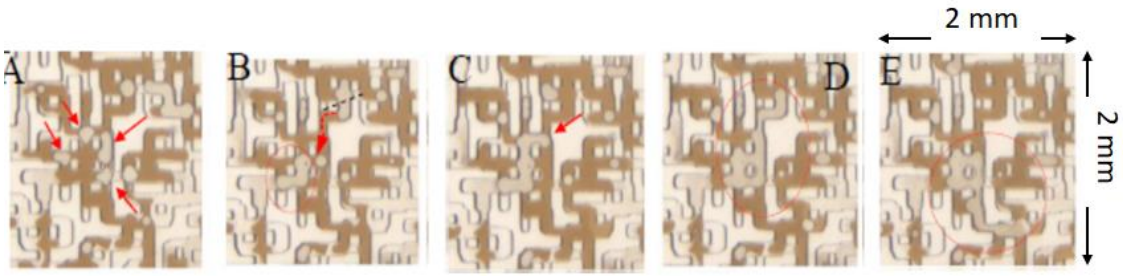

Figure 5-2 micromodel snapshots of (A) formation of third phase bubbles, (B) aggregation of the bubbles to form a third phase batch, (C) combined multiple patches to create a third phase chunk (D and E) third phase chunk displacing the stationary oil blobs during secondary CWI [73]

Mahzari et al. [146] observed a unique behaviour of the third phase towards the end of secondary CWI, in that the third phase saturation showed a decreasing trend, where the gas phase stayed in contact with the surrounding oil until the interface between them vanished, resulted in a brighter liquid phase. Furthermore, towards the end of CWI, continuous mass transfer of CO_2 to oil would extract more intermediate hydrocarbon components, which would bring about favourable conditions for miscibility potential between the third gas phase and oil phase. This phenomenon exhibits the importance of the presence of intermediate hydrocarbon components in live oil if we are fully to reproduce the processes taking place during CWI.

According to Mahzari et al., the third phase formed after 4.5 hours, equivalent to 2 pore volumes of injected half-saturated CW in tertiary mode (post-waterflood) in their third pore-scale visualisation experiment [73]. Moreover, the injection of half-saturated CW led to a reduction in the volume of the formed gas phase within the oil phase. On other words, the carbonation level in the injected brine would certainly have a significant influence on the mass transfer of CO_2 from the carbonated water into the resident oil. As a result, the tertiary half-saturated CWI leads to a higher oil saturation than with fully-

saturated CWI. Figure 5-3 shows the variation in oil saturation and maximum third-phase saturation based on different injection modes and carbonation levels, where the various responses to different injection scenarios could be explained by the volume of the third phase formed during CWI.

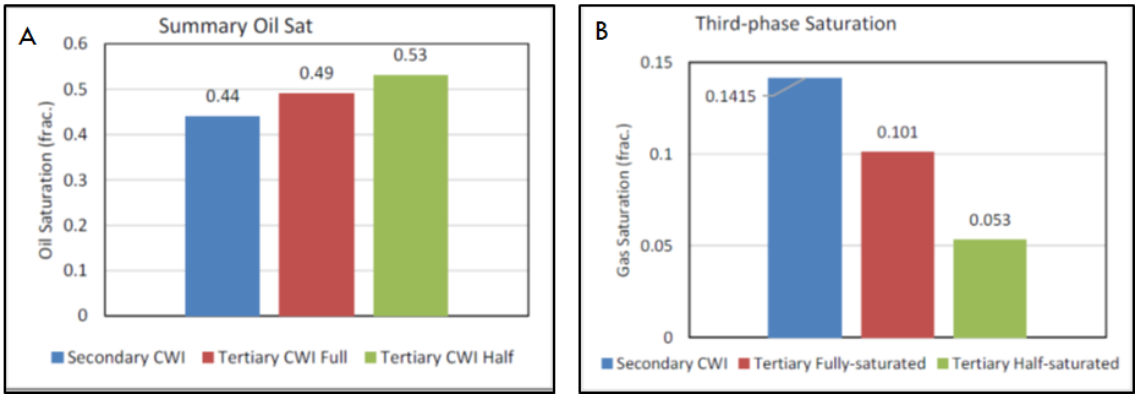

Figure 5-3 (A) the calculated oil saturation in visualisation experiments at the end of three injection scenarios (B) the estimated third-phase saturation during three visualisation experiments [73]

5.4 Core Displacement Experiments

Building on the above, a trial of a new set of core displacement experiments were undertaken to solidify the method proposed for numerically modelling the performance of carbonated water injection in a live oil system. Specific experiments are presented in which CW is injected in a fully-saturated (gas-dissolved) oil system reservoir core that were performed by Mahzari et al. [73] Three initial conditions were considered: secondary fully-saturated CWI where initial oil saturation was at an irreducible water saturation of 0.173, while in tertiary fully-saturated CWI the remaining oil saturation was residual oil saturation after conventional waterflooding. In the third experiment, meanwhile, half-saturated CW was injected to displace the oil in secondary mode. In these experiments, the reservoir oil was a recombination of stock tank reservoir crude oil (S) with four gas components (C_1, C_2, C_3, nC_4) at a gas-oil ratio of 435 SCF/STB (77.5 cc/cc). The three experiments were performed using the same core at a temperature of 212 °F and reservoir pressure of 3100 psi. Worth to be mentioned that all the experimental data and results were performed and measured by Mahzari et al. [73, 146] and some of the results were published in their papers while the other results were provided to me within Heriot-Watt university research group. Then, I had the opportunity to utilize these results to implement my method to simulate the performance of CWI.

5.4.1 Fluid Samples

A stock tank crude oil S which contains about 19 Mol% of intermediate components (iC_4-C_6), was recombined with make-up gas that had four hydrocarbon components (C_1-nC_4) at a gas oil ratio of 77.5 ccGas/ccoil (~ 435 scf/stb) to create the reservoir oil used in core displacement experiments. The full composition is set out in table 5-1. The oil was characterised as a light crude oil that has an API gravity of 27.3° and a dead oil viscosity at the test temperature of 212 °F was 2.22 cp.

Table 5-1 Crude S stock tank oil composition and make-up gas for reservoir oil recombination [73]

Hydrocarbon Components	STO Composition (Mol%)	Make-up gas (Mol%)
C_1	0.041	53.42
C_2	0.801	25.79
C_3	3.803	13.25
iC_4	0.965	-
nC_4	4.656	7.54
iC_5	2.295	-
nC_5	4.489	-
C_6	7.009	-
C_7	5.767	-
C_8	5.39	-
C_9	5.008	-
C_{10+}	59.776	-

The properties of the live oil are presented in table 5-2. The oil was fully saturated with the dissolved gas in such a way that the live oil saturation pressure equalled the test pressure of 3100 psi at a reservoir temperature of 212 °F. The oil characterized as low viscous oil.

Table 5-2 measured basic live oil properties of crude S [73]

Live oil saturation pressure at 212 °F	3100 psi
Gas-oil ratio (Rs)	435.7 SCF/STB
Stock tank API gravity	27.3°
Stock tank oil viscosity at 212 °F	2.22 cp
Live oil viscosity	0.829
Formation Volume Factor	1.239

The brine used in the experiments was prepared to represent a seawater brine with a salinity of 59046 ppm using the ionic contents showed in table 5-3. The seawater brine was enriched with CO_2 at the required carbonation level in test conditions to make-up the fully-saturated carbonated water. The CO_2 content of the fully-saturated water at test conditions was 22.33 ccCO_2/cc Brine (~ 125 scf/bbl). Meanwhile, the volume of CO_2 was reduced to prepare the half-saturated CW which has CO_2 content of 11.34 ccCO_2/cc Brine (~ 63.7 scf/bbl).

Table 5-3 Composition of the seawater brine used in the coreflood experiments [73]

Ion	Concentration, ppm
Na^+	18300
Ca^{++}	650
Mg^{++}	2439
Cl^-	32200
SO_4^{--}	4290
HCO_3^-	120
TDS	59046

5.4.2 Core Samples

A composite carbonate core made by five core plugs was used during the coreflood experiments where its wettability was restored to a mixed-wet state through ageing with reservoir live oil. The composite core was cleaned, dried and then its irreducible water saturation (S_{wi}) was attained. Next, the core was aged using dead oil for three weeks. Then, the recombined live oil was injected to displace the dead oil until the recorded gas-oil ratio reached the initial value measured during the recombination process.

The average permeability of the composite carbonate core, measured with the formation brine at the test pressure, temperature and porosity are shown in table 5-4, along with the core dimensions and pore volume.

Table 5-4 the physical and rock properties of the composite core used in the coreflood experiments [73]

Length (cm)	Diameter (cm)	Porosity (%)	Pemeability (md)	PV (cc)
25.74	3.793	25.83	88.277	75.13

5.4.3 Coreflood Tests and Results

5.4.3.1 Tertiary Fully-Saturated CWI (EXP01 SWF – TCWI)

After establishing the initial water saturation of 17.3% pore volume (PV), the seawater injected, where it was pre-equilibrated with methane to prevent the presence of mass transfer and to strip off of methane content from reservoir oil. After injecting about 6 PV of conventional seawater, a pump flood was performed to surpass the end-effects and recover any oil retained in the outlet of the core, in order to establish the residual oil saturation across the core. The differential pressure across the core increased until the seawater broke through, then it declined as the oil movement reduced and the system reached its equilibrium where single-phase flow of water occurred. As a result of this, the oil recovery after secondary conventional water flooding was 40.7 % of OOIP. Subsequently, fully-saturated carbonated water containing 22.33 cc of CO_2 per cc of seawater was injected at the same injection rate in tertiary mode (post-waterflood). Additional oil of 14.6 % of OOIP was recovered after injecting 6 PV of carbonated water. Figure 5-4 demonstrates the full sequences of conventional seawater flooding followed by tertiary CWI oil recovery and differential pressure across the core.

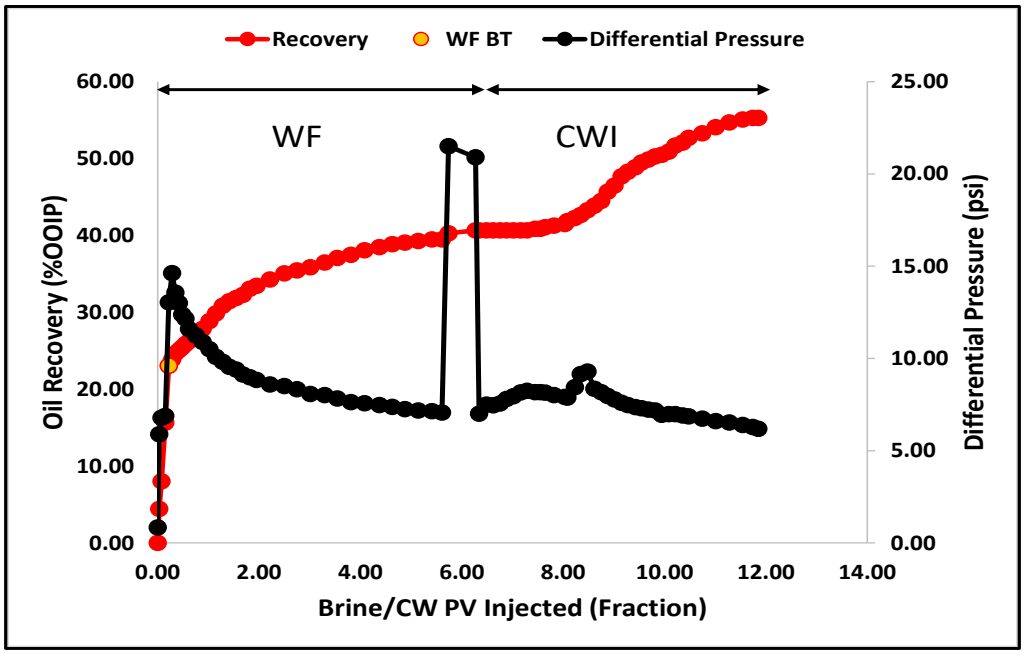

Figure 5-4 oil recovery and differential pressure across the core during secondary WF and tertiary CWI in crude S – EXP01 [73]

5.4.3.2 Secondary Fully-Saturated CWI (EXP02-SCWI)

For the secondary CWI, all the operational parameters from the tertiary CWI core displacement test were retained. In this experiment, the core was flooded with fully CO_2-enriched water after establishing the initial oil and water saturations at 83% and 17% PV, respectively. The injection of CW continued until a total of about 5.8 pore volume had been injected, by which point an oil recovery of 54.7 % of OOIP had been produced. Figure 5-5 shows the profiles of oil recovery and differential pressure across the core during secondary CWI.

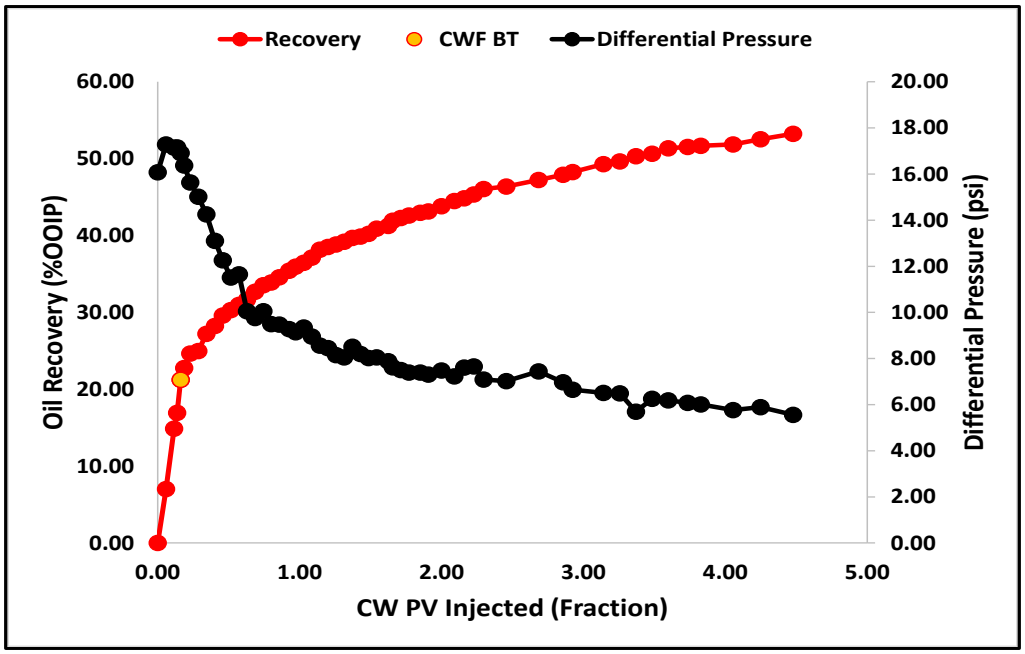

Figure 5-5 recorded oil recovery and differential pressure across the core during secondary fully-saturated CWI in crude S EXP02 [73]

5.4.4 Third Phase Saturation during Tertiary CWI

Considering the tertiary CWI core displacement experiment, residual oil saturation (S_{orw}) only remained in the porous medium after secondary conventional water flooding, whereby no further oil production took place. The observation from the direct pore-scale experiment that was performed in the same conditions determined that the total hydrocarbon saturation during CWI would remain constant whereas the new phase was formed as part of the total hydrocarbon saturation. The recorded oil production data during the tertiary CWI core displacement test was used to calculate the average oil saturation in the core through the test. The residual oil saturation (S_{orw}) after conventional

waterflooding was 0.4908, and this was assumed to be equal to the total hydrocarbon saturation during tertiary CWI. Then, the average (gas) saturation was calculated using equation 3-2, which expressed the physics observed in pore-scale experiments, as shown in figure 5-6. The assumption in using this method was that the mechanisms caused by the formation of the third phase were the main contributors to the oil production, neglecting the contribution of normal oil swelling and oil viscosity reduction. As a result, the oil saturation would decreased while the new phase saturation would increase.

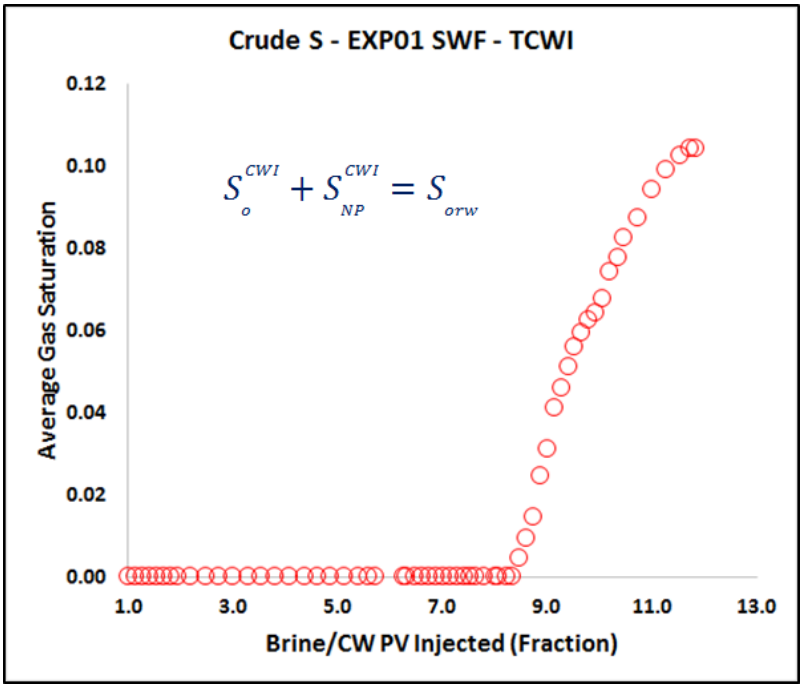

Figure 5-6 calculated average (gas) new phase saturation during tertiary full-saturated CWI of coreflood EXP01

The other process resulting from the presence of the third phase is the creation of a three-phase flow region in which a two-phase flow regime would no longer govern the saturation distributions. Additional aspects of multi-phase flow should therefore be considered while simulating the process of injecting carbonated water, and these can be extrapolated from the pore-scale observations. Experimentally, during conventional waterflooding, the water follows its flowing path leaving a significant amount of oil saturation that could not be produced. Observations of pore-scale micromodel experiments revealed that the formation of the new gaseous phase occurred in a scattered manner within the residual oil. Continuous injection of the carbonated water results in an increase in the number and volume of the bubbles in the gas phase within the oil due to continuous and non-equilibrium CO_2 dissolution into oil. The influence of this mechanism serves to enlarge the oil volume further, such that the detached oil blobs are

connected and remobilise to form a continuous low mobility flow of oil. Through this mechanism, a relationship between the formed gas phase and oil can be generated in which the new gas saturation grows in parallel with the reduction in the oil saturation, although the sum of the oil and gas saturations would remain constant to residual oil saturation (S_{orw}). The residual oil saturation during CWI is therefore a function of the gas saturation. An analogy of this concept could be the linear interpolation between the two extreme values, which are residual oil saturation to water (S_{orw}) and residual oil saturation to gas (S_{org}), proposed by Fayers [103] in their study the of Stone I three-phase formulation [100], as follows:

$$S_{om} = S_{orw} - \alpha(S_{gt}) \qquad \text{Equation 5-1}$$

Where S_{om} is the minimal oil saturation in the three-phase region related to S_{orw}, and S_{gt} is trapped gas saturation; in our case, this can be the new (gas) phase saturation, which most likely would be trapped within the oil at its early stage. The coefficient (α) would be a constant value equal to 1, to relate the growth in the gas saturation to the reduction in the oil saturation as the main mechanism responsible for oil recovery during carbonated water injection, as demonstrated in figure 5-7.

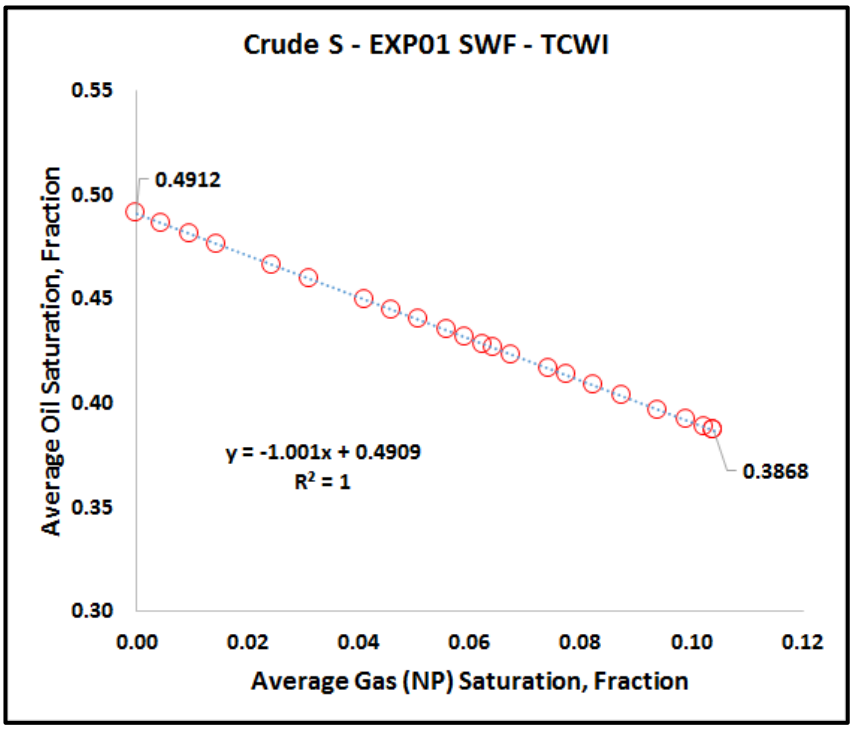

Figure 5-7 minimal oil saturation between two extreme residual oil saturations during the formation of the gas phase in tertiary CWI

The three-phase region during CWI can be considered as an "in-situ WAG" type of EOR, but the third phase would generate a local three-phase flow with a relatively higher trapped gas saturation, whereas the cyclic injection of gas and water in the WAG process would require a good sweep efficiency of both injection fluids, i.e. water and gas, to bring about residual oil saturation reduction.

For general three-phase flow in porous media, three phase relative permeability is taking into an account for the interaction of flow between the different phases. Due to the complex and time-consuming nature of three phase relative permeability measurements, three phase oil relative permeability formulations are often interpolated from water-oil and oil-gas two phase relative permeability data. Various three-phase relative permeability correlations have been proposed to predict the oil's relative permeability in three phase region, but the most widely used are Stone I and II, Baker, and linear models. Among these mentioned models, Stone I [100] is the most representative for idealising the three-phase flow regime during CWI in a live oil system where an additional phase is formed.

5.5 Simulating the Performance of CWI

A methodology has been established to simulate the performance of CWI core displacement tests by analysing the physics taking place in pore-scale micromodel observations. As a result of that, a new set of CWI coreflood experiments using reservoir oil performed by Mahzari et al. are modelled to history match the tertiary CWI core displacement test and predict the secondary CWI and tertiary half-saturated CWI coreflood experiments [73].

5.5.1 Model Description

A linear one-dimensional model was constructed to build the reservoir grid system. Figure 5-8 illustrates the schematic 1D cross-section in which a core about 25.7 cm (0.844 ft) long and almost 3.8 cm (0.124 ft) in diameter is discretised into 100 grids in the x direction and a single grid in both the y and z directions in Cartesian horizontal orientation. Since the rock properties of the composite cores were measured as a whole core, it was anticipated that the simulation model would have a constant porosity of

0.2583 and an average isotropic permeability of 88.3 md. After that, the model was simulated using the CMG-GEM compositional simulator [106].

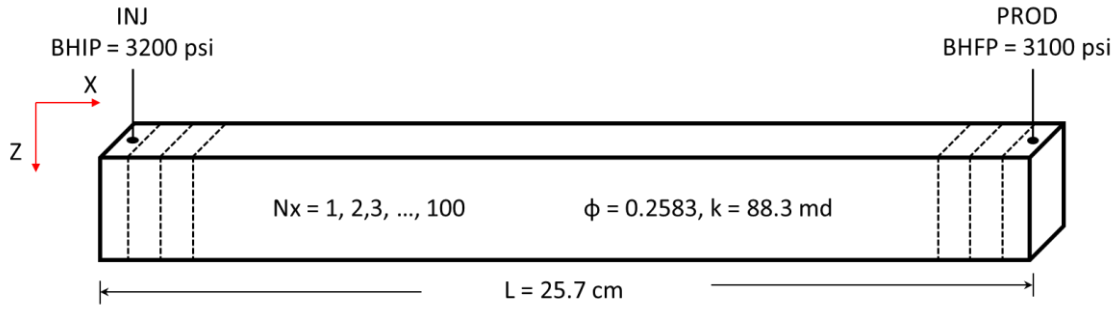

Figure 5-8 Schematic diagram showing the 1D model setup for Crude-S coreflood experiments

The carbonated water was injected by invoking the solubility feature. Henry's Law was used to model the solubility of CO_2 in brine, which was measured to be 22.3 cc of CO_2 per cc of brine (125 scf/bbl) at test conditions of 3100 psi and 212 °F with a brine salinity of 59046 ppm. Thus, carbonated water (CW) was defined as an aqueous phase that has 0.97548 gmol per kg water of CO_2 molality soluble in brine and was injected using a single well, called the 'injector' at i=1. The second well defined in the model was the 'producer' at i=100. The well at the outlet was constrained by a constant bottom-hole flowing pressure of 3100 psi, which was the test pressure, whereas the injection well was constrained with a constant injection rate of 0.00905 bbl/day.

5.5.2 Modelling Reservoir Fluids

The crude oil (S) used in these tests was a low viscous black oil with an API gravity of 27.3° and stock tank oil viscosity of 2.22 cp at a test temperature of 212 °F. Four component gases (C_1, C_2, C_3, and nC_4) were used as a make-up gas to be recombined with stock tank oil at gas-oil ratio of 435 scf/stb to generate the reservoir live oil. The reservoir oil was fully saturated with gas whose saturation pressure of 3100 psi was equal to the test pressure. The live oil viscosity at test conditions was 0.829 cp.

The composition of the recombined live oil was calculated through a global material balance similar to the procedure described in chapter 4. Figure 5-9 shows the reservoir oil after recombining the four components making up the gas with stock tank oil at the required gas-oil ratio. Peng-Robinson's (1978) cubic equation of state, coupled with the Jossi-Stiel-Thodos (JST) viscosity model, were tuned at the test temperature of 212 °F

using the CMG-WinProp^{TM} fluid modelling software package to reproduce the measured fluid properties that are listed in table 5-6.

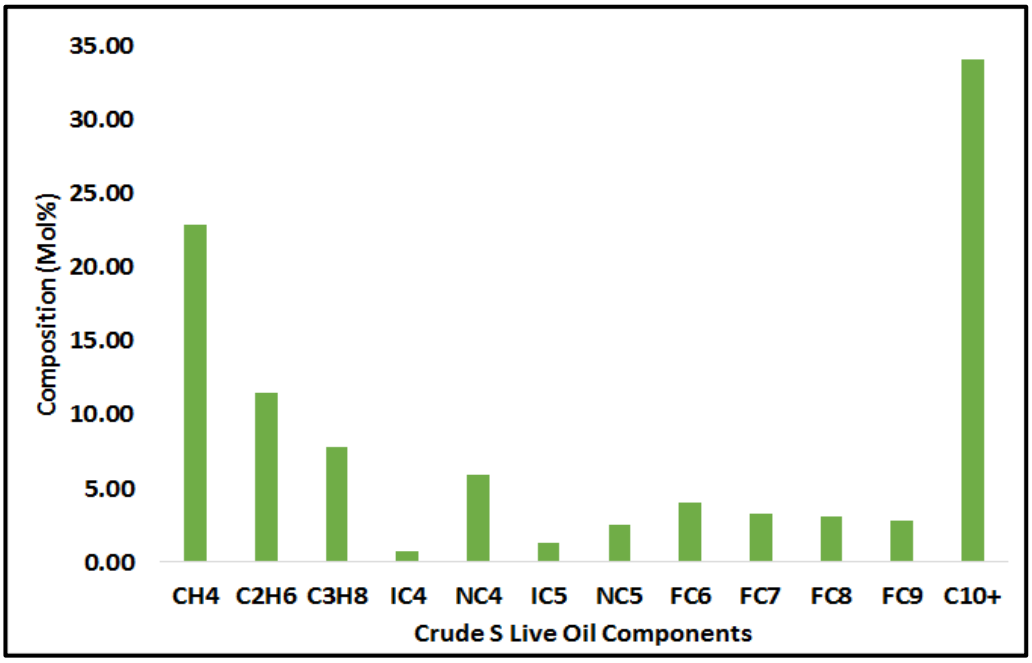

Figure 5-9 recombined reservoir live oil – crude (S)

Reservoir oil contains twelve individual hydrocarbon components, including C10+ which represents the pseudo-component, and CO_2 which represents non-hydrocarbon components. The hydrocarbon interaction coefficient exponent (PVC3) is a real number used to generate the binary interaction coefficients between hydrocarbon components, del_{ij}, and this was adjusted from the typical value of 2 to be 1.8408. Additionally, critical properties of C_{10+} such as pressure, temperature, molecular weight, and volume shift were used in the regression process to repeat the measured saturation pressure and separator test; for example, GOR, oil formation volume factor and oil gravity. A thorough description of the reservoir live oil after the EOS had been tuned is set out in table 5-5, while figure 5-10 shows the phase diagram of the recombined oil before and after the regression process. On the other hand, the JST correlation was tuned by adjusting its exponent parameter and polynomial coefficients 2, 3, 4 with C_{10+} critical molar to regenerate the stock tank oil and live oil viscosities under measured conditions.

Table 5-5 detailed description of crude (S) live oil

Components	Composition	MW	Pc	Tc	ω	Volume
	Mol%		atm	K		Shift
CO_2	0.000	44.01	72.80	304.20	0.225	0.000
C_1	22.854	16.04	45.40	190.60	0.008	0.000
C_2	11.479	30.07	48.20	305.40	0.098	0.000
C_3	7.840	44.09	41.90	369.80	0.152	0.000
iC_4	0.723	58.12	36.00	408.10	0.176	0.000
nC_4	5.888	58.12	37.50	425.20	0.193	0.000
iC_5	1.314	72.15	33.40	460.40	0.227	0.000
nC_5	2.571	72.15	33.30	469.60	0.251	0.000
FC_6	4.014	86.00	32.46	507.50	0.275	0.000
FC_7	3.303	96.00	30.97	543.20	0.308	0.000
FC_8	3.087	107.00	29.12	570.50	0.351	0.000
FC_9	2.868	121.00	26.94	598.50	0.391	0.000
C_{10+}	34.061	350.22	11.58	883.83	1.016	0.258

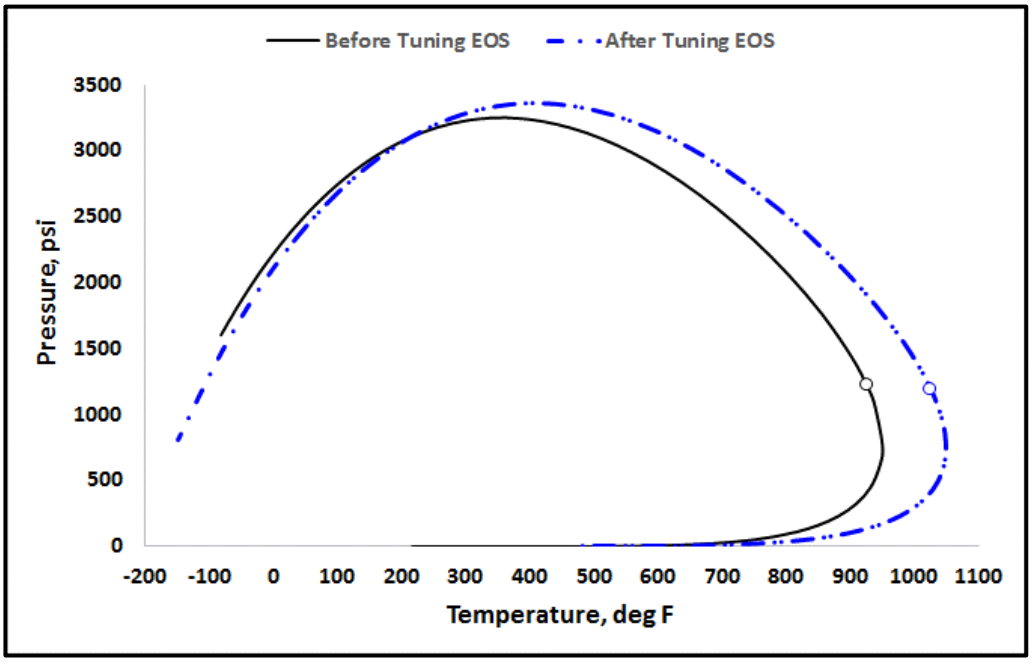

Figure 5-10 phase diagram of crude (S) live oil before and after EOS tuning

The resultant fluid properties after tuning the cubic EOS are displayed in table 5-6, and these were aligned with the experimental values that were measured during the coreflood test.

Table 5-6 comparison between the basic fluid properties that calculated by EOS and the measured values of crude (S) live oil

Parameter	Saturation Pressure (psi)	GOR (SCF/STB)	FVF (bbl/STB)	API Gravity	Oil Viscosity (cp)	
					Live Oil	STO
Measured [73]	3100.0	435.7	1.239	27.3	0.829	2.22
Modelled	3100.1	435.5	1.245	27.3	0.829	2.25

Henry's Law constant was adjusted to reproduce the gas (CO_2) water ratio of 125 scf/bbl that characterised the solubility of CO_2 in brine. The adjusted Henry's Law constant and molar volume at infinite dilution were 5981.368 atm and 0.036141, respectively, and at a reference pressure of 3100 psi, whereas about 1.672 mol% of CO_2 was soluble in brine.

As can be noticed, the data regarding the basic fluid properties are not enough for further adjustment of the EOS to predict CO_2-oil mixture phase behaviour characterisation during mass transfer of CO_2 from carbonated brine to oil. While the binary interaction coefficients between CO_2 and hydrocarbon components controlled the modelling of the CO_2-oil mixture characterisation through the mixing rule in the EOS, and the solubility of CO_2 in brine had been adjusted by Henry's Law, then the average gas saturation, which was estimated in the tertiary CWI coreflood test, was used as a guide to tuning the EOS to model the fluid-fluid interaction process occurring during CWI to generate the third phase.

5.5.3 Reproducing the Formation of the Third Phase

The current cubic equation of state could not thermodynamically model the behaviour of polar molecules such as water. Coupling the model of CO_2 solubility in brine with the cubic equation of state could therefore provide a robust and reliable model for predicting phase equilibria of high-pressure multiple components containing CO_2 and hydrocarbon mixtures by cubic equation of state along with estimating gases solubilities in brine by Henry's Law. In addition to a representative cubic equation of state that could accurately predict vapour pressure, the ability of a CEOS to correlate and predict the phase equilibria of mixtures depends strongly upon the mixing rule applied. The most generally-used rule to extend an EOS to mixtures of non-polar molecules is to apply van der Waals one-fluid mixing rules. The van der Waals mixing rules are capable of accurately representing

vapour-liquid equilibria for a non-polar system using only one binary-interaction parameter (k_{ij}).

On the other hand, the solubility of gas in the aqueous phase is estimated from Henry's Law constants, taking into consideration the effect of salt, which is handled by using the scaled-particle theory (SPT) to modify Henry's Law constants derived for pure water. The connection between the cubic equation of state and Henry's Law is established by the interaction parameter and the fugacity coefficient of the specific component through a flash calculation process of various phases (oil, gas and water). In this case, the flash calculation would be predominantly controlled by CO_2 mass transfer from CW to oil and the changes in the phase behaviour of the contacted oil which subsequently leads to the formation of the new-gaseous phase. The fugacity coefficient of the CO_2 component in vapour and liquid are estimated using the cubic equation of state and are a function of pressure, temperature, and phase composition, whereas the fugacity coefficient of CO_2 in aqueous phase is being estimated from Henry's law. More details of the process had been explained through chapter 3 in this research.

During CWI, the mass transfer of CO_2 from the aqueous phase to oil phase is the essential process driving the subsequent mechanisms that result in improved oil recovery. For that reason, the fugacity coefficient of CO_2 in the aqueous phase was kept as predicted by Henry's Law, whereas the fugacity coefficients of CO_2 in vapour and liquid were changed based on the binary interaction parameters of CO_2 to hydrocarbon components. Based on that, the partitioning coefficient (k_{iw}) was calculated in order to estimate the mole fraction of CO_2 in both aqueous and oil phases. Next, the liquid phase was examined as it reached a stable equilibrium since the vapour (gas) phase is formed whenever the liquid (oil) phase is not stable.

Utilising the average gas saturation profile calculated during the tertiary CWI core displacement experiment, the binary interaction coefficients of CO_2 to hydrocarbon components were adjusted to approximate the fugacity coefficients of CO_2 in both vapour and liquid phases, resulting in a non-stable oil phase that in turn produces the gas phase. Figure 5-11 displays the estimation of gas phase saturation (blue lines) by various binary interaction parameters realisations, where the optimum solution, indicated by the red line, reproduces the historical average gas saturation profile.

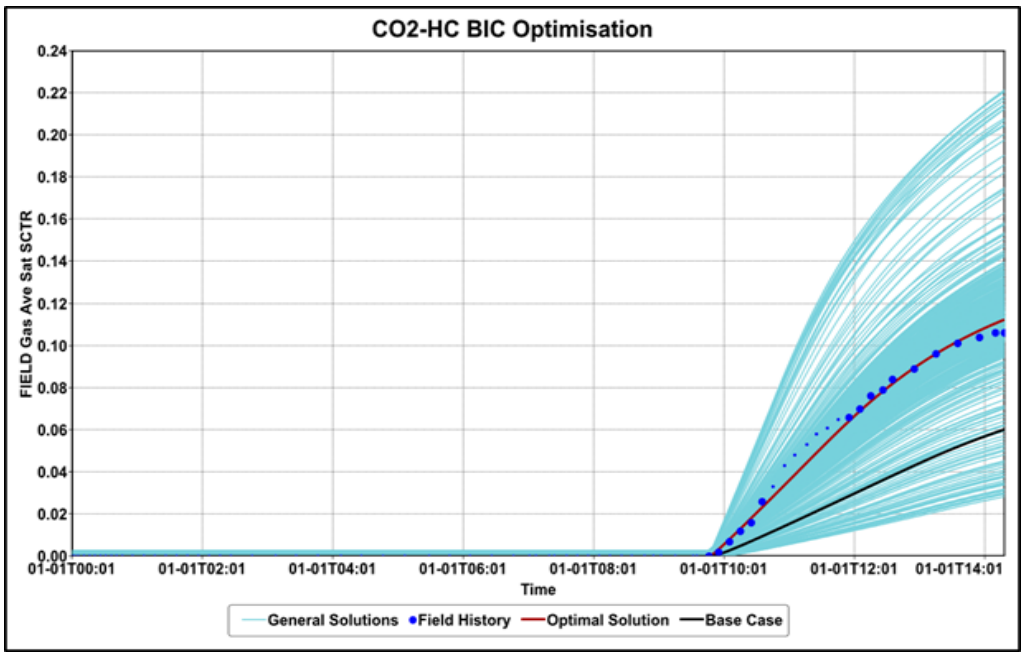

Figure 5-11 impact of adjusting the BICs in EOS with the aim of generating the third phase saturation during the tertiary CWI core displacement test

5.5.4 History Matching EXP01-SWF-TCWI

The purpose of the coreflood experiments was to estimate the flow function to convincingly represent the behaviour of the flow in a porous medium. Thus, one of the consequences of simulating core displacement tests would be obtaining the relative permeability and capillary pressure functions of the target displacement scenario. The secondary conventional water injection coreflood experiment was history matched in order to calculate the flow function containing water-oil relative permeability and capillary pressure. The constructed 100 grid-block one-dimensional model was used in a compositional simulator (CMG-GEM) connected to an assisted history matching machine (CMOST) to obtain the flow function. The LET formulations, developed by Lomeland et al. [130, 147], were integrated so as to develop flexible correlations for calculating the relative permeability and the correlation of Skjaeveland et al. [148] was used to calculate the capillary pressure function for mixed-wet reservoirs. Usually, the calculated saturation functions are less confident within saturation ranges attained after breakthrough of the displacing fluid, i.e. water, in an unsteady-state of a two-phase flow. The early water breakthrough in the secondary water flood experiment, however, results in a relatively wide range of saturation changes achieved after breakthrough, which could lead to a more reliable saturation function with respect to water saturation.

As a lesson learned from the previous simulation exercise, the adjustment of BICs was combined with oil-gas relative permeability optimisation to achieve a comprehensive history matching of the performance of carbonated water injection in tertiary mode. Therefore, the global objective function included the main objective variables as expressed in equation 5-2, that leads the optimizer on altering the input parameters to minimise the difference between the measured and simulated data. Those objective variables are the cumulative oil production volume, bottom-hole injection pressure and oil and gas saturation.

$$M = \sum_{i=1}^{N_p}\left[W_{oi}\left(V_{oi}^{EXP} - V_{oi}^{SIM}\right)^2\right] + \sum_{i=1}^{N_p}\left[W_{BHIPi}\left(BHIP_i^{EXP} - BHIP_i^{SIM}\right)^2\right] + \sum_{i=1}^{N_p}\left[W_{Sgi}\left(S_{gi}^{EXP} - S_{gi}^{SIM}\right)^2\right] + \sum_{i=1}^{N_p}\left[W_{Soi}\left(S_{oi}^{EXP} + S_{oi}^{SIM}\right)^2\right] \quad \text{Equation 5-2}$$

The number of observation points in cumulative oil production and oil and gas saturation was about 35 points in each of these objective function variables while double that number of observation points recorded in bottom-hole injection pressure for digitised recording in this case. On the other hand, the input parameters of tuning EOS and estimating the oil-gas relative permeability generated 19 parameters in which they should be adjusted to reach the optimum solution. While ten input parameters represent the binary interaction coefficients of CO_2 and hydrocarbon components as listed in table 5-7, the L.E.T oil-gas relative permeability correlation including Soirg, Sgcrit, Krgcl and oil and gas LET exponents which are Lg, Eg, Tg, Log, Eog and Tog; represented by nine input parameters.

After setting up the global objective function and assigning the input parameters, the CMG DECE optimiser performed to accomplish 3500 simulation runs as shown in figure 5-12 to minimise the percentage of global error upon achieving the optimum solution. The rate of global history-matching error initially was about 12% then reduced below 2% in the matched solution. Although the global error reached 2% after 500 simulation runs, however, it took another 3000 simulation runs to fine-tune the input parameters for acceptable matching of all objective function variables. The analysis of input parameters effectiveness shows the most significant parameters in overall were the BIC_CO2_C10p and oil-to-gas relative permeability. Those two parameters effected more in oil and gas saturation, as explained in table 5-7. The critical gas saturation and the start of gas mobility have a great impact on bottom-hole injection pressure.

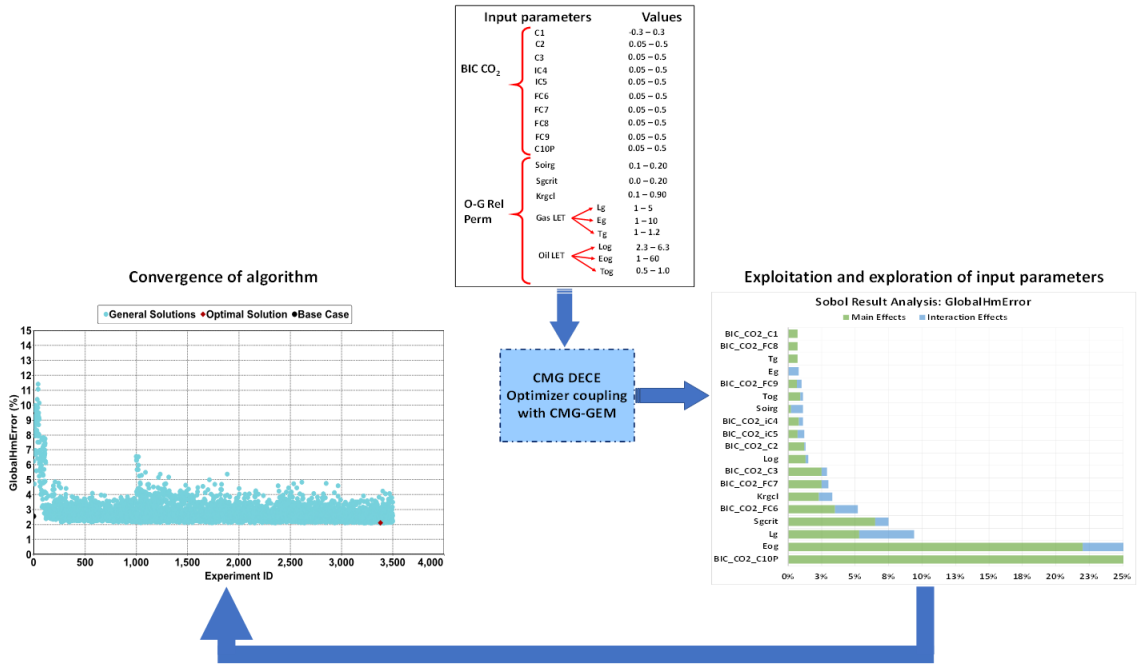

Figure 5-12 flow diagram of assisted-history matching for tertiary CWI core displacement in mixed-wet core

Table 5-7 effectiveness matrix of input parameters on objection functions of tertiary CWI core displacement in mixed-wet core

Input Parameters	Objective Function				
	GlobalHmError	Gas Saturation	Oil Saturation	Cumulative Oil Production	BHIP
$BIC\_CO_2\_C1$	0.7%	0.5%	1.1%	0.5%	0.8%
$BIC\_CO_2\_C2$	1.3%	1.0%	2.4%	0.7%	1.0%
$BIC\_CO_2\_C3$	2.9%	0.6%	1.7%	8.5%	0.9%
$BIC\_CO_2\_iC4$	1.1%	0.7%	0.3%	2.6%	0.9%
$BIC\_CO_2\_iC5$	1.2%	0.1%	0.8%	2.6%	1.1%
$BIC\_CO_2\_FC6$	4.2%	0.1%	0.7%	**15.3%**	0.5%
$BIC\_CO_2\_FC7$	3.0%	0.1%	0.5%	**10.4%**	0.8%
$BIC\_CO_2\_FC8$	0.7%	0.1%	0.9%	0.8%	1.2%
$BIC\_CO_2\_FC9$	1.0%	1.0%	1.4%	1.1%	0.5%
$BIC\_CO_2\_C10P$	**37.0%**	**88.1%**	**51.1%**	5.1%	3.6%
Soirg	1.1%	0.1%	0.9%	2.8%	0.6%
Sgcrit	7.5%	4.3%	0.5%	3.0%	**22.1%**
Krgcl	3.3%	0.8%	0.7%	**10.7%**	1.0%
Lg	9.4%	5.1%	0.6%	0.1%	**31.8%**
Eg	0.8%	0.1%	0.6%	0.5%	2.1%
Tg	0.7%	0.1%	0.5%	1.9%	0.5%
Log	1.5%	0.1%	1.5%	1.4%	2.9%
Eog	**28.1%**	0.5%	**39.2%**	**36.3%**	**36.2%**
Tog	1.1%	0.7%	0.8%	1.0%	1.8%

Through this, the non-unique solutions would be reduced with more historical data used in the assisted history matching technique. For a further quality check of this method of optimising the BIC's, however, the correlations in Kato et al. [138] and Nikos et al. [142] were selected to estimate CO_2-hydrocarbon binary interaction coefficients, as shown in table 5-8. Figures 5-13 and 5-14 represent the simulated average oil and gas saturations using different sets of CO_2-HC BICs. CO_2-HC BIC's estimated with Nikos et al.'s correlation, could roughly reproduce the calculated average oil and gas saturations. Obviously, there is no clear trend that should be followed in adjusting the binary interaction coefficients to better simulate the formation of the gas phase and its mechanism in reducing the oil saturation. Thus, in the absence of an assisted history matching engine to adjust the CO_2-HC BICs, Nikos et al.'s correlation would be useful as an initial guess of those BICs; then adjustment of the CO_2-C_1 and CO_2-plus fraction BICs would be sufficient to achieve the match. Kato et al.'s correlation, however, would increase the dissolution of CO_2 in oil and delay the formation of the gas phase, which would affect the oil phase behaviour by sharply reducing the oil viscosity and slightly increasing the oil density, as demonstrated in figure 5-15. Furthermore, the other CO_2-HC BIC sets simulate early formation of the gas phase, which results in increasing the oil density due to extraction of hydrocarbon components to the gas phase. A fuller knowledge of the changes in oil density and viscosity that occur during CWI would therefore lead to a more accurate tuning of the EOS to replicate the phase behaviour changes resulting from CO_2 mass transfer from CW to the oil phase.

Table 5-8 CO_2-hydrocarbon BICs were estimated using various methods

Method / CO_2 BIC	Nikos et al. [142]	Kato et al. [138]	CMOST Assist-HM
CH4	-0.0919	0.1867	0.3055
C2H6	0.2152	0.1530	0.4660
C3H8	0.1324	0.1364	0.3628
IC4	0.1195	0.1310	0.2345
NC4	0.1151	0.1278	0.2345
IC5	0.1089	0.1226	0.2278
NC5	0.1071	0.1197	0.2278
FC6	0.1050	0.1173	0.1013
FC7	0.1047	0.1148	0.4325
FC8	0.1051	0.1127	0.1198
FC9	0.1065	0.1114	0.3358
C10+	0.1453	0.0709	0.2255

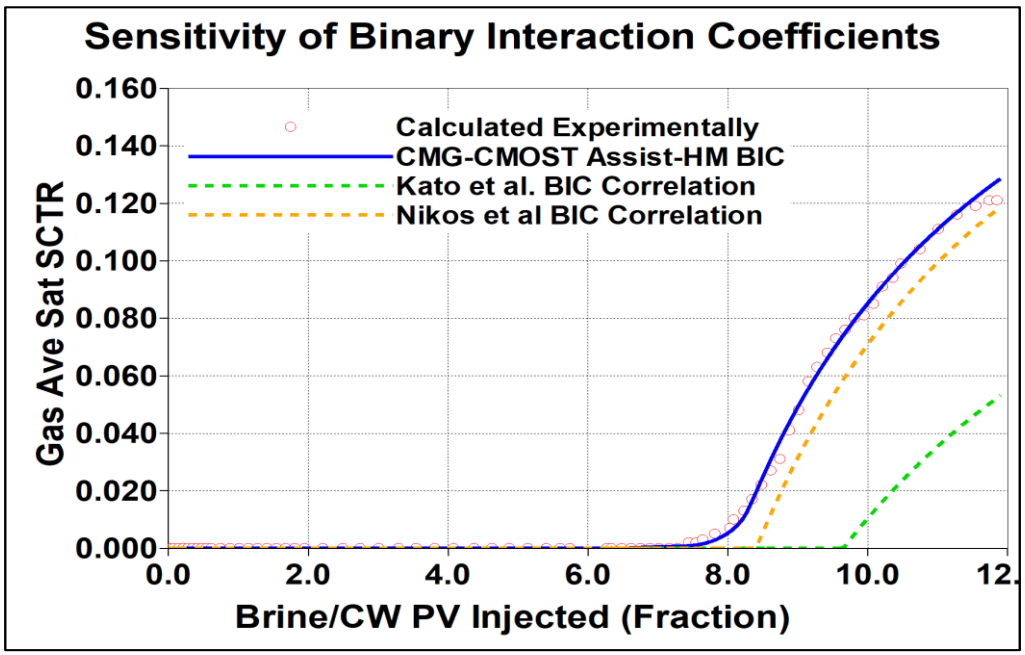

Figure 5-13 sensitivity of CO_2-hydrocarbon binary interaction coefficients between values obtained through assist history matching and values calculated using generalized correlation for simulating the average gas saturation

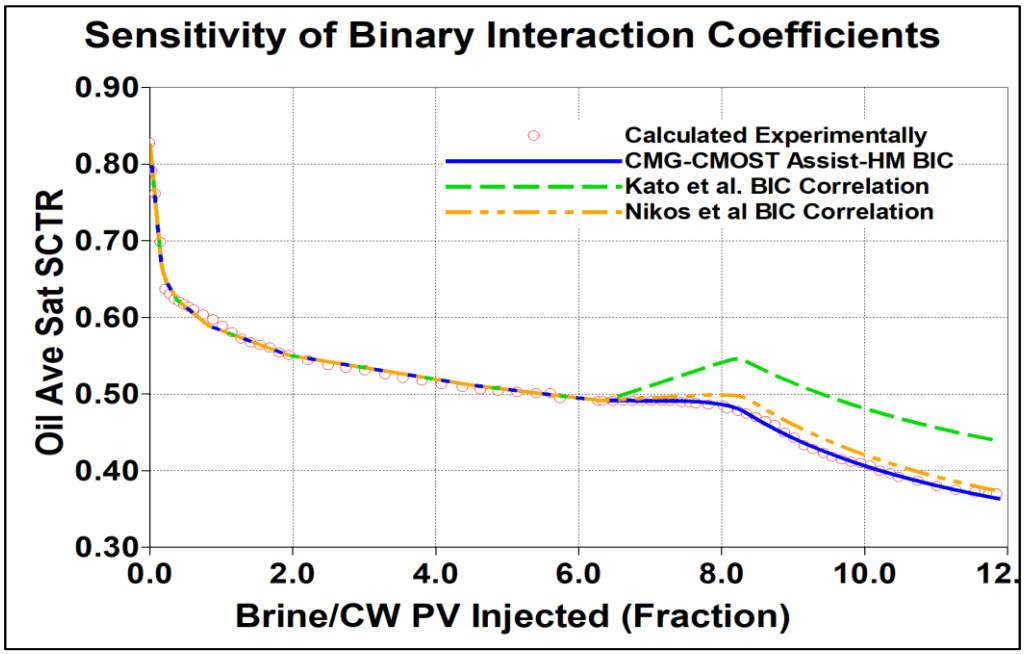

Figure 5-14 sensitivity of CO_2-hydrocarbon binary interaction coefficients between values obtained through assist history matching and values calculated using generalized correlation for simulating the average oil saturation

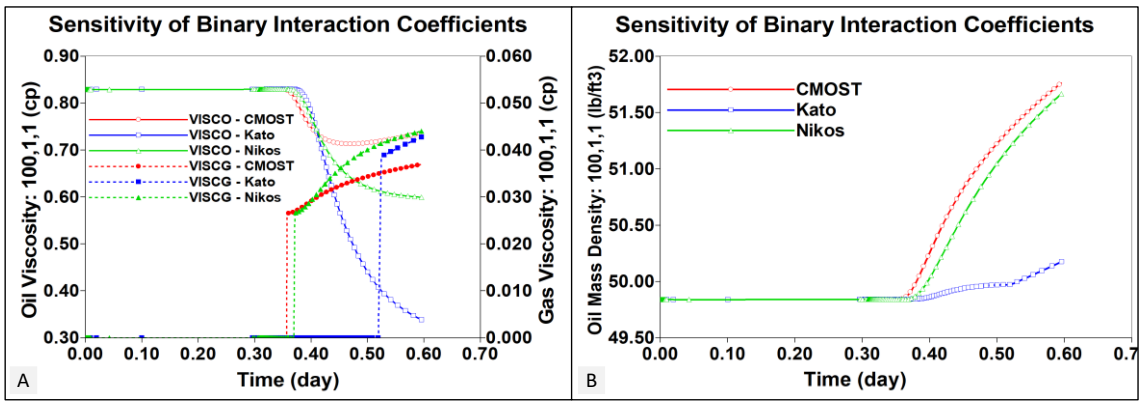

Figure 5-15 sensitivity of CO_2-HC BIC sets in the estimation of the phase behaviour in terms of oil (solid lines) and gas (dashed lines) viscosities and oil density in the last grid block (100, 1, 1)

Figure 5-16A shows the gas density of the two CO_2-HC BIC sets closest to the calculated experimental values. Nikos et al.'s correlation exhibits higher gas density than that predicted by the assisted history matching engine. The reason for this is the lower values of the CO_2 BIC to heavy hydrocarbon components calculated by Nikos et al.'s correlation, since this leads to the capability of CO_2 to extract heavier components to the gas phase, as shown in figure 5-16B. The author could therefore draw a relationship between CO_2-HC BICs and the ability of CO_2 to extract these components to the gas phase, since increasing the values of the BICs would reduce the ability of CO_2 to extract the hydrocarbon components, accordingly limiting the CO_2 dissolution in oil. Although this relationship could be predictable in the case of heavy hydrocarbon components, for light hydrocarbon components (C_1-C_4), the author was not able to obtain a clear relationship that would optimise their binary interaction coefficients to CO_2, maybe since their acentric factors were less than those of CO_2.

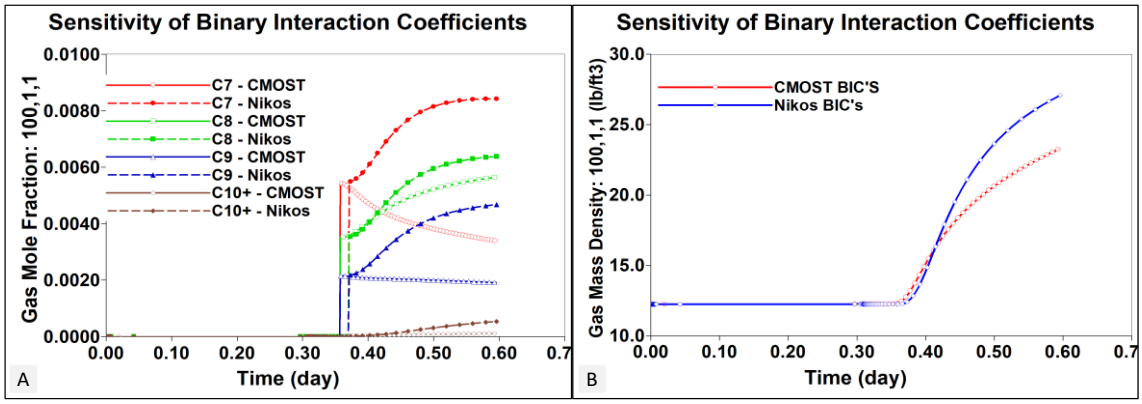

Figure 5-16 sensitivity of CO_2-HC BIC sets for the estimation of the gas density, and the role of C_7 plus fractions in changing the gas density

Having implemented the assist history matching technique [128], the experimental results could be equitably replicated by the simulation in order to estimate the water-oil relative permeability and capillary pressure functions, as demonstrated in figures 5-17 and 5-18. Thereafter, CO_2-hydrocarbon BICs in the EOS were optimised to reproduce the average gas and oil saturations, while the LET parameters for oil-gas relative permeability formulations, as shown in table 5-10 and figure 5-21B, were modified to history match the performance of CWI in tertiary mode. Through the history matching trail, the physics observed and interpreted in direct pore-scale visualisations was considered and translated into simulation terms. For example, the linear relationship between increasing gas saturation and a reduction in oil saturation was formulated using a Stone I three-phase relative permeability function, with a high critical gas saturation to achieve a unity alpha factor.

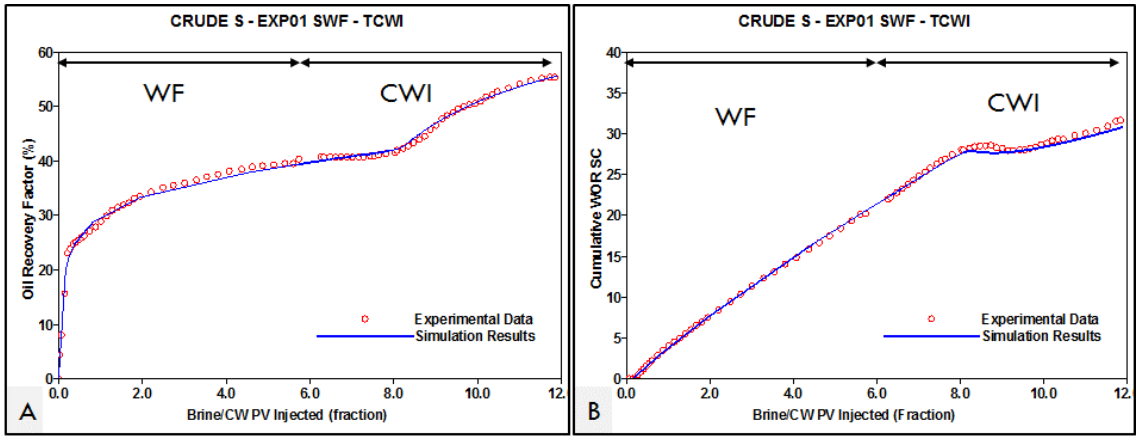

Figure 5-17 history matched (A) oil recovery and (B) cumulative WOR compare to the experimental values during SWF and TCWI core displacement test EXP01

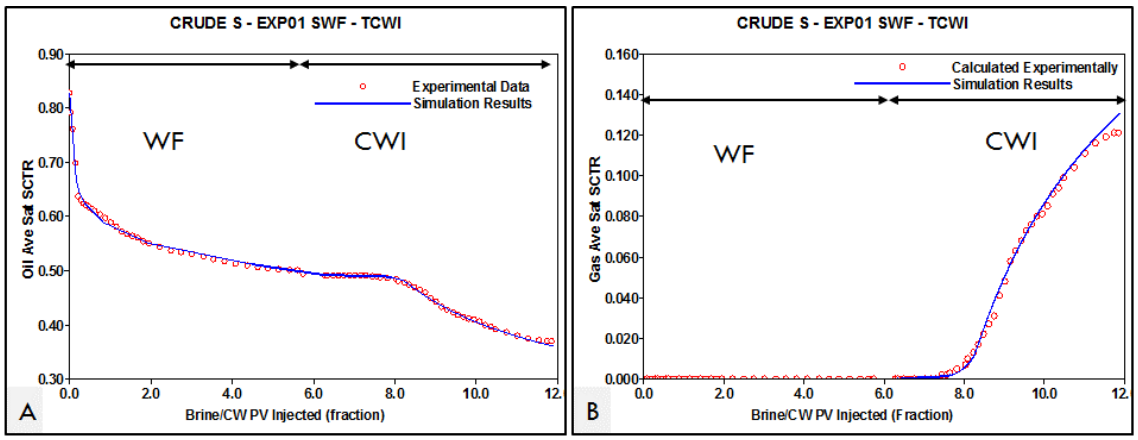

Figure 5-18 simulated (A) average oil saturation and (B) average gas saturation in comparison with calculated experimental values in EXP01 SWF-TCWI

5.5.4.1 Effects of Multiple-Components Recombination on Performance of CWI

Unlike the previous experiment in chapter 3, where the increasing trend in differential pressure across the core during CWI (figure 3-25) was one of the measurable factors influencing the formation of the new (gas) phase, in this experiment, the differential pressure increased during CWI until the production of oil started; then the trend of differential pressure declined, as demonstrated in figure 5-20. This can be explained as follows:

- A dissimilar wettability in both cores although they faced the same aging procedure to turn them into a mixed-wet state. In practice, however, the water-oil relative permeability obtained in the previous experiment (figure 3-27A) showed a weak water-wet wettability. According to the definition of water-wet, as shown in figure 5-19, water occupied the small pores and created a small film surrounding the oil which occupied the larger pores. Then, the gas-phase was formed and grew within the trapped oil in large pores as a result of contact between CW and oil [149]. Consequently, the differential pressure across the core showed an increasing trend. On the other hand, the water-oil relative permeability obtained in this experiment (figure 5-21A), displayed a mixed to weak oil-wet wettability, where the oil occupied the small pores and established a small film surrounding the large pores, as illustrated in figure 5-19 [149]. Moreover, the new gaseous phase was formed and grew in small pores in the trapped oil, as a result of contact between the CW and oil. Then, the differential pressure across the core increased, indicating the formation of the third phase, then decreased when the oil started to be displaced from the small pores. Seyyadi et al., however, performed secondary CWI displacements experiments in aged and un-aged cores using methane-saturated oil [70]. The un-aged core represented water-wet wettability and the aged one was assumed to be mixed-wet wettability. In both experiments, the differential pressure increased even after water breaking through, indicating that the initial wettability would not affect the behaviour of the differential pressure. The compositional behaviour that occurred due to CO_2 mass transfer from CW to oil would therefore have a great impact on differential pressure.

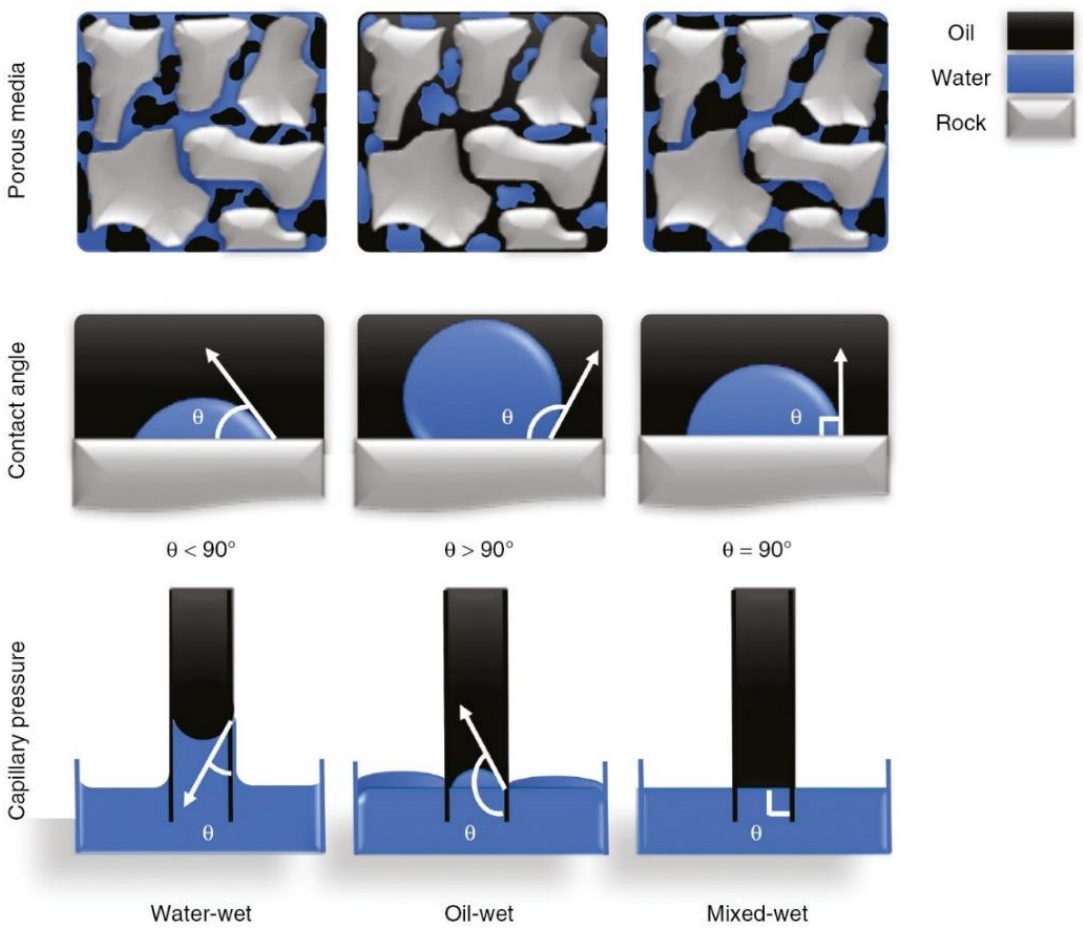

Figure 5-19 illustration of the definition of wettability in porous media with oil/water/rock and their contact angles and capillary pressure behaviour [150]

- In the previous experiment, the live oil is methane-saturated oil; while in this experiment, the live oil is recombined stock tank oil with make-up gas which has multiple intermediate hydrocarbon components (C_2 to C_4). When the new gas phase formed in methane-saturated oil during CWI, that phase mainly contained methane and, after further carbonated water injection, CO_2. Then, the interfacial tension between the new gas phase and the oil was much higher, avoiding any potential for miscibility between the phases, even though C_{7+} components were extracted from the oil. Additionally, due to the immobility process of the formed gas phase, the differential pressure across the core was increased. In the other experiment, however, whenever the new gas phase formed with the live oil, this phase contained multiple intermediate hydrocarbon components in addition to CO_2. Thus, the interfacial tension between gas and oil exhibited a decreasing trend, with more extraction of hydrocarbon compounds from the oil to the gas phase, and this created favourable miscibility conditions. Then, the gas phase was displaced with oil, causing a decline in differential pressure across the core.

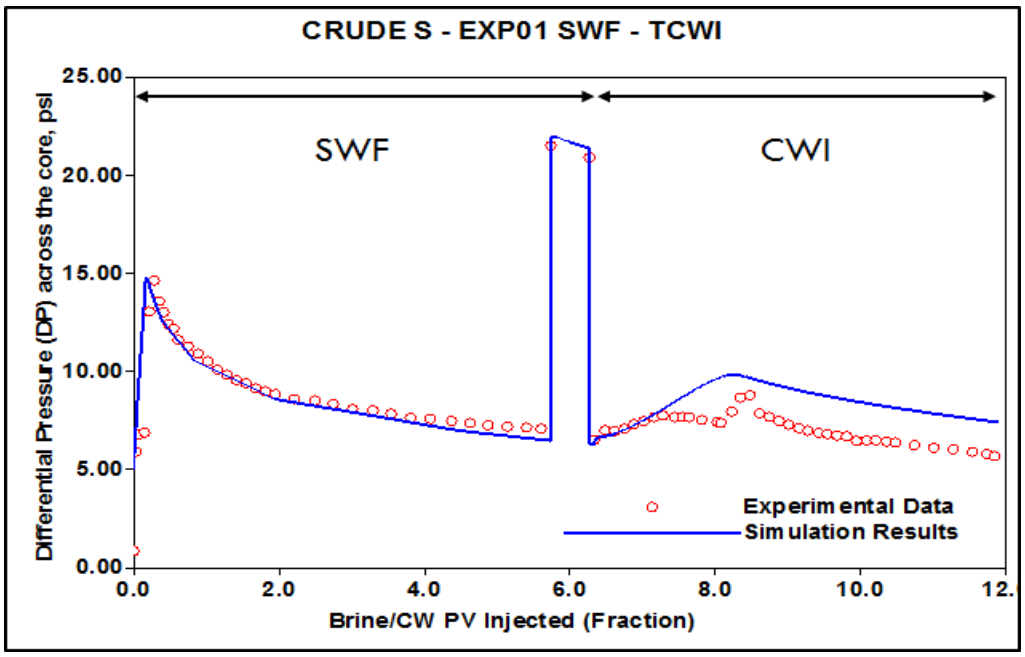

Figure 5-20 the simulated differential pressure with recorded experimental data in EXP01 showing a gradual increase then a decline after the oil production commenced, even with formation of the third phase

The estimated water-oil, oil-gas relative permeability and capillary pressure functions that resulted from history matching the experimental data, considering the tuned EOS to reproduce the average gas saturation while injecting the carbonated water, are shown in figures 5-21 and 5-22. Based on Craig's [132] criteria for recognising the oil-wet wettability of the core based on water-oil relative permeability curves, the connate water saturation was less than 0.2. The saturation at which the relative permeabilities of oil and water are equal should be less than 0.5, and the end point of the relative permeability of water at residual oil saturation ($k_{rw|Sorw}$) is greater than 0.5. Thus, based on Craig's criteria, figure 5-21A might represent the water-oil relative permeability of a mixed-wet core, because the end point of oil relative permeability at connate water saturation ($k_{row|Swi}$) is greater than 0.7, which contradicts the suggested criteria where ($k_{row|Swi}$) should be less than 0.7. Tables 5-9 and 5-10 represent the end points of water-oil and oil-gas relative permeabilities, along with the LET correlation parameters obtained during the history matching process. A critical gas saturation of 20% is essential to simulate the displacement of the oil phase during the formation of the new (gas) phase. The high critical gas saturation and very low gas relative permeability values are the common estimation in depressurisation processes and carbonated water injection, since in both cases the solution gas is released. In a depressurisation process, the reservoir pressure is decreased at a constant rate, which leads to the formation of gas bubbles when the pressure reduces below the saturation pressure. In the carbonated water process,

meanwhile, the CO_2 transferred from CW extracts the hydrocarbon components, forming bubbles of gas that are surrounded by the oil phase. Then in both mechanisms, the formed gas, although initially in immobile bubbles, accumulated to form apparent oil swelling.

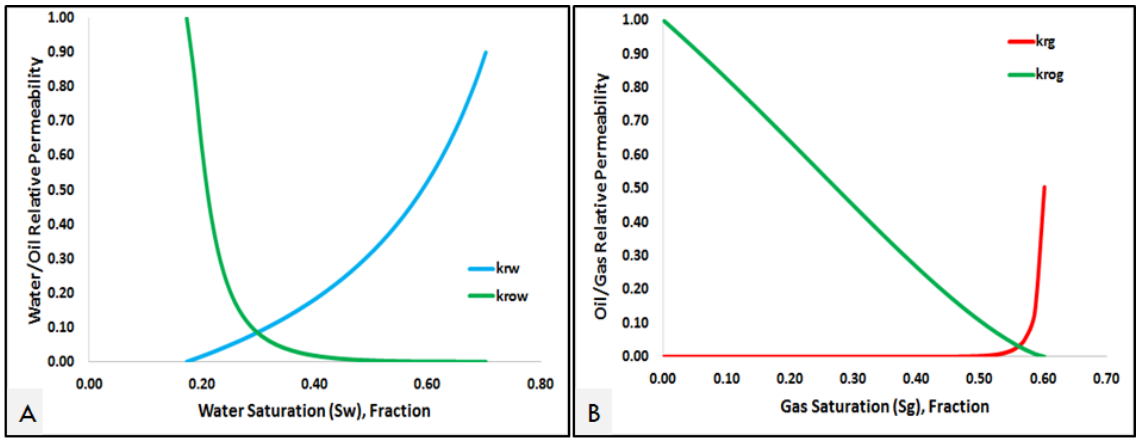

Figure 5-21 obtained relative permeability curves from history matching the EXP01 coreflood experiment (A) water-oil relative permeability and (B) oil-gas relative permeability

Table 5-9 obtained water-oil relative permeability end points and LET correlation exponents

S_{wi}	S_{wcrit}	S_{oirw}	S_{orw}	k_{rwiro}	k_{rocw}
0.173	0.173	0.297	0.297	0.90	1.00
L_w	**E_w**	**T_w**	**L_{ow}**	**E_{ow}**	**T_{ow}**
1.00	2.96	1.00	2.54	47.9	1.51

Table 5-10 obtained oil-gas relative permeability end points and LET correlation exponents

S_{oirg}	S_{org}	S_{gcon}	S_{gcrit}	k_{rogcg}	k_{rgc}
0.225	0.225	0	0.20	1.00	0.604
L_g	**E_g**	**T_g**	**L_{og}**	**E_{og}**	**T_{og}**
10	50	1.0	1.3	1.0	1.0

A history match of the secondary water injection part was done using an assisted history matching machine (CMG-CMOST) to estimate the oil-gas relative permeability and capillary pressure functions simultaneously. Skjaeveland et al. [148] developed a correlation equation to estimate the capillary pressure function in a mixed wet core (equation 5-3 below).

$$P_c = \frac{c_w}{\left(\frac{S_w - S_{wcon}}{1 - S_{wcon}}\right)^{a_w}} + \frac{c_o}{\left(\frac{1 - S_w - S_{oirw}}{1 - S_{oirw}}\right)^{a_o}} \qquad \text{Equation 5-3}$$

Where, the a's and c's are correlation constants, as presented in table 5-11, with one set for imbibition and another for drainage. Figure 5-22 demonstrates the estimated capillary

pressure curves to achieve reasonable history matched differential pressure, including for the pump flood region.

Table 5-11 estimated capillary pressure parameters

c_w	a_w	c_o	a_o
0.32	0.34	-0.105	0.4325

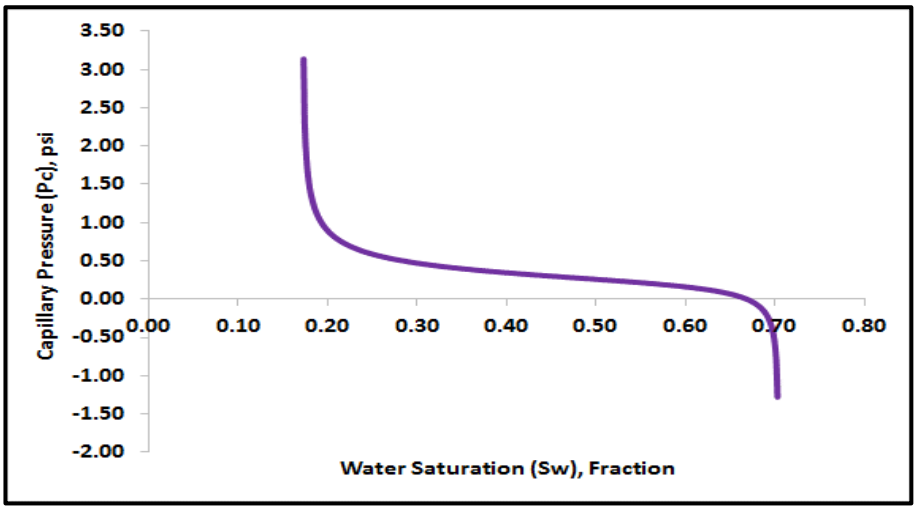

Figure 5-22 calculated capillary pressure function during history matching the performance of secondary waterflooding in EXP01

One of the consequences of using this method is the assumption that the formation of the gas phase is tied with the decreasing oil saturation. In other words, the gas saturation would remain zero, even though the carbonated water was injected and CO_2 mass transfer to oil phase occurred. In that respect, there was a slight difference between the simulated produced CO_2 concentrations and the CO_2 concentrations recorded during the experiment, as illustrated in figure 5-23.

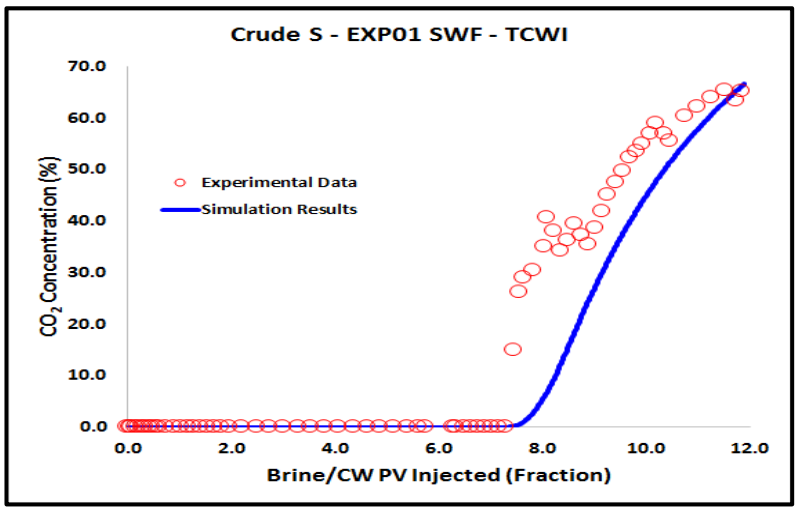

Figure 5-23 comparison between produced CO_2 in simulation and the recorded experimental values

5.5.5 Prediction EXP02-SCWI

Reservoir simulation prediction is a tool to validate the quality of the history matched model. Prediction helps to recognise the limitations and uncertainties involved in the reservoir simulation models. In core-scale simulation, predicting the secondary CWI core displacement test would corroborate the applied method to tune the EOS and the companion flow functions as a result of history matching the TCWI coreflood test. Therefore, using the tuned PR-EOS and flow function obtained from replicating the performance of the tertiary CWI (EXP01) coreflood test, secondary fully-saturated CWI core displacement test (EXP02) is numerically predicted to generate its performance results, which then can be compared with the experimental data.

As a result of that, the numerically simulated SCWI coreflood test predicts the increasing trend of oil recovery comparable to the experimental data. Although, the predicted oil recovery shows relatively smaller values after water breakthrough than the measured data, nevertheless, the ultimate oil recovery is in good agreement with the experimental values, as demonstrated in figure 5-24A. Before the breakthrough, the carbonated water behaves similar to conventional water flooding, where the displacement efficiency between two immiscible fluids, based on their mobility ratio, is the principal process in oil recovery and water production, as shown in figure 5-24B. Thus, obtaining a proper water-oil flow function would predict the performance of secondary CWI. Figure 5-25 shows reasonable prediction of average oil saturation with experimentally calculated values, indicating that the method used to tune the EOS to reproduce the gas saturation is sufficient to replicate the performance of CWI in secondary mode.

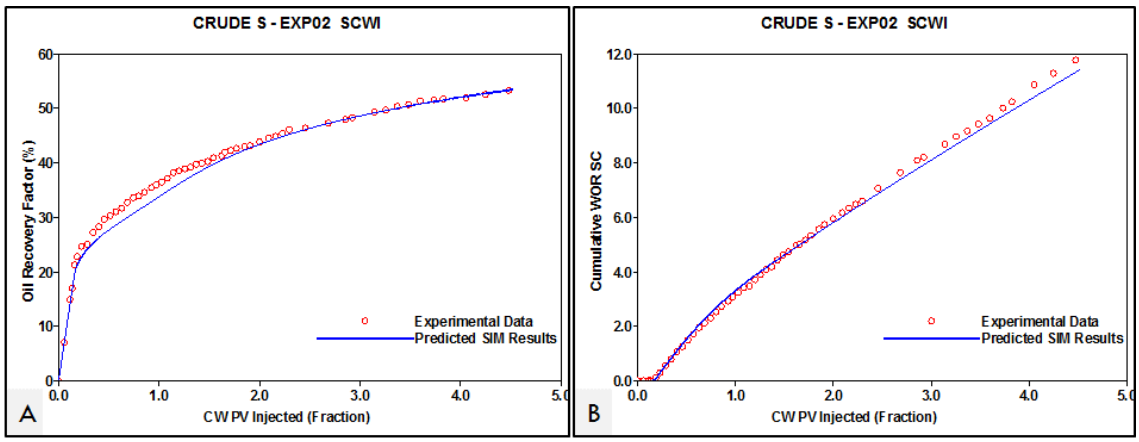

Figure 5-24 (A) comparison of predicted oil recovery and measured values during SCWI, and (B) the predicted cumulative WOR compared with the recorded data from EXP02-SCWI

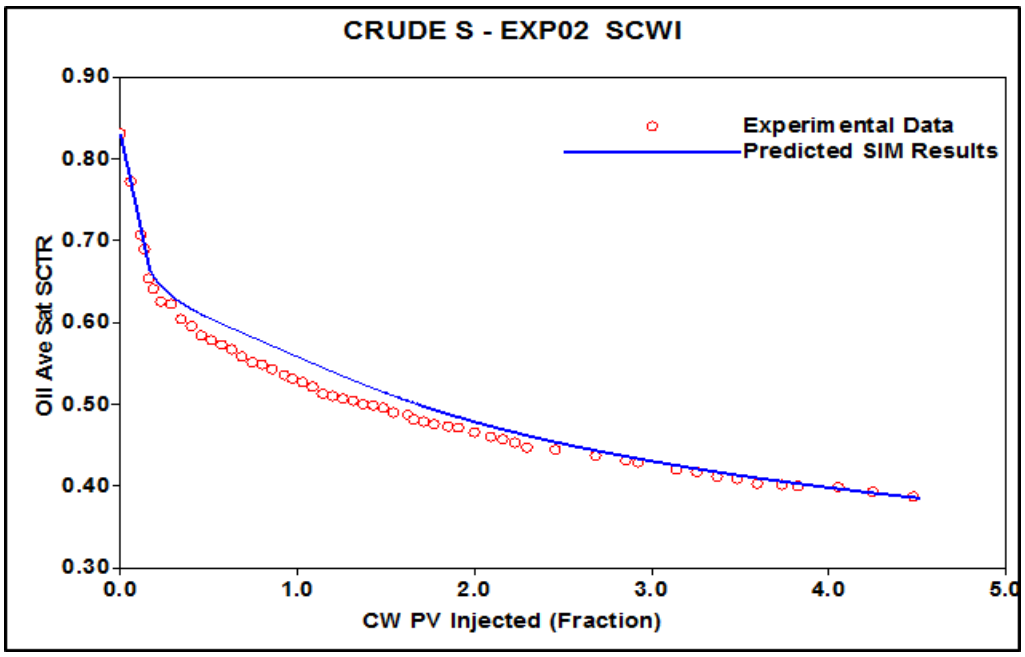

Figure 5-25 predicted average oil saturation against experimentally calculated oil saturation of EXP02-SCWI

5.5.5.1 Role of CO_2 Diffusion in Oil and Mechanical Dispersion

The equation of state assumed instantaneous equilibrium and complete mixing among the three phases (oil, gas and water) while carrying out the flash calculation. This means that the mass transfer of CO_2 from the carbonated water to oil occurs instantaneously without CO_2 molecular diffusion into oil or CO_2 dispersion in the grid block. Figure 5.26 shows a one-dimensional cross-section of CO_2 concentration in oil and water close to water breakthrough time, as indicated by the oil and water saturation cross-sections. The carbonated water has transferred all of its CO_2 to the resident oil, which results in water that is free of CO_2 at the front. Accordingly, more CO_2 from the injected carbonated

water is saturated the oil behind the front. The core displacement experiment that was performed in [73], however, recorded the breakthrough of CO_2 ahead of water, verifying the presence of CO_2 diffusion and dispersion within the oil that can be extrapolated from the direct pore-scale observations. In those experiments, the third phase was formed in a scattered manner and was not restricted in the contacted area between carbonated water and oil.

Even though Sayyedi et al. found earlier breakthrough of water than CO_2 by about 0.3 PV during SCWI in their slim tube test [69], since the slim tube contained well sorted Ottawa sand in a 60-ft long coil that creates 30% porosity and permeability of 6 darcy, unlike the reservoir core, the high permeability and well-sorted pore structure diminishes the effect of dispersion on CO_2 mass transfer from carbonated water to oil.

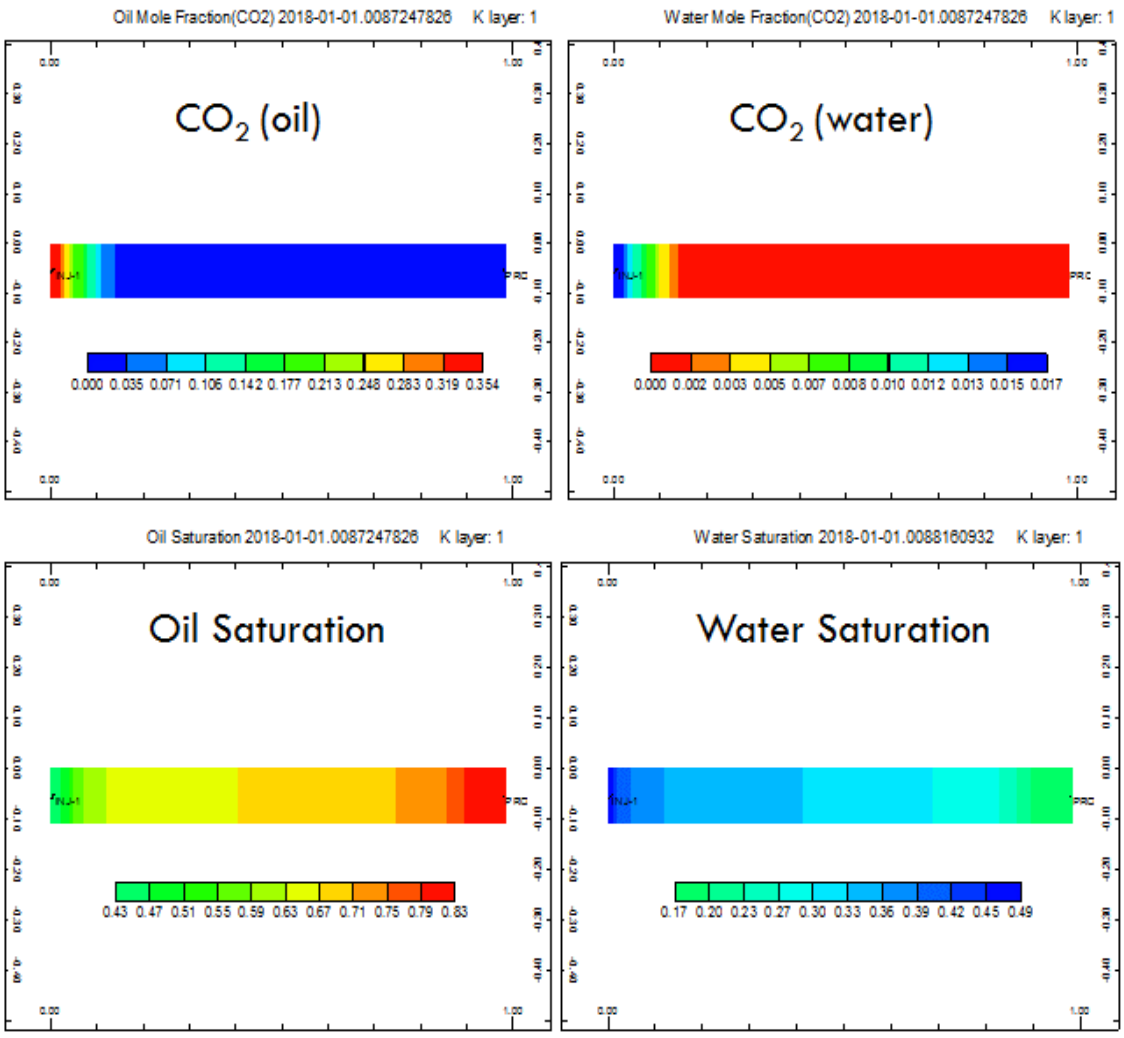

Figure 5-26 top cross-sections are the simulated CO_2 concentrations in oil and water close to water breakthrough, as indicated by the bottom cross-sections, which show oil and water saturation along the core close to water breakthrough

Experimentally, CO_2 and water broke through after 0.18 PV and 0.2 PV of injected carbonated water, respectively. On other hand, as illustrated in figure 5-27B, the simulation model expected a much more pronounced delay in CO_2 breakthrough than that of water, indicating inappropriate mixing of CO_2 among the three phases (water, oil and gas) in the model calculated by the simulator. While the simulator predicted the gas-liquid ratio reasonably well (in figure 5-27A), its over-estimation of the GLR after water breakthrough could be related to its under-estimation of the predicted oil recovery during this period. The non-equilibrium and dynamic mixing that resulted from CO_2 mass transfer from carbonated to oil is more related to the pore structure in porous media. In other words, the degree of heterogeneity in reservoir rock controls the local velocity and occupancy of oil and water in the pores, and consequently the saturation of oil with CO_2 and the formation of the new (gas) phase.

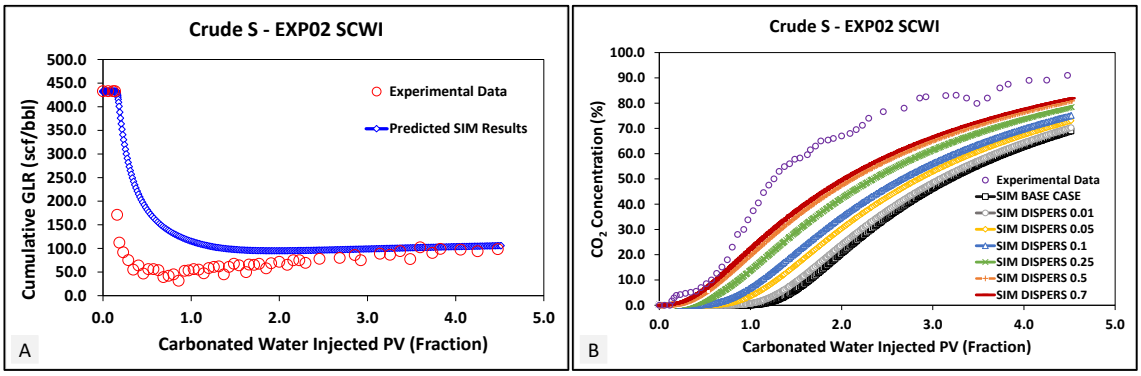

Figure 5-27 (A) the simulated GLR in comparison with the measured GLR during SCWI in EXP02 and (B) the recorded mole percentage of CO_2 concentration during the experiment in comparison with different simulation scenarios on the impact of mechanical dispersion on earlier CO_2 production

There are two mass transfer processes that take place when CO_2 dissolves in oil during CWI: solution and diffusion. It is known that solution occurs rapidly while diffusion is a much slower process. Diffusion happens when a system is not in equilibrium, where the molecules (in this case CO_2) move from one point to another due to concentration differences, temperatures and pressure gradients. It is self-governing process of any of the convective forces in the system; and is known to play an important role in immiscible CO_2 displacement [99]. Several authors [151-155] have stated the advantages of diffusion: namely, that it helps CO_2 to dissipate within the oil, speed up the reduction in oil viscosity, and increase the oil rate. The diffusion coefficients of CO_2 in water and oil phases during carbonated water injection were determined [156], in research on the effects of operational parameters such as saturation pressure, temperature and phase volumes on CO_2 diffusion in both phases. A linear relationship was found to exist

between saturation pressure and diffusion coefficients, and also the increased temperature reduces the time required for phases to reach equilibrium. At the interface between water and oil, the CO_2 mass transfer is the predominant process, which is faster than the molecular diffusion [157]. The role of CO_2 molecular diffusion therefore weakens in carbonated water injection, where the mass transfer is controlling the process.

Furthermore, if the diffusion occurs at the molecular level, it can be defined as dispersion, which is the mixing of fluids that occurs when one fluid displaces another, caused by local velocity gradients, heterogeneity of the rock and mechanical mixing [158]. Non-uniform pore distribution in heterogeneous rock leads to incomplete mixing at the pore level, which is not the case in a slim tube apparatus, where the water breaks through earlier than CO_2 due to the more homogeneous and uniform pore structure, reflecting the actuality of fluid-fluid interaction mechanisms.

As a result of that, the dispersion was used to evaluate its effects on the simulation of the distribution of CO_2 within porous media. As illustrated in figure 5-27B, introducing CO_2 diffusion in oil alone led to no significant improvement on CO_2 movement ahead of water. Consequently, the dispersion factor was used to reproduce the effects of mixing on scattered CO_2 distribution within porous media. Increasing the length of the dispersion effect would expand the dissipation of CO_2 into oil, resulting in oil that saturates CO_2, and flows ahead of water. Figure 5-28 shows a one-dimensional cross-section of CO_2 concentration in oil and water, close to water breakthrough, after including in the simulation model the CO_2 diffusion and dispersion. The former was based on an oil coefficient of 3.9582E-5 cm^2/sec (which was calculated using McManamey and Woolen's correlation [159]), while the latter involved a dispersion length of 0.7 ft. The carbonated water now transferred its CO_2 into oil across a longer distance before the water became free of CO_2. Thus, the CO_2 became more widely spread within the oil such that the produced oil contained CO_2 before the water breaking through.

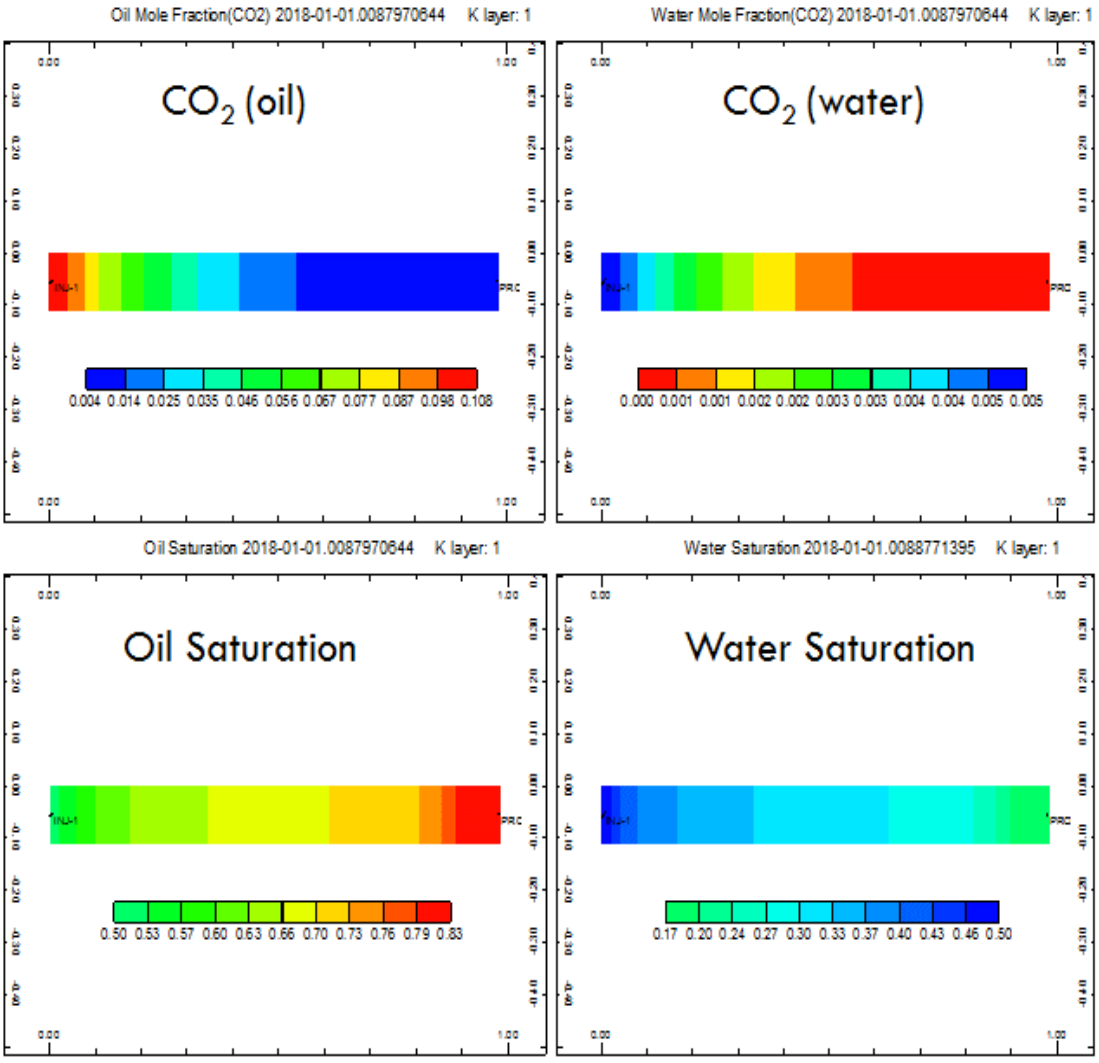

Figure 5-28 top cross-sections are the simulated CO_2 concentrations in oil and water close to water breakthrough, as indicated by the bottom cross-sections which are oil and water saturations along the core close to water breakthrough after introducing into the simulation model both CO_2 diffusion in oil and a dispersion of 0.7 ft

Selecting the dispersion factor in which both CW and oil would be mixed together to repeat the earlier CO_2 breakthrough ahead of water had a negative effect on the oil recovery, but a positive one on the differential pressure across the core, as shown in figure 5-29. In other words, while the dispersion factor would properly distribute the CO_2 within oil, thus replicating the phenomena observed in direct pore-scale experiments, the amount of the new (gas) phase formed would be substantially reduced, which affects the numerical performance of the CWI simulation.

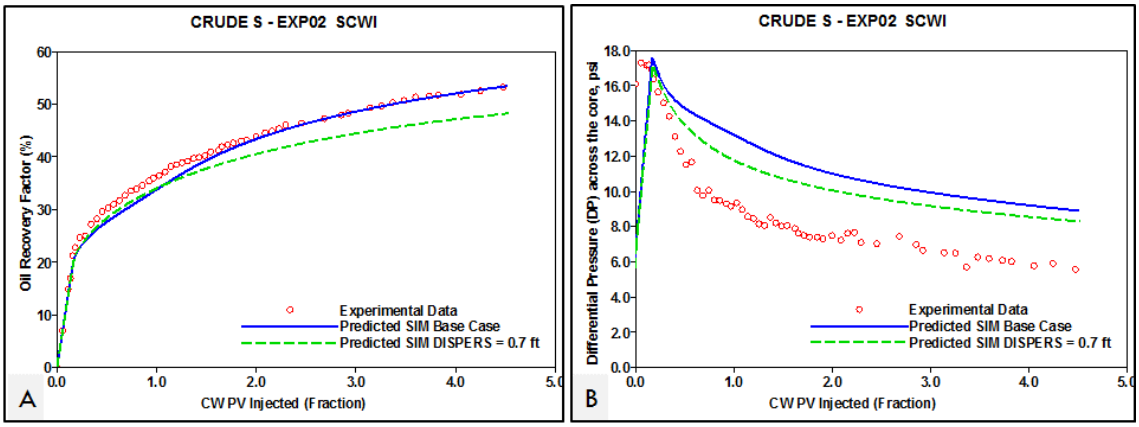

Figure 5-29 simulated oil recovery and differential pressure with and without introducing CO_2 diffusion in oil and a dispersion factor

5.5.5.2 Impact of Mineral Dissolution

Fluid-rock interactions induced by CWI could also alter the geochemical system equilibrium between the porous rock and the injected brine [160]. Injecting carbonated water into carbonate rock increases the chances of dissolution and precipitation of minerals constituting the porous rock [161]. Thus, the injection of CO_2-enriched brine into core samples can result in severe modifications of the pore structure, which can either improve or impair the absolute permeability depending on the driven geochemical processes (i.e. dissolution or precipitation processes) [162]. Those changes in the petrophysical properties of the rock depend on the type of mineralogical accumulation, the composition of injected brine, and also the thermodynamic conditions [160]. The flow regime within a porous medium controls the reaction time required for the process to take place [163]. For example, in the near wellbore region, where the flow is turbulent and directed into the rock, the geochemical equilibrium is strongly affected and wormholes may form due to heterogeneous dissolution patterns of carbonate rock. Further from the injection well, however, the flow is expected to be uniform and laminated, where a homogeneous alteration of the pore structure occurs [163]. Egermann et al. demonstrated the dependency of the evolution of the porosity-permeability on the degree of dissolution, which is extremely reliant on the pore structure [164]. They detected that within two porosity-unit enhancement of porosity due to rock dissolution, the evolution of the permeability could reach up to 70%. Also, they indicated that the biggest cause of porosity-permeability evolution is the homogeneous alteration of pore structure as a result of uniform and laminated flow in the core.

This evolution of the rock structure is not only observed at laboratory level but evidence for it has been reported in the field. Dissolution of anhydrite was observed using thin-section analysis in samples cored in a CO_2 flooded area far from injection wells in dolomite reservoir rock, Denver unit, Wasson field [165]. In 1979, enhancement of well injectivity by 50% was reported while injecting WAG-CO_2 in the SACROC field, which was attributed to rock dissolution [166].

Mahzari et al., however, denied the impact of rock dissolution on the performance of CWI, even though they observed the pattern of wormholes due to heterogeneous dissolution on the rock inlet, as demonstrated in Figure 5-30, and the rock had a mineral content of 93% calcite [73]. As a small fraction of the dissolved CO_2 in brine is converted into a weak carbonic acid according to reaction formula 5-4, then that weak acid had the potential to react with the host rock formation (calcite, dolomite, anhydrite, etc.) as indicated in reaction formula 5-5 for calcite.

$$CO_{2(aq)} + H_2O \leftrightarrow H_2CO_{3(l)} \leftrightarrow H^+ + HCO_3^- \qquad \text{Equation 5-4}$$

$$H^+ + HCO_3^- + CaCO_3 \leftrightarrow Ca^{2+} + 2HCO_3^- \qquad \text{Equation 5-5}$$

Also, there was a reduction of 2.17% in the weight of the core sample that was observed the wormholes on its inlet indicating sort of mineral dissolution occurrence. Experimentally, the differential pressure across the core during CWI, in either in tertiary or secondary modes, was lower than that is during conventional water injection, although during CWI, three phases (water, oil and new gas) are flowing in the core, unlike the flowing of two phases (water and oil) during conventional water injection. The author believed there dissolution of minerals resulted in an evolution in the permeability that initially occurred during tertiary CWI. That evolution affected the differential pressure across the core, as shown in figure 5-31B. If the assumption of the change in permeability due to rock dissolution improved up to 50%, which is equivalent to 132 md, then the simulation model would predict the reduction in the differential pressure comparatively well. The predicted oil recovery would not be changed as the increase in differential pressure corresponded to the improvement in absolute permeability (figure 5-31A), which leads to the relative permeability being maintained, according to Darcy's Law, equation 5-6.

$$q_o = \frac{k_{ro} k A}{\mu_o} \frac{dp_o}{L}$$ Equation 5-6

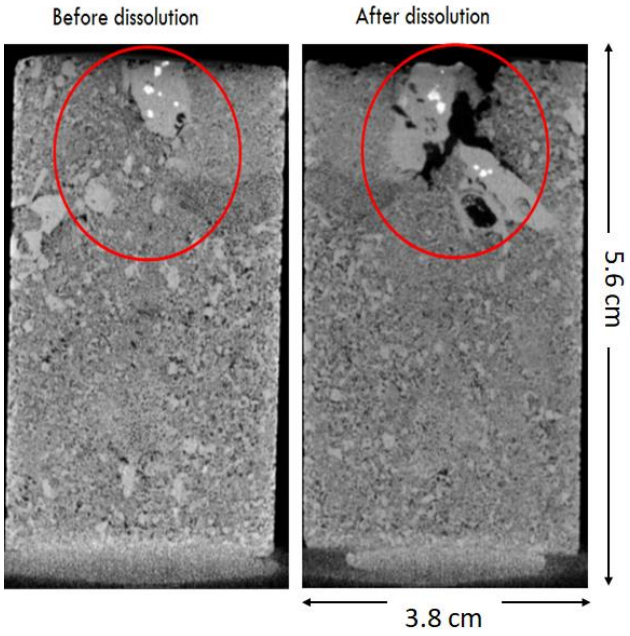

Figure 5-30 CT-scan images of the core sample before and after mineral dissolution while injecting carbonated water (red circle is showing the formation of wormholes at the inlet of the core) [73]

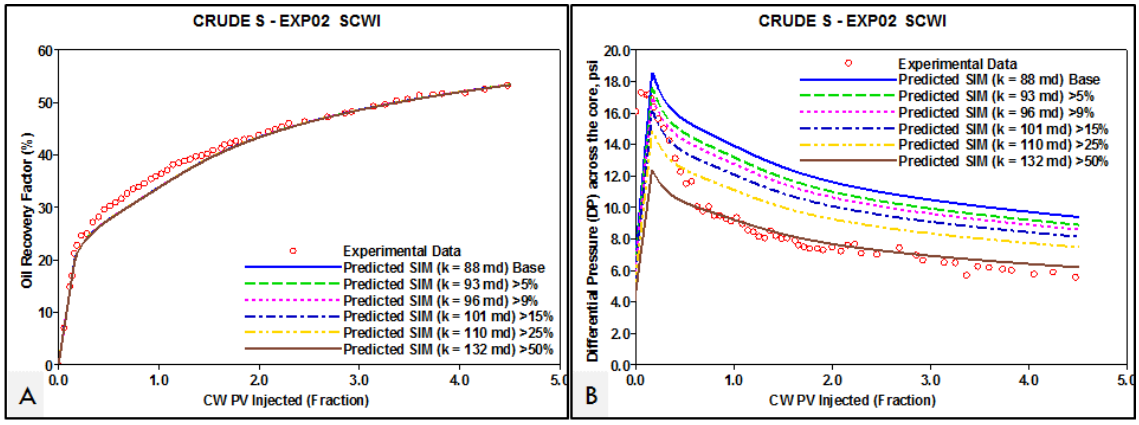

Figure 5-31 sensitivity of the impact of the change in permeability due to dissolution of minerals on differential pressure across the core during SCWI EXP02

5.5.6 Effect of Carbonation Level on Oil Recovery

The carbonation level (CL) is known as the amount of CO_2 that is soluble in water. Thus, the solubility of CO_2 in water is affected by several factors, such as temperature, pressure and water salinity. Temperature and brine salinity have an inverse relationship with the solubility of CO_2 in brine: i.e. the solubility decreases with increasing temperature and salinity. On the other hand, the solubility of CO_2 in brine increases with increasing pressure. The amount of CO_2 in carbonated water therefore plays an essential role in oil

recovery as it influences the mechanisms responsible for improving oil recovery, such as oil swelling, reduction of oil viscosity and formation of the third phase.

Mahzari et al. performed a tertiary CWI displacement experiment where the injected carbonated water contained 50% of the CO_2 that can be dissolved in it [73]. Their proposal was that the carbonation level of the injection brine would affect the process of CO_2 mass transfer from CW into oil through the partitioning coefficient, which would be constant given a specific pressure and temperature. In their pore-scale visualisation experiments, the reduction of oil saturation and the quantity of third phase saturation were less when injecting half-saturated CW than when injecting fully-saturated CW. Also, the oil recovery of the tertiary fully-saturated CWI core displacement experiment was 5.5% higher than that of the tertiary half-saturated CWI, whereas the simulation model predicts 8.2% higher oil recovery during tertiary fully-saturated CWI than during tertiary half-saturated CWI core displacement experiments, as demonstrated in figure 5-32.

Experimentally, the relationship between carbonation level and oil recovery could not be interpreted linearly, i.e., reducing the carbonation level to 50% would not decrease the oil recovery by the same percentage; rather the additional oil recovery in a half-saturated case was two-thirds of that in the fully-saturated case. In the simulation model, however, the oil recovery is a linear function of the carbonation level, which leads to under-estimation of the performance of CWI when its carbonation level is below 100%. The reason for this could be related to the initial estimate of the partitioning coefficient by dividing the mole fraction of CO_2 among the two phases (water and oil) based on a fixed value, which may be less than the actual value. Furthermore, as shown in figure 4-12 in previous chapter, the partitioning coefficient of CO_2 between water and oil shows an increasing trend, whereas in the EOS calculation, a fixed partitioning coefficient value is suggested in all flash calculation stages, which creates an inflexible mass transfer of CO_2 between the two phases.

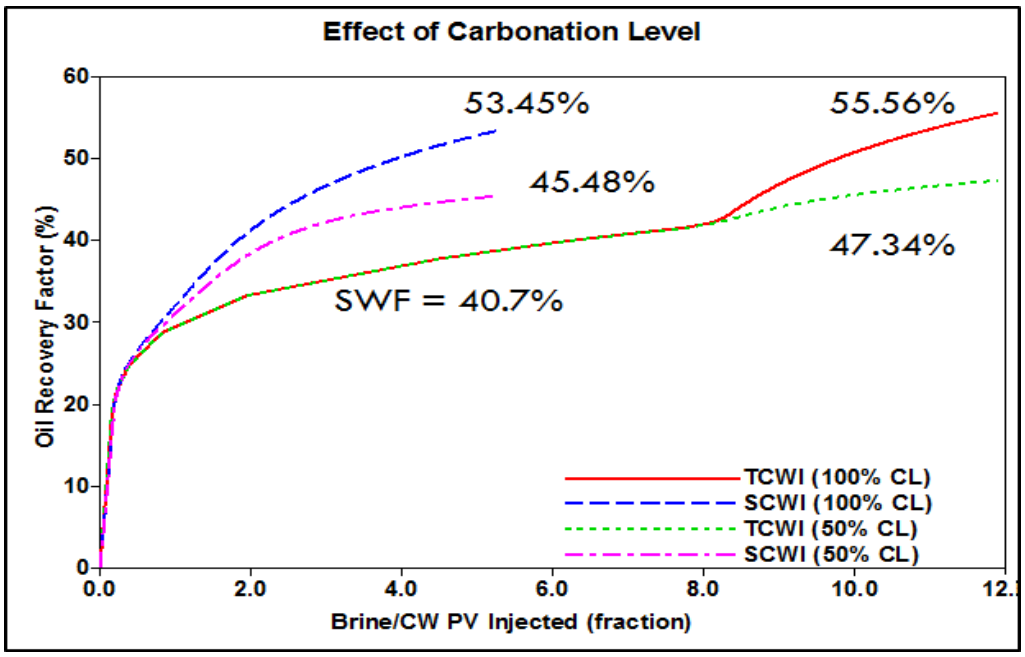

Figure 5-32 Effect of carbonation level on oil recovery during CWI in different modes

5.6 Summary and Conclusions

To verify and evaluate the capability of the developed methodology to predict the performance of CWI in a real reservoir environment, simulations of different sets of core displacement experiments were performed in this chapter. The coreflood experiments were performed using a mixed-wet reservoir carbonate core that was saturated with reservoir live oil at the initial water saturation. First, the saturation of the new (gas) phase was calculated using the experimental data from the tertiary CWI displacement test by analysing the direct pore-scale visualisations, and the suitable three-phase function was selected to be Stone I.

Then, the initial tuning of the cubic equation of state was accomplished to reproduce the basic fluid properties and to modify Henry's Law constant of CO_2 solubility in water at test conditions and brine salinity. After that, following the same procedure as in water-wet case, a simulation of conventional the waterflooding period was performed in order to history match the test results and obtained water-oil relative permeability and capillary pressure functions. Then, advanced EOS tuning was accomplished by adjusting the binary interaction coefficients of CO_2 and hydrocarbon compounds with the CMG-CMOST assisted history matching engine to simulate the calculated new (gas) saturation. Other generalised correlations were used to calculate the CO_2-HC binary interaction coefficients and to compare their simulated average oil and gas saturations with those

produced by the assisted history matching task. The CO_2-HC BIC's calculated by Nikos et al.'s correlation simulated the closest match to the experimentally calculated values in addition to the CO_2-HC BICs obtained through the assisted history matching, which makes Nikos et al.'s correlation a good initial guess in the absence of an advanced PVT test and a suitable assisted history matching engine. Selecting the right set of CO_2-HC BICs depends mainly on reproducing the oil and formed gas phase behaviour changes that occur when CO_2 is being transferred from the CW to the oil, however. A sort of relationship between the CO_2-HC BIC, mainly in heavy hydrocarbon components (C_{7+} fractions), and the ability of CO_2 to extract these hydrocarbon components was established to evaluate the increase in CO_2 dissolution in oil numerically.

Next, the secondary CWI displacement experiments were predicted reasonably well in respect to oil recovery, average oil saturation and cumulative WOR, using the tuned EOS and estimated saturation functions in history matching tertiary CWI. There was a significant difference between the predicted differential pressure and that recorded experimentally, however; also the simulation model predicted a delay in CO_2 production compared to the measured values, which could be related to the effect of dispersion on the distribution of CO_2 in the oil, with a consequent effect on the formation of the gas phase. The dispersion effect is a localised process near the injection region where the flow is heterogeneous and turbulent, and its effect diminished further into the reservoir, as explained by the injection of carbonated water in a slim tube apparatus, representing uniform and laminar flow in the reservoir. Overall, we found that dispersion had an influence on the early production of CO_2, extending the dissolution of CO_2 for about 0.7 ft.

The change in permeability due to rock dissolution would also affect the differential pressure across the core leading to poor differential pressure predictions by the simulation model. The injection of carbonated water into the carbonate core that contains calcite could lead to severe changes in pore structure, which could either improve or impair the permeability of the rock. In our case, the rock dissolution caused improvement of rock permeability resulting in a reduction of differential pressure across the core.

The effect of carbonation level on the performance of CWI in secondary and tertiary modes was also studied. In the core displacement experiments, the relationship between the carbonation level and improving oil recovery could not interpreted linearly. Whereas

in the simulation modelling, a reduction in CL by 50% results in a decrease in oil recovery by the same percentage due to the fixed partitioning coefficient value in all flash calculation stages calculated by EOS, rather than a variable partitioning coefficient as calculated in the multiple-contacts equilibrium PVT test.

Chapter 6 – Technical Quality of Simulating CWI on the Reservoir-Scale

6.1 Introduction

In previous chapters, the simulation of CWI was systematically studied at the core-scale. It was explained that coupling the CO_2 solubility in brine in the form of Henry's Law with a cubic equation of state would provide an appropriate modelling scheme to simulate the performance of CWI using compositional simulators, taking in consideration of the physics observed in direct pore-scale experiments. Then, it was demonstrated that an appropriate selection of CO_2-hydrocarbon BICs and oil-gas relative permeabilities, with a three-phase oil relative permeability function would reproduce the experimental results seen in the CWI core displacement experiments.

The effect of any enhanced oil recovery (EOR) method is limited to its results on the laboratory-scale, except if it is tested at the reservoir scale, such as in a field pilot test. It is essential to shift to the field pilot testing of the performance of enhanced oil recovery methods so as to translate the results from the laboratory-scale into a real reservoir environment where other variables such as reservoir heterogeneity, thickness and gravitational effects may influence that performance. Field testing, however, requires significant preparation, starting from the design of the project to drilling the required wells, building the suitable surface facilities and ending with implementation. Furthermore, it might takes months to years for the applicability of a particular method for enhancing oil recovery to be proved technically and economically.

6.2 Trials of CWI on the Field-Scale

In 1959, JW Martin [167] published a patented study on the process of recovering oil from oil fields involving the use of critically carbonated water. That CWI trial took place in Allegany County near Richburg, New York in 1947. A slug of carbonated water was injected after secondary waterflooding until the oil structure was partially filled with partially carbonated water. This was then followed by a bank of conventional water. After the treatment with partially carbonated water, an enhancement in water injection capacity was noted since the water injection rates increased to about 35 bbl/day, which was more than before the treatment. Also, the oil production rate increased to 1045 barrels per acre

in the first year of implementing carbonated water whereas the yearly oil production rate by waterflooding alone had been 92 barrels per acre.

At the same time, the first commercial CWI field applications were being carried out in Dewey-Bartlesville field in Washington County, Northeast Oklahoma [168-170]. The K&S project was the first commercial carbonated water injection, beginning in 1958, followed by Project 33 which received carbonation in 1959. Then, lastly, the Post Oak project received a partial carbonated injection in 1960. In all three projects, the flood process started with a small slug of LPG to displace the remaining light hydrocarbon prior to carbonated water injection. Followed by controlled injections of CO_2 and water containing 50 ppm of surfactant, which was stopped after 3-4 months while the carbonation continued for about a year in each project, before being chased by plain water injection. The results of the carbonated water injection process were an improvement in the injectivity by about three times that of the nearby conventional waterflooding. Additionally, the average additional oil recovery for the K&S project and Project 33 was 43% higher than the original estimates for conventional waterflooding. The incremental oil recovery was equivalent to 4% pore volume.

Another field application of CWI was conducted in the Bartlesville sand formation of the Domes unit in north-eastern Oklahoma in 1965 [171]. The first stage of the project consisted of nine enclosed five-spot patterns. Carbonated water that had a CO_2 solubility of 82 scf/bbl, was injected as a slug, followed by plain water. The projected additional oil recovery was assumed to be 12% pore volume, and 9% pore volume if only a 25 % carbonated slug of carbonated water injected. The performance of the carbonated water in this case was not satisfactory, however, because of the relatively low waterflood recovery. On the other hand, the material balance of the gas produced indicated that less than 900 tons out of the 5000 tons of CO_2 injected were actually produced, meaning that most of CO_2 injected was retained in the reservoir. Additionally, de Nevers [172] explained that the low oil production of 110 MSTB in the second stage of the project, which was one third of the estimated volume, was due to poor sweep efficiency and vertical fractures. Table 6-1 summarised the field applications of CWI and their main reservoir properties and performance results. The enhancement of water injectivity and the increase in oil production were resulted from injecting the carbonated water, however, some reservoir characterisation such as vertical fractures would have a negative impact on the performance of CWI.

Table 6-1 Summary of the main field trials on carbonated water injection and their main results

Field Location and Year		Project type	CW Injection method	Reservoir and fluid properties	Main results
Allegany County, NY 1947		Pilot test	Tertiary Slug of CW followed by WF (economically depleted reservoirs)	- P_{res} =800 psi and T_{res} = 65°F - low permeability	- enhancement in water injection capacity from 55 bbl/day to 90 bbl/day - Increase in oil production by 1135%
Dewey-Bartlesville field, OK	K&S Project, 1958	Commercial tertiary CWI	A year of CWI in tertiary mode followed by WF (Economically depleted reservoirs)	- porosity = 17% and permeability = 50 md	- three times improvement in the injectivity than conventional WF - 37% additional oil more than estimated WF by 5 years lower
	Project 33, 1959			- thin oil layer with gas cap and bottom water drive	- the project life increased by unlocking extra oil production
	Post Oak Project 1960			- the presence of gas cap results in saturated oil	- 47% average additional oil recovery for K&S and Project 33 over estimated WF
				- medium-low oil viscosity of 6 cp	- doubled the water injection rate - oil production increased from 300 to a peak of 860 bbl per day
Domes unit, OK 1961		Sateged commercial tertiary CWI	- one third of the estimated reservoir PV followed by plain WF	- average porosity = 14% and permeability = 22 md	- active mass transfer of CO2 from CW to reservoir oil leads to oil viscosity reduction up to 1.9 cp and 15% oil swelling
				- medium-low oil viscosity of 10 cp at 98F	- almost 4100 tons out of 5000 tons injected CO2 retained in the reservoir
				- under-saturated oil with API gravity of 32°	- poor sweep efficiency and vertical fractures were the cause of low oil recovery

6.3 Overall Approach

Convenient simulation modelling before the implementation of pilot testing is essential to forecast the performance of the targeted EOR method. The simulation model proposed in this thesis is adequate in capturing most of the physics that were obtained in core flood displacement experiments and fluid-fluid interaction PVT tests during the investigation of carbonated water injection as EOR method. The simulation model has the right prediction tools to forecast the technical efficiency to proceed to the application of a carbonated water injection on a reservoir scale.

This chapter, therefore, carries out a technical quality screening study of the process of simulating CWI on the reservoir scale, using different reservoir models, beginning with a homogeneous single layer model and then a SPE-5 comparative solution model representing homogeneous multi-layer models. The synthetic 3-D homogeneous model has rock properties similar to the mixed-wet carbonate rock in the previous chapter. In this model, a comparison study between conventional water injection and carbonated water injection was achieved using different comparative parameters like the influence on improving oil recovery of injection rates during specific pore volumes injected, the effectiveness of dispersion on CWI on the field-scale, the effect of the level of CO_2 enrichment of the water, and the impact of the timing of the carbonated water injection in tertiary mode.

After that, a comparison study was carried out of the performance of CWI and other injection methods such as conventional waterflooding, CO_2 and methane injection, in order to evaluate suitable situations for the implementation of carbonated water injection. The SPE-5 comparative solution model, which is classified as a homogeneous model, containing three layers of fixed porosity and permeability, was used to achieve this study. This study also assessed the obtained oil-gas relative permeability during CWI in injection of the conventional gas and its influences in oil recovery compare to typical oil-gas relative permeability related to gas injection. Then, various CO_2 injection methods were simulated against carbonated water injection in secondary and tertiary modes to assess the incremental oil recovery at various PVI, the net CO_2 utilisation factor, and CO_2 storage.

6.3.1 Statistical Estimates for RF, UF_{netCO2}, CO_2 Retention, and Storage

Four statistical indicators were selected to evaluate the performance of carbonated water injection in comparison with other CO_2 injection methods. The amount of oil that may be recovered from the reservoir is termed the incremental oil recovery and is expressed as a recovery factor (RF) in terms of a percentage of OOIP (%OOIP). The net CO_2 utilisation factor is the amount of CO_2 required to produce a barrel of oil during the CO_2 injection, and is usually stated in units of thousands of cubic feet of CO_2 per stock tank barrel of oil produced (MSCF/STB). The CO_2 retention factor is the amount of CO_2 stored relative to the CO_2 injected, including all means of storage, such as trapped CO_2 in gas form or dissolved in oil and water. The CO_2 storage is the percentage of CO_2 that could be stored in the total reservoir pore volume that could be accessible to the CO_2 injection [173, 174]

6.4 Homogeneous Box Model

6.4.1 Model Description

A synthetic three-dimensional model was constructed to assess the performance of CWI on the reservoir scale. The rock and fluid properties were the same as those of the mixed-wet carbonate core displacement experiments in chapter 5. That is, the oil used in those experiments represented reservoir oil that contains multiple component gases, and the reservoir conditions for mixed-wet experiments were similar to real reservoir conditions, so as to reduce the uncertainty in respect to phase behaviour and compositional changes due to CO_2 mass transfer. The reservoir was 1000 ft x 1000 ft x 100 ft. The model consisted of two vertical production and injection wells, and the locations of those wells were chosen to represent a quarter 5 spot well pattern. In other words, the production and injection wells were diagonally in opposite corners of the model, as demonstrated in figure 6-1. The reservoir was under-saturated at an initial reservoir pressure of 4000 psi and a temperature of 212 °F.

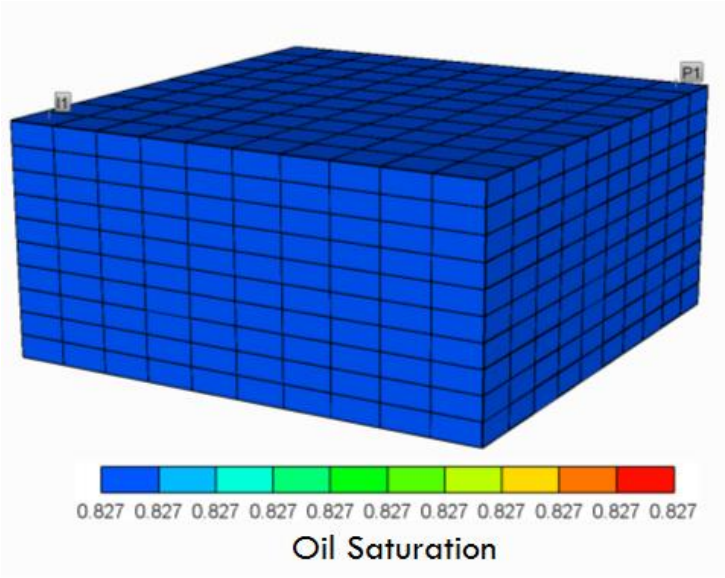

Figure 6-1 3-D homogeneous model

The CMG-GEM compositional simulator that was used in all the previous simulation models, was used again in this simulation. The sensitivity of the grid in the X-Y directions and layering (table 6-2) was analysed with secondary WF and CWI to create the required gridding option. The carbonated water was injected by invoking the solubility feature. Henry's Law was used to model the solubility of CO_2 in brine, which was estimated to be 135 scf/bbl at a reservoir pressure of 4000 psi and 212 °F in a brine salinity of 59046 ppm. Thus, carbonated water (CW) is defined as an aqueous phase that has 1.01 gmol per kg water of CO_2 molality soluble in brine.

Table 6-2 X-Y grid size and layers sensitivity analysis

Horizontal area		Vertical Layers	
No. of X-Y Grids	Grid size (ft)	No. of Layers	Grid size (ft)
3	500	1	100
6	250	2	50
10	150	4	25
20	75	5	20
30	50	10	10
50	30	20	5
75	20		

In the reservoir simulation, the selection of the optimum size for the grid blocks was done in such a way as to minimise the effect of numerical dispersion and to obtain a reasonable simulation time and computational load, then the results of the simulation would become independent of grid size. Figure 6-2 shows the oil recovery from the secondary WF and CWI process at various grid blocks in the X-Y direction and across a number of layers.

After ten grids in the X-Y direction, both WF and CWI were unresponsive to more refining of the grids, whereas increasing the number of layers up to ten layers would improve the sweep efficiency, consequently enhancing the oil recovery. After ten layers, however, the change in recovery became negligible. Based on this sensitivity analysis, the model was discretised into 10x10x10 grid blocks to resolve the flow accurately, and this was used in the subsequent simulations. In this simulation model, the oil composition and tuned EOS, along with the estimated saturation functions that were obtained when simulating the mixed-wet core displacement experiments, were used in the prediction of conventional WF and CWI. In the simulation model, the CO_2 partitioning coefficient between the aqueous and oil was first calculated using the fugacity equilibrium method, where the oil phase behaviour was calculated using PR-EOS, while the solubility of the CO_2 in the aqueous phase was estimated using Henry's Law. Only hydrocarbon and CO_2 were allowed to be in the oil and gas phases, i.e., no water vaporisation, while no hydrocarbons were soluble in the aqueous phase. The properties of the homogeneous model are given in table 6-3.

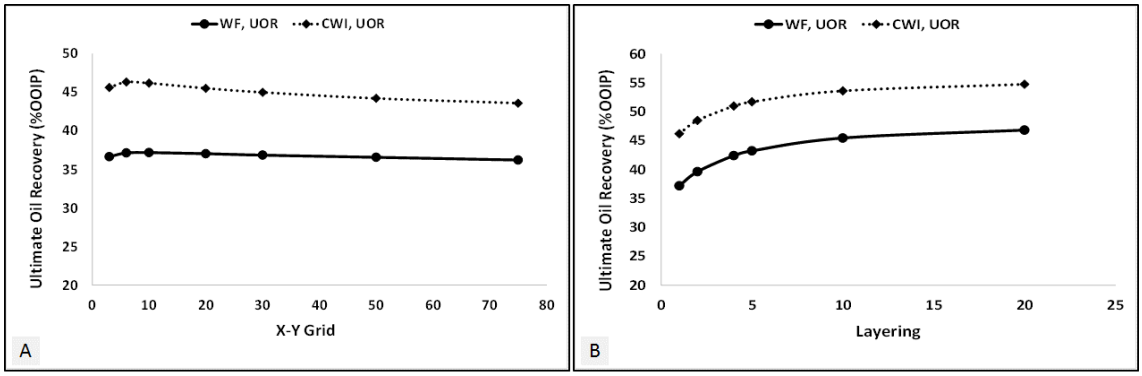

Figure 6-2 grid size (X-Y grid and layers) sensitivity of secondary WF and CWI

Table 6-3 grid properties of the synthetic 3D homogeneous model

Initial reservoir pressure, psi	4000
Reservoir temperature, °F	212.00
Grid Size, ft	150x150x10
Porosity, fraction	0.2583
Permeability (kx = ky = kz), md	88.277
Reservoir PV, MM res bbl	10.351
OOIP, MMSTB	6.9371
Initial water saturation (Swi), fraction	0.173
Reservoir depth, ftss	8450
Oil viscosity, cp	0.90
Water viscosity, cp	0.33

The production and injection wells were perforated across all the reservoir layers. The initial reservoir pressure was set to be 900 psi above the core displacement experiments, which was 3100 psi, where the production well was constrained by a constant minimum bottomhole flowing pressure of 3100 psi so as to prevent any accumulation of secondary gas cap around the well. The production rate was fixed at 3500 STBD. Other well economic constraints for the production well were set at a minimum oil rate of 5 STBD, maximum water cut of 99% and a maximum GOR of 15 Mscf/stb. Thus, the economic limits were controlled on the basis of the layers, which means that if any layer reached these limits, it was automatically shut-in. The maximum allowable bottomhole injection pressure was limited to be 6000 psi assuming a fracture gradient of 0.8 psi/ft at a datum depth of 8450 ftss. The injection well was controlled by the injection rate. The model was customised to predict the performance over 25 years, whereas the injection rate was varied to inject the specified pore volume over that period, as demonstrated in table 6-4.

Table 6-4 various injection rates over 25 years

Injection Rates (STBD)	Total PVI
1135	1.00
1705	1.50
2270	2.00
2835	2.50
3405	3.00
3970	3.50
4540	4.00

6.4.2 Simulation Results

6.4.2.1 Secondary WF and CWI

The performances of the secondary WF and CWI were predicted in order to investigate the effect of total injected fluid on ultimate oil recovery. It was shown in the coreflood experiments that the secondary CWI produced 13.5% more oil than that from secondary WF, at 4 PV of injected fluid. This incremental oil recovery was related to CO_2 dissolution in oil and the formation of the gas phase, which enlarged the oil volume, subsequently improving oil mobility. To evaluate this at the reservoir scale, figure 6-3 shows the ultimate oil recovery of secondary CWI in comparison with that of secondary WF versus the total pore volume injected (PVI). It was shown that the oil recovery in secondary WF was maintained at 45% with no further enhancement as more water pore volume was injected, while the oil recovery in secondary CWI showed an increasing trend

as more CW pore volume was injected. Additional CO_2 introduced to the system therefore led to extra oil recovery. The incremental oil recovery at 4 PVI, however, was 8.19 % of OOIP, which was lower than that in the core displacement experiments.

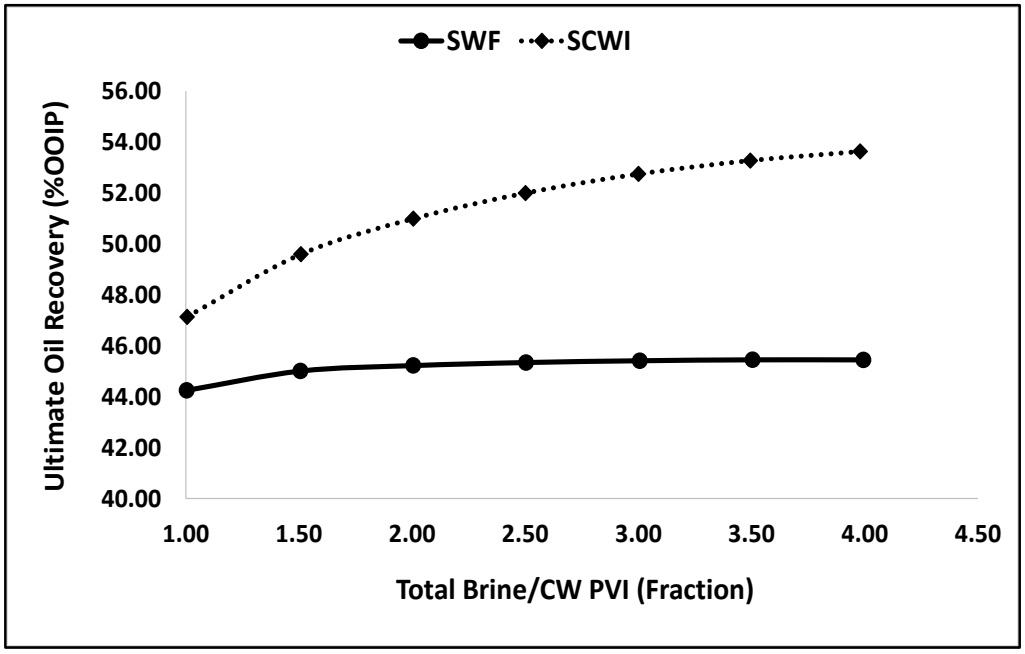

Figure 6-3 ultimate oil recovery of secondary WF and CWI with total brine/CW PVI

It was the increase in CO_2 in aqueous phase arising from the injection of more CW pore volume that resulted in additional oil recovery, rather than the increase in the injection rate. Figure 6-4 shows the oil recovery of SWF and SCWI at various injection rates within the specified injecting pore volume of 1.5 PVI. An increase in injection rate led to a reduction in the amount of oil that could be recovered, where the water broke through faster at greater injection rates, leading to poor sweep efficiency, and subsequently leaving more remaining oil saturation un-swept. With about a fixed volume of CO_2 soluble in brine (equivalent to a CO_2 injection rate of 143 res bbl/day), however, the incremental oil recovery was maintained at an average of 4.77 % of OOIP.

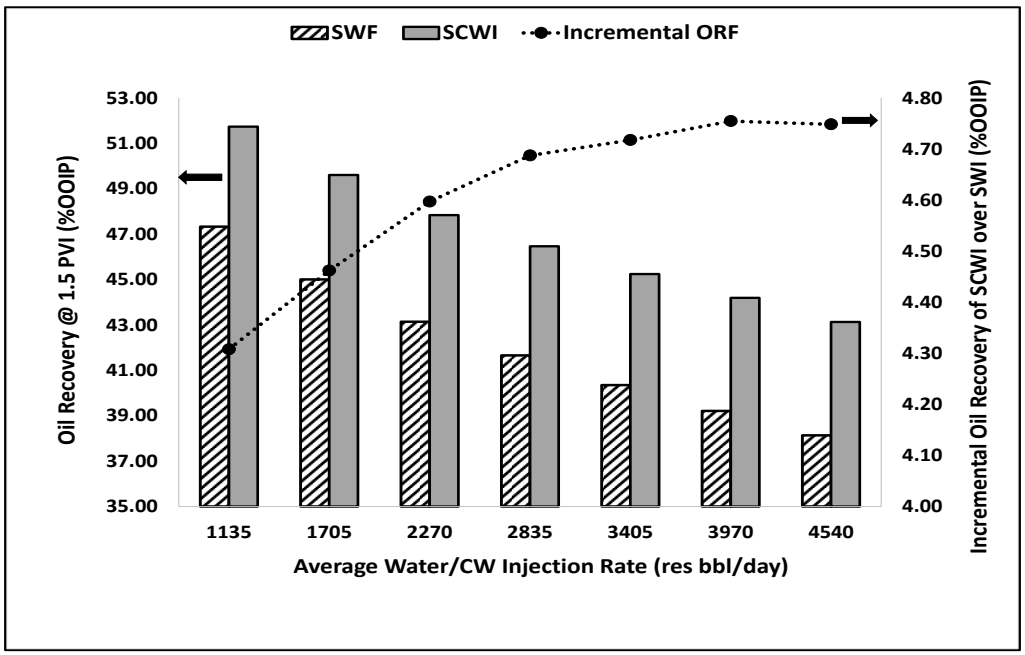

Figure 6-4 oil recovery of SWF and SCWI and incremental oil recovery at 1.5 PVI of various injection rates

Effectiveness of dispersion on CWI

As explained in the previous chapter, introducing the dispersion factor through which both CW and oil would be mixed together to repeat the earlier CO_2 breakthrough ahead of water, had a negative impact on the oil recovery when simulating the performance of the CW core displacement experiment. In reservoir-scale simulation, therefore, a dispersion factor of 1000 ft was introduced to predict the early breakthrough of CO_2 ahead of water, as shown in figure 6-6B. Thus, the dispersion effect on the reservoir-scale significantly reduced the CO_2 retention, which is the percentage of stored CO_2 in the reservoir, as demonstrated in figure 6-5B, while it is relatively insensitive to the oil recovery, as shown in figure 6-5A. Then, the effect of dispersion on oil recovery was diminished at the larger scale where the flow away from the injector would be uniform and steady rather than the unsteady and turbulent flow near the wellbore.

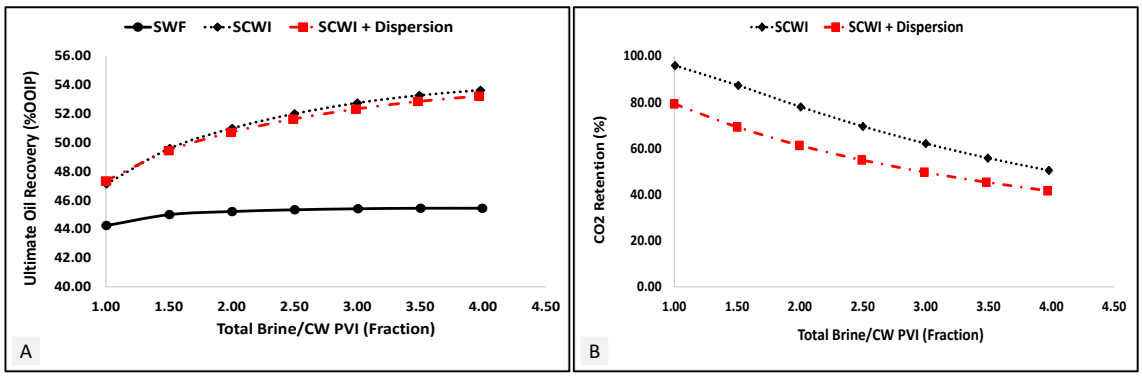

Figure 6-5 (A) ultimate oil recovery over total injected PV for the SWF, SCWI and SCWI scenarios with dispersion (B) CO_2 retention comparison between SCWI with and without the dispersion effect

One scenario was selected to investigate the role of dispersion in the mechanisms of CWI for enhancing oil recovery. Figure 6-6A showed the oil recovery of SCWI with and without the dispersion effect when an injection rate of about 3400 bbl/day was implemented. In this case, there was a slight enhancement in oil recovery after water breakthrough from 0.5 to 1.5 PVI as a result of the better distribution of the CO_2 in the oil improving the oil mobility; thereafter the oil recovery followed the same trend as with no dispersion. At this point in the dispersion effect case, the gas phase had not yet formed, as shown in figure 6-8, which indicated that the steady dissolution of the CO_2 in oil was preventing the formation of a new phase. While the production of CO_2 occurred after the water breakthrough by almost 0.5 PVI in (without dispersion) simulation scenario, the CO_2 broke through the same time as water breakthrough in (with dispersion) simulation scenario as shown in figure 6.6B. The early breakthrough of CO_2 results from the non-uniform distribution of CO_2 within the oil which was caused by the dispersion effect. In other words, the mass transfer of CO_2 from CW to oil was not concentrated in the focused location which could lead to forming an additional phase but it rather scattered distribution.

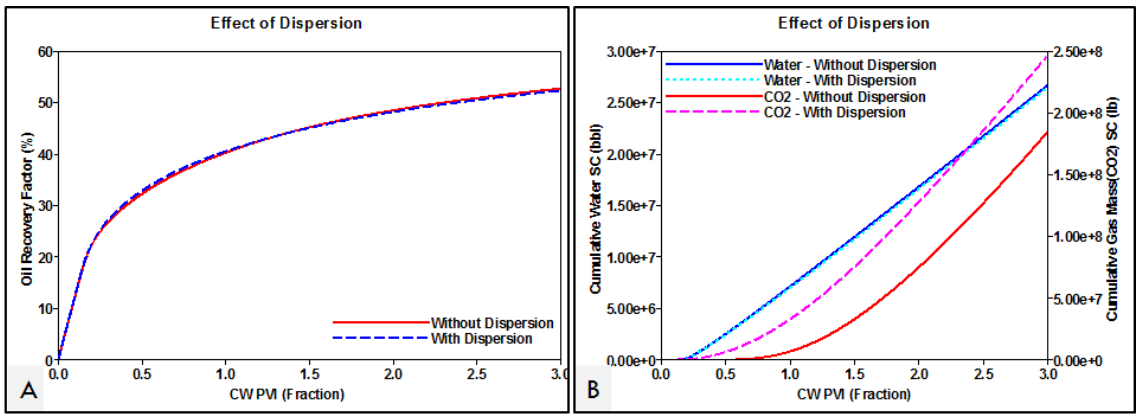

Figure 6-6 effect of dispersion on (A) oil recovery factor of SCWI and (B) cumulative water and CO_2 mass productions

Introducing the dispersion effect helped to improve the diffusion of the CO_2 in the oil and water in such a way that the water would not be depleted of its content of CO_2 since it limited the CO_2 mass transfer to oil around the injection well area only, rather than distributing it across the whole reservoir, as illustrated in figure 6-7. In this way, the formation of the free gas phase was delayed since the oil had not reached its saturation limit in respect to CO_2. On the other hand, the mobility of oil was enhanced.

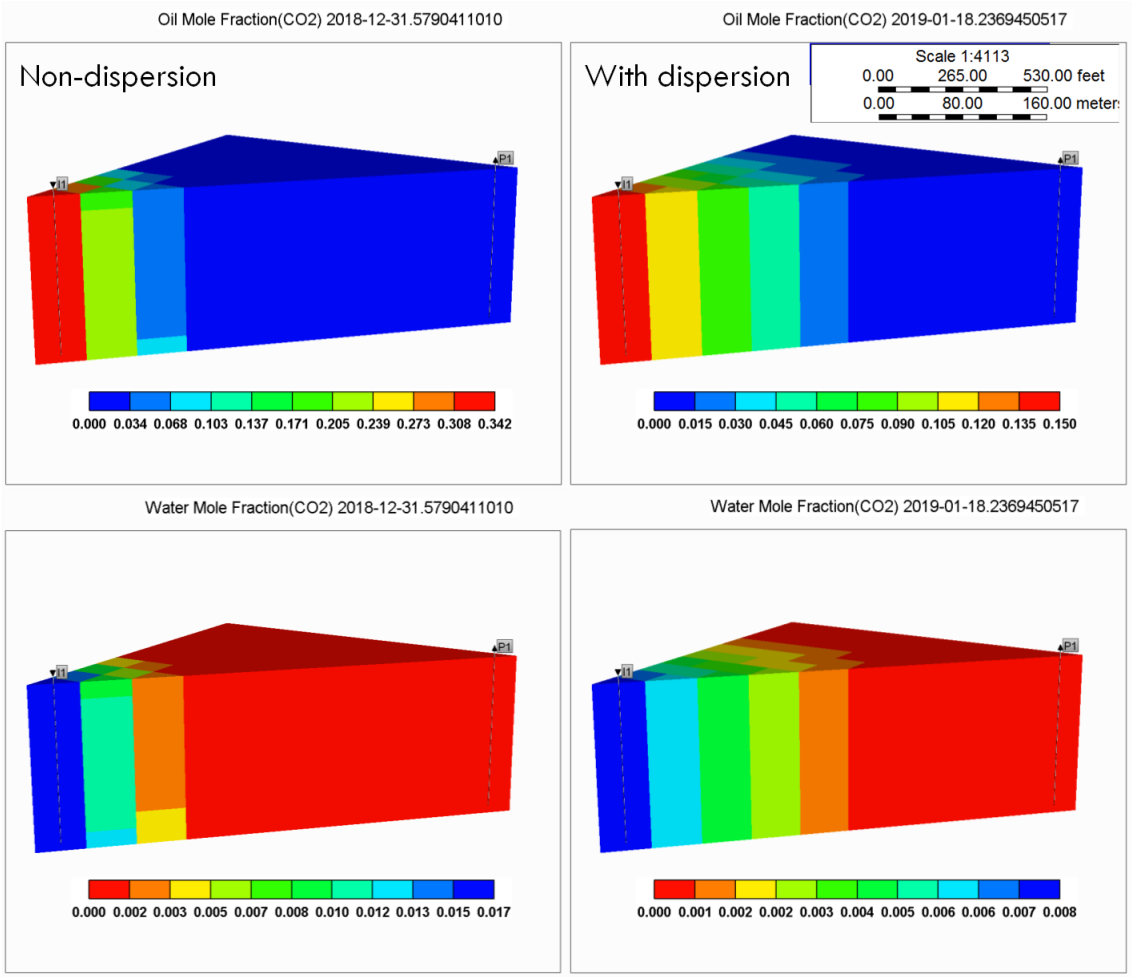

Figure 6-7 effect of dispersion on CO_2 concentration in oil (top) and water (bottom) at time of water breakthrough (0.12 PVI)

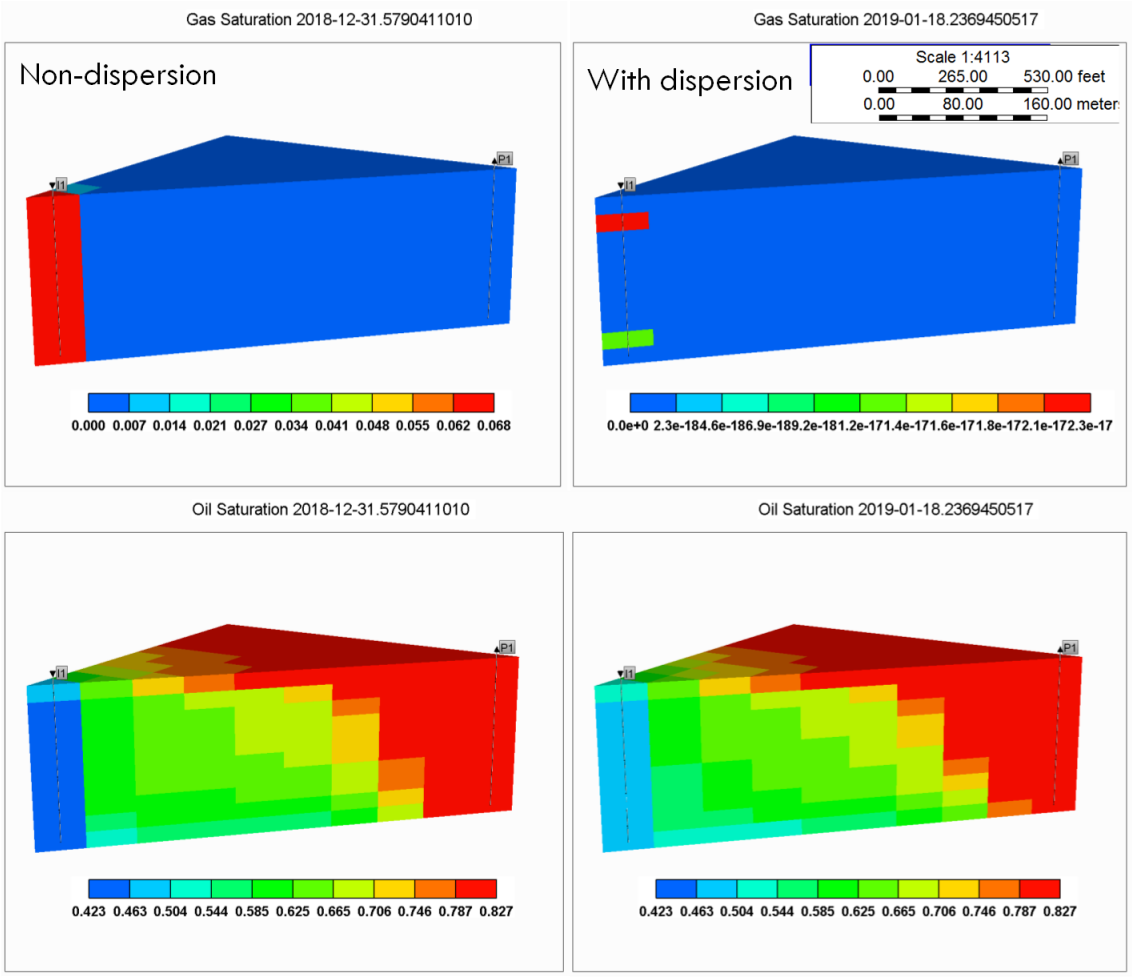

Figure 6-8 effect of dispersion on the formation of the gas phase (top gas saturation) and oil sweep efficiency (bottom oil saturation) at time of water breakthrough (0.21 PVI)

Impact of carbonation level

Experimentally, when carbonation level was reduced by 50%, the oil recovery reduced by about 30% compared to when the carbonation level was 100%. Although 50% oil recovery was predicted by the simulation when the carbonation level was 50%, this was almost 20% lower than that in the core displacement experiment. The simulation practice, however, was sufficient to present qualitative results of the impact of the carbonation level on oil recovery. On the reservoir-scale, therefore, reducing the solubility of CO_2 in brine, either by increasing the brine salinity or reducing the pressure in the isothermal reservoir, served to reduce the oil recovery and the CO_2 storage in the reservoir. In the simulation forecasting model, various carbonation levels were implemented, to predict the performance of SCWI in producing additional oil, as illustrated in table 6-5.

Table 6-5 CO_2 solubility in brine for different carbonation levels

Carbonation level (%)	CO_2 solubility in brine, scf/bbl
100	135.046
75	101.285
50	67.523
25	33.762

Figures 6-9 and 6-10 demonstrate the role of various carbonation levels in secondary CWI, and the effect on the oil recovery and CO_2 retention. In terms of oil recovery, the reduction of the level of the CO_2 in the brine clearly impaired the amount of CO_2 transferred to the oil, thereby weakening the CW mechanisms that would enhance oil recovery, such as the reduction in oil viscosity and the increase in oil swelling. In addition, the oil would not become fully saturated with CO_2 so as to form the additional gas phase that is crucial to recover more oil. On the other hand, the dominant mechanism of CWI performance was the formation of immobile gas phase resulting from saturating the oil with CO_2 due to the mass transfer of CO_2 from CW. Therefore, reducing the CO_2 enrichment in CW limited the saturation of the oil, consequently reducing the volume of the gas phase that was formed. This then resulted in a reduction in the CO_2 storage (CO_2 retention), as demonstrated in figure 6-10. As with the oil recovery, the CO_2 storage was dependent on the volume of the gas phase that was trapped in the reservoir, since this served both to produce additional oil and at the same time to store more CO_2 in-situ.

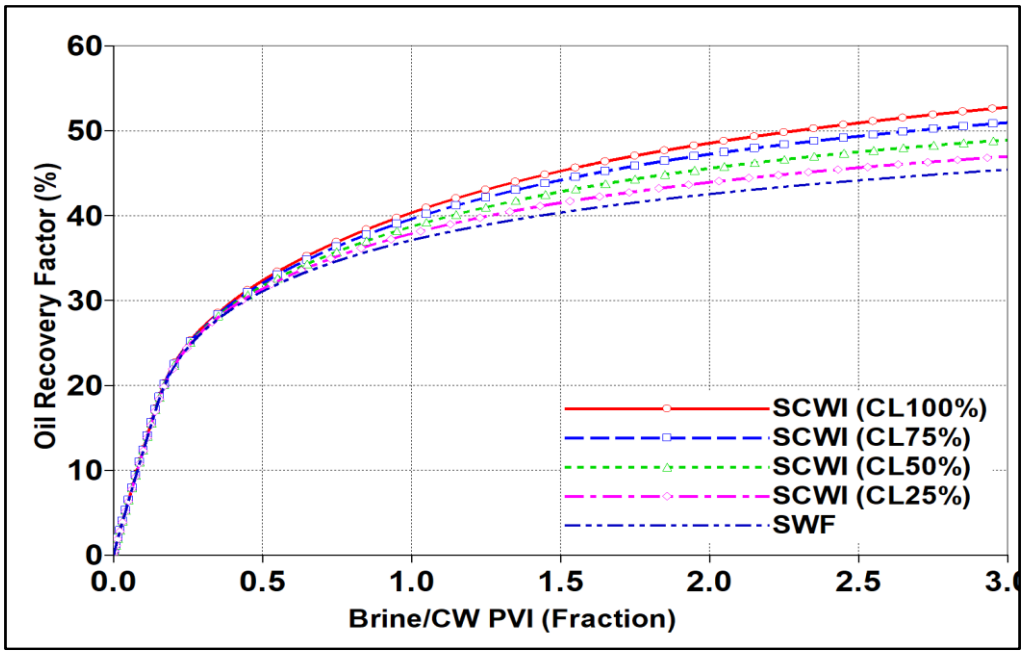

Figure 6-9 Impact of carbonation level on oil recovery during secondary CWI

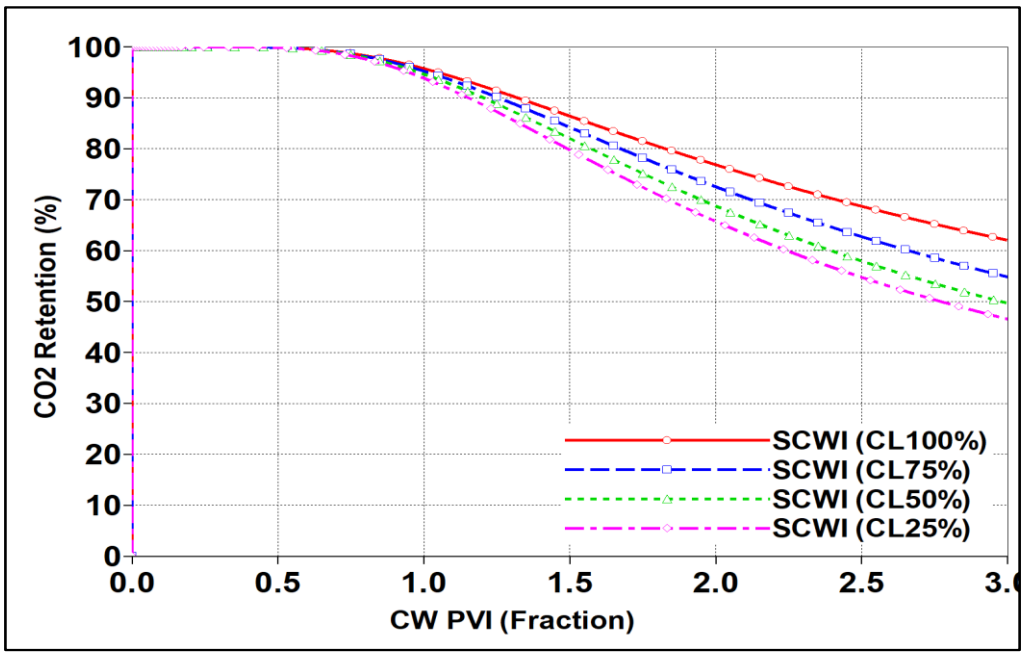

Figure 6-10 impact of carbonation level on CO_2 retention during secondary CWI

6.4.2.2 Tertiary CWI

It is more likely that the injection of carbonated water for enhancing oil recovery and CO_2 storage will be implemented in tertiary mode rather than the secondary recovery method, especially if the performance of conventional waterflooding was adequate to produce the oil, taking in consideration the technical and economic circumstances. Hence, the performance of tertiary CWI (post-WF) was studied after several pore volumes of injected conventional water. In the simulation model, the water broke through after about 0.2 PVI, when 22% of oil in place had been recovered. The sensitivity analysis of tertiary CWI was carried out by injecting CW up to a total injecting pore volume of 4.0 after 0.1, 0.3, 0.5 and 0.7 PVI of plain water so as to evaluate the consequences for oil recovery and CO_2 storage of a delay in injecting CW. Figures 6-11 and 6-12 compare the oil recovery and CO_2 retention of SCWI and tertiary CWI at various pore volumes of injected WF. It can be observed that injecting CW initially at the beginning was by far superior in enhancing oil recovery than doing so in tertiary CWI, while to get better CO_2 sequestration credits, the longer the injection of CWI in tertiary mode was postponed the more the percentage of stored CO_2 increased.

It is worth mentioning that this 3D model prediction was consistent with the experimental results reported in CWI core displacement experiments, in that the oil recovery due to secondary CWI was more than that in tertiary CWI in cases of water-wet and mixed-wet cores.

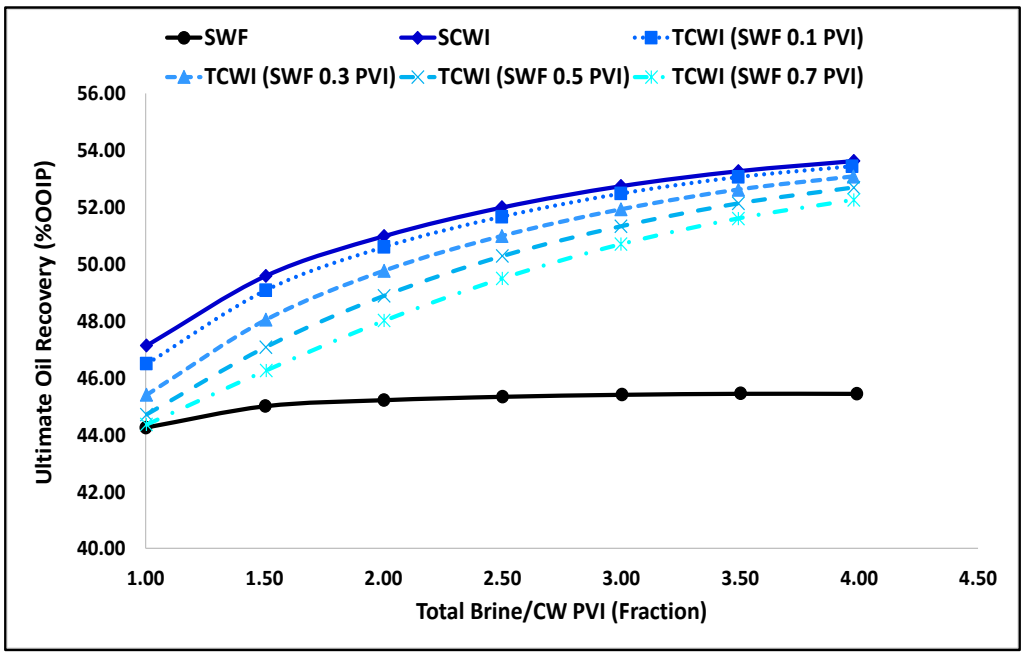

Figure 6-11 comparison of oil recovery between SCWI and tertiary CWI at various SWF PVI

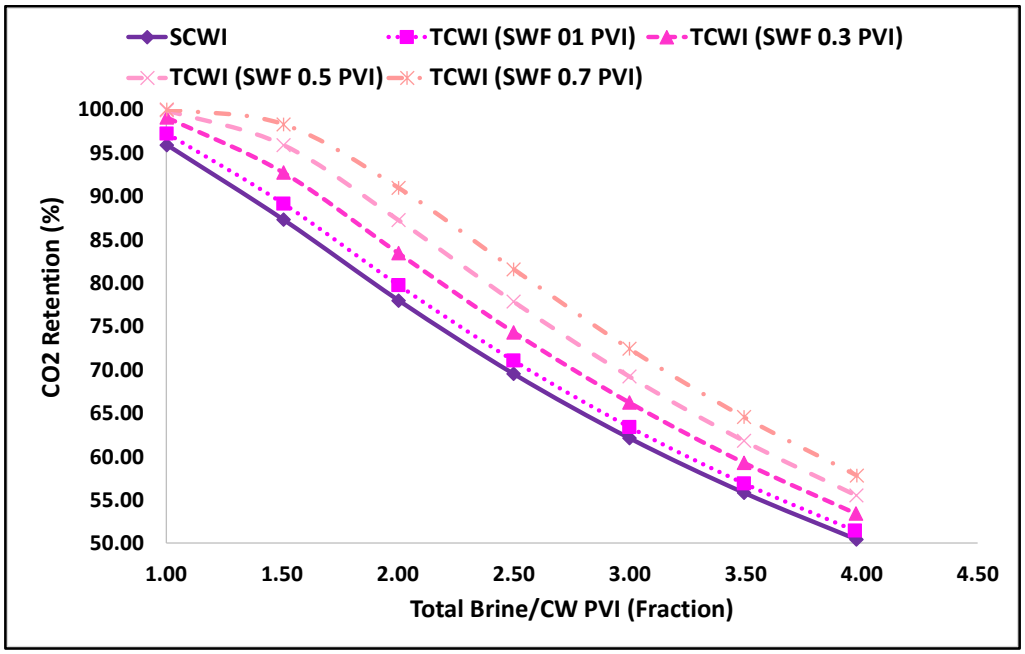

Figure 6-12 comparison of CO_2 retention between SCWI and tertiary CWI at various SWF PVI

In summary, there was a relationship between the incremental oil recovery and CO_2 retention with and the total CO_2 PV injected that is soluble with brine. While injecting more CO_2 that is soluble in brine produced additional oil, it reduced the CO_2 storage, since the oil saturated with CO_2, along with the formed gas phase, were produced from the reservoir, as clarified in figures 6-13 and 6-14. Therefore, the earlier the carbonated water was injected, the greater the oil recovered but the smaller the amount of CO_2 stored.

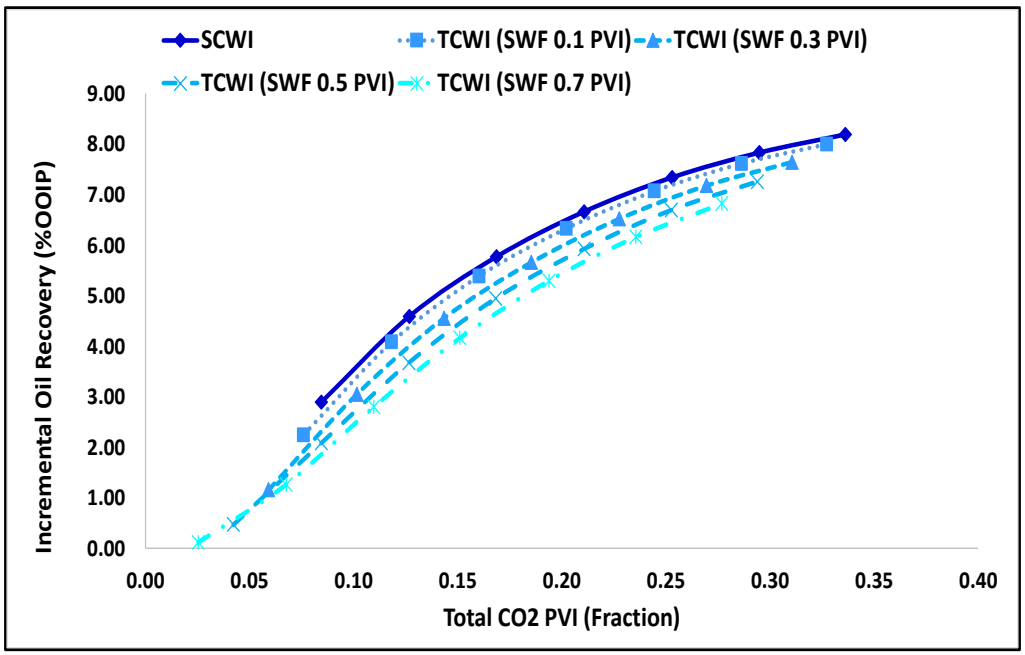

Figure 6-13 a relationship between incremental oil recovery with total CO_2 PVI

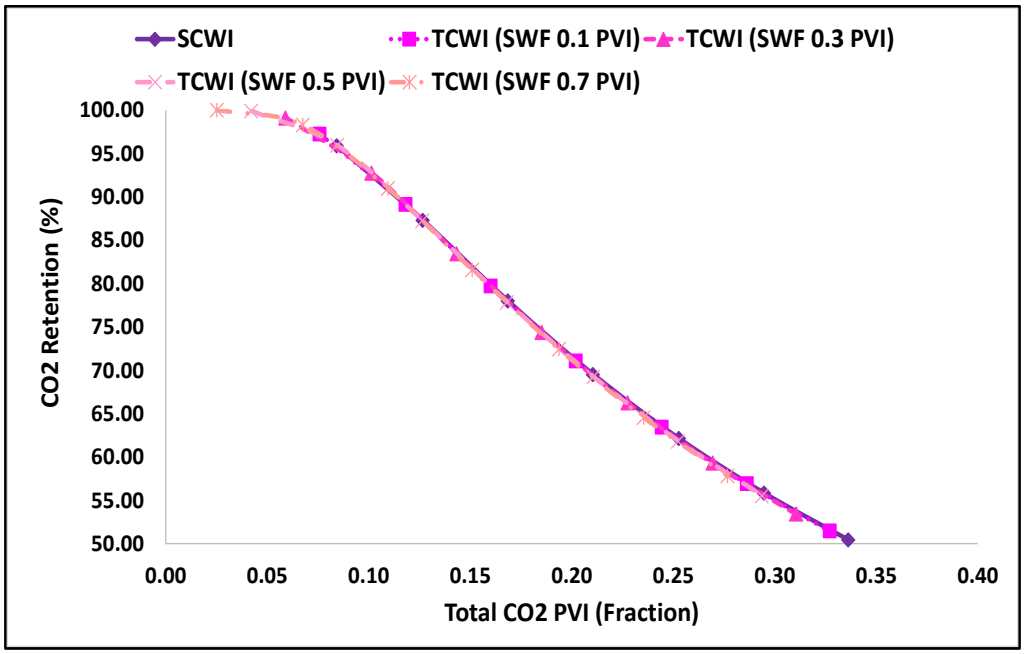

Figure 6-14 a relationship between CO_2 retention with total CO_2 PVI

6.5 SPE-5 Comparative Solution Model

6.5.1 Model Description

For the purpose of the comparison, the SPE-5 comparative solution model, which was introduced by Killough and Kossack in 1987, was used [175]. The reservoir dimension in the model was 3500 ft in the x and y directions, with a reservoir thickness of 100 ft. The initial water saturation was 17.3 %PV. The reservoir contained three layers of

different thicknesses and horizontal and vertical permeabilities, as shown in table 6-6, but with a uniform porosity of 0.3. The reservoir pressure and temperature were initially set at 4000 psi and 212 °F, respectively, and therefore the reservoir was under-saturated with oil where the oil saturation pressure is 3100 psi. In this simulation model, the saturation functions, including the relative permeability set and capillary pressure and oil composition with the tuned EOS, were retained as those estimated in the previous simulation of the mixed-wet core displacements in section 5.5.4, chapter 5. The reservoir oil, meanwhile, was generated by recombining the stock tank oil with multiple hydrocarbon gases (C_1-C_4), representing the reality of reservoir oil.

Table 6-6 reservoir properties in the SPE-5 grid model

Reservoir Layer	Thickness, ft	Horizontal Permeability k_h, md	Vertical Permeability, k_v, md	Anisotropy ratio (k_v/k_h)
1	20	500	50	0.100
2	30	50	50	1.000
3	50	200	20	0.125

Sensitivity analysis of the number of grids in the x and y directions and layers was carried out in respect to secondary waterflooding and CWI using the CMG-GEM compositional simulator to acquire the optimum gridding and layering option, in which the effect of numerical dispersion would be minimal while achieving a reasonable simulation time and use computational memory and storage. The results are shown in table 6-7. The carbonated water was injected by invoking the solubility feature. Henry's Law was used to model the CO_2 solubility in brine, which was estimated to be 135 scf/bbl at the reservoir pressure of 4000 psi and 212 °F and with a brine salinity of 59046 ppm. Thus, carbonated water (CW) is defined as an aqueous phase that has 1.01 gmol of CO_2 per kg water of CO_2 molality soluble in brine. Figure 6-15 demonstrates the oil recovery of secondary WF and CWI at different X-Y grid blocks and with variations in the number of layers. The simulation results became independent of grid size, when the number of grids increased to more than 19 grids and after about 10 layers. The reservoir model was discretised into 29x29x10 gridblocks which had 8410 grids, to be used in the subsequent simulation scenarios. In the simulation model, the hydrocarbon components were not allowed to be soluble in brine, while only the CO_2 and hydrocarbon components were allowed to exist in the oil and gas phases. The partitioning of CO_2 between oil and aqueous phases was calculated based upon the fugacity equilibrium equation, where the

oil fugacity calculated using the cubic EOS and the aqueous fugacity was determined using Henry's Law. The gas phase was then able to form due to the unstable oil phase and the equilibrium coefficient calculated internally through the cubic EOS.

Table 6-7 Sensitivity of X-Y grid size and number of layers

Horizontal Area		Vertical Layers			
X-Y Grid	Grid Size, ft	Layers	Grid size, ft		
7	500.00	3	20	30	50
15	233.33	6	2	2	2
19	184.21		10	15	25
29	**120.69**	**10**	**10**		
35	100.00	12	4	3	5
47	74.47		5	10	10
		20	5		

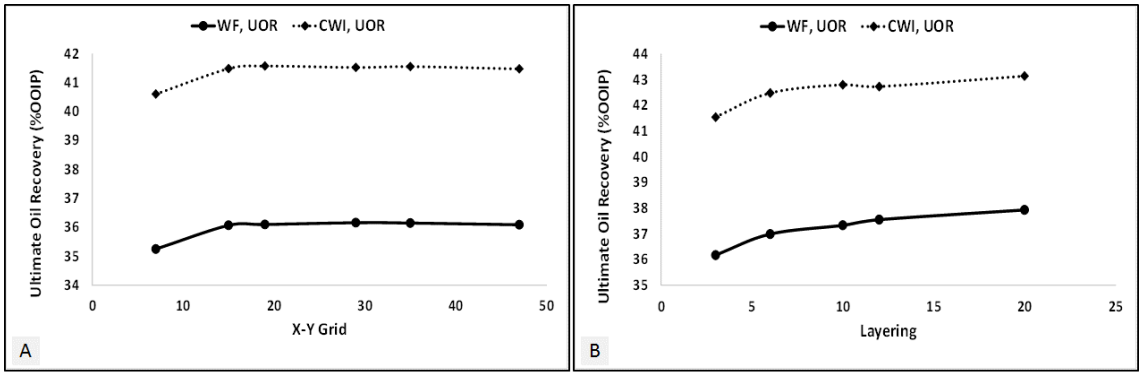

Figure 6-15 oil recovery at different X-Y grid sizes and number of layers

The stock tank original oil in place (STOOIP) was 43.866 million STB, and the reservoir pore volume was 367.5 million reservoir cubic feet. Figure 6-16 represents the grid top of the SPE-5 reservoir model where the reservoir depth at datum is 8450 ftss.

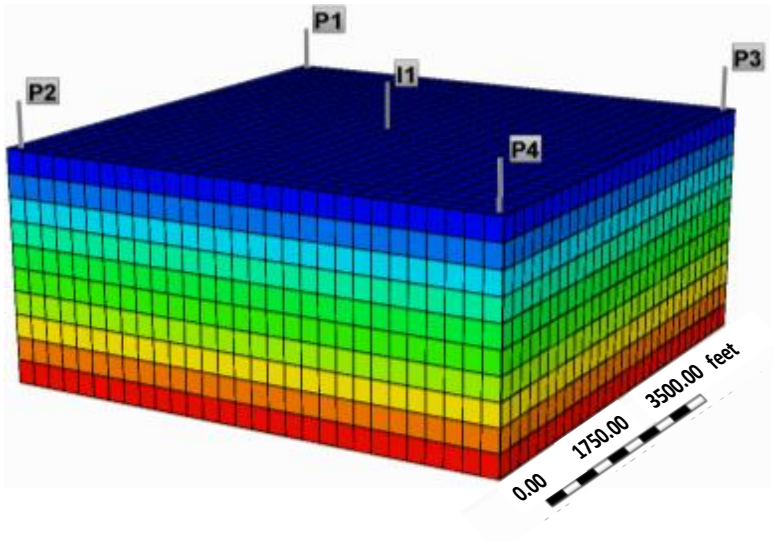

Figure 6-16 SPE-5 reservoir model showing the inverted five-spot pattern

An inverted five-spot pattern was selected to locate the well in the reservoir model. The pattern contains four production wells located at each corner of the model, and one injection well located at the centre of the model. The production wells were constrained based on a minimum bottomhole flowing pressure of 3100 psi to avoid any accumulation of secondary gas caps around the wells. The other constraint was the maximum oil production rate of 4000 STBD per well to gain 13.32 % yearly oil recovery. The well economic constraints were not considered in this simulation task as the maximum oil recovery and CO_2 storage should be reached in order to continue with the technical screening among all the proposed injection methods. The injection well was controlled by a reservoir injection rate set to attain the same injected pore volume in various injection methods. The surface injection rate would be more influenced by the formation volume factor that was in turn affected by the reservoir pressure. The sensitivity of the perforating layers was studied to assess the impact of injecting and producing layers on the displacement efficiency in secondary water injection and CWI. Table 6-8 displays the oil recovery after injecting 1 PV of either conventional water or CW for each of the perforation scenarios. Apparently, the perforation layers had a negligible effect on oil recovery in both SWF and SCWI, however scenario no. 7 was selected in all the simulations, whereby the injection is in layer 3 and the production is from all layers. Injection in the second layer was avoided because of low injectivity in comparison with other cases.

Table 6-8 Different injection and production perforation layer cases and their oil recovery at 1 PVI of SWF and CWI

Case No.	Injection layer	Production layer	SWF, Oil Recovery (%)	SCWI, Oil Recovery (%)
1	1	3	32.12	35.01
2	3	3	32.82	35.63
3	1	1	33.01	35.05
4	3	1	32.99	35.72
5	1,2,3	1,2,3	33.38	36.06
6	1	1,2,3	32.88	35.74
7	**3**	**1,2,3**	**33.56**	**36.37**
8	1	2,3	32.27	35.17
9	3	1,2	33.08	35.80

It should be noted that the simulation model was defined so that the screening criteria for a CO_2-EOR project is met. That is, the CO_2 minimum miscibility pressure (MMP) was estimated using the predefined correlations. Glaso presented a generalised correlation for

predicting CO_2-MMP that required multiple-contact miscible displacement of reservoir fluid by CO_2 [176]. His correlation was a function of reservoir temperature and C_{7+} molecular weight of the stock tank oil. The correlation was as follows:

$$\mathrm{MMP_{CO_2}} = 810.0 - 3.404\mathrm{M_{C_{7+}}} + \left(1.700 \times 10^{-9}\mathrm{M_{C_{7+}}^{3.7370}e^{786.8M_{C_{7+}}^{-1.058}}}\right)\mathrm{T} \quad \text{Equation 6-1}$$

Where M_{C7+} is the C_{7+} molecular weight of stock tank oil and T is the reservoir temperature in degrees Fahrenheit. The MMP was estimated to be 3041 psi. Glaso's correlation under-estimated MMP, however, because the intermediate components were not considered in the calculation. Another improved MMP correlation for CO_2 injection was therefore developed by Yuan et al. [177]. Their approach was to use the analytical theory for MMP calculations developed from cubic equation of state. The approach covered a wide range of temperature and reservoir fluids. Their MMP correlation was a function of reservoir temperature, molecular weight of C_{7+}, and percentage of intermediate components (C_2 to C_6) in the oil. The developed correlation was as follows:

$$\mathrm{MMP_{CO_2}} = a_1 + a_2M_{c7+} + a_3P_{C2-6} + \left(a_4 + a_5M_{c7+} + a_6\frac{P_{C2-6}}{M_{C7+}}\right)T + (a_7 + a_8M_{C7+} + a_9M_{C7+}^2 + a_{10}P_{C2-6})\mathrm{T}^2 \quad \text{Equation 6-2}$$

Where M_{C7+} is the C_{7+} molecular weight of stock tank oil, P_{C2-6} is the percentage of intermediate components in reservoir oil, T is the reservoir temperature in degrees Fahrenheit, and a_1 to a_{10} are coefficients determined from regression data as shown in table 6-9. The MMP was calculated to be 6503 psi.

Table 6-9 Yuan et al. CO_2 MMP correlation coefficients

a_1	-1.4634E+03
a_2	6.6120E+00
a_3	-4.4979E+01
a_4	2.1390E+00
a_5	1.1667E-01
a_6	8.1661E+03
a_7	-1.2258E-01
a_8	1.2883E-03
a_9	-4.0152E-06
a_{10}	-9.2577E-04

Two correlations gave different CO_2-MMP pressures, in that the first correlation [176] estimated miscible CO_2 injection at simulation model reservoir pressure of 4000 psi, while the calculated MMP from the other correlation [177] suggested immiscible CO_2 injection at reservoir pressure. A third correlation was therefore used to decide whether the CO_2 injection would be immiscible or miscible with reservoir oil at the proposed reservoir conditions. Specifically, Khazam et al. established a new simple reliable correlation to calculate the CO_2 MMP covering a wide ranges of pressure between 1544 to 6244 psia and oil API gravity of 28° to 50° [178]. Their CO_2 MMP correlation was mainly a function of saturation pressure, API, reservoir temperature, and solution gas oil ratio (Rs). Their correlation was as follows:

$$MMP_{CO_2} = 5578 + 10.37 * T + 0.929 * P_b + 10220 * \frac{API}{Rsi} - 166.3 * API - 8.71 * P_b * \frac{API}{Rsi} \quad \text{Equation 6-3}$$

Where, T is the reservoir temperature in degrees Fahrenheit, P_b is the oil bubble point pressure in psi, API is oil API gravity, and R_{si} is the solution gas oil ratio in scf/stb. The CO_2 MMP was calculated to be 5826 psi. Additionally, Khazam et al. developed another correlation which was more complex than equation 6-3 [178]. The CO_2-MMP was estimated to be similar to that found from the simple correlation. As a result of this procedure, the injected CO_2 would be immiscible with the specified oil composition at reservoir conditions.

The oil-gas relative permeability curves that were obtained while reproducing the CWI process in the mixed-wet carbonate core displacement experiment were suitable to model the flow behaviour of the formed new (gas) phase in which the immobility and slow movement were the flow characteristics of that gas. Hence, the high values of critical gas saturation, and very low gas relative permeability, were the main features necessary to mimic the performance of CWI. Whereas, a classic gas displacement, represented by typical oil-gas relative permeability curves, characterised the immiscible CO_2 injection as an EOR method. Although, the tertiary CO_2 injection after secondary CWI was relatively predictable using oil-gas relative permeability estimated for CWI in the water-wet core displacement test. Moreover, oil-gas relative permeability curves for CO_2 injection were generated based on the intention of mimicking the flow behaviour of CO_2 in a carbonate reservoir that possessed rock properties close to the reservoir model. As a

result, the oil-gas relative permeability curves for a mixed wet core that were used in Agada et al. [179], were incorporated in the model used in this study, as shown in figure 6-17.

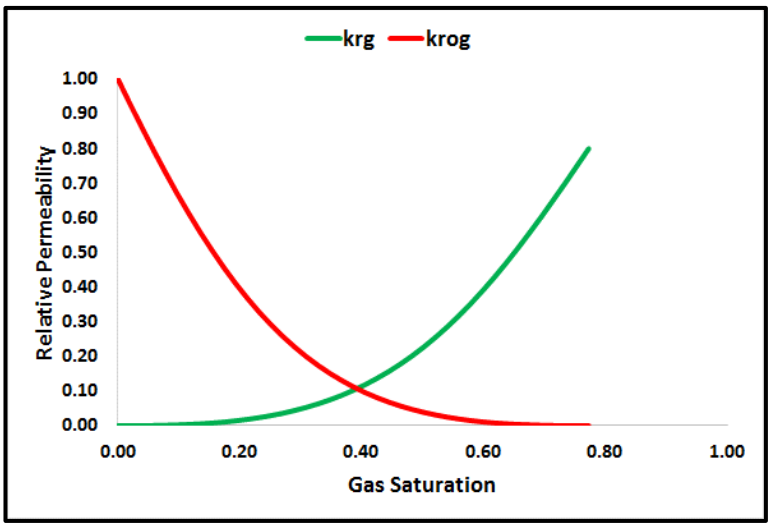

Figure 6-17 a typical oil-gas relative permeability curves produced following those in [179]

6.5.2 Simulation Results

6.5.2.1 Secondary CWI vs. Other Injection Methods

The performance of secondary CWI was investigated in comparison with other injection methods, i.e. secondary WF, immiscible CO_2 and methane injection. Seven injection rates were selected to inject the specified pore volume over 25 years, as explained in table 6-10. Both CO_2 and methane injections were selected in order to provide a fair comparison among two immiscible gas injection methods since CO_2 mechanisms such as oil viscosity reduction and the oil swelling effect do not exist with methane injection. However, methane injection is considered one of the lean gas injection methods similar to nitrogen injection, where their minimum miscibility pressure is higher than 5000 psi. The primary usage of lean gas injection in oil pools is pressure maintenance in oil reservoirs to maintain productivity and oil displacement to production wells. Depending on gas injection composition and reservoir pressure usually more than 5000 psi, lean gases contain mainly methane, tend to vaporize the intermediate hydrocarbon components in the C_5 to C_{12} range developing an in-situ gas that is sufficiently rich with those intermediate hydrocarbons to create miscibility with the reservoir oil [180].

The comparison between WF and CWI was investigated in the previous model, and the performance of WF in this reservoir model was considered as the base case.

Table 6-10 different reservoir injection rates over 25 years with their equivalent surface injection rates

Injection rate, RES BBL/DAY	Total PVI @ 25 Years	Water injection rate, STB/DAY	CO_2 Injection rate, MMSCF/DAY	Methane injection rate, MMSCF/DAY
3585	0.50	3570	5.42	3.32
7170	1.00	7149	10.94	6.67
10755	1.50	10735	16.53	10.03
14340	2.00	14327	22.20	13.43
17925	**2.50**	**17922**	**28.03**	**16.86**
21510	3.00	21497	34.11	20.38
25095	3.50	24760	40.13	23.96

Figure 6-18 shows the ultimate oil recovery for the four injection methods versus the total pore volume injected. It was demonstrated that the oil recovery arising from secondary conventional water flooding (SWF) remained at 40.3 % of OOIP, with no further improvement as water continued to be injected. On the other hand, the oil recovery during CWI improved as the injection of CW was active: the more CO_2 was dissolved in oil, the more the formation of the gas phase increased. There were two processes that occurred at pore level in which the oil-gas relative permeability. At values of gas saturation below the critical gas saturation, the enlargement of the gas phase inside the oil in the grid served to reduce the oil saturation by displacing the oil to neighbouring grids. Then, once the gas saturation became higher than the critical gas saturation, and as a result of gravity, the gas moved vertically to upper layers, sweeping the oil in its way. This means that during CW areal and vertical displacement efficiency would be more effective. Whereas the advantages of immiscible CO_2 injection into oil reservoirs lie in the attendant reduction of oil viscosity and oil swelling effects [145, 181-183]. This created complexities, however, due to adverse mobility and gravity effects stemming from the low viscosity and density of CO_2 and methane in comparison to reservoir oil. The density and viscosity of CO_2 were 39.302 lbm/ft^3 and 0.05048 cp, respectively, methane were 9.0168 lbm/ft^3 and 0.02058 cp, respectively. In comparison, the oil density and viscosity were 50.2891 lbm/ft^3 and 0.904 cp, respectively, at simulation reservoir pressure and temperature. Thus, viscosity fingering and gravity tonguing are problems that cause flow instabilities and early breakthrough of injected CO_2 or methane [184, 185]. As a result, the forecasted oil recoveries during CO_2 and methane injection were very low, even after continuous injection of the gases.

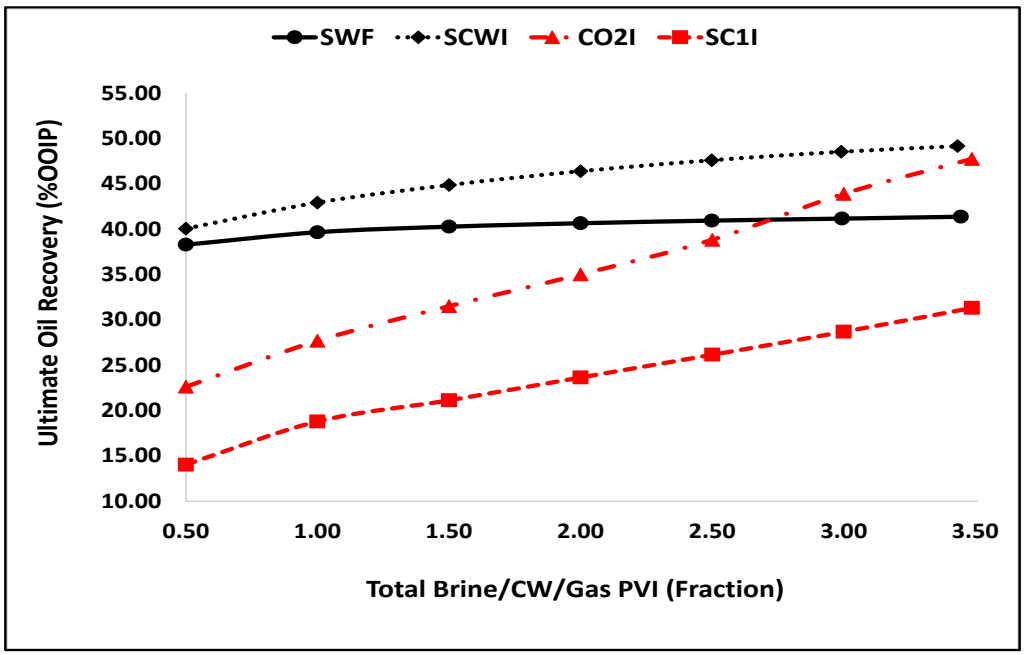

Figure 6-18 ultimate oil recovery of secondary CWI in comparison with other injection methods

The simulation model predicted more efficient CO_2 retention during SCWI than during CO_2 injection, as shown in figure 6-19A. The volume of stored CO_2 in CWI was much less than that in CO_2 injection as illustrated in figure 6-19B, however, due to the limited amount of CO_2 that was soluble in brine.

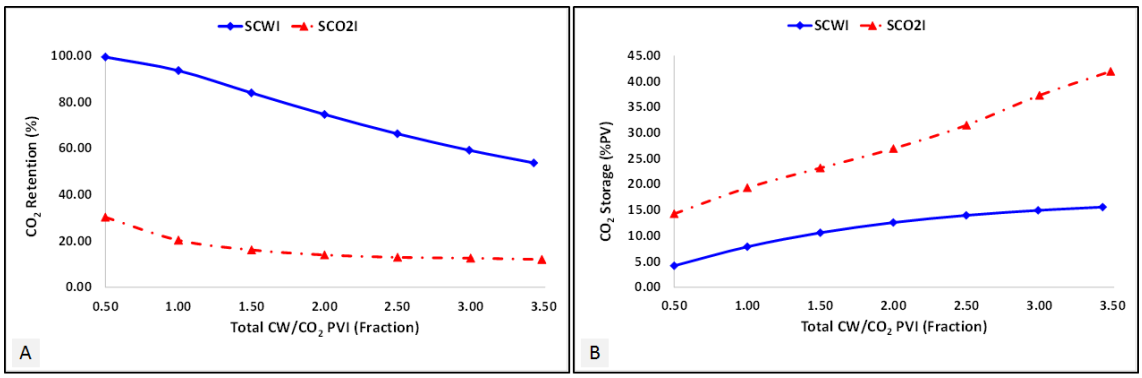

Figure 6-19 (A) CO_2 retention and (B) CO_2 storage during SCWI and SCO_2I with different injection rates

6.5.2.2 Sensitivity of Oil-Gas Relative Permeability

For the purpose of assessing the effect of oil-gas relative permeability on the performance of secondary CWI and CO_2 injection, a reservoir injection rate of 17925 res bbl/day was selected in this analysis. At this injection rate, the voidage replacement ratio of SWF, SCWI and secondary CO_2 injection ranged from about 0.9 to 1.0, as shown in figure 6-20, which created a favourable sweep efficiency in the reservoir. The voidage replacement ratio is the ratio of total injection rate to total production rate.

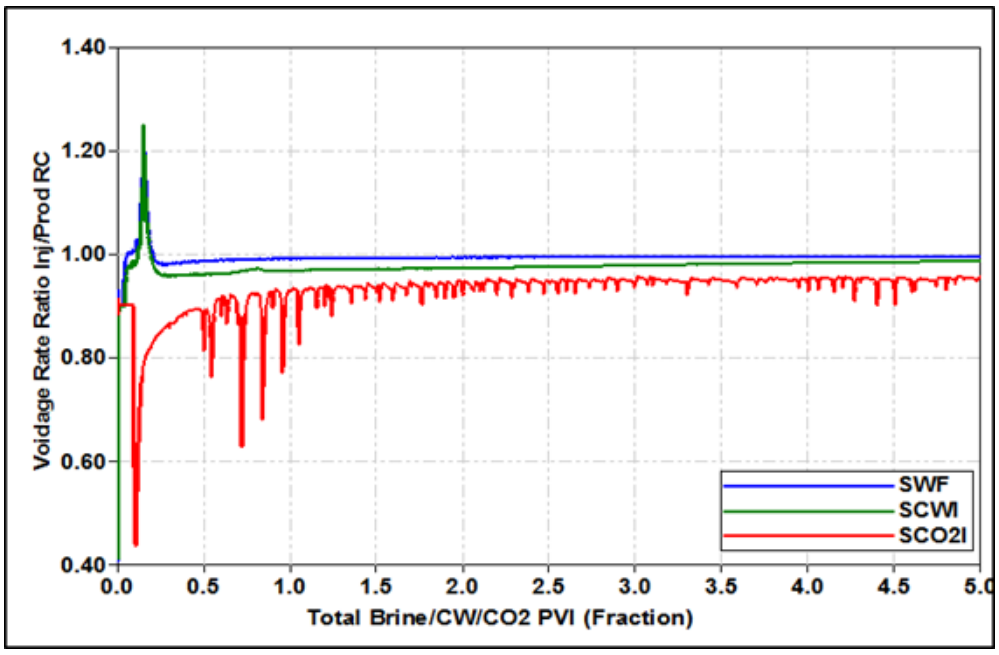

Figure 6-20 instantaneous voidage replacement ratio of SWF, SCWI and SCO_2I versus pore volume injected

Figure 6-21 shows the oil recovery of SWF as a base case, and two cases of secondary carbonated water injection (SCWI) and secondary CO_2 injection (SCO_2I), where the oil-gas relative permeability was obtained during CWI and is the typical one to represent conventional gas injection, while the other graph shows the comparison in respect to CO_2 retention. In SCWI, having an optimum oil-gas relative permeability that demonstrates the physics observed in the direct pore-scale experiments was crucial to recovering additional oil and storing larger amounts of CO_2. After 2 PVI, in the SCWI case where the typical oil-gas relative permeability was used, the oil recovery started to level off at around 50.5 % of OOIP, whereas in the other case, using the oil-gas relative permeabilities that preserved the physics of the CWI process, there was 4.6 % of OOIP additional oil recovery as a result of the high critical gas saturation and low gas relative permeability. The CO_2 retention was 11 % less when using a typical oil-gas relative permeability as demonstrated in figure 6-22. On the other hand, the CO_2 injection performed better when using an oil-gas relative permeability with a high critical gas saturation and low values of gas relative permeability. The reason for this is that the trapped CO_2 would have more time to dissolve into the oil before CO_2 breakthrough, consequently increasing the oil mobility as result of oil viscosity reduction and oil swelling. The improvement in CO_2 retention during CO_2 injection was due to the CO_2 that was trapped as result of using the CWI oil-gas relative permeability. Overall, the efficiency of carbonated water in respect to storing CO_2 was higher than that with CO_2 injection. This sensitivity is showing the importance of using an oil-gas relative

permeability which models the mechanisms of the carbonated water injection process in enhancing oil recovery. Through this practice, the oil-gas relative permeability that obtained for conventional CO_2 injection would not be useful to reproduce the performance of CWI as the (new) gas phase trapped mechanism is a critical influencer for enhanced oil recovery.

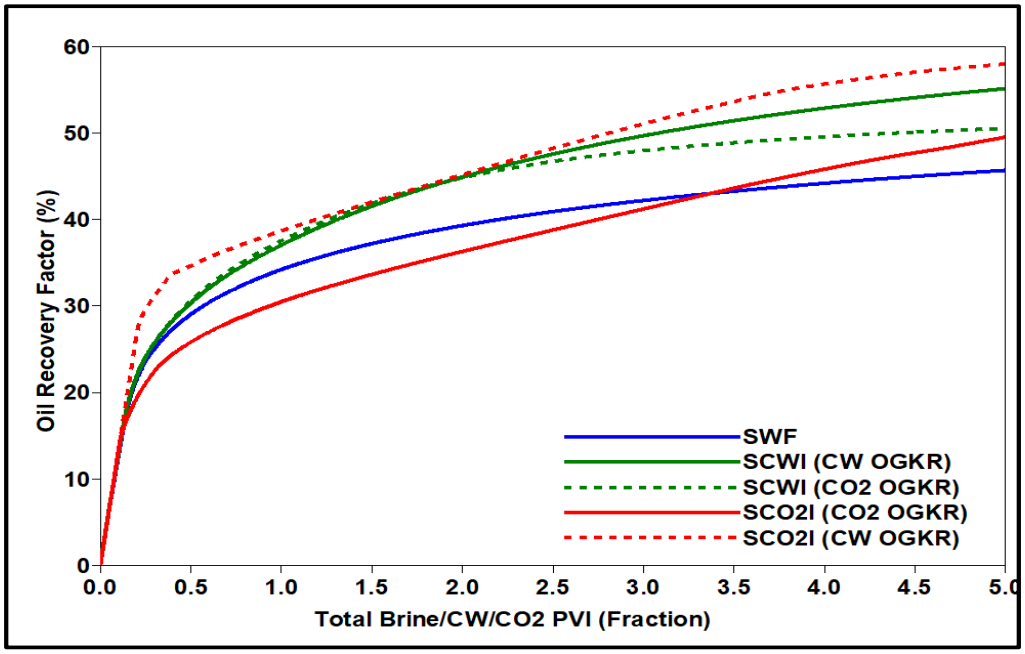

Figure 6-21 impact of oil-gas relative permeability on oil recovery for secondary CWI and CO_2 injection (solid lines represent the results when using the oil-gas relative permeability from CW and the dashed lines representing the results when using the oil-gas relative permeability from CO_2I)

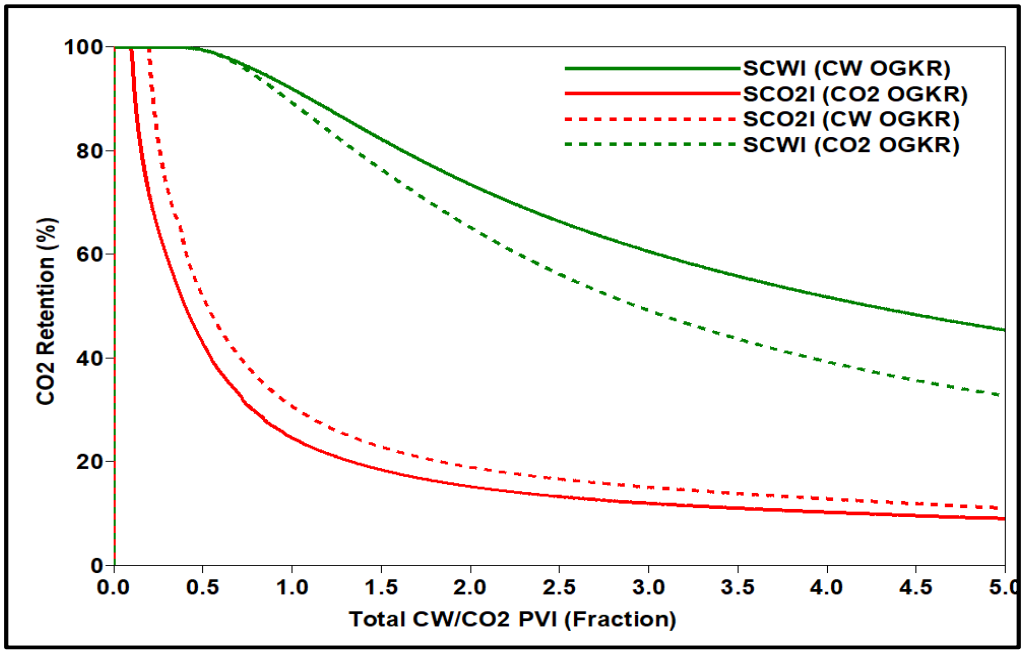

Figure 6-22 *impact of oil-gas relative permeability on* CO_2 retention *for secondary CWI and* CO_2 *injection* (solid lines represent the results when using the oil-gas relative permeability from CW and the dashed lines representing the results when using the oil-gas relative permeability from CO_2I)

6.5.2.3 Secondary CWI vs. Various CO_2 Injection Methods

As can be seen in the preceding section, the discrepancy between gas injection density and the viscosity of the reservoir oil leads to poor sweep efficiency as a result of gravity override and viscous fingering, thence early CO_2 breakthrough. Conversely, water-alternating gas (WAG) injection, and simultaneous water and gas (SWAG) injection strategies could enhance the mobility of the injected gas (CO_2) by increasing the water saturation, thereby decreasing the CO_2 saturation within the pores. The WAG and SWAG processes are combinations of efficient macroscopic displacements associated with water injection, and microscopic displacement as a result of the CO_2 injection mechanisms.

Secondary CO_2 WAG (hereafter, SWAG) and secondary simultaneous WAG (hereafter, SSWAG) injection were therefore considered in the comparison with secondary CWI. The SWAG cycle was designed to inject water for three months before injecting CO_2 for a further three months, and the WAG slug size ratio was 1:1. The reservoir injection rate was 17925 res bbl/day. The sensitivity of the WAG cycle and slug size were not studied, nor the effect of hysteresis as they were not in the scope of work of this thesis. The SSWAG injection was designed to inject 50% of the daily reservoir rate (about 8962.5 res bbl/day) of CO_2 in the bottom five layers, and the other 50% of the daily reservoir injection rate in the top five layers. This design was different from the formal SSWAG where the CO_2 and water were injected simultaneously at the same perforated layers.

Figures 6-23 and 6-24 demonstrate the total oil recovery of four injection methods (SCWI, SCO_2I, SWAGI, and SSWAGI) in secondary mode, as well as their CO_2 utilisation factors. It is worth noticing that the net CO_2 utilisation factor was calculated based on the cumulative CO_2 injection divided by cumulative oil production, not the incremental cumulative oil, since as all the methods were implemented in secondary mode. Introducing the SWAG and SSWAG injection strategies improved the oil recovery and reduced the net CO_2 utilisation factor better than conventional CO_2 injection within 1.5 PVI; however the SCWI still had the highest ultimate oil recovery and the best net CO_2 utilisation factor.

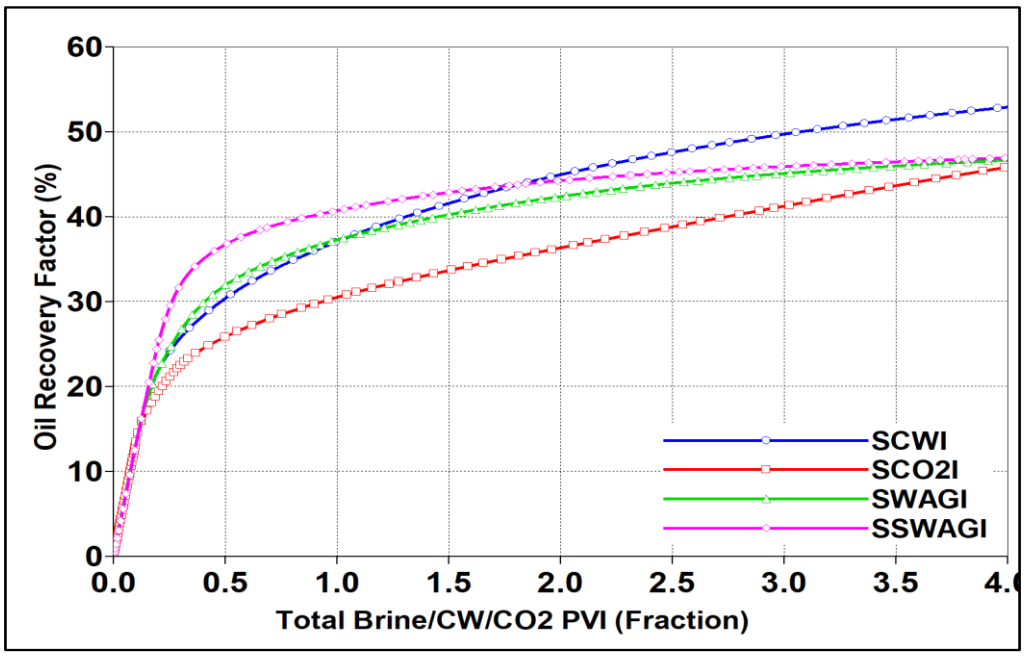

Figure 6-23 oil recovery of four CO_2-related injection methods versus total pore volume injected

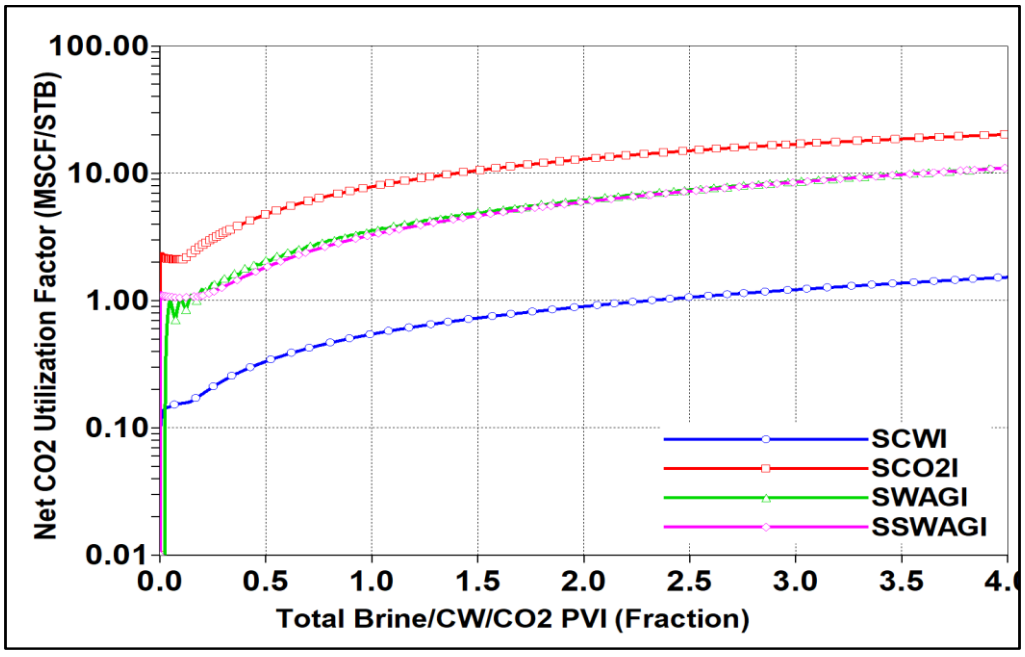

Figure 6-24 CO_2 utilisation factor of four CO_2-related injection methods versus total pore volume injected

The ability of CW to store the injected CO_2 kept its premier position among the other CO_2 injection methods, as shown in figure 6-25. The CO_2 retention of SCWI declined to 55% after 4 PVI, which means that 45% of CO_2 was stored in the reservoir, either as dissolved in oil, solute in brine, or trapped in the form of gas. There was a huge difference between the volume of injected CO_2 as gas during SCO_2, SWAG and SSWAG injection, and the amount of injected CO_2 that was soluble in brine during SCWI. Specifically, the CO_2 storage as pore volume was the lowest in SCWI, as illustrated in figure 6-26. The CO_2 storage increased with additional pore volumes of injected CW, however; in contrast to

SWAG and SSWAG where the CO_2 storage was maintained after several pore volume of injected CO_2. Due to the cyclic process in CO_2 WAG injection, hysteresis is common, and this managed the trapping of CO_2 due the dependency of relative permeability and capillary pressure on the phase's saturation. Thence, only the hysteresis had the ability to show the advantage of residual CO_2 trapping, and thereby safe CO_2 storage, while reducing the CO_2 mobility and producing additional oil [186, 187]. This means that the additional sensitivity of the effect of hysteresis on the performance of the WAG process should be elaborated and compared against CWI.

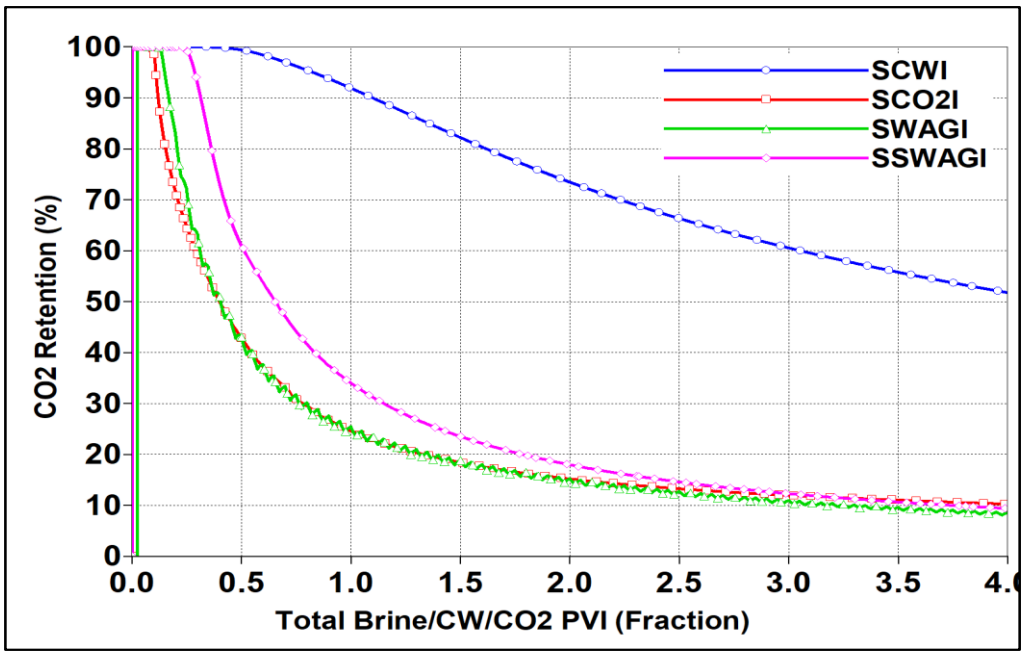

Figure 6-25 CO_2 retention in various CO_2-related injection methods

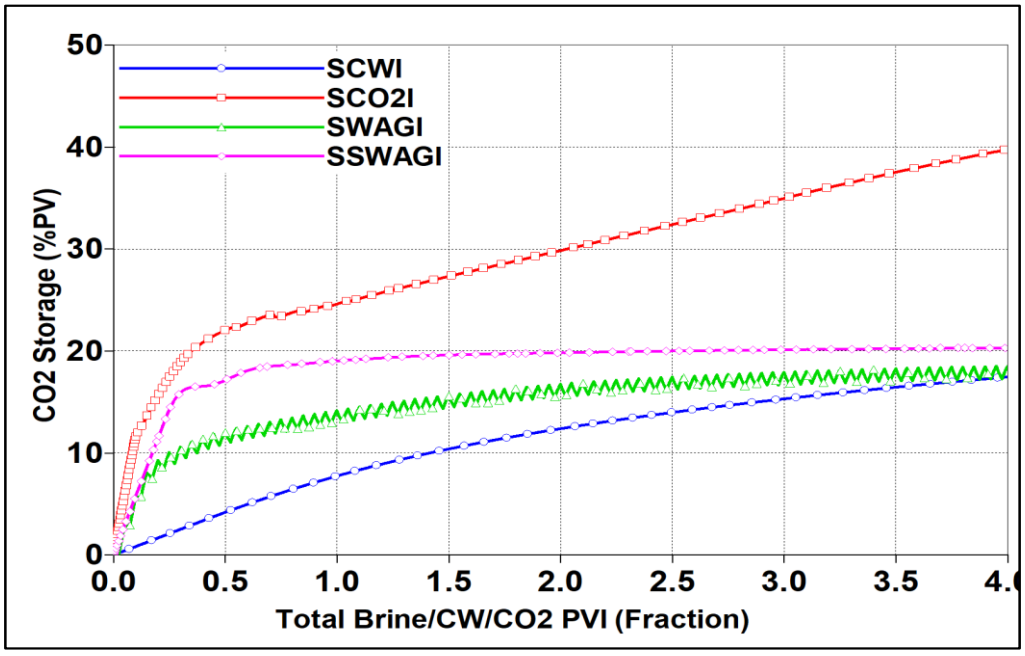

Figure 6-26 percentage of CO_2 pore volume storage in various CO_2-related injection methods

6.5.2.4 Tertiary CWI vs. various CO_2 Injection Methods

Usually, the enhanced oil recovery methods are implemented in tertiary mode (post-WF), thus taking advantage of waterflooding (WF) displacement mechanisms in recovering the initial oil before the water breaks through the production wells. The performance of tertiary CWI was therefore studied after injecting 0.5 PV of conventional water, and this was compared with other CO_2-related injection methods such as continuous tertiary CO_2 injection (TCO_2I), water-alternating gas injection (TWAG), and simultaneous water-and gas injection (TSWAG). The injection and production constraints remained the same as in secondary injection. Secondary conventional water (WF) was injected up to 0.5 PV, which was about five years of water injection, and in that time the oil recovery reached 29.04 % of OOIP. At 0.5 PV of injection, both WF and CWI produced almost the same amount of oil, as shown in figure 6-27. Thus, the mechanisms of CWI for enhancing oil recovery took place after 0.5 PVI.

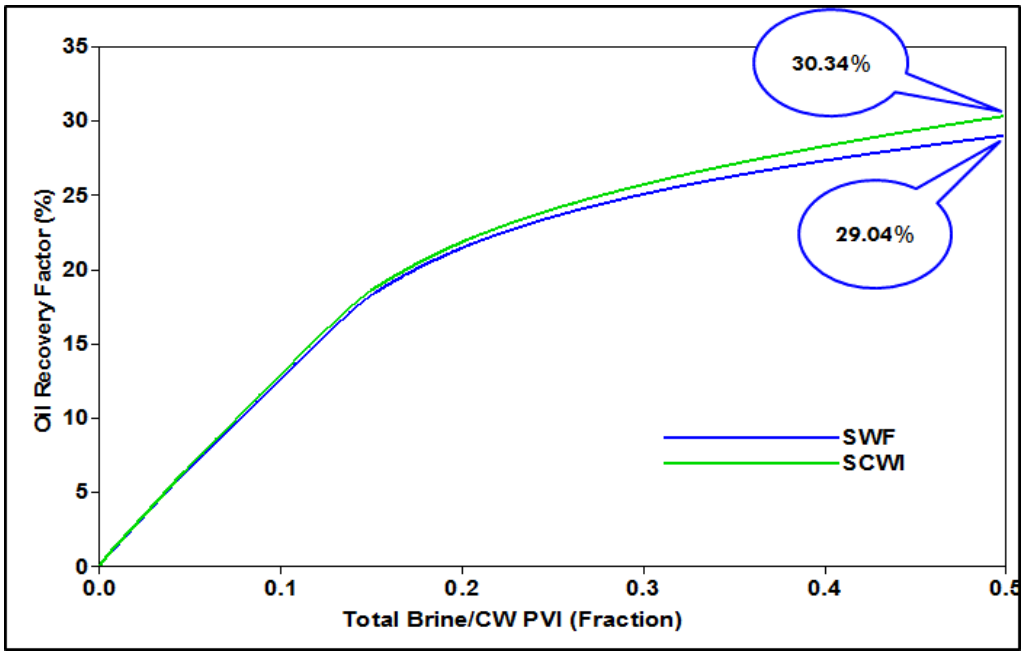

Figure 6-27 oil recovery of SWF and SCWI at 0.5 PVI

Figures 6-28 and 6.29 display the incremental oil recovery of TCWI, TCO_2I, TWAGI and TSWAGI, along with their net CO_2 utilisation factors. The features of continuous CO_2 injection, TWAG, and TSWAG injection were the immediate response in the form of enhanced oil recovery, compared to TCWI, where the gradual improvement of oil recovery was the noticeable phenomenon. During CWI, a constant mass transfer of CO_2 took place from carbonated water to oil, thereby leading to the steady formation of the

gas phase, which would trap most of the CO_2, thus taking the most advantage of the dissolution of CO_2 in oil and improving oil recovery more than the other CO_2 injection methods. Also, CWI provided better utilisation of CO_2 to recover additional oil, which represents an efficient utilisation of a small volume of CO_2 to recover more oil. This is important given that the major factors controlling the profitability of CO_2-EOR recovery methods are the availability of CO_2 at economical prices, usually with 2-3 $MSCF [30, 188], and the net CO_2 utilisation factor of 1000 standard cubic feet of CO_2 to recover an additional barrel of oil. The net CO_2 utilisation factor will vary from one optimised CO_2 project to another, however. Broome et al., in their 1986 review of US EOR projects, [189], estimated a need for 5.5 MSCF of CO_2 per additional oil barrel, and this was confirmed by Jeschke et al. [190] through their estimation of a net CO_2 utilisation factor of 4-6 MSCF/bbl for a successful CO_2-EOR project.

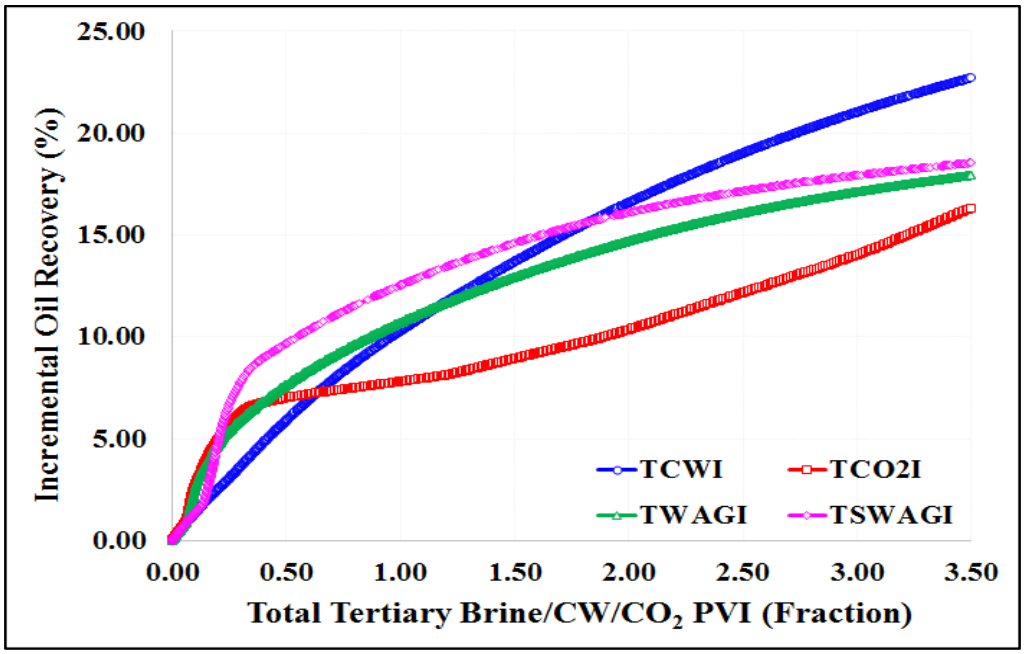

Figure 6-28 incremental oil recovery of tertiary CWI and CO_2-related injection methods versus total pore volume injected

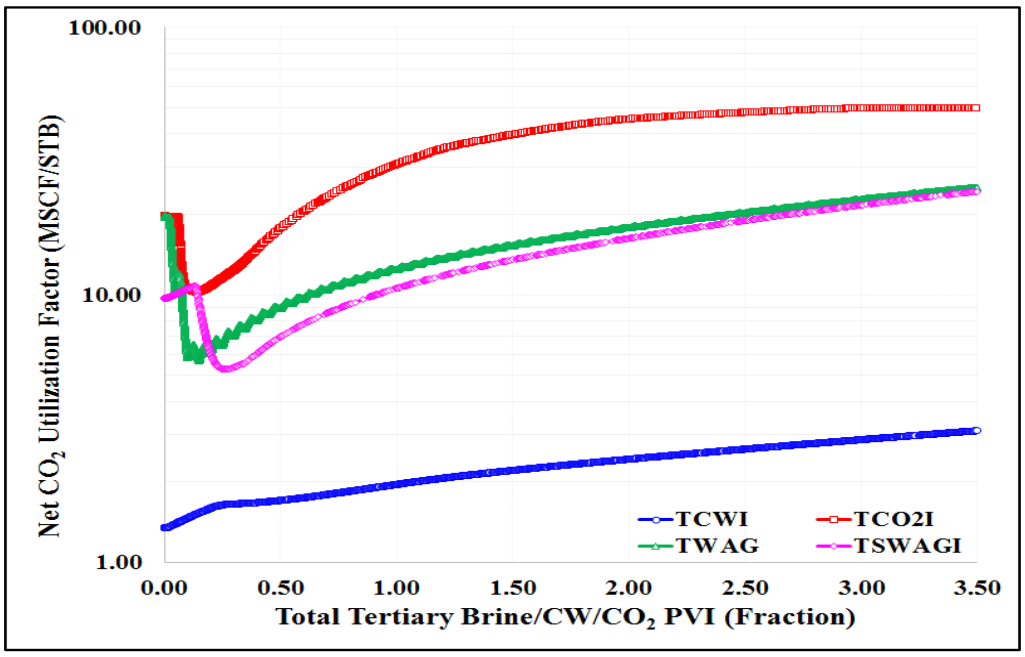

Figure 6-29 net CO_2 utilisation factor of tertiary CWI and CO_2-related injection methods versus total pore volume injected

Nonetheless, CWI had the most efficient process to store CO_2 in the reservoir while producing additional oil in the tertiary mode as illustrated in figure 6-30. Although the efficiency of continuous CO_2 injection in storing CO_2 was poor, it still had the ability to store a higher volume of CO_2 since a greater volume of CO_2 was injected, as shown in figure 6-31. The WAG process helped in controlling the CO_2 injection and resulted in more additional oil recovery than continuous CO_2 injection, but the total volume of CO_2 that could be stored was reduced since the water displaced the gas and oil in each cycle where the effect of hysteresis was negligible. The trapping mechanism of simultaneous water-and-gas injection, in which injecting the water at the top and CO_2 at the bottom could prevent the CO_2 gas from migrating to the top reservoir as a result of gravity segregation resulted in additional oil recovery and CO_2 storage.

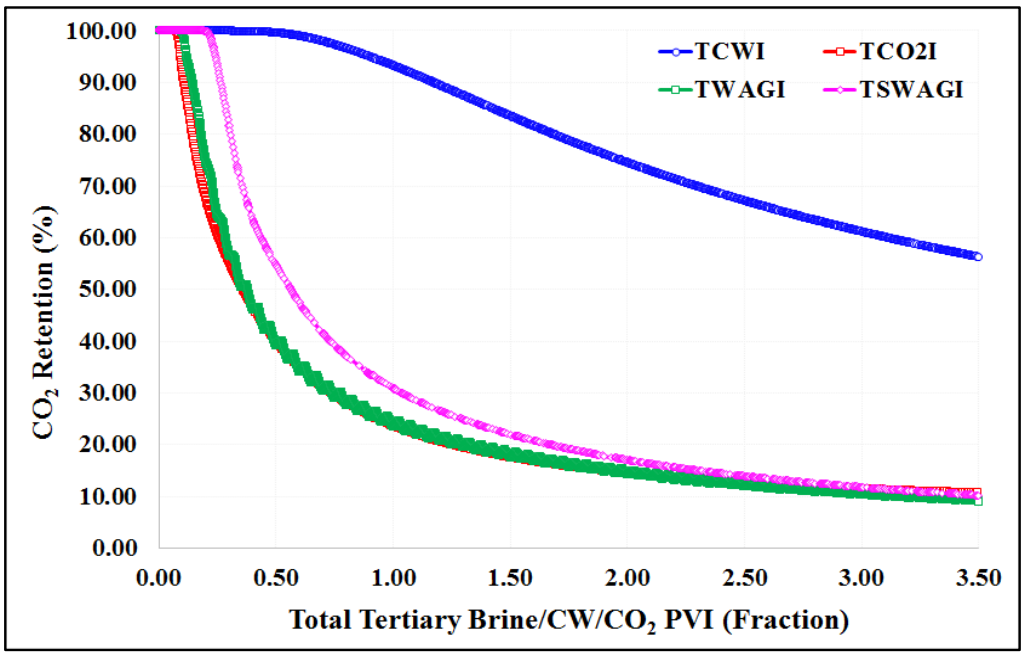

Figure 6-30 CO_2 retention in the tertiary mode of various CO_2-related injection methods

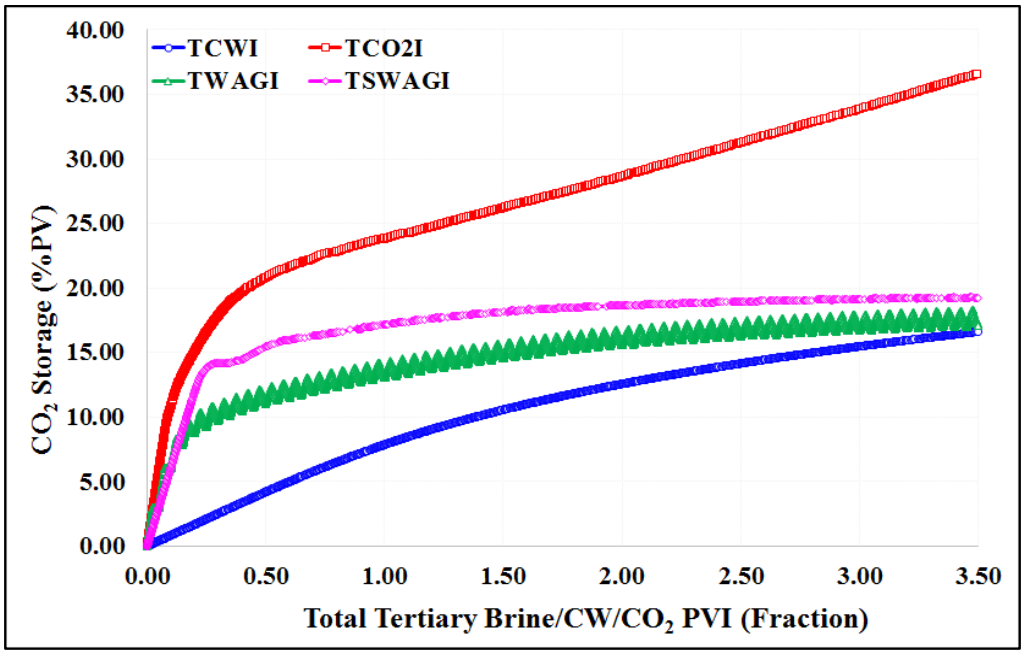

Figure 6-31 percentage of CO_2 pore volume stored in the tertiary mode of various CO_2-related injection methods

Considering the cross-section of the distribution of oil and gas saturation for different CO_2-EOR injection methods after injecting 1.5 pore volume of either CW, CO_2 or water-CO_2 in tertiary mode for TCWI, TCO2I, TWAGI, and TSWAGI in figures 6-32 and 6-33. During tertiary CWI, the CO_2 was transferred from carbonated water into oil, in which the dissolution of CO_2 in oil resulted in a reduction of oil viscosity and swelling effects. Moreover, the continuous mass transfer of CO_2 from the carbonated water would saturate the oil, and this CO_2 would strip the light hydrocarbon components from the oil to form

the gas phase. The formation of the gas phase within the oil leads to swelling, which causes the oil to be displaced, since the gas, initially, would be trapped. Furthermore, the density of the formed gas is less than the oil density and the gas phase would be migrated to the upper layers as a result of gravity segregation. With low gas relative permeability, however, the migrated gas would reduce the gas breakthrough while displacing the oil in the top layer. Additionally, the injected carbonated water would displace the oil in the bottom layers. This process thus established a uniform macro-sweep efficiency displacement, and the CO_2 transferred from the carbonated water enhanced this micro-sweep efficient.

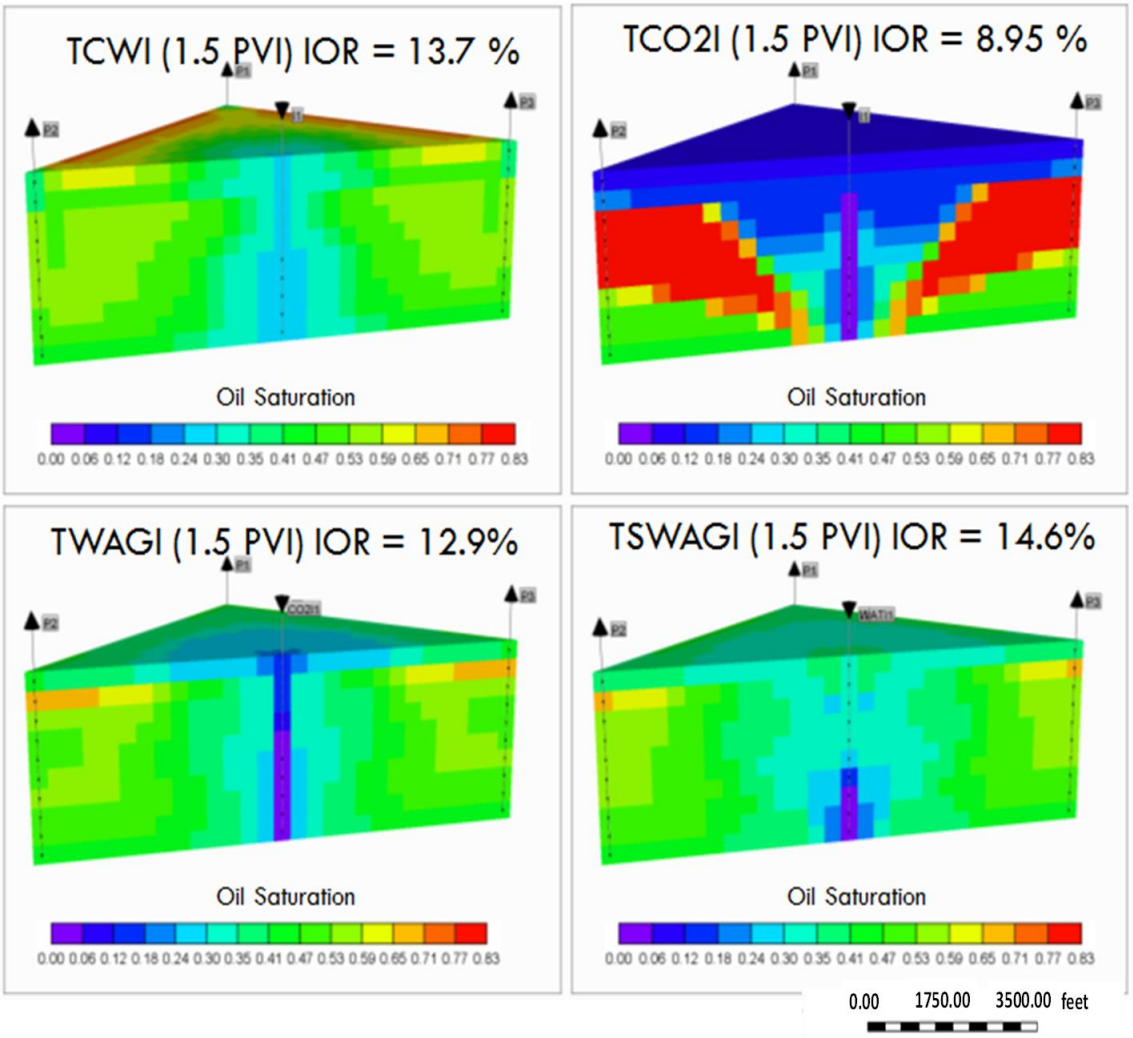

Figure 6-32 cross-section of oil saturation after injecting 1.5 PV of (left top) TCWI, (right top) TCO_2I, (left bottom) TWAGI, and (right bottom) TSWAGI

In other CO_2 injection methods, meanwhile, the injected CO_2 would drift upwards, leaving a lot of remaining saturation of oil that would not be displaced. For example, in continuous CO_2 injection, the contrast between CO_2 and oil densities caused the gas to

override the oil as a result of gravity segregation. The effect of gas override would be reduced in TWAGI and TSWAGI, but that effect would exist away from the injection well causing poor sweep efficiency after injecting several pore volumes. In the absence of hysteresis, the displacement efficiency in water-alternating gas and simultaneous water-and-gas injection would be severely affected by gas overriding problems.

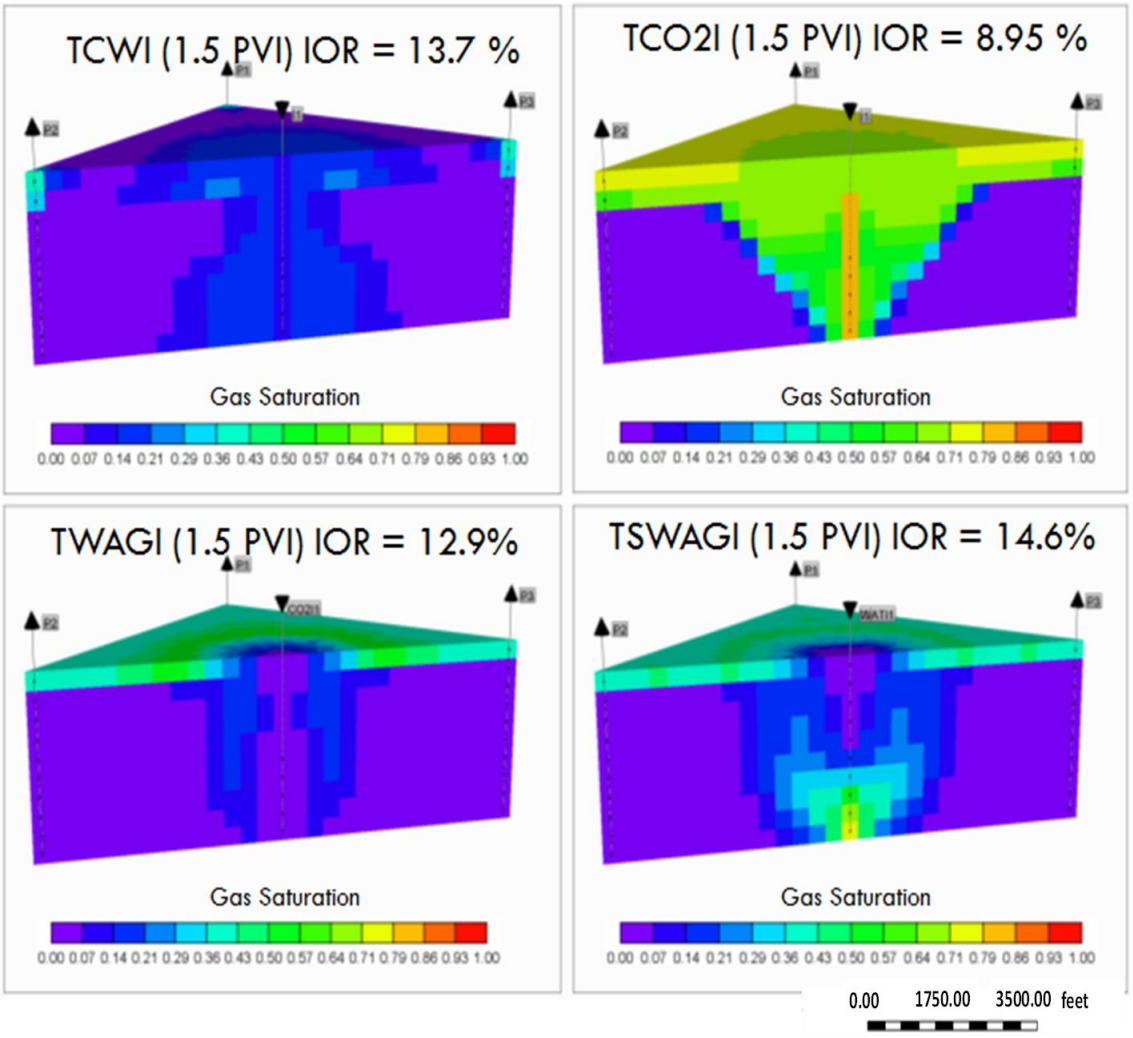

Figure 6-33 cross section of gas saturation distribution after injecting 1.5 PV of (left top) TCWI, (right top) TCO_2I, (left bottom) TWAGI, and (right bottom) TSWAGI

The mechanisms that are engaged in the performance of CWI to produce additional oil thus provide a steady displacement efficiency that maximises the oil recovery and at the same time stores the CO_2. In fact, the CO_2 content in brine plays a crucial part in the performance of CWI, although it is limited by the content of CO_2 that is soluble in brine. Although the solubility of CO_2 in brine is higher compared to other gases, the mass of CO_2 transferred by carbonated water into oil is still very low compared to other CO_2 injection methods. As the simulation shows, the oil recovery during carbonated water

injection is a function of the carbonation level; i.e. the amount of CO_2 soluble in brine. So, the low CO_2 content in brine can adversely affect the performance of CWI, thereafter reducing the oil recovery. The opposite is also true, however, and therefore using a CO_2 solubility promoter (called a co-solvent) to increase the CO_2 content in water prior to injection would improve the production of additional oil even more since it would enable more CO_2 to be transferred to the reservoir oil, with a consequent greater reduction in oil viscosity, more oil swelling, and finally a more pronounced formation of the gas phase will displaced more oil.

CO_2 solubility promoters can be divided into two categories: chemical adsorbent agents and physical promoters. Chemical absorption is characterised by increasing the CO_2 content in water through a chemical reaction between the gas (CO_2) component and the adsorbent agent in the water. The disadvantage of this kind of co-solvent, however, lies in the resistance of CO_2 to being transferred from carbonated water and dissolving in the oil; thus a slug of demoter, or heated fluid, would be required to release the CO_2 from the carbonated water [90].

Winston suggested a carbonated water injection regime in which the CO_2 content in brine is increased by a chemical CO_2 solubility promoter. First, a slug of CW containing a CO_2 solubility promoter should be injected in the reservoir. Then, a slug of CO_2 solubility demoter or heated fluid would be injected to release the CO_2 from the CW and transfer it to the reservoir oil [191, 192]. He suggested several CO_2 solubility promoters, such as ammonia, sodium carbonate, potassium carbonate, or any other weak base chemicals. Meanwhile, the CO_2 solubility demoters could be any weak acids that are commonly used for well stimulation treatment in oil field operations, such as hydrochloric, acetic and hydrofluoric acids.

Conversely, the physical absorbents do not chemically react with the adsorbed CO_2 and thus allow the mass transfer of CO_2 from carbonated water to oil. Methanol, acetone, normal methyl pyrrolidone (NMP), and alkanes, such as nC_4 and nC_{10}, could be used as physical adsorbent materials [90].

One example of a physical co-solvent is acetone, and several studies have proved that the presence of acetone in water would increase the CO_2 solubility significantly [193, 194].

6.5.2.5 Tertiary CO_2 Injection Methods after SCWI

Figures 6-34 and 6-35 display a comparison of the incremental oil recovery and CO_2 storage during tertiary continuous CO_2 injection, water-alternating CO_2 gas injection and simultaneous water-and-CO_2 gas injection after secondary conventional water injection and carbonated water injection. The typical oil-gas relative permeability curve was used to predict the performance of TCO_2I, TWAGI and TSWAGI after secondary carbonated water injection without considering the hysteresis effect. Their performance was weakened compared to after conventional water injection. The absence of a gas trapping mechanism and the presence of oil that was saturated with CO_2 would cause that decline in oil recovery and CO_2 storage since the injected gas would displace the trapped gas that formed during CWI. Also, with more CO_2 injection, the oil would become denser as a result of the stripping of its hydrocarbon compounds by the injected CO_2.

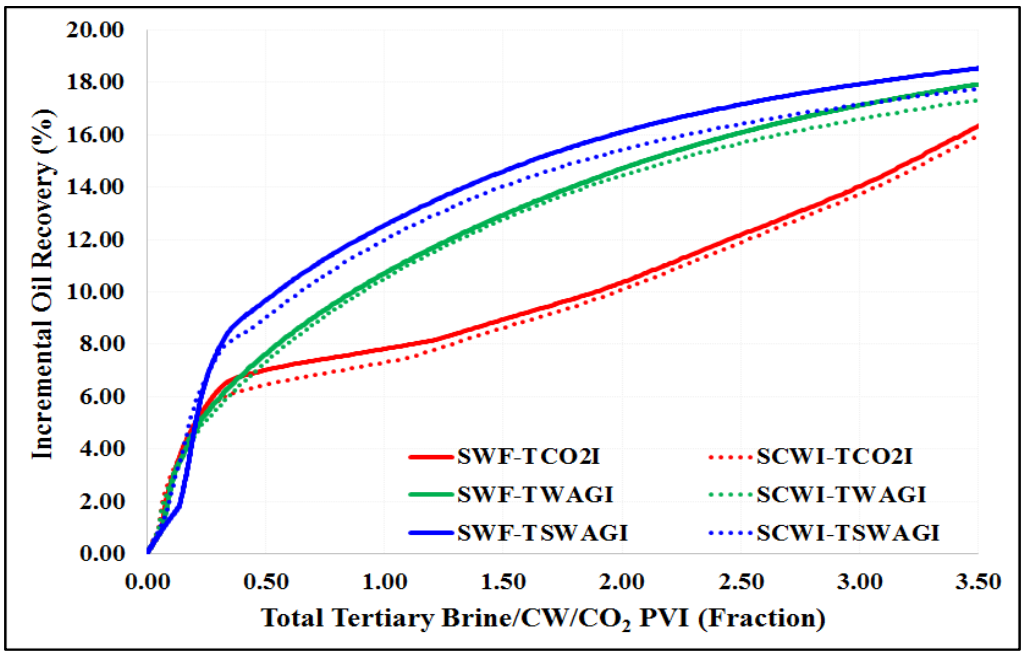

Figure 6-34 comparison of incremental oil recovery during tertiary CO_2 injection methods after SCWI (dashed lines) and those after SWF (solid lines)

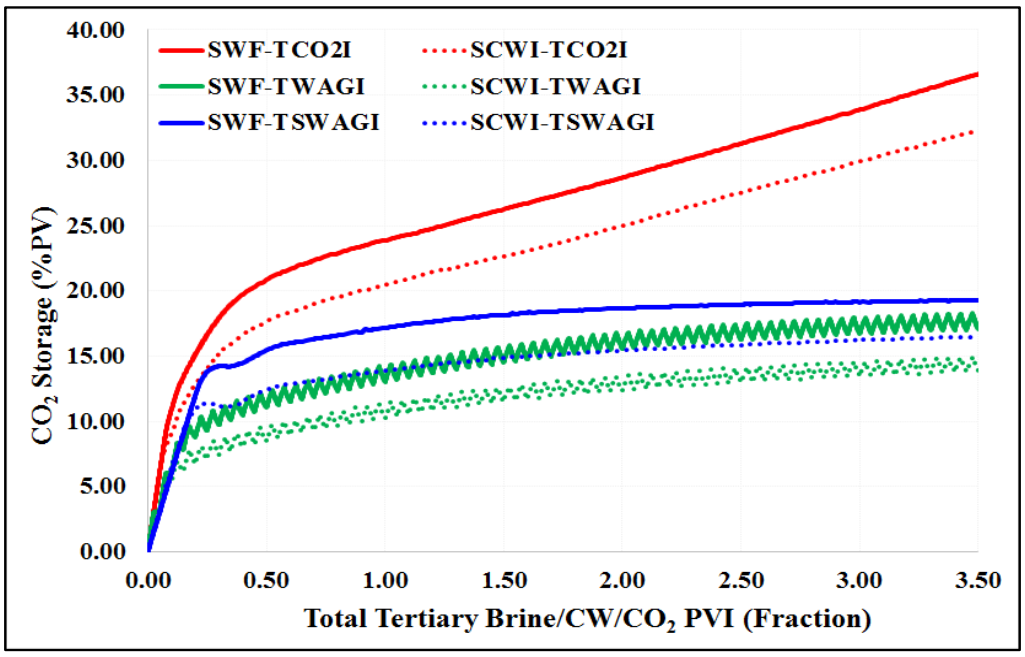

Figure 6-35 comparison of CO_2 storage during tertiary CO_2 injection methods after SCWI (dashed lines) and those after SWF (solid lines)

The performance of tertiary CO_2 injection after secondary CWI was relatively predictable using the obtained oil-gas relative permeability while history matching the experimental results in water-wet core displacement injection, as explained in section 3.7.4.3 of chapter 3. Based on that, the oil-gas relative permeability that was estimated while history matching and predicting the performance of CWI in mixed-wet core displacement experiments was used to forecast the performance of tertiary continuous CO_2 injection, water-alternating gas injection and simultaneous water-and-gas injection. The results were remarkable, as shown in figures 6-36 and 6-37. The incremental oil recovery jumped immediately after injecting 0.3 PV of simultaneous water-and-CO_2 gas to reach 38.6 % of OOIP, and about 60 %PV of CO_2 was stored due to the trapping mechanism of CO_2, as expressed by a critical gas saturation of 0.2 and the very low gas relative permeability. After 1.5 PVI, however, no further improvement in either oil recovery or CO_2 storage was noticed. It is worth mentioning that the injected water in TWAG and TSWAGI was carbonated water; hence, the mechanisms of carbonated water were activated and magnified by the additional injected CO_2. Unifying the oil-gas relative permeability and considering the hysteresis effect to reproduce the carbonated water injection and other CO_2 injection methods would therefore provide reasonable forecasting of the performance of these methods in terms of additional oil recovery, net CO_2 utilisation factor, CO_2 retention and storage.

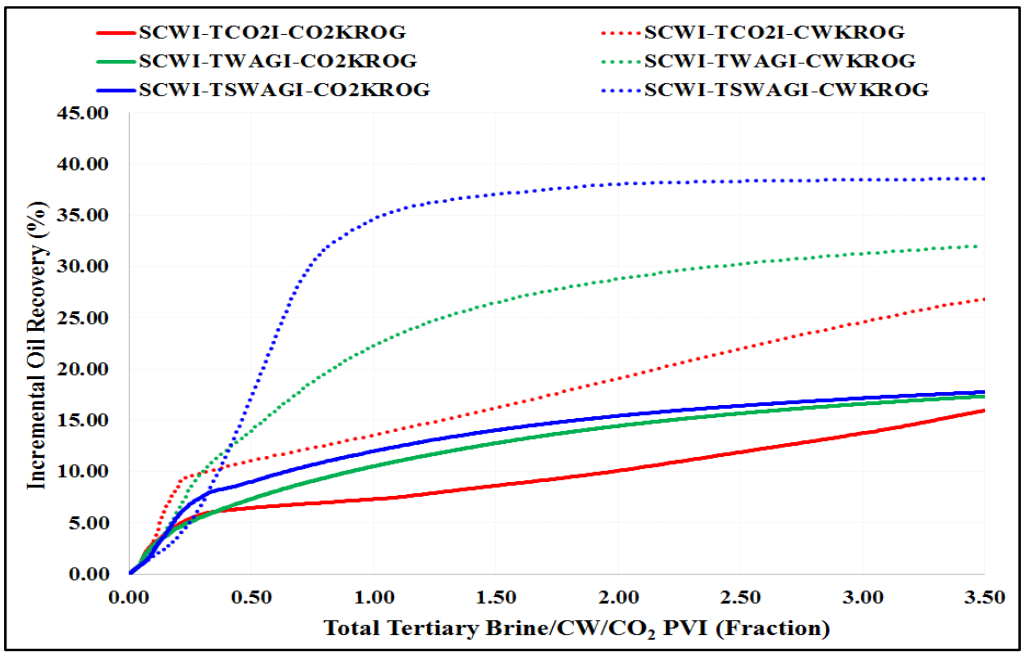

Figure 6-36 comparison of incremental oil recovery during tertiary CO_2 injection methods after SCWI using oil-gas relative permeability during CWI (dashed lines) and those using typical gas injection oil-gas relative permeability (solid lines)

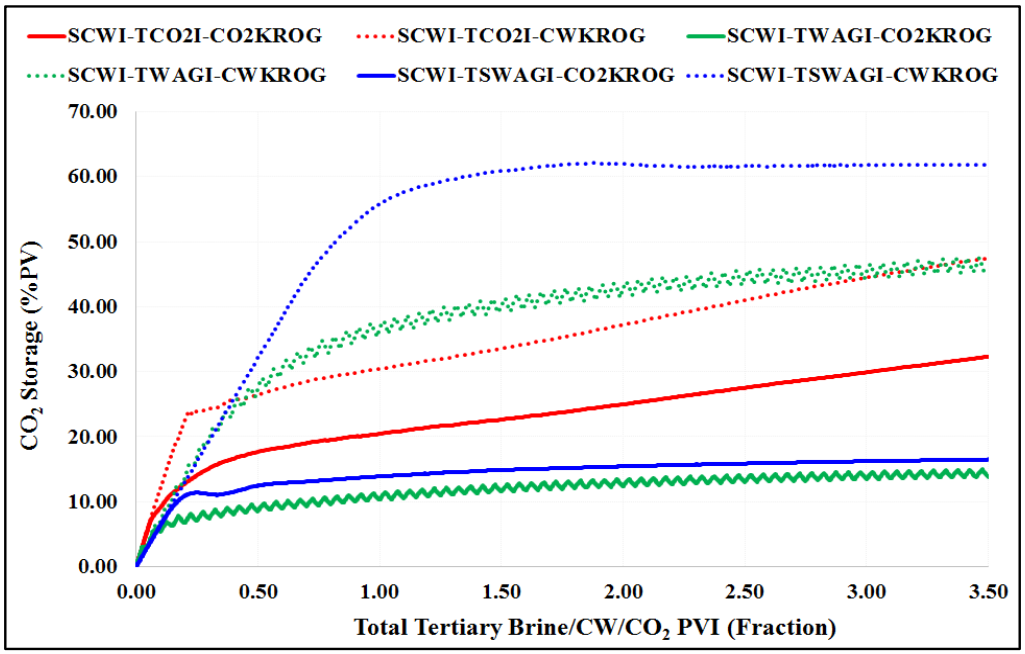

Figure 6-37 comparison of CO_2 storage during tertiary CO_2 injection methods after SCWI using oil-gas relative permeability during CWI (dashed lines) and those using typical gas injection oil-gas relative permeability (solid lines)

6.6 Operational Concerns Associated with CWI

Although the results that have been obtained in core experiments and field trials demonstrate a promising incremental oil recovery resulting from CWI, the application of CWI processes has been relatively limited in practice, mainly due to lack of understanding of the mechanisms involved in the performance of CWI. Also, operational concerns

associated with CWI such as preparing CWI, and corrosion problems, may contribute to the limited use of this technology.

6.6.1 Preparing CWI

Injecting the carbonated water at a larger scale under the desired reservoir pressure and temperature could be considered as one of the main operational concerns. Two methods could be useful in achieving an appropriate mixture of CO_2 and water to generate carbonated water. The first method is to undertake the mixing at the reservoir wellbore where a slug of LPG (liquefied petroleum gaseous) is first injected to displace the remaining light hydrocarbon prior to carbonated water injection. Controlled amounts of CO_2 and water are then injected to achieve the required carbonation level. This method was adopted in 1958 in the Dewey-Bartlesville field [170, 195]. The other method is using well-known technologies to make carbonated water at the surface using a gas infusion (GI) generator. The GI generator contains hydrophobic micro hallow fibres that extend the surface area between the water and gas to achieve high mass transfer efficiency, as shown in figure 6-38, i.e. bubble free CO_2 transfer, to produce high dissolved gas concentrations at elevated pressures [90, 196].

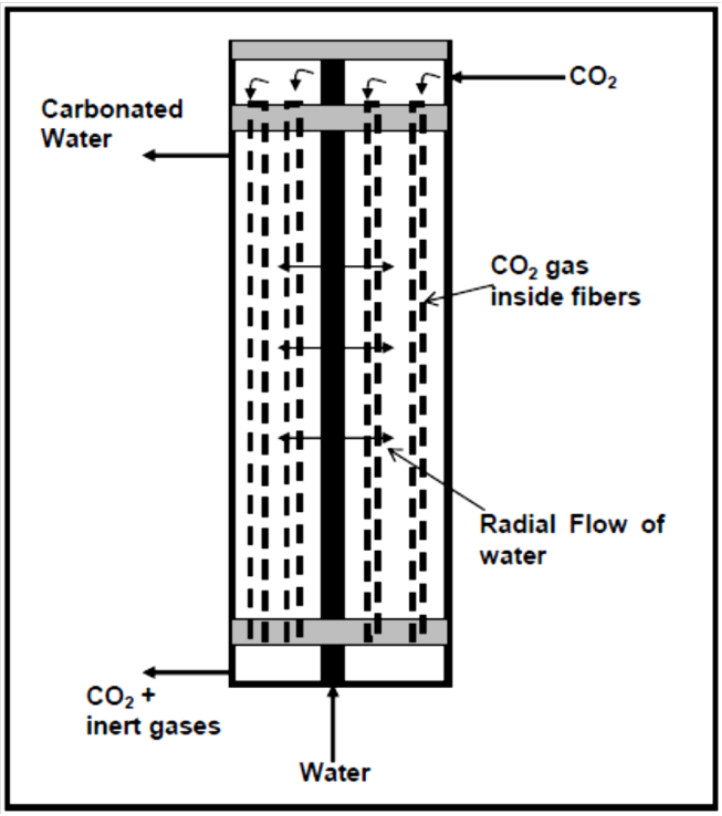

Figure 6-38 Schematics of CO_2 mass transfer process in a Gas Infusion Unit [197]

6.6.2 Corrosion Problems

Another operational problem associated with CWI is the corrosion of injection and production facilities as a result of the formation of carbonic acid (H_2CO_3), which is a secondary product resulting from the dissolution of CO_2 in water [198]. Significant amounts of this acid will reduce the water pH, which might accelerate the corrosion of carbon steel. The controlling factors of this process have been found to be the partial pressure of CO_2, temperature, the pH of the CW, and the fluid velocity within the pipes [199].

Despite the concerns that carbonic acid may harm the facilities through corrosion [200], no evidence of corrosion was reported from the production wells or surface facilities in the first K&S commercial carbonated water injection project, apart from that observed during conventional water flooding [170]. Moreover, the CO_2 injection lines were re-used several times during the staging of the CO_2 injection without any observation of corrosion due to the separation of processes of injecting the CO_2 and the water, since the mixing occurred in the reservoir itself. Another study of the effect on equipment of injecting CW during the CWI pilot in the Slaughter field, Texas, reported no weakening in the stainless steel and aluminium bronze material thicknesses during the test period [201]. In any CO_2 injection project, however, the protection from corrosion of injection and production wells, along with surface facilities, should be undertaken as a matter of course, especially when the CO_2 is injected in tertiary mode after conventional water flooding.

6.7 Summary and Conclusion

A technical quality screening study of simulating CWI in reservoir-scale was achieved using two homogeneous models to evaluate the performance of CWI in comparison with conventional water flooding and also among other gas-based injection methods, specifically immiscible CO_2 and methane. The oil composition and tuned EOS, in addition to the obtained saturation functions, that were estimated in simulating the mixed-wet core displacement experiments were used to carry out the screening. The technical quality screening study concluded the following:

- The behaviour of CWI followed the conventional waterflooding behaviour in selecting the number of gridblocks to overcome the numerical dispersion effects associated with numerical simulation. Moreover, there was a negligible effect of perforated layers on the performance of SWF and SCWI.

- The performance of secondary CWI in comparison with the performance of conventional WF was predicted using the simulation models. The results showed that the incremental oil recovery by CWI was increased as more CW pore volume was injected whereas no significant improvement in oil recovery was evident in secondary WF when more water pore volume was injected. On the reservoir scale, however, the incremental oil recovery was lower than that in core displacement experiments at the same PVI.

- Increasing the CO_2 content in the aqueous phase by injecting more CW pore volume, rather than increasing the injection rate, resulted in an increase in the incremental oil recovery.

- The dispersion effect on incremental oil recovery was diminished on the reservoir scale since the flow away from the injector would be uniform and steady rather than turbulent and unsteady as when near the wellbore, which allowed enough time to achieve an equilibrium between carbonated water and oil. The dispersion effect did significantly reduce the CO_2 storage efficiency of CWI on the reservoir scale, however, due to the fast breakthrough of CO_2 that was dissolved in both oil and aqueous phases.

- Lowering the carbonation level would reduce the CO_2 content in water which weakened the mechanisms responsible for enhancing oil recovery during CWI. Since the CO_2 storage in CWI depended on the amount of the gas phase that was trapped in the reservoir, then lowering the carbonation level would reduce the amount of trapped gas, subsequently reducing the CO_2 storage efficiency (CO_2 retention)

- The earlier the implementation of CWI, the more oil would be recovered but the less CO_2 stored. The secondary CWI could produce higher oil recovery than that in tertiary CWI, which was consistent with the published experimental data.

- A comparison between secondary and tertiary CWI and secondary and tertiary continuous gas (CO_2) injections showed better oil recovery during SCWI and TCWI. The poor oil recovery during secondary and tertiary gas injection was related to flow instabilities, problems due to adverse mobility and gravity effects leading to gravity overrides.

- The simulation predicted more efficient CO_2 retention during SCWI and TCWI than that during continuous CO_2 injection, however, the volume of stored CO_2 during SCWI and TCWI was much lower than that in CO_2 injection due to the low amount of CO_2 that was soluble in brine compared to CO_2 injection.

- Having optimum oil-gas relative permeability was extremely important to obtain the actual performance of CWI in producing additional oil and storing more CO_2.

- Even after implementing the water-alternating gas and simultaneous water-and-gas processes without the hysteresis effect to enhance the mobility of injected gas (CO_2), the SCWI still had the highest ultimate oil recovery and the best net CO_2 utilisation factor. Furthermore, the ability of CWI to store the injected CO_2 makes it a leading CO_2 injection method. Hysteresis, however, plays a critical role in showing the advantage of residual CO_2 trapping, and thereby safe CO_2 storage, while reducing the CO_2 mobility and producing additional oil. Therefore, the effect of hysteresis on the performance of WAG processes should be considered and compared against CWI.

- On the reservoir scale, the gas phase formed with the oil as a result of the transfer of CO_2 from carbonated water into oil enlarged the hydrocarbon volume which caused the oil to be displaced. Then, since the density of the formed gas is less than the oil density, and once the gas phase reached its critical saturation, it migrates to the upper layers at low relative permeability as a result of gravity segregation; meaning that the oil is displaced to the top layer while the injected

carbonated water is displaces the oil in the bottom layers. Through this process, a steady and efficient macro and micro sweep displacement was established. The CO_2 content in brine was therefore the key controller of the performance of CWI. Therefore, using a CO_2 solubility promoter to increase the CO_2 content in water would improve this process leading to additional oil recovery.

- The results of the prediction of the tertiary CO_2 injection methods using the oil-gas relative permeability that explained CWI mechanisms, produced the highest oil recovery and the largest CO_2 storage. This case was simulated based on the predicted results of CO_2 injection after secondary CWI in water-wet core displacement experiments where the performance of tertiary CO_2 injection was relatively predictable using the same oil-gas relative permeability as that obtained during SCWI.

Chapter 7 – Conclusions and Recommendations

This chapter presents the main conclusions of this research. In addition, some recommendations for future work are provided for the researchers to study the process of CWI in depth and thus strengthen its impact on improving oil recovery.

This thesis provided a new methodology for the numerical simulation of the process of carbonated water injection for enhanced oil recovery in live oil systems. This research sought to model CWI core displacement experiments, taking into consideration the actual physics that occurred in the direct pore-scale visualisations during the CWI process. Furthermore, the results from core-scale simulations were up-scaled to evaluate the CWI process at the reservoir scale.

7.1 Conclusions

The recent research on injecting carbonated water in live oil systems has revealed that the formation of the new (gas) phase during the CWI process could be the predominant mechanism underpinning the performance of CWI for enhancing oil recovery.

Thus, when the carbonated water (CW) is injected and comes into contact with reservoir live oil, the mass of CO_2 is transferred from CW to the oil due to the contrast in the solubility of CO_2 between the two immiscible fluids. The dissolution of CO_2 in oil enhanced the oil mobility as a result of a reduction in the viscosity of the oil and the effect of oil swelling. In live oil systems, however, where the oil is initially saturated with dissolved gas, the CO_2 transferred into the oil expels the light hydrocarbon components in order to dissolve more CO_2 in the oil. The vaporised hydrocarbon components form gas bubbles within the oil which bring about a bigger increase in oil volume than that in normal oil swelling. The continuous transfer of CO_2 from CW to the oil phase would enlarge the gas phase with more hydrocarbon in addition to CO_2. Then, the gas phase bubbles would merge together displacing the trapped oil to be recovered by upcoming carbonated water.

7.1.1 Numerical Simulation of CWI in Core-Scale

Based on the physics directly observed in pore-scale visualisation experiments, a new methodology was developed to estimate the complex processes leading to gas saturation in the core during CWI, and an equation of state (EOS) was tuned to reproduce the dynamic of the fluids' phase behaviour and the new phase formation. Due to the formation of a new phase arising from the dissolution of CO_2 into the oil, three phases exist and flow together in the porous medium, and therefore additional aspects of multiphase flow regimes are considered when simulating the carbonated water injection process.

Two sets of core displacement experiments were chosen to be studied systematically using the proposed methodology. The first set of coreflood experiments was simulated in a water-wet sandstone core using methane-saturated oil as the live oil system. The other set of coreflood experiments was simulated in a mixed-wet carbonate core using a reservoir live oil system.

Firstly, an approach was developed to calculate the average saturation of the gas phase in the core during tertiary CWI based on the mechanisms observed through direct pore-scale visualisations and so as to overcome the difficulties in measuring the gas saturation. Then, this gas saturation was used to tune the EOS through parametrising the binary interaction coefficients (BICs) between CO_2 and hydrocarbon compounds in order to model the oil and gas phases' behaviours to produce the gas saturation. After that, the saturation functions, including relative permeabilities and capillary pressure, were estimated to history-match and predict the coreflood experimental data. The results demonstrated that, by incorporating the proposed methodology, the complex processes taking place during CWI could be captured.

The main conclusions that can be drawn from the simulation and history matching attempts are as follows:

- The mixing between CO_2 and oil in the form of CO_2-hydrocarbon binary interaction coefficients in the EOS would affect the simulation of CO_2 partitioning in water and oil, and also the instability of oil phase that forms a gas phase to reach equilibrium.

- Generalised correlations were taken from [138] and [142] to calculate the CO_2-HC binary interaction coefficients and to compare their simulated average oil and gas saturations with those produced through the assisted history matching task. The results revealed that selecting the right set of CO_2-HC BICs mainly depends on replicating the behaviour changes exhibited by the oil and formed gas phases when CO_2 is transferred from CW to oil.

- The need for a negative CO_2-C_1 binary interaction coefficient was a result of the presence of a high polar compound, i.e., water, in which the CO_2 and methane soluble in brine produce high interaction forces in front of the opposite repulsive forces between them.

- The heavy hydrocarbon components (C_{7+} fractions) were found to control the dissolution of CO_2 in the oil via the ability of CO_2 to extract these hydrocarbon compounds to the gas phase.

- The formation of the new gaseous phase would necessitate utilising a three-phase oil relative permeability model where the formed gas increased the volume of the hydrocarbon saturation. At the same time, the carbonated water displaced the swollen oil in the three-phase region. This means that reducing the oil saturation is a function of increasing the gas phase saturation, representing the fact that the gas is completely trapped in the porous medium. Thus, the relative permeability of the oil is a function of both gas and water saturations in the three-phase region in which the relative permeability to oil in the three-phase region could be expressed using the Stone I model.

- The mechanism through which the gas phase is formed, and the characteristics of oil-gas relative permeability in the context of high critical gas saturation and low values of gas relative permeability during CWI, are similar to those in depressurisation (blow-out) processes, where the pressure is depleted below the saturation pressure and bubbles of dissolved gas form that enlarge the oil volume.

- The full sequence of secondary waterflooding and subsequent tertiary CWI could be history matched successfully to obtain one set of oil-water and gas-oil relative

permeabilities. These indicated the acceptable potential of the commercial simulators to model the underlying mechanisms once the dominant physics are understood and implemented in the simulation. The secondary CWI could be matched and relative permeabilities could be estimated.

- The prediction of tertiary CO_2 injection using the proposed method in history matching the secondary CWI was generally acceptable to model the compositional changes during conventional CO_2 injection.

- The prediction in respect to the secondary CWI displacement experiment in a mixed wet core was reasonably achieved in terms of oil recovery, average oil saturation and cumulative WOR using the tuned EOS and estimated saturation functions in history matching tertiary CWI.

- The dispersion effect is a localised process nearby the injection region where the flow is heterogeneous and turbulent and its effect diminished further into the reservoir, as explained by the injection of carbonated water in a slim tube representing the uniform and laminar flow in the reservoir.

- The injection of carbonated water into a carbonate core that contains calcite could lead to significant changes in pore structure, which could either improve or impair the permeability of the rock. In our case, the rock dissolution caused improvement of rock permeability resulting in a reduction of differential pressure across the core.

- In the core displacement experiments, the relationship between the carbonation level and incremental oil recovery could not interpreted linearly. In contrast, in the simulation modelling, a 50 % reduction in the carbonation level resulted in a 50 % decrease in oil recovery due to the fixed partitioning coefficient value in all flash calculation stages that were calculated by the EOS, rather than the variable partitioning coefficient as calculated in the multiple-contacts equilibrium PVT test.

- The successful history matching of the coreflood experiments implies a good potential to simulate large scale cases of carbonated water injection if the simulator is trained to capture the pertinent physics.

7.1.2 CW Multiple-Contacts Equilibrium in Live Oil Systems

Knowledge of the changes that take place in the phase behaviour during the CWI process is essential to assess the partitioning of CO_2 among the three phases and how this affects the fluid flow in a porous medium. In this study, the carbonated water was brought into contact with under-saturated oil in a series of multiple-equilibrium contacts to describe the compositional change of CO_2-oil mixtures during these CW contacts. The resultant phases were measured to track the transferred CO_2 among different phases, and to characterise the phase behaviour occurring in the oil phase and the subsequent new phase. A comprehensive interpretation of the physical fluid properties, including the solubility of CO_2 in oil, the solubility of gases in water, the swelling factor and changes in the saturation pressure. In addition, the physical properties of the third phase were measured in order to tune the cubic-EOS. The tuned EOS was then used to validate the history matched method proposed in water-wet core displacement experiments. The following conclusions were summarised from this study:

Multiple-Contacts Equilibrium PVT Test (MCET)

- There was a dual mass transfer between carbonated water and oil where light hydrocarbon components, mainly C_1 to C_3, transferred from oil to the brine while CO_2 transferred from CW to oil.

- An incessant mass transfer of CO_2 took place into the oil. This could be surmised through the low GWR after each contact, even after the oil became saturated with CO_2 and formed a gas phase.

- The continuous dissolution of CO_2 into the oil from the CW would lead to steady compositional changes in the oil and the formation of a gas phase, even though the oil was under-saturated with hydrocarbon gases.

- The formation of the new gas phase during CWI depends on the amount of dissolve gas in oil. The continuous and dynamic dissolution of CO_2 into the oil phase that takes place during the interphase mass transfer happening during CWI would expel the lighter hydrocarbon components of the oil forming a new gaseous phase with tendency to enlarge the oil phase much more than the effect of normal oil swelling.

- The formation of the new gas phase occurred after the oil became saturated with CO_2, observed in the form of increasing saturation pressure. The new phase was characterised as a gaseous phase, whose composition soon after its initial formation was mainly methane (C_1). In fully saturated oil and in under-saturated oil, its composition contains a higher concentration of CO_2 than other light hydrocarbon components. The reason behind these phenomena is the initial saturation level of each type of oil.

- The formation of the new phase enhanced the mass transfer of CO_2 from the aqueous phase to the oil phase, which was clearly estimated during the calculation of the CO_2 partition coefficient between the two immiscible phases.

Modelling MCET

- By adjusting the binary interaction coefficients between CO_2 and hydrocarbon components, the mass transfer of CO_2 from CW to oil changes and, as a result, the new (gas) phase formed containing the light hydrocarbon components. Henry's Law controls the solubility of various gases in brine and this, together with the flash calculation and the partitioning coefficients of soluble gases in brine to oil, was used to reproduce the mass transfer of those gases from CW to oil and vice versa.

- The main difference between the two manually adjusted BIC sets was the negative CO_2-C_1 BIC in the one named MCET 2^{ND} (-ve) EOS, which were able to predict the dissolution of CO_2 in oil through a noticeable increase in oil saturation pressure. The tuned EOS has the ability to reproduce the measured GOR and swelling factor before the formation of the gas phase. On the other hand, it was

difficult to estimate accurately the GOR after the gas phase formed, most likely due to the inaccuracy of the measured value.

- Successful prediction of the composition and volume of the new (gas) phase was compared to the composition measured after the sixth CW equilibrated contact. The tuned EOS, however, calculated the extraction of more C_{4+} than the measured experimental composition.

- The tuned cubic EOS calculated a continuing increase in reservoir oil density and reduction in oil viscosity before the phase split to form gas phase. After the phase split, both oil density and viscosity demonstrated an increasing trend. The results of this fluid modelling cannot conclusively evaluate the characterisation of the CO_2-oil mixture in terms of its viscosity and density, although the equation of state could predict the general behaviour of CO_2-oil mixture, which was as reported in the literature.

Validation of the Core Displacement Experiments' History Matching Method

- Changing the CO_2-C_1 BIC towards more negative values would decrease the solubility of CO_2 in oil, consequently shrinking the oil swelling and the rate of oil viscosity reduction. A positive CO_2-C_1 BIC would limit the CO_2 dissolution in the oil phase after the oil became saturated with CO_2, whereas the negative CO_2-C_1 BIC allowed the oil continually to dissolve more CO_2.

- Generally, the PVT-tuned EOS simulation scenarios could realistically predict the increase in differential pressure across the core and gave a good indication of appropriateness of the oil-gas relative permeability curves that were obtained, and also the effect of the binary interaction coefficients on the fluid phase behaviour.

- The prediction of tertiary CO_2 injection in test no. 3, using a second EOS, showed that the performance of tertiary CO_2 injection was over estimated where the EOS was tuned to model the phase behaviour change in oil due to CO_2 mass transfer from carbonated water to oil without taking into consideration the compositional changes that take place during conventional CO_2 injection.

7.1.3 Technical Quality of Simulating CWI on a Reservoir Scale

A technical quality screening study of the process of simulating CWI on the reservoir scale was achieved using two homogeneous models to evaluate the performance of CWI in comparison with conventional water flooding and also among other gas-based injection methods, specifically immiscible CO_2 and methane. The oil composition and tuned EOS, in addition to the obtained saturation functions that were estimated in simulating the mixed-wet core displacement experiments were used to carry out the screening. The technical quality screening study concluded the following:

- The performance of secondary CWI was predicted using the simulation models and compared with the performance of conventional WF. The results showed that the incremental oil recovery due to CWI increased as more CW pore volume was injected, whereas there was no significant improvement in oil recovery due to secondary WF when more water pore volume injected. On the reservoir scale, however, the incremental oil recovery was lower than that in the core displacement experiments at the same PVI.

- The dispersion effect on incremental oil recovery was diminished in the reservoir-scale as the flow away from the injector would be uniform and steady rather than turbulent and unsteady as it was near the wellbore. This allowed enough time to achieve an equilibrium between carbonated water and oil. The dispersion effect on reservoir scale significantly reduced the CO_2 storage efficiency of CWI due to the fast breakthrough of CO_2 that was dissolved in both oil and aqueous phases.

- Lowering the carbonation level would reduce the CO_2 content in water, weakening the CW mechanisms responsible for enhancing oil recovery during CWI. Since the CO_2 storage in CWI depended on the amount of gas phase formed, and how much was trapped in the reservoir, lowering the carbonation level would reduce the amount of trapped gas, subsequently reducing the efficiency of the CO_2 storage.

- Even after implementing the water-alternating gas and simultaneous water-and-gas processes without a hysteresis effect to enhance the mobility of the injected gas (CO_2), the SCWI still had the highest ultimate oil recovery and the best net

CO_2 utilisation factor. Furthermore, the ability of CWI to store the injected CO_2 makes it preeminent among other CO_2 injection methods. Hysteresis, however, plays a critical role in showing the advantage of residual CO_2 trapping, and thereby safe CO_2 storage, while reducing the mobility of the CO_2 and producing additional oil. Therefore, the effect of hysteresis on the performance of WAG processes should be considered and compared against CWI.

- On the reservoir scale, the gas phase formed with the oil as a result of the transfer of CO_2 from carbonated water into the oil enlarges the hydrocarbon volume which causes the oil to be displaced. Then, since the density of the formed gas is less than the oil density, once the gas phase reaches its critical saturation, it migrates to the upper layers at low relative permeability as a result of gravity segregation, thereby displacing the oil in the top layers while the injected carbonated water displaces the oil in the bottom layers. Through this process, a steady and efficient macro and micro sweep displacement was established. Through this process, the CO_2 content in brine is the key controller of the performance of CWI. Using a CO_2 solubility promoter to increase the CO_2 content in water would therefore improve this process leading to additional oil recovery.

7.2 Practical guidelines to simulate the performance of CWI

One of the main objectives that setup in this thesis, is to provide practical guidelines for the numerical simulating the performance of CWI and its influences on EOR. The following flow-diagram (figure 7-1) explains the steps that could be followed to successfully simulate the performance CWI and predict its results for further design and implementation as an EOR method. The building block in which the procedure of simulating CWI performance would gain its effectiveness is the assumption of the formation of a new (gas) phase as a result of mass transfer of CO_2 from CW to oil and stripping the oil from its lightest hydrocarbon components. Furthermore, a new gas-phase would be the predominant mechanism in enhancing oil recovery mainly in live oil systems rather than the normal oil swelling and reduction of oil viscosity.

Depending upon the availability of experimental laboratory results, the procedure of simulating the performance of CWI would follow the conventional way where the tuning

of the cubic equation of state to model the mass transfer of CO_2 from CW to oil and subsequently the formation of new gas phase, based on the designated CW multiple-equilibrium contact (CW-MCET) PVT test. In this PVT test, a series of equilibrium contacts between CW and oil is performed to measure the composition of oil after each contact, to quantify the formation of a new phase as volume and composition, and any related change the oil phase behaviour that happens through the diffusion of CO_2 in oil. Then, adjusting the binary interaction coefficients of CO_2 and hydrocarbon components accordingly to reproduce the test results.

In the absence of representative PVT test in which through it the EOS could be tuned, calculating the saturation of new gas phase during tertiary CWI and then utilize the results in tuning the EOS, would be another route in simulating the performance of CWI. Several reasons make this method adequate in modelling the injecting of CW in live oil systems, which are

- In conventional waterflooding, the formation of a gas phase and the presence of its saturation would not be possible due to the type of displacement between two immiscible liquid phase.

- All the performed direct pore-scale experiments of injecting CW in live oil systems revealed on the formation of new gas phase that trapped within the oil phase causing a drastic increase in oil swelling.

- Calculating the saturation of new gas phase during tertiary CWI after no further oil production in secondary conventional WF would eliminate the possibility of interfering of WF mechanisms in the calculation procedure, for example, reduction of oil saturation is not resulting from water displaced oil.

- CO_2-HC BIC's are the only parameters in vdW1f mixing rules which responsible in the mass transfer of CO_2 from CW to oil phase taking into consideration the unchanged effect of CO_2-H_2O BIC in the process.

Optimising the CO_2-HC BIC's alone would lead to a non-unique solution, then I recommend combining the oil-gas relative permeability parameters and CO_2-HC BIC's

in an optimisation procedure in which reduce the impact of non-uniqueness setup on history-matching the core displacement experiments.

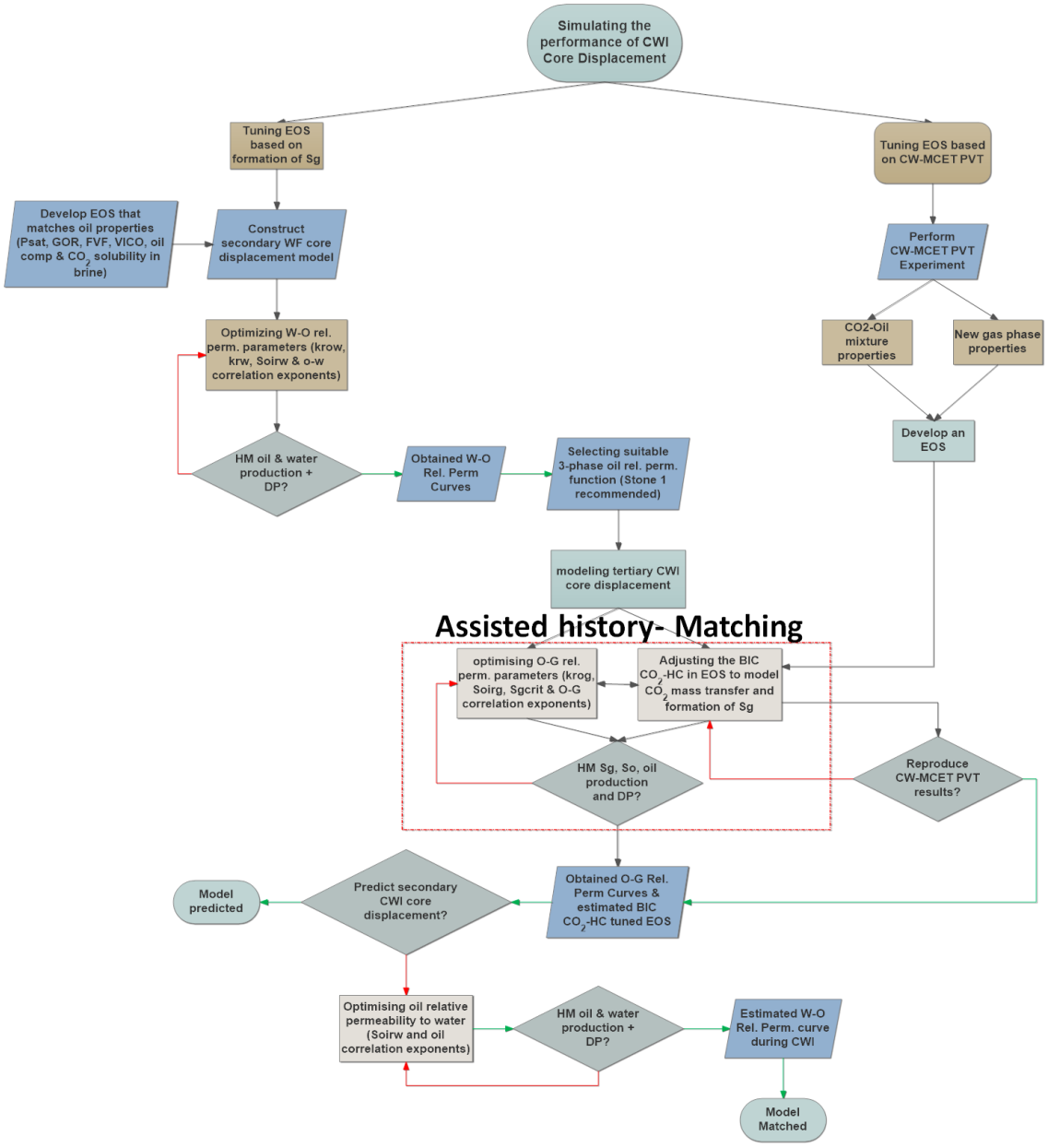

Figure 7-1 flow diagram of the practical guidelines in successfully simulating the performance of CWI core displacement experiments

7.3 Future works and recommendation

In this thesis, the numerical simulation of CWI process in live oil systems was performed through the development of a methodology to tune the equation of state that was coupled with CO_2 solubility in brine estimated by Henry's Law to reproduce the formation of the gas phase, then modelling the flow behaviour of three phases in porous media. The main assumption in this methodology, however, was that the formation of gas phase during

CWI is the predominant mechanism in improving oil recovery, and that the impact of other mechanisms, such oil viscosity reduction and normal oil swelling, have only smaller impacts. Some recommendations are made for future work:

- To evaluate and implement the method which I proposed in simulating the performance of CWI and obtaining the parameters that responsible for successful modelling the impact of injecting CW on enhancing oil recovery, a one-dimensional simulation modelling where the flow only exists linearly in the x-direction was applied. A one-dimensional modelling represents the underlying simulation model where Buckley-Leverett type water displacement. However, it was used in the newly proposed method to translate the observed physics from direct-pore scale experiment to be utilised numerically in the simulation. After proving and validating the technique in simulating CWI, it is recommended using two or three dimensions modelling for future simulation of CWI using the practical guidelines that mentioned earlier. The 2D models allow the evaluation of vertical or areal sweep efficiency and water/oil displacements in geostatistical cross-section, and then a generation of pseudo-relative permeability (2 phase upscaling).

- As the equation of state was tuned based on the fluid-fluid interaction between the carbonated water and the oil during CWI, the tuned results could only model the compositional changes in oil and subsequent gas phases due to CWI. Tuning an EOS to model the phase behaviour of a CO_2-oil mixture in both the conventional CO_2 injection and CWI is therefore essential to train the compositional simulation model to predict both scenarios. This could happen through designing an advance PVT test containing the CO_2 swelling and CW multiple-equilibrium contacts tests to describe the CO_2-oil mixture compositional changes and measure the fluid properties accordingly.

- The differential pressure across the core behaved differently in the two sets of experiments. The continuously increasing trend of differential pressure was the noticeable feature in methane-saturated oil system, whereas an increasing then declining trend of differential pressure was the obvious feature in the multiple-gas components-saturated oil system. Thus, the presence of multiple component

gases dissolved in oil affects the performance of CWI. The gas formed as a result of CWI contains multiple components gases. Thus, the interfacial tension between the formed gas and the oil would decrease with more extraction of hydrocarbon components from the oil to the gas phase, which will create favourable miscibility conditions. It is therefore recommended to perform a series of coreflood experiments studying the role of dissolved gas in the CWI process, especially in respect to a shift from immiscible to miscible conditions.

- Hysteresis has more of an effect in the WAG process, while the critical gas saturation (trapped gas) is the essential factor in the CWI process. Performing a WAG injection core displacement test that involves injecting cycles of CW and CO_2 is therefore recommended to obtain a common oil-gas relative permeability with hysteresis which reflects the performance of both processes.

- The experimental core displacement results showed early breakthrough of CO_2 ahead of water breakthrough, while in the slim tube experimental results, the water broke through earlier than the CO_2, indicating that the produced water contained zero CO_2 and the equilibrium between CW and oil occurred instantaneously. It is therefore recommended to perform a CW multiple-contact equilibrium test where the carbonated water in the first contact between water and oil is used to contact new oil in a subsequent contact and so on, in order to measure the CO_2 content in water after each contact.

References

1. *Global Energy & CO2 Status Report 2017*. 2017, International Energy Agency (IEA).

2. *International Energy Outlook 2017*. 2017, U.S. Energy Information Administration (EIA).

3. *Climate Change 2014 Synthesis Report*. 2014, Intergovernmental Panel on Climate Change (IPCC).

4. Keller, K., D. McInerney, and D.F. Bradford, *Carbon dioxide sequestration: how much and when?* Climatic Change, 2008. **88**(3-4): p. 267.

5. Hite, J.R., M.L. Blanton, M.I. Kuhlman, and W.B. Fair. *Managing Risk in EOR Projects*. in *SPE Latin America and Caribbean Petroleum Engineering Conference*. 2012. Society of Petroleum Engineers.

6. Luckow, P., E.A. Stanton, B. Biewald, J. Fisher, F. Ackerman, and E. Hausman, *2013 Carbon Dioxide Price Forecast.* Synapse Energy Economics, 2013.

7. Kokal, S. and A. Al-Kaabi, *Enhanced oil recovery: challenges & opportunities.* World Petroleum Council: Official Publication, 2010. **64**.

8. Glover, P., *Chapter 3: Reservoir Drivers, Formation Evaluation MSC course notes.* Aberdeen University, 2001: p. 19-26.

9. Fettke, C.R., *The Bradford oil field Pennsylvania and New York*. 1938, Pennsylvania Geological Survey. p. 298-301.

10. Alagorni, A.H., Z.B. Yaacob, and A.H. Nour, *An overview of oil production stages: enhanced oil recovery techniques and nitrogen injection.* International Journal of Environmental Science and Development, 2015. **6**(9): p. 693.

11. Al-Anazi, B.D., *Enhanced oil recovery techniques and nitrogen injection.* CSEG Recorder, 2007: p. 28-33.

12. Atia, A. and K. Mohammedi, *A Review on the Application of Enhanced Oil/Gas Recovery through CO2 Sequestration.* Carbon Dioxide Chemistry, Capture and Oil Recovery, 2018: p. 241.

13. Enick, R.M., D.K. Olsen, J.R. Ammer, and W. Schuller. *Mobility and Conformance Control for CO2 EOR via Thickeners, Foams, and Gels--A Literature Review of 40 Years of Research and Pilot Tests*. in *SPE improved oil recovery symposium*. 2012. Society of Petroleum Engineers.

14. Hargrove, B., L. Melzer, and L. Whitman. *A status report on North American CO2 EOR production and CO2 supply*. in *16th Annual CO2 Flooding Conference, Midland, Tx. Dec*. 2010.

15. Gozalpour, F., S.R. Ren, and B. Tohidi, *CO2 EOR and storage in oil reservoir.* Oil & gas science and technology, 2005. **60**(3): p. 537-546.

16. Sahimi, M., M.R. Rasaei, and M. Haghighi, *Gas injection and fingering in porous media*, in *Gas Transport in Porous Media*. 2006, Springer. p. 133-168.

17. Holm, L. and V. Josendal, *Mechanisms of oil displacement by carbon dioxide.* Journal of petroleum Technology, 1974. **26**(12): p. 1,427-1,438.

18. Yellig, W. and R. Metcalfe, *Determination and Prediction of CO2 Minimum Miscibility Pressures (includes associated paper 8876).* Journal of Petroleum Technology, 1980. **32**(01): p. 160-168.

19. Stalkup Jr, F.I., *Status of miscible displacement.* Journal of Petroleum Technology, 1983. **35**(04): p. 815-826.

20. Stalkup, F., *Miscible Displacement, SPE Monograph Volume 8, Henry L. Doherty Series, Dallas*. 1983, ISBN 0-89520-319-7.

21. Stalkup, F.I., *Displacement Behavior of the Condensing/Vaporizing Gas Drive Process*. 1987, Society of Petroleum Engineers.

22. Martin, D.F. and J. Taber, *Carbon dioxide flooding.* Journal of Petroleum Technology, 1992. **44**(04): p. 396-400.

23. Mungan, N., *Carbon Dioxide Flooding-fundamentals.* 1981.

24. Bennion, B. and S. Bachu. *Relative permeability characteristics for supercritical CO2 displacing water in a variety of potential sequestration zones*. in *SPE Annual Technical Conference and Exhibition*. 2005. Society of Petroleum Engineers.

25. Bennion, D.B. and S. Bachu. *Permeability and relative permeability measurements at reservoir conditions for CO2-water systems in ultra low permeability confining caprocks*. in *EUROPEC/EAGE Conference and Exhibition*. 2007. Society of Petroleum Engineers.

26. Bachu, S. and B. Bennion, *Effects of in-situ conditions on relative permeability characteristics of CO2-brine systems.* Environmental Geology, 2008. **54**(8): p. 1707-1722.

27. Kulkarni, M.M., *Multiphase mechanisms and fluid dynamics in gas injection enhanced oil recovery processes.* 2005.

28. Riazi, M., M. Sohrabi, M. Jamiolahmady, S. Ireland, and c. Brown, *Oil Recovery Improvement Using CO2-Enriched Water Injection*. 2009, Society of Petroleum Engineers.

29. Sohrabi, M., M. Riazi, M. Jamiolahmady, S. Ireland, and C. Brown. *Mechanisms of oil recovery by carbonated water injection*. in *SCA annual meeting*. 2009.

30. (NETL), N.E.T.L., *Carbon Dioxide Enhanced Oil Recovery; Untapped Domestic Energy Supply and Long Term Carbon Storage Solution*. US Department of Energy.

31. Shakhashiri, B.Z. *Carbon Dioxide Phase Behavior*. 2008; Available from: http://www.scifun.org/.

32. Batema, C. *What Makes CO2 Soluble in H2O*. 13 March 2018; Available from: https://sciencing.com/co2-soluble-h2o-18452.html.

33. ToolBox, E. *Solubility of Gases in Water*. 2008 6 June 2018]; Available from: https://www.engineeringtoolbox.com/gases-solubility-water-d_1148.html

34. Iglauer, S., *Dissolution trapping of carbon dioxide in reservoir formation brine–a carbon storage mechanism*, in *Mass Transfer-Advanced Aspects*. 2011, InTech.

35. Dodds, W., L. Stutzman, and B. Sollami, *Carbon dioxide solubility in water.* Industrial & Engineering Chemistry Chemical & Engineering Data Series, 1956. **1**(1): p. 92-95.

36. Steel, L., Q. Liu, E. Mackay, and M.M. Maroto-Valer, *CO2 solubility measurements in brine under reservoir conditions: A comparison of experimental and geochemical modeling methods.* Greenhouse Gases: Science and Technology, 2016. **6**(2): p. 197-217.

37. Duan, Z. and R. Sun, *An improved model calculating CO2 solubility in pure water and aqueous NaCl solutions from 273 to 533 K and from 0 to 2000 bar.* Chemical geology, 2003. **193**(3-4): p. 257-271.

38. Duan, Z., R. Sun, C. Zhu, and I.-M. Chou, *An improved model for the calculation of CO2 solubility in aqueous solutions containing Na+, K+, Ca2+, Mg2+, Cl−, and SO42−.* Marine Chemistry, 2006. **98**(2-4): p. 131-139.

39. Hildebrand, J.H., *A critique of the theory of solubility of non-electrolytes.* Chemical reviews, 1949. **44**(1): p. 37-45.

40. Simon, R. and D. Graue, *Generalized correlations for predicting solubility, swelling and viscosity behavior of CO2-crude oil systems.* Journal of Petroleum Technology, 1965. **17**(01): p. 102-106.

41. Welker, J., *Physical properties of carbonated oils.* Journal of Petroleum Technology, 1963. **15**(08): p. 873-876.

42. Chung, F., R. Jones, and T. Burchfield. *Recovery of viscous oil under high pressure by CO2 displacement: A laboratory study*. in *International Meeting on Petroleum Engineering*. 1988. Society of Petroleum Engineers.

43. Srivastava, R., S. Huang, and S. Dyer, *Measurement and prediction of PVT properties of heavy and medium oils with carbon dioxide*. 1995, UNITAR, New York, NY (United States).

44. Emera, M. and H. Sarma. *A genetic algorithm-based model to predict co-oil physical properties for dead and live oil*. in *Canadian International Petroleum Conference*. 2006. Petroleum Society of Canada.

45. Chung, F.T., R.A. Jones, and H.T. Nguyen, *Measurements and correlations of the physical properties of CO2-heavy crude oil mixtures.* SPE reservoir engineering, 1988. **3**(03): p. 822-828.

46. Rostami, A., M. Arabloo, A. Kamari, and A.H. Mohammadi, *Modeling of CO 2 solubility in crude oil during carbon dioxide enhanced oil recovery using gene expression programming.* Fuel, 2017. **210**: p. 768-782.

47. Miller, J.S. and R.A. Jones. *A laboratory study to determine physical characteristics of heavy oil after CO2 saturation*. in *SPE/DOE Enhanced Oil Recovery Symposium*. 1981. Society of Petroleum Engineers.

48. DeRuiter, R., L. Nash, and M. Singletary, *Solubility and Displacement Behavior of a Viscous Crude With CO2 and Hydrocarbon Gases. SPE Res Eng 9 (2): 101–106*. 1994, SPE-20523-PA. http://dx. doi. org/10.2118/20523-PA.

49. Martin, J.W., *Additional oil production through flooding with carbonated water.* Producers Monthly, 1951. **15**(7): p. 18-22.

50. Holm, L., *CO2 Requirements in CO2 Slug and Carbonated Water Recovery Processes.* Producer Monthly. September, 1963.

51. Riazi, M., M. Jamiolahmady, and M. Sohrabi, *Theoretical investigation of pore-scale mechanisms of carbonated water injection.* Journal of Petroleum Science and Engineering, 2011. **75**(3–4): p. 312-326.

52. Riazi, M., M. Sohrabi, and M. Jamiolahmady, *Experimental Study of Pore-Scale Mechanisms of Carbonated Water Injection.* Transport in Porous Media, 2011. **86**(1): p. 73-86.

53. Sohrabi, M., N.I. Kechut, M. Riazi, M. Jamiolahmady, S. Ireland, and G. Robertson, *Safe storage of Co2 together with improved oil recovery by Co2-enriched water injection.* Chemical Engineering Research and Design, 2011. **89**(9): p. 1865-1872.

54. Sohrabi, M., N.I. Kechut, M. Riazi, M. Jamiolahmady, S. Ireland, and G. Robertson, *Coreflooding Studies to Investigate the Potential of Carbonated Water Injection as an Injection Strategy for Improved Oil Recovery and CO2 Storage.* Transport in Porous Media, 2012. **91**(1): p. 101-121.

55. Johnson, W., R. Macfarlane, J. Breston, and D. Neil, *Laboratory experiments with carbonated water and liquid carbon dioxide as oil recovery agents.* Prod. Monthly, 1952. **17**.

56. Ahmadi, M.A., M. zeinali Hasanvand, S.S. Behbahani, A. Nourmohammad, A. Vahidi, M. Amiri, and G. Ahmadi, *Effect of operational parameters on the performance of carbonated water injection: Experimental and numerical modeling study.* The Journal of Supercritical Fluids, 2016. **107**: p. 542-548.

57. Lake, L., G. Carey, G. Pope, and K. Sepehrnoori, *Isothermal, multiphase, multicomponent fluid flow in permeable media.* In Situ;(United States), 1984. **8**(1).

58. Saxon Jr, J., J. Breston, and R. Macfarlane, *Laboratory tests with carbon dioxide and carbonated water as flooding mediums.* Prod. Monthly, 1951. **16**.

59. Holm, L., *Carbon dioxide solvent flooding for increased oil recovery.* 1959.

60. Van Dijk, C., *Carbonated water flood*, in *Shell Internal Research Report R 1189*. 1965.

61. Dumore, J., J. Hagoort, and A. Risseeuw, *A One-Dimensional Analytical Model for Carbonated Waterflooding*. 1982, Shell Internal Research Report.

62. Falls, A., *Analysis of an Idealized Carbonated Waterflood in the South Wasson/Clearfork Formation*. 1986, Shell Internal Research Report.

63. Falls, A., A. Cherubini, and S. Seunsom, *The response of South Wasson/Clearfork crude to carbonated water in an etched-glass model*, in *Shell Internal Research Report BRC-1350*. 1986.

64. Gorell, S. and A. Falls, *Status of Carbonated Waterflooding Research*. 1986, Shell Internal Research Report.

65. Sohrabi, M., M. Riazi, M. Jamiolahmady, S. Ireland, and C. Brown. *Carbonated water injection (CWI) studies*. in *29th Annual Workshop & Symposium, IEA Collaborative Project on Enhanced Oil Recovery*. 2008.

66. Sohrabi, M., M. Riazi, M. Jamiolahmady, N.I. Kechut, S. Ireland, and G. Robertson, *Carbonated water injection (CWI)–A productive way of using CO2 for oil recovery and CO2 storage.* Energy Procedia, 2011. **4**: p. 2192-2199.

67. Kechut, N.I., M. Riazi, M. Sohrabi, and M. Jamiolahmady, *Tertiary Oil Recovery and CO2 Sequestration by Carbonated Water Injection (CWI)*. 2010, Society of Petroleum Engineers.

68. Sohrabi, M., A. Emadi, S.A. Farzaneh, and S. Ireland. *A thorough investigation of mechanisms of enhanced oil recovery by carbonated water injection*. in *SPE Annual Technical Conference and Exhibition*. 2015. Society of Petroleum Engineers.

69. Seyyedi, M., P. Mahzari, and M. Sohrabi, *An integrated study of the dominant mechanism leading to improved oil recovery by carbonated water injection.* Journal of Industrial and Engineering Chemistry, 2017. **45**: p. 22-32.

70. Seyyedi, M., M. Sohrabi, and A. Sisson, *Experimental investigation of the coupling impacts of new gaseous phase formation and wettability alteration on improved oil recovery by CWI.* Journal of Petroleum Science and Engineering, 2017. **150**: p. 99-107.

71. Seyyedi, M., P. Mahzari, and M. Sohrabi, *A comparative study of oil compositional variations during CO 2 and carbonated water injection scenarios for EOR.* Journal of Petroleum Science and Engineering, 2018. **164**: p. 685-695.

72. Seyyedi, M. and M. Sohrabi, *Pore-scale investigation of crude oil/CO2 compositional effects on oil recovery by carbonated water injection.* Industrial & Engineering Chemistry Research, 2017. **56**(6): p. 1671-1681.

73. Mahzari, P., P. Tsolis, S.A. Farzaneh, M. Sohrabi, S. Enezi, A.A. Yousef, and A.A. Eidan. *A Comprehensive Experimental Study of Pore-Scale and Core-Scale Processes During Carbonated Water Injection Under Reservoir Conditions*. in *SPE Kingdom of Saudi Arabia Annual Technical Symposium and Exhibition*. 2017. Society of Petroleum Engineers.

74. Kechut, N.I., M. Sohrabi, and M. Jamiolahmady, *Experimental and Numerical Evaluation of Carbonated Water Injection (CWI) for Improved Oil Recovery and CO2 Storage*. 2011, Society of Petroleum Engineers.

75. Tavakolian, M., M. Sohrabi, M. Jami, and S. Ireland. *Significant improvement in oil recovery and CO2 storage by carbonated water injection (CWI)*. in *Third EAGE CO2 Geological Storage Workshop*. 2012.

76. Dong, Y., B. Dindoruk, C. Ishizawa, E.J. Lewis, and T. kubicek, *An Experimental Investigation of Carbonated Water Flooding*. 2011, Society of Petroleum Engineers.

77. Dong, Y., C. Ishizawa, E. Lewis, and B. Dindoruk. *Carbonated water flood: what we observed in sand pack experiments*. in *International Symposium of the Society of Core Analysts, Austin, Texas, USA*. 2011.

78. Mosavat, N. and F. Torabi, *Performance of Secondary Carbonated Water Injection in Light Oil Systems.* Industrial & Engineering Chemistry Research, 2014. **53**(3): p. 1262-1273.

79. Mosavat, N. and F. Torabi, *Experimental evaluation of the performance of carbonated water injection (CWI) under various operating conditions in light oil systems.* Fuel, 2014. **123**: p. 274-284.

80. Kechut, N.I., M. Jamiolahmady, and M. Sohrabi, *Numerical simulation of experimental carbonated water injection (CWI) for improved oil recovery and CO2 storage.* Journal of Petroleum Science and Engineering, 2011. **77**(1): p. 111-120.

81. Seyyedi, M., M. Sohrabi, A. Sisson, and S. Ireland, *Quantification of oil recovery efficiency, CO2 storage potential, and fluid-rock interactions by CWI in heterogeneous sandstone oil reservoirs.* Journal of Molecular Liquids, 2018. **249**: p. 779-788.

82. Anderson, W.G., *Wettability literature survey-part 3: the effects of wettability on the electrical properties of porous media.* Journal of petroleum technology, 1986. **38**(12): p. 1,371-1,378.

83. Anderson, W., *Wettability Literature Survey—Part 4: Effects of Wettability on Capillary Pressure. JPT 39 (10): 1283–1300*. 1987, SPE-15271-PA. DOI: 10.2118/15271-PA.

84. Masalmeh, S.K., *The effect of wettability heterogeneity on capillary pressure and relative permeability.* Journal of Petroleum Science and Engineering, 2003. **39**(3-4): p. 399-408.

85. Anderson, W.G., *Wettability Literature Survey Part 5: The Effects of Wettability on Relative Permeability.* Journal of Petroleum Technology, 1987. **39**(11): p. 1453-1468.

86. Anderson, W.G., *Wettability literature survey-part 6: the effects of wettability on waterflooding.* Journal of petroleum technology, 1987. **39**(12): p. 1,605-1,622.

87. Morrow, N.R., *Wettability and its effect on oil recovery.* Journal of Petroleum Technology, 1990. **42**(12): p. 1,476-1,484.

88. Grape, S.G., *Imbibition flooding with CO_2-enriched water*. 1990, Texas A&M University.

89. Yang, D., Y. Gu, and P. Tontiwachwuthikul, *Wettability determination of the crude oil− reservoir brine− reservoir rock system with dissolution of CO 2 at high pressures and elevated temperatures.* Energy & Fuels, 2008. **22**(4): p. 2362-2371.

90. Riazi, M., *Pore scale mechanisms of carbonated water injection in oil reservoirs*. 2011, Heriot-Watt University.

91. Seyyedi, M., M. Sohrabi, and A. Farzaneh, *Investigation of rock wettability alteration by carbonated water through contact angle measurements.* Energy & Fuels, 2015. **29**(9): p. 5544-5553.

92. Seyyedi, M. and M. Sohrabi, *Enhancing water imbibition rate and oil recovery by carbonated water in carbonate and sandstone rocks.* Energy & Fuels, 2015. **30**(1): p. 285-293.

93. De Nevers, N., *A Calculation Method for Carbonated Water Flooding.* 1964.

94. Buckley, S.E. and M. Leverett, *Mechanism of fluid displacement in sands.* Transactions of the AIME, 1942. **146**(01): p. 107-116.

95. Welge, H., E.F. Johnson, S. Ewing Jr, and F. Brinkman, *The linear displacement of oil from porous media by enriched gas.* Journal of Petroleum Technology, 1961. **13**(08): p. 787-796.

96. Ramesh, A.B. and T.N. Dixon, *Numerical Simulation of Carbonated Waterflooding In A Heterogeneous Reservoir*. 1973, Society of Petroleum Engineers.

97. Shenawi, S.H. and C.H. Wu, *Compositional Simulation of Carbonated Waterfloods in Naturally Fractured Reservoirs*. 1994, Society of Petroleum Engineers.

98. Shelton, J. and F. Schneider, *The effects of water injection on miscible flooding methods using hydrocarbons and carbon dioxide.* Society of Petroleum Engineers Journal, 1975. **15**(03): p. 217-226.

99. Grogan, A. and W. Pinczewski, *The role of molecular diffusion processes in tertiary CO2 flooding.* Journal of petroleum technology, 1987. **39**(05): p. 591-602.

100. Stone, H., *Probability model for estimating three-phase relative permeability.* Journal of Petroleum Technology, 1970. **22**(02): p. 214-218.

101. Stone, H., *Estimation of three-phase relative permeability and residual oil data.* Journal of Canadian Petroleum Technology, 1973. **12**(04).

102. Baker, L.E., *Three-Phase Relative Permeability Correlations*. 1988, Society of Petroleum Engineers.

103. Fayers, F., *Extension of Stone's method 1 and conditions for real characteristics in three-phase flow.* SPE Reservoir Engineering, 1989. **4**(04): p. 437-445.

104. Aziz, K. and A. Settari, *Petroleum reservoir simulation. 1979.* Applied Science Publ. Ltd., London, UK: p. 30-38.

105. Ltd., C.M.G., *CMG-GEM User Manual.* 2015.

106. Ltd., C.M.G., *CMG-WinProp User Manual.* 2015.

107. Whitson, C.H. and M.R. Brulé, *Phase behavior*. Vol. 20. 2000: Henry L. Doherty Memorial Fund of AIME, Society of Petroleum Engineers ….

108. Van Der Waals, J.D., *On the Continuity of the Gaseous and Liquid States*. 1873, Univeriteit Leiden, Leiden, The Netherlands.

109. Redlich, O. and J.N. Kwong, *On the thermodynamics of solutions. V. An equation of state. Fugacities of gaseous solutions.* Chemical reviews, 1949. **44**(1): p. 233-244.

110. Soave, G., *Equilibrium constants from a modified Redlich-Kwong equation of state.* Chemical engineering science, 1972. **27**(6): p. 1197-1203.

111. Peng, D.-Y. and D.B. Robinson, *A new two-constant equation of state.* Industrial & Engineering Chemistry Fundamentals, 1976. **15**(1): p. 59-64.

112. Robinson, D.B. and D.-Y. Peng, *The characterization of the heptanes and heavier fractions for the GPA Peng-Robinson programs*. 1978: Gas processors association.

113. Privat, R. and J.-N. Jaubert, *Thermodynamic models for the prediction of petroleum-fluid phase behaviour*, in *Crude Oil Emulsions-Composition Stability and Characterization*. 2012, IntechOpen.

114. Barrios, O.M., C. Olivera-Fuentes, and F.L. Figueira, *Generalized Correlation of Binary Interaction Parameters in Cubic Equations of State for Hydrocarbon/CO, Hydrocarbon/HS and CO,/HS Systems.* CHEMICAL ENGINEERING, 2011. **24**: p. 589.

115. Coutinho, J.A., G.M. Kontogeorgis, and E.H. Stenby, *Binary interaction parameters for nonpolar systems with cubic equations of state: a theoretical approach 1. CO 2/hydrocarbons using SRK equation of state.* Fluid phase equilibria, 1994. **102**(1): p. 31-60.

116. Mehra, R.K., R.A. Heidemann, and K. Aziz, *Computation of multiphase equilibrium for compositional simulation.* Society of Petroleum Engineers Journal, 1982. **22**(01): p. 61-68.

117. Nghiem, L. and R. Heidemann. *General acceleration procedure for multiphase flash calculation with application to oil-gas-water systems*. in *Proceedings of the 2nd European Symposium on Enhanced Oil Recovery*. 1982.

118. Li, Y.K. and L.X. Nghiem, *Phase equilibria of oil, gas and water/brine mixtures from a cubic equation of state and Henry's law.* The Canadian Journal of Chemical Engineering, 1986. **64**(3): p. 486-496.

119. Mansoori, J., *Compositional modeling of CO2 flooding and the effect of CO2 water solubility.* 1982.

120. Chang, Y.-B., B.K. Coats, and J.S. Nolen. *A compositional model for CO 2 floods including CO 2 solubility in water*. in *Permian Basin Oil and Gas Recovery Conference*. 1996. Society of Petroleum Engineers.

121. Enick, R. and S. Klara, *Effects of CO2 solubility in brine on the compositional simulation of CO2 floods.* SPE reservoir engineering, 1992. **7**(02): p. 253-258.

122. Cysewski, G.R. and J.M. Prausnitz, *Estimation of gas solubilities in polar and nonpolar solvents.* Industrial & Engineering Chemistry Fundamentals, 1976. **15**(4): p. 304-309.

123. Nghiem, L.X. and Y.-K. Li, *Computation of multiphase equilibrium phenomena with an equation of state.* Fluid Phase Equilibria, 1984. **17**(1): p. 77-95.

124. Cancelliere, M., D. Viberti, and F. Verga, *Assisted history matching for petroleum reservoirs in the social computing era.* American Journal of Applied Sciences, 2013. **10**(8): p. 901.

125. Abdollahzadeh, A., *Adaptive algorithms for history matching and uncertainty quantification*. 2014, Heriot-Watt University.

126. Coats, K., J. Dempsey, and J. Henderson, *A new technique for determining reservoir description from field performance data.* Society of Petroleum Engineers Journal, 1970. **10**(01): p. 66-74.

127. Thomas, L.K., L. Hellums, and G. Reheis, *A nonlinear automatic history matching technique for reservoir simulation models.* Society of Petroleum Engineers Journal, 1972. **12**(06): p. 508-514.

128. Ltd., C.M.G., *CMG-CMOST User Manual.* 2015.

129. Akbarabadi, M., M. Borges, A. Jan, F. Pereira, and M. Piri, *A Bayesian framework for the validation of models for subsurface flows: synthetic experiments.* Computational Geosciences, 2015. **19**(6): p. 1231-1250.

130. Lomeland, F., E. Ebeltoft, and W.H. Thomas. *A new versatile relative permeability correlation*. in *International Symposium of the Society of Core Analysts, Toronto, Canada*. 2005.

131. Kontogeorgis, G.M. and G.K. Folas, *Thermodynamic models for industrial applications: from classical and advanced mixing rules to association theories*. 2009: John Wiley & Sons.

132. Craig, F.F., *The reservoir engineering aspects of waterflooding*. Vol. 3. 1971: HL Doherty Memorial Fund of AIME New York, NY.

133. Grattoni, C., R. Hawes, and R. Dawe. *Relative permeabilities for the production of solution gas from waterflood residual oil*. in *SCA-9817, International Symposium of the SCA*. 1998.

134. Egermann, P. and O. Vizika, *A new method to determine critical gas saturation and relative permeability during depressurization in the near-wellbore region.* Petrophysics, 2001. **42**(04).

135. Owens, W. and D. Archer, *The effect of rock wettability on oil-water relative permeability relationships.* Journal of Petroleum Technology, 1971. **23**(07): p. 873-878.

136. Morrow, N.R., P.J. Cram, and F. McCaffery, *Displacement studies in dolomite with wettability control by octanoic acid.* Society of Petroleum Engineers Journal, 1973. **13**(04): p. 221-232.

137. Whitson, C.H., *Characterizing hydrocarbon plus fractions.* Society of Petroleum Engineers Journal, 1983. **23**(04): p. 683-694.

138. Kato, K., K. Nagahama, and M. Hirata, *Generalized interaction parameters for the Peng—Robinson equation of state: carbon dioxide—n-paraffin binary systems.* Fluid Phase Equilibria, 1981. **7**(3-4): p. 219-231.

139. Graboski, M.S. and T.E. Daubert, *A modified Soave equation of state for phase equilibrium calculations. 2. Systems containing CO2, H2S, N2, and CO.* Industrial & Engineering Chemistry Process Design and Development, 1978. **17**(4): p. 448-454.

140. Nishiumi, H., T. Arai, and K. Takeuchi, *Generalization of the binary interaction parameter of the Peng-Robinson equation of state by component family.* Fluid Phase Equilibria, 1988. **42**: p. 43-62.

141. Valderrama, J.O., A.A. Ibrahim, and L.A. Cisternas, *Temperature-dependent interaction parameters in cubic equations of state for nitrogen-containing mixtures.* Fluid Phase Equilibria, 1990. **59**(2): p. 195-205.

142. Varotsis, N., G. Stewart, A. Todd, and M. Clancy, *Phase behavior of systems comprising North Sea reservoir fluids and injection gases.* Journal of petroleum technology, 1986. **38**(11): p. 1,221-1,233.

143. Kordas, A., K. Tsoutsouras, S. Stamataki, and D. Tassios, *A generalized correlation for the interaction coefficients of CO2—hydrocarbon binary mixtures.* Fluid Phase Equilibria, 1994. **93**: p. 141-166.

144. Emera, M. and H. Sarma, *Prediction of CO2 solubility in oil and the effects on the oil physical properties.* Energy Sources, Part A, 2007. **29**(13): p. 1233-1242.

145. Grigg, R.B. *Dynamic phase composition, density, and viscosity measurements during CO2 displacement of reservoir oil*. in *SPE International Symposium on Oilfield Chemistry*. 1995. Society of Petroleum Engineers.

146. Mahzari, P., P. Tsolis, M. Sohrabi, S. Enezi, A.A. Yousef, and A.A. Eidan, *Carbonated water injection under reservoir conditions; in-situ WAG-type EOR.* Fuel, 2018. **217**: p. 285-296.

147. Lomeland, F., E. Ebeltoft, and W. Hammervold Thomas. *A new versatile capillary pressure correlation*. in *Paper SCA 2008-08 presented at the International Symposium of the Society of Core Analysts held in Abu Dhabi, UAE*. 2008.

148. Skjaeveland, S., L. Siqveland, A. Kjosavik, W. Hammervold, and G. Virnovsky. *Capillary pressure correlation for mixed-wet reservoirs*. in *SPE India Oil and Gas Conference and Exhibition*. 1998. Society of Petroleum Engineers.

149. Donaldson, E.C. and R.D. Thomas. *Microscopic observations of oil displacement in water-wet and oil-wet systems*. in *Fall Meeting of the Society of Petroleum Engineers of AIME*. 1971. Society of Petroleum Engineers.

150. Moghadam, A.M. and M.B. Salehi, *Enhancing hydrocarbon productivity via wettability alteration: a review on the application of nanoparticles.* Reviews in Chemical Engineering, 2018.

151. Schmidt, T., Leshchyshyn, T.H., Puttagunta, V.R., *Diffusion of Carbon Dioxide into Athabasca Bitumen,* in *33rd Annual Technical Meeting of the Petroleum Society of CIM*. 1982: Calgary, Canada.

152. C. Bardon, L.D. *CO2 injection to enhance heavy oil recovery*. in *Heavy Crude Oil Recovery*. 1984. Martinus Nijhoff Publishers.

153. De Boer, R., S. Wellington, and K. Tschiedel, *Measurements on CO2-diffusion through unusually resistive layers on oil—water interfaces.* Colloids and surfaces, 1984. **9**(1): p. 79-83.

154. Grogan, A., V. Pinczewski, G.J. Ruskauff, and F. Orr Jr, *Diffusion of CO2 at reservoir conditions: models and measurements.* SPE reservoir engineering, 1988. **3**(01): p. 93-102.

155. Renner, T., *Measurement and correlation of diffusion coefficients for CO2 and rich-gas applications.* SPE reservoir engineering, 1988. **3**(02): p. 517-523.

156. Shu, G., M. Dong, H. Hassanzadeh, and S. Chen, *Effects of Operational Parameters on Diffusion Coefficients of CO2 in a Carbonated Water–Oil System.* Industrial & Engineering Chemistry Research, 2017. **56**(44): p. 12799-12810.

157. Trevisan, O.V., S.V. Araujo, R.G.D. Santos, and J.A. Vargas. *Diffusion coefficient of CO2 in light oil under reservoir conditions using X-Ray computed tomography*. in *OTC Brasil*. 2013. Offshore Technology Conference.

158. Lake, L.W., *Enhanced oil recovery.* 1989.

159. McManamey, W. and J. Woollen, *The diffusivity of carbon dioxide in some organic liquids at 25 and 50 C.* AIChE Journal, 1973. **19**(3): p. 667-669.

160. André, L., P. Audigane, M. Azaroual, and A. Menjoz, *Numerical modeling of fluid–rock chemical interactions at the supercritical CO2–liquid interface during CO2 injection into a carbonate reservoir, the Dogger aquifer (Paris Basin, France).* Energy conversion and management, 2007. **48**(6): p. 1782-1797.

161. Svec, R. and R. Grigg. *Physical effects of WAG fluids on carbonate core plugs*. in *SPE Annual Technical Conference and Exhibition*. 2001. Society of Petroleum Engineers.

162. Grigg, R. and R. Svec. *Co-injected CO2-brine interactions with Indiana Limestone*. in *SCA2003-19, presented at the Society of Core Analysts Convention SCA*. 2003.

163. Egermann, P., B. Bazin, and O. Vizika. *An experimental investigation of reaction-transport phenomena during CO2 injection*. in *SPE Middle East Oil and Gas Show and Conference*. 2005. Society of Petroleum Engineers.

164. Egermann, P., S. Bekri, and O. Vizika, *An integrated approach to assess the petrophysical properties of rocks altered by rock-fluid interactions (CO2 injection).* Petrophysics, 2010. **51**(01).

165. Mathis, R. and S. Sears. *Effect of CO 2 Flooding on Dolomite Reservoir Rock, Denver Unit, Wasson (San Andres) Field, TX*. in *SPE Annual Technical Conference and Exhibition*. 1984. Society of Petroleum Engineers.

166. Kane, A., *Performance review of a large-scale CO2-WAG enhanced recovery project, SACROC Unit Kelly-Snyder Field.* Journal of Petroleum Technology, 1979. **31**(02): p. 217-231.

167. Martin, J.W., *Process of recovering oil from oil fields involving the use of critically carbonated water*. 1959, Google Patents.

168. Hickok, C., R. Christensen, and H. Ramsay Jr, *Progress review of the K&S carbonated waterflood project.* Journal of petroleum technology, 1960. **12**(12): p. 20-24.

169. Christensen, R. *Carbonated waterflood results--Texas and Oklahoma*. in *Annual Meeting of Rocky Mountain Petroleum Engineers of AIME*. 1961. Society of Petroleum Engineers.

170. Hickok, C.W. and H.J. Ramsay, Jr., *Case Histories Of Carbonated Waterfloods In Dewey-Bartlesville Field*. 1962, Society of Petroleum Engineers.

171. Scott, J. and C. Forrester, *Performance of domes unit carbonated waterflood-first stage.* Journal of petroleum technology, 1965. **17**(12): p. 1,379-1,384.

172. De Nevers, N., *Carbonated Water Flooding: Is it a Lab Success and a Field Failure?* 1966.

173. Peck, W.D., N.A. Azzolina, J. Ge, C.D. Gorecki, A.J. Gorz, and L.S. Melzer, *Best Practices for Quantifying the CO2 Storage Resource Estimates in CO2 Enhanced Oil Recovery.* Energy Procedia, 2017. **114**: p. 4741-4749.

174. Peck, W.D., N.A. Azzolina, J. Ge, N.W. Bosshart, M.E. Burton-Kelly, C.D. Gorecki, A.J. Gorz, S.C. Ayash, D.V. Nakles, and L.S. Melzer, *Quantifying CO2 storage efficiency factors in hydrocarbon reservoirs: A detailed look at CO2 enhanced oil recovery.* International Journal of Greenhouse Gas Control, 2018. **69**: p. 41-51.

175. Killough, J. and C. Kossack. *Fifth comparative solution project: evaluation of miscible flood simulators*. in *SPE Symposium on Reservoir Simulation*. 1987. Society of Petroleum Engineers.

176. Glaso, O., *Generalized minimum miscibility pressure correlation (includes associated papers 15845 and 16287).* Society of Petroleum Engineers Journal, 1985. **25**(06): p. 927-934.

177. Yuan, H., R. Johns, A. Egwuenu, and B. Dindoruk. *Improved MMP correlations for CO2 floods using analytical gas flooding theory*. in *SPE/DOE symposium on improved oil recovery*. 2004. Society of Petroleum Engineers.

178. Khazam, M., T. Arebi, T. Mahmoudi, and M. Froja, *A new simple CO 2 minimum miscibility pressure correlation.* Oil Gas Res, 2016. **2**(120): p. 2472-0518.1000120.

179. Agada, S., S. Geiger, and F. Doster, *Wettability, hysteresis and fracture–matrix interaction during CO2 EOR and storage in fractured carbonate reservoirs.* International Journal of Greenhouse Gas Control, 2016. **46**: p. 57-75.

180. Whitson, C.H. and M.R. Brulé, *Phase behavior*. SPE Monograph Series. Vol. 20. 2000: Henry L. Doherty Memorial Fund of AIME, Society of Petroleum Engineers …. 233.

181. Lansangan, R. and J. Smith, *Viscosity, density, and composition measurements of CO2/West Texas oil systems.* SPE reservoir engineering, 1993. **8**(03): p. 175-182.

182. Wang, G. *A study of crude oil composition during CO2 extraction process*. in *SPE California Regional Meeting*. 1986. Society of Petroleum Engineers.

183. Tsau, J.-S., L.H. Bui, and G.P. Willhite. *Swelling/extraction test of a small sample size for phase behavior study*. in *SPE improved oil recovery symposium*. 2010. Society of Petroleum Engineers.

184. Kurowski, P., C. Misbah, and S. Tchourkine, *Gravitational instability of a fictitious front during mixing of miscible fluids.* EPL (Europhysics Letters), 1995. **29**(4): p. 309.

185. Moortgat, J., *Viscous and gravitational fingering in multiphase compositional and compressible flow.* Advances in Water Resources, 2016. **89**: p. 53-66.

186. Burnside, N. and M. Naylor, *Review and implications of relative permeability of CO2/brine systems and residual trapping of CO2.* International Journal of Greenhouse Gas Control, 2014. **23**: p. 1-11.

187. Spiteri, E.J., R. Juanes, M.J. Blunt, and F.M. Orr, *A new model of trapping and relative permeability hysteresis for all wettability characteristics.* Spe Journal, 2008. **13**(03): p. 277-288.

188. Elwy, M., A.Y. Zekri, R.A. Almehaideb, and H.H. Al-Attar. *Optimization of CO2 WAG Processes in Carbonate Reservoirs-An Experimental Approach*. in *Abu Dhabi International Petroleum Conference and Exhibition*. 2012. Society of Petroleum Engineers.

189. Broome, J., J. Bohannon, and W. Stewart, *The 1984 Natl. Petroleum Council Study on EOR: An Overview*. Journal of Petroleum Technology, 1986. **38**(08): p. 869-874.

190. Jeschke, P., L. Schoeling, and J. Hemmings. *CO2 flood potential of California oil reservoirs and possible CO2 sources*. in *SPE Annual Technical Conference and Exhibition*. 2000. Society of Petroleum Engineers.

191. Shu, W.R., *Carbonated waterflooding for viscous oil recovery using a CO2 solubility promoter and demoter*. 1983, Google Patents.

192. Shu, W.R., *Carbonated waterflooding for viscous oil recovery*. 1984, Google Patents.

193. Jödecke, M., J. Xia, Á. Pérez-Salado Kamps, and G. Maurer, *Solubility of Carbon Dioxide in Aqueous, Salt-Containing Solutions of Methanol or Acetone.* Chemical Engineering & Technology: Industrial Chemistry-Plant Equipment-Process Engineering-Biotechnology, 2004. **27**(1): p. 31-34.

194. Jödecke, M., Á. Pérez-Salado Kamps, and G. Maurer, *Experimental investigation of the solubility of CO2 in (acetone+ water).* Journal of Chemical & Engineering Data, 2007. **52**(3): p. 1003-1009.

195. Hickok, C.W., R.J. Christensen, and H.J. Ramsay, Jr., *Progress Review of the K&S Carbonated Waterflood Project.* 1960.

196. Li, T.M., M. Ioannidis, and I. Chatzis, *Recovery of non-aqueous phase liquids from ground sources*. 2007, Google Patents.

197. Mosavat, N., *Utilization of Carbonated Water Injection (CWI) as a Means of Improved Oil Recovery in Light Oil Systems: Pore-Scale Mechanisms and Recovery Evaluation*. 2014, Faculty of Graduate Studies and Research, University of Regina.

198. De Waard, C. and D. Milliams, *Carbonic acid corrosion of steel.* Corrosion, 1975. **31**(5): p. 177-181.

199. De Waard, C., U. Lotz, and A. Dugstad. *Influence of Liquid Flow Velocity on CO~ 2 Corrosion: A Semi-Empirical Model*. in *CORROSION-NATIONAL ASSOCIATION OF CORROSION ENGINEERS ANNUAL CONFERENCE-*. 1995. NACE.

200. Browning, D. *CO2 corrosion in the Anadarko Basin*. in *SPE Deep Drilling and Production Symposium*. 1984. Society of Petroleum Engineers.

201. Blackford, T. *Carbonated waterflood implementation and its impact on material performance in a pilot project*. in *SPE annual technical conference and exhibition*. 1987. Society of Petroleum Engineers.